CDT
Centre de
Développement
Technologique

**ÉCOLE
POLYTECHNIQUE
DE MONTRÉAL**

-- REPORT --

STUDY OF THE EFFECT OF TITANIUM AND SULPHUR ON THE THOUGHNESS PROPERTIES OF WELD METAL DEPOSITS FROM LOW HYDROGEN ELECTRODES

prepared for:

CANADIAN LIQUID AIR LTD
5035 Rouen Street
Montréal (Québec) H1V 1J3

August 1987

CDT PROJECT P1079

CDT
Centre de Développement Technologique
École Polytechnique de Montréal

CDT PROJECT P1079
DSS CONTRACT No. 15SQ23440-5-9211

CONTRACT REPORT NO. 15Q 85-00222

-- REPORT --

STUDY OF THE EFFECT OF TITANIUM AND SULPHUR ON THE THOUGHNESS PROPERTIES OF WELD METAL DEPOSITS FROM LOW HYDROGEN ELECTRODES

prepared for:

CANADIAN LIQUID AIR LTD
R & D Research Laboratory
5035 Rouen Street
Montréal (Québec) H1V 1J3

by:

Sylvain St-Laurent, Eng.
Larry Cutler, Ph.D.
Gilles L'Espérance, Ph.D.
Department of Metallurgical Engineering
ECOLE POLYTECHNIQUE DE MONTREAL

submitted by:

LE CENTRE DE DÉVELOPPEMENT TECHNOLOGIQUE
DE L'ECOLE POLYTECHNIQUE DE MONTREAL
Campus de l'Université de Montréal
Case postale 6079, Succursale A
Montréal (Québec) H3C 3A7

MICROMEDIA

250 pp

August 1987

Gilles L'Espérance, Ph.D.
Project Director

TABLE OF CONTENTS

	PAGE
TABLE OF CONTENTS	iv
LIST OF FIGURES	ix
LIST OF TABLES	xiv
CHAPTER 1 INTRODUCTION	1
CHAPTER 2 LITERATURE REVIEW	4
2.1 INTRODUCTION	4
2.2 MICROSTRUCTURE OF THE AS-DEPOSITED WELD METAL IN MICROALLOYED STEELS	5
2.2.1 Methods of Classification	5
2.2.2 Description of the Constituent Phases	8
2.2.2.1 Primary Ferrite (PF)	8
2.2.2.2 Acicular Ferrite (AF)	8
2.2.2.3 Ferrite with a Second Phase (FS)	8
2.2.2.4 Ferrite Carbide Aggregates (FC)	9
2.2.2.5 Other constituents	9
2.2.3 Sequence of Formation of the Weld Metal Microstructures	10
2.3 TOUGHNESS OF THE AS-DEPOSITED WELD METAL	11
2.3.1 Effect of Microstructure	11
2.3.2 Effect of Austenite Grain Size	13
2.3.3 Influence of Cooling Rate	14
2.3.3.1 Influence of Δt (1200/800)	14
2.3.3.2 Influence of Δt (1200/800) on Austenite Grain Size	15
2.3.4 Effects of Alloy Additions	17
2.3.4.1 General Effects	17
2.3.4.2 Carbon Equivalent	17
2.3.4.3 Carbon	18
2.3.4.4 Manganese	20
2.3.4.5 Silicon	20
2.3.4.6 Titanium and Boron	22
2.3.4.7 Oxygen	25
2.3.4.8 Aluminium	29
2.3.4.9 Sulphur	29
2.3.4.10 Nitrogen	30
2.3.4.11 Other Elements	31
2.4 ROLE OF INCLUSIONS	31
2.4.1 General Effects	31
2.4.2 Influence of Inclusions Size and Distribution	32
2.4.2.1 Optimum Size and Distribution	32
2.4.2.2 Influence of Size Distribution	33

PAGE

2.4.2.3 Effect of Oxygen Levels on Average Inclusion Size..... 36
2.4.2.4 Effect of the Flux on the Inclusion Size..... 36
2.4.3 Influence of Chemical Composition of the inclusions..... 37
2.4.3.1 General Trends..... 37
2.4.3.2 Effect of Aluminium..... 38
2.4.3.3 Influence of Ti..... 42
2.4.3.4 Microanalysis of Inclusions..... 43

2.5 MECHANISMS FOR THE NUCLEATION OF ACICULAR FERRITE.... 46
2.5.1 Nucleation Thermodynamics..... 46
2.5.2 Epitaxial Relationships Between Inclusions and Ferrite..... 47
2.5.3 Strain Induced Nucleation..... 48
2.5.4 Nucleation on an Inert Substrate..... 50
2.5.5 Localized Variation in the Composition of the Matrix Near the Inclusions..... 50

CHAPTER 3 EXPERIMENTAL TECHNIQUES..... 51

3.1 WELD METAL PREPARATION..... 51
3.1.1 Composition of the Weld Metal..... 51
3.1.1.1 Technique of Chemical Analysis..... 51
3.1.1.2 Compositions of the Weld Metal Studied..... 51
3.1.2 Electrode Fabrication..... 51
3.1.3 Welding Techniques..... 54

3.2 TOUGHNESS EVALUATION OF WELD METAL DEPOSITS..... 60
3.2.1 Experimental Procedure..... 60
3.2.2 Types of As-Deposited Weld Metal Studied..... 61
3.2.3 Data Reduction..... 62
3.2.4 Fractography..... 64

3.3 MICROSCOPIC EXAMINATION..... 65
3.3.1 Regions Examined..... 65
3.3.2 Metallographic Examination..... 65
3.3.3 Quantitative Inclusion Analysis..... 66

CHAPTER 4 EXPERIMENTAL RESULTS..... 70

4.1 MICROSTRUCTURAL ANALYSIS OF LARGE FINAL PASS AS-DEPOSITED WELDS..... 70
4.1.1 Quantitative Microstructural Analysis..... 70
4.1.2 Effect of Ti on Microstructure..... 70
4.1.3 Effect of S on Microstructure..... 73
4.1.4 Effect of Ca and Al additions on Microstructure 73

PAGE

4.2 INCLUSION ANALYSES OF EXPERIMENTAL AS-DEPOSITED LARGE PASS WELDS 76
4.2.1 Inclusion Size Distributions 76
4.2.1.1 General Aspects 76
4.2.1.2 Effect of Ti on Inclusion Size Distributions 76
4.2.1.3 Effect of S on Inclusion Size Distributions 82
4.2.1.4 Effect of O plus S on Volume Fraction of Inclusions 82
4.2.2 Chemical Composition of Inclusions 84
4.2.2.1 General Aspects 84
4.2.2.2 Effect of Ti on Chemical Composition of Inclusions 84
4.2.2.3 Effect of S on Chemical Composition of Inclusions 96
4.2.2.4 Effect of Al and Ca on Chemical Composition of Inclusions 98
4.2.2.5 Heterogeneous Nature of the Inclusions 99

4.3 TOUGHNESS OF THE EXPERIMENTAL WELDS 100
4.3.1 As-deposited Weld Metal 100
4.3.1.1 Results of Charpy Impact Tests 100
4.3.1.2 Effect of Ti on Toughness 107
4.3.1.3 Effect of S on Toughness 107
4.3.1.4 Effect of Ca and Al on Toughness 108
4.3.1.5 Effect of Nitrogen on Toughness 108
4.3.2 Instrumented Impact Tests of the As-Deposited Weld Metal 109
4.3.2.1 Introduction 109
4.3.2.2 Effect of Ti 109
4.3.2.3 Effect of S 110
4.3.2.4 Effects of Ca and Al 114
4.3.2.5 Cleavage Fracture Resistance of As-deposited Weld Metal 119
4.3.3 Fractographic Studies 120
4.3.3.1 General Trends 120
4.3.3.2 Effect of Ti 124
4.3.3.3 Effect of S 129
4.3.3.4 Effect of Ca and Al 129
4.3.3.5 Effect of Nitrogen 131
4.3.4 Toughness of Standard CSA Welds 135

CHAPTER 5 DISCUSSION 141

5.1 ROLE OF INCLUSIONS ON THE DEVELOPMENT OF THE WELD METAL MICROSTRUCTURE 141
5.1.1 Effect of Inclusion Chemistry 141
5.1.1.1 Effect of Ti 141
5.1.1.2 Effect of S and Deoxidizing Agents, Ca and Al 145

PAGE

5.1.1.3 Comparison with Results of Other Workers..... 146
5.1.2 Effect of the Inclusion Size, Density and distribution..... 149
5.1.2.1 Effect of austenite grain size..... 149
5.1.2.2 Nucleation of Acicular Ferrite..... 152
5.1.3 Proposed Mechanism for the Nucleation of Acicular Ferrite..... 160
5.1.3.1 Nucleation on the Ti rich Phase..... 160
5.1.3.2 Estimation of the Surface Area of the Ti rich Phases..... 160
5.1.3.3 Relationship between the AF/Fγ and the Total Available Surface Area of Ti-rich Phase per unit Volume..... 161
5.1.3.4 Ti-Al Weld..... 167
5.1.3.5 Comparison of the Proposed Model with those of other Researchers..... 170

5.2 MICROSTRUCTURE-TOUGHNESS RELATIONSHIPS FOR EXPERIMENTAL LARGE PASS WELDS..... 176
5.2.1 Introduction..... 176
5.2.2 General Trends..... 178
5.2.2.1 Effects of Acicular Ferrite..... 178
5.2.2.1.1 Effect on Dynamic Strength 178
5.2.2.1.2 Effect on Cleavage Fracture Resistance..... 182
5.2.2.2 Effect of Inclusion Density on Critical Cleavage Fracture Stress..... 185
5.2.3 Effect of Ti on As-deposited Weld Strength and Toughness..... 187
5.2.3.1 Effect on Strength..... 187
5.2.3.2 Effect on Cleavage Fracture Resistance and T_{50} Temperature..... 191
5.2.3.3 Proposed Model for the Cleavage Fracture Process in Weld Metal Containing Significant Quantities of AF..... 194
5.2.3.4 Effect on Impact Resistance above the Impact Transition Temperature..... 196
5.2.4 Effect of S on Toughness..... 198
5.2.5 Effect of Ca on Toughness..... 199
5.2.6 Effect of Al on Toughness..... 201
5.2.7 Effect of Nitrogen on Toughness..... 202
5.2.8 Possible Avenues for Improved Toughness in As-deposited Weld Metal..... 206

5.3 COMPARAISON BETWEEN EXPERIMENTAL LARGE PASS WELDS AND CONVENTIONAL CSA TEST WELDS..... 208
5.3.1 Toughness..... 208
5.3.2 The conventionel welds TiM-1 and SM-1..... 211
5.3.2.1 Effect of Inclusions on the Microstructural Development..... 211

PAGE

5.3.2.3 Microstructure-Toughness Relationships..... 217

CONCLUSIONS..... 219

REFERENCES..... 225

LIST OF FIGURES

		PAGE
FIGURE 2.1	: As-Deposited Weld Microstructures Showing the Various Microstructural Constituents.....	7
FIGURE 2.2	: Continuous Cooling Curve Illustrating the Sequence of Formation of the Weld Metal Microstructures.....	10
FIGURE 2.3	: Transformation Sequence for Various Weld Metal Microstructures..... A) Polyganol and Side Plate Ferrite B) Acicular Ferrite C) Bainite	12
FIGURE 2.4	: Relationship Between Prior-Austenite Grain Size and Quantity of Grain Boundary Ferrite.....	14
FIGURE 2.5	: Influence of Δt (1200/800) on Austenite Grain Size....	15
FIGURE 2.6	: Effect of Δt (800/500) on the Quantity of Acicular Ferrite and the Austenite to Ferrite Transformation Temperatures.....	16
FIGURE 2.7	: Relationship Between Carbon Equivalent and the Proportions of Microstructural Components.....	18
FIGURE 2.8	: Effect of Carbon Concentration on Impact Transition Temperatures.....	19
FIGURE 2.9	: Effect of Manganese Concentration on Microstructural Development.....	21
FIGURE 2.10	: Effect of Ti Level on the Quantity of Acicular Ferrite	23
FIGURE 2.11	: Mechanism by which Titanium and Boron Influence Weld Metal Toughness and Microstructure.....	24
FIGURE 2.12	: Relations Between Inclusion Volume Fraction and..... A) O Content and B) Sum of O and S Contents	25
FIGURE 2.13	: Effect of O Level on Transition Temperatures of Weld Metal.....	26
FIGURE 2.14	: Schematic Diagram of the Effect of O Content on Continuous Cooling Curves..... A) Low O B) Medium C) High	28
FIGURE 2.15	: Two Types of Particle Distributions Observed By Chuen	34

PAGE

FIGURE 2.16 : Influence of Intergranualar Inclusion Density on Austenite Grain Size..... 35

FIGURE 2.17 : Influence of Intragranualar Inclusion Density on Quantity of Acicular Ferrite..... 35

FIGURE 2.18 : Influence of Al Content on the Transition Temperature Of Weld Metal In Si-Mn-Al-Ti Data From Terashima and Hart..... 38

FIGURE 2.19 : Variation of the Transition Temperature As a Function of Ti and Al Levels after Devillers et al..... 39

FIGURE 2.20 : Relation Between the $(\%Al)/(\%O)^2$ Ratio and..... 40
A) Transition Temperature and
B) Average Inclusion Diameter After the Data of Terashima and Hart

FIGURE 2.21 : Optimum O Content (Lowest Transtition Temperature for a Given Al Content According to Results of Devillers and Terashima and Hart..... 41

FIGURE 2.22 : Role of Ti on Acicular Ferrite Content for Small Al Additions as a Function of Carbon Equivalent (pcm). Data of Bonnet et al..... 42

FIGURE 2.23 : Heterogeneous Nature of Two Inclusions on Carbon Replicas..... 43
A) Micrograph of Particle
B) C) and D) X-Ray Spectra from Various Regions

FIGURE 2.24 : Effect of Ti Concentrations on the Chemical Composition of Inclusions..... 45

FIGURE 2.25 : Ratio of Surface Energy of Inclusions and the Austenite Grain Boundaries to the Energy of Homogeneous Nucleation..... 46

FIGURE 2.26 : Thermal Coefficients of Expansion for Various Phases. 49

FIGURE 3.1 : Details of Weld Test Assembly and Standard Charpy Specimens..... 55

FIGURE 3.2 : Details of the Preparation of the Modified Test Plate..... 56

FIGURE 3.3 : Details of Sub-Sized Charpy Specimen..... 58

FIGURE 3.4 : Location of Charpy Specimens in the Modified Weld Test Plate..... 59

PAGE

FIGURE 3.5 : Typical Load-Time Trace and Associated Energies for an Impact Test..... 63

FIGURE 4.1 : Typical Optical Microstructure for TiL Weld..... 72

FIGURE 4.2 : Typical Optical Microstructure for TiM..... 72

FIGURE 4.3 : Typical Optical Microstructure for TiH Weld..... 74

FIGURE 4.4 : Typical Optical Microstructure for SM Weld..... 74

FIGURE 4.5 : Typical Optical Microstructure for SH Weld..... 75

FIGURE 4.6 : Typical optical Microstructure for Ti-Ca Weld..... 75

FIGURE 4.7 : Typical Optical Microstructure for Ti-Al Weld..... 77

FIGURE 4.8 : Inclusion Size Distributions for TiL, TiM and TiH Welds..... 78

FIGURE 4.9 : Inclusion Size Distributions for TiM, SM and SH Welds. 79

FIGURE 4.10 : Inclusion Size Distributions for TiM, Ti-Ca and Ti-Al. 80

FIGURE 4.11 : Relationship between (O+S) and Volume Fraction of Inclusions..... 83

FIGURE 4.12 : Relative Intensity of the Major Elements as a Function of Inclusion Diameter for TiL..... 86

FIGURE 4.13 : Relative Intensity of the Major Elements as a Function of Inclusion diameter for TiM..... 87

FIGURE 4.14 : Relative Intensity of the Major Elements as a Function of Inclusion Diameter for TiH..... 88

FIGURE 4.15 : Relative Intensity of the Major Elements as a Function of Inclusion Diameter for SM..... 89

FIGURE 4.16 : Relative Intensity of the Major Elements as a Function of Inclusion Diameter for SH..... 90

FIGURE 4.17 : Relative Intensity of the Major Elements as a Function of Inclusion Diameter for Ti-Ca..... 91

FIGURE 4.18 : Relative Intensity of the Major Elements as a Function of Inclusion Diameter for Ti-Al..... 92

FIGURE 4.19 : Relative Intensity of Ti in Inclusions as a Function of Ti Content of the Weld Metal..... 93

PAGE

FIGURE 4.20 : Calculated Total Contents of Ti, S, Si and Mn in the Inclusions as a Function of Ti Content of the Weld.... 95

FIGURE 4.21 : Calculated Total Contents of Ti, S, Si and Mn in the Inclusions as a Function of S Content of the Weld..... 97

FIGURE 4.22 : Summary of the Effects of Weld Metal Composition on the Inclusion Chemistry..... 101

FIGURE 4.23 : Typical Inclusion of SM Weld which shows the Heterogenious Nature of Inclusions..... 102
A) Micrograph of the Inclusion
B), C) and D) Energy Dispersive X-ray Spectra from Regions 1, 11 and 111

FIGURE 4.24 : Impact Transition Curve for Standard Charpy tests of Welds with Varying Ti Additions..... 103

FIGURE 4.25 : Impact Transition Curves for Standard Charpy Tests for Welds with Varying Sulphur Additions..... 104

FIGURE 4.26 : Impact Transitions Curves for Standard Charpy Tests of Welds with Ca and Al Additions..... 105

FIGURE 4.27 : Effect of N on Impact Energy for TiM Weld..... 111

FIGURE 4.28 : Load-Temperature Diagrams for TiL, TiM and TiH Welds.. 112

FIGURE 4.29 : Load-Displacement Curves for TiL, TiM and TiH Welds... 113

FIGURE 4.30 : Load-Temperature Diagrams for TiM, SM and SH Welds.... 115

FIGURE 4.31 : Load-Displacement Curves for TiM, SM and SH Welds 116

FIGURE 4.32 : Load-Temperature Diagrams for TiM and TiCa Welds..... 117

FIGURE 4.33 : Load-Displacement Diagrams for TiM and TiCa Welds Tested at $0^{o}C$..... 118

FIGURE 4.34 : Load-Temperature Diagrams for TiM and TiAl Welds..... 122

FIGURE 4.35 : Load-Displacement Curves for TiM and TiAl Welds Tested at $0^{o}C$..... 123

FIGURE 4.36 : Fractograph and oblique Sections of TiL Weld Impact Tested at $-30^{o}C$..... 126
A) Fractograph
B) Oblique Section

PAGE

FIGURE 4.37 : Fractograph and oblique Section of TiM Weld Impact Tested at -30°C..... 127
A) Fractograph
B) and C) Oblique Sections

FIGURE 4.38 : Fractograph and Oblique Section of TiH Weld Impact Tested at -30°C..... 128
A) Fractograph
B) Oblique Section

FIGURE 4.39 : Fractograph and oblique Section of SM Weld Impact Tested at -30°C..... 130
A) and C) Fractographs
B) and D) Oblique Sections

FIGURE 4.40 : Fractograph and Oblique Sections of TiCa Weld Impact Tested at -30°C..... 132
A) and B) Oblique Sections
C) Fractograph

FIGURE 4.41 : Fractographs of TiAl Weld Tested at 0°C..... 133

FIGURE 4.42 : Fractograph and Oblique Sections of TiM Welds with Low and High Levels of N, Impact Tested at -30°C..... 134
A) Oblique Section of Low N Weld
B) and C) Fractograph and Oblique Section of High N Weld

FIGURE 4.43 : Impact Transition Curves for Industrial Weld Deposits from Electrodes with Varying Ti Additions..... 137

FIGURE 4.44 : Impact Transition Curves for Industrial Weld Deposits from Electrodes with Varying Sulphur Additions..... 138

FIGURE 4.45 : Impact Transition Curves for Industrial Weld Deposits from Electrodes with Ca or Al Additions..... 139

FIGURE 5.1 : Micrograph showing that the Inclusions of TiL Weld have not Played an Active Role on the Microstructure.. 142

FIGURE 5.2 : Micrograph showing that the inclusions of TiM Weld are Preferential Sites for the Nucleation of Acicular Ferrite..... 142

FIGURE 5.3 : Nucleation of Acicular Ferrite at Inclusions for SM Weld..... 143

FIGURE 5.4 : Nucleation of Acicular Ferrite at Inclusions for Ti-Al Weld..... 143

FIGURE 5.5 : Nucleation of Acicular Ferrite at Inclusions for Ti-Al Weld..... 144

LIST OF TABLE

		PAGE
TABLE 2.1	: Classification and Terminology of Microstructures of Low C Low Alloy Steel Weld Metal (2).....	6
TABLE 3.1	: Chemical Composition of Standard Industrial Type Multi-Pass Welds.....	52
TABLE 3.2	: Chemical Composition of the Experimental Welds With Large Last Pass.....	53
TABLE 3.3	: Welding Parameters and Thermal Cycle for Weld Specimens.....	57
TABLE 3.4	: Weld Metal Microstructural Classification.....	67
TABLE 3.5	: Experimental Conditions.....	69
TABLE 4.1	: Results of Quantitative Microstructural Analysis.....	71
TABLE 4.2	: Effects of Composition on Inclusion Size Distributions	81
TABLE 4.3	: Average Relative Intensity of the X-Ray Peaks for the Principal Elements Found in the Inclusions.....	85
TABLE 4.4	: Results of Standard Charpy Tests for the Electrodes with Varying Ti Concentrations.....	103
TABLE 4.5	: Results of Standard Charpy Tests for the Electrodes with Varying S Concentrations.....	104
TABLE 4.6	: Results of Standard Charpy Tests for the Electrodes with Ca and Al Additions.....	105
TABLE 4.7	: Results of Full Size Charpy Tests for the Experimental Test Plates.....	106
TABLE 4.8	: Results of 5x5 Charpy Tests for Experimental Welds with Varying Ti Concentrations.....	106
TABLE 4.9	: Dynamic Yield and Fracture Properties of Experimental Weld metal.....	120
TABLE 4.10	: Results of Charpy Tests for Industrial Weld Deposits from Electrodes with Varying Ti Additions (Ti Serie).	137
TABLE 4.11	: Results of Charpy Tests for Industrial Weld Deposits from Electrodes with Varying Sulphur additions.....	138
TABLE 4.12	: Results of Charpy Tests for Industrial Weld Deposits from Electrodes with Varying Ca and Al Additions.....	139

PAGE

FIGURE 5.6 : Proportion of AF in the Weld as a Function of the Relative Intensity of Ti in the Inclusions..... 147

FIGURE 5.7 : Proportion of AF in the Weld with Varying Sulphur Content as a Function of the Relative Intensity of S in the Inclusions..... 148

FIGURE 5.8 : Austenite Grain Size (represented by the ratio S/L) as a Function of Inclusion Density (N_A) for the Welds except TiL..... 151

FIGURE 5.9 : Proportion of AF as a Function of the Austenite Grain Size (S/L)..... 156

FIGURE 5.10 : Proportion of AF as a Function of the Inclusion Density 157

FIGURE 5.11 : The Ratio AF/Fγ as a Function of the Inclusion Density (N_A) for the Weld with Varying Sulphur Content..... 158

FIGURE 5.12 : The Ratio AF/Fγ as a Function of $(N_A x A_{inc})$..... 159

FIGURE 5.13 : Schematic illustrating the Spherical Cap which is the Form Assumed for the Ti-rich Phase present in the Inclusions..... 163

FIGURE 5.14 : Percentage of the Inclusion Surface Area Occupied by the Ti-rich Phase as a Function of the Relative Intensity of Ti in Inclusions..... 163

FIGURE 5.15 : The Nucleation Efficiency Ratio, AF/F*, as a function of $(N_A x A_{Ti})$..... 167

FIGURE 5.16 : Dynamic Yield Strength at -30°C as a Function of AF Content..... 180

FIGURE 5.17 : Critical Cleavage Fracture Stress as a Function of AF Content..... 184

FIGURE 5.18 : Deviation in the Critical Cleavage Fracture Stress as a Function of the Inclusion Density Over 1 μm..... 186

FIGURE 5.19 : Dynamic Yield Strength at -30°C as a Function of Ti content..... 188

FIGURE 5.20 : AF Content in the Weld as a Function of Ti Content.... 190

FIGURE 5.21 : Effect of N no Absorbed Energy for Charpy Tests at -30°C and -40°C..... 203

FIGURE 5.22 : Load-Temperature Diagram for the TiM Weld with 100 and 180 ppm N..... 204

PAGE

FIGURE 5.23 : Micrograph Showing the Caracteristic Microstructure of the Weld TiM-I..... 212

FIGURE 5.24 : Micrograph Showing the Caracteristic Microstructure of the Weld SM-I..... 212

FIGURE 5.25 : Inclusion Size Distribution of TiM-I and SM-I Welds... 214

FIGURE 5.26 : Relative Intensities of Si, S, Ti and Mn as a Function of the Inclusion Diameter for TiM-I and SM-I Welds.... 217

		PAGE
TABLE 4.13	: Transition Temperature for the Industrial test plates	140
TABLE 5.1	: Summary of the Principal Values used in the Calculation of $N_A x A_{Ti}$	166
TABLE 5.2	: Summary of the Quantitative Microstructural and Inclusion Analysis	213

CHAPTER ONE

INTRODUCTION

The ever increasing concern for the prevention of brittle fracture in welded structures has lead to the need for improved notch toughness of the weld metal at lower temperatures. Electrodes for the Shielded Metal Arc Welding (SMAW) procedure which can garantee Charpy V-notch toughness of 27 J at -45°C in the vertical position, are presently available on the market. The toughness, however, can vary drastically with welding procedure and position.

The possible development of welded structures for the Arctic environment will increase even further the the notch toughness requirements. Charpy V-notch toughness of 27 to 50 J at -60 °C has already been requested for ice breakers so the consistent achievment of such values in the weld metal is of major concern.

The main aim of this study is to achieve consistantly these low temperature impact properties. More specifically, SMAW consumables are the object of this study since they are most likely to satisfy such requirements. In the industry, although a number of filler metals are claimed to give acceptable notch toughness values at temperatures down to -60 °C (SAW or FCAW filler metals) SMAW is usually the procedure chosen when a critical application (requiring more consistent values at -60 °C) is encounted because of the

ability to use SMAW in all positions. In addition, the highest toughness values are obtained at a given temperature with this technique. It was thus concluded that "low hydrogen" SMAW electrodes should be investigated first.

In addition, the work centered on the as-deposited area of the weld metal as it is usually the area exhibiting the lowest toughness values [3,55-59]. This, however, is not always observed. For example, welds regions which have been hardened as a result of thermal cycling during subsequent passes may have lower toughness than the as-deposited weld metal. This, however, is not the case for low hydrogen filler metals.

For this reason, a special welding procedure was developed to allow notch toughness samples to be taken from welds with the largest amount of as deposited metal possible. This required a substantial number of experiments since SMAW deposits are usually made of a large number of small superimposed passes. It was intented to compare the results obtained with this technique with those obtained with a standard multipass welding procedure for all weld metal deposits (CSA type).

The final aspect of this work is the role played by alloying additions on the microstructural development and hence on the weld metal toughness. Alloying elements such as Mn, Mo, Si, C, etc..., directly affect the microstructure due to their effect on hardenability and more indirectly by their effect on the chemistry and inclusions size distribution formed during solidification [19, 31, 36, 58]. Of particular interest in this regard are oxygen, sulphur and titanium. In this study, the effect of three titanium levels (0.002, 0.005 and 0.02%wt), of three sulphur levels for a given amount of Ti (0.005% found to be the optimum value in the Ti series) and of two strong deoxidants (Ca and Al) have been systematically investigated.

This report is divided in five main chapters. First, a literature survey will be presented followed by a description of the experimental techniques used to characterize in detail the microstrucutre and the toughness properties of the welds. In the next chapter, all of the results for the microstructural and toughness characterization are given. The discussion that follows first presents the effects of alloying elements on the microstructural development, particularly, the formation and role of inclusions on the nucleation of acicular ferrite which is responsible for high toughness values. The microstructure-toughness relationships for the experimental welds are then discussed followed by those for the standard CSA welds. Finally, several conclusions, summarizing the main findings of this investigation, are given.

CHAPTER TWO

LITERATURE REVIEW

2.1 INTRODUCTION

In absence of major defects in the heat affected zone or the base metal, it is the weld melt zone that has the lowest toughness. Increases in the toughness of this zone will therefore increase the overall toughness of the welded joint.

To find welding techniques that will improve the toughness of the melt zone, it is imperative to have a good understanding of the metallurgical factors affecting the microstructure and toughness in this region. In this Chapter, a summary of the effects of these factors on the microstructural development of the weld metal is presented , with special attention being given to the size, distribution and composition of inclusions and the role of inclusions on the formation of acicular ferrite. Also, the terminology that has been used to describe the various microstructural components is discussed.

2.2 MICROSTRUCTURE OF THE AS-DEPOSITED WELD METAL IN MICROALLOYED STEELS

2.2.1 Methods of Classification

The microstructural characteristics of the as-deposited weld metal depend on three subsequent phase transformations[1], namely:

1 - Formation of primary δ ferrite from the liquid phase

2 - Transformation to austenite (δ->γ)

3 - Transformation to ferrite (γ->α)

Although the first two will certainly have an influence, the γ->α transformation ultimately determines the weld metal microstructure.

A number of distinct phases can form during the γ->α transformation in microalloyed steel welds. The terminology used to describe these phases varies, however, with the author[2-13] and has resulted in a certain ambiguity when comparing results from different sources. This is in spite of the efforts of Davey and Widgery[11], Abson and Dolby[9,10] and Pargeter and Dolby[12] to normalize the terminology. Table 2.1 gives a summary of the terminology that has been used to describe the various constituents.

Throughout this report, the terminology of Abson and Dolby[10] is used. Figure 2.1 summarizes this nomenclature and illustrates in optical photomicrographs the corresponding structures in weld metal.

TABLE 2.1

CLASSIFICATION AND TERMINOLOGY OF MICROSTRUCTURES

OF LOW C LOW ALLOY STEEL WELD METAL[2]

Dube, C.A. Aaronson, H.I. Cochrane, R.C.	Widgery, D.J.	Abson, D.J.	Japanese Researchers (4)	Others (4)
Allotriomorphic (Polygonal) Ferrite	Proeutectoid Ferrite	Grain Boundary Ferrite	Proeutectoid Ferrite, Grain Boundary Ferrite, Polygonal Ferrite	Proeutectoid Ferrite, Grain Boundary Ferrite, Block Ferrite
		Polygonal Ferrite	Polygonal Ferrite	Ferrite Islands
Primary & Secondary Ferrite Sideplates	Lamellar Component	Ferrite with Aligned M-A-C	Ferrite Sideplate, Lath-Like Ferrite	Ferrite Sideplate, Lath Ferrite Upper Bainite
Intragranular Ferrite Plates	Acicular Ferrite	Acicular Ferrite	Acicular Ferrite, Needle Like Ferrite,	Acicular Ferrite, Fine Bainitic Ferrite
Lath Martensite Twinned Martensite	Martensite	Martensite M-A	Martensite M-A High-C Martensite	Martensite M-A Lath Ferrite
Upper Bainite			Upper Bainite	

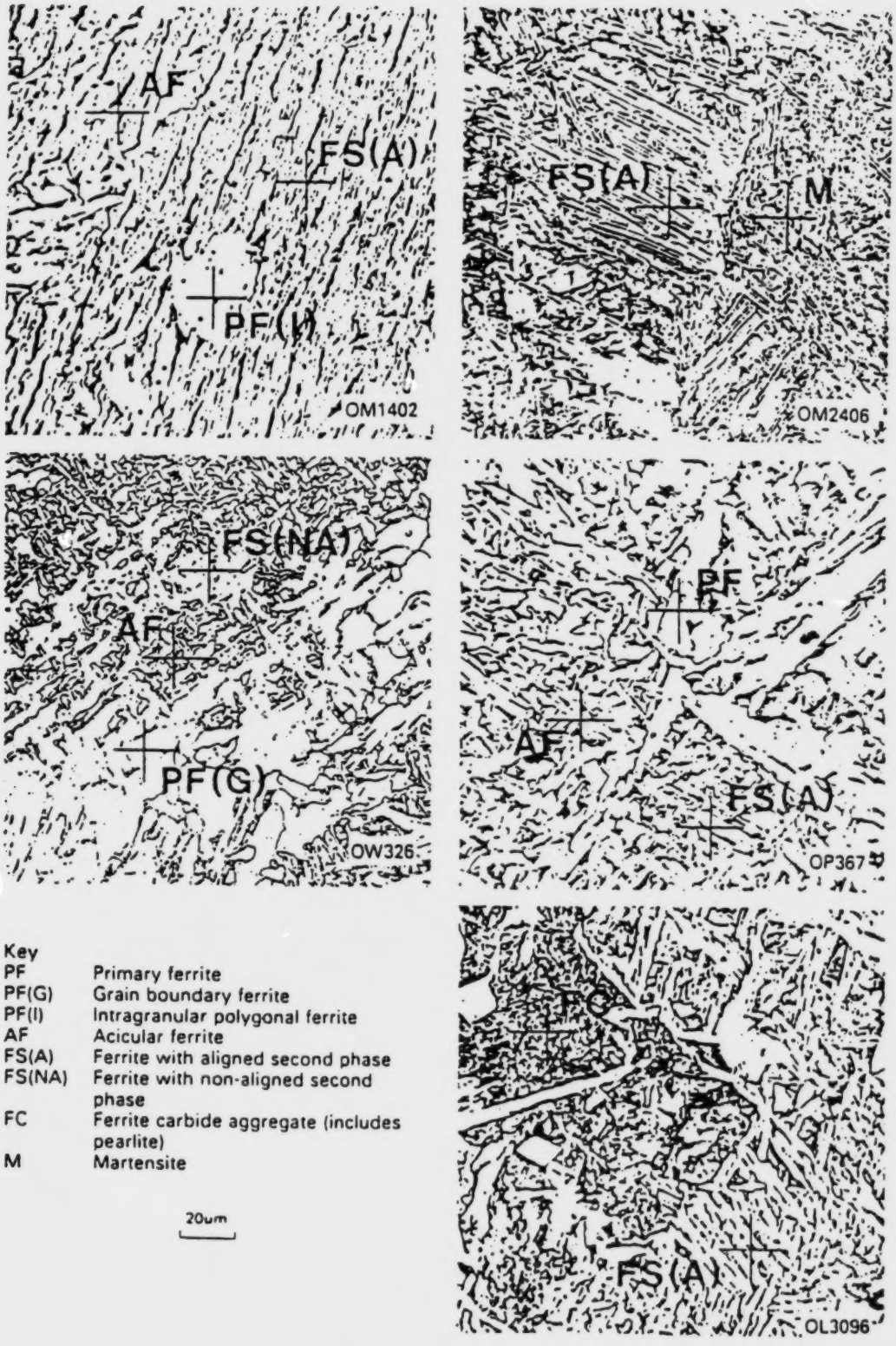

FIGURE 2.1 AS-DEPOSITED WELD MICROSTRUCTURES SHOWING THE VARIOUS MICROSTRUCTURAL CONSTITUENTS[12]

2.2.2 Description of the Constituent Phases

2.2.2.1 Primary Ferrite (PF)

Primary ferrite[10,12] can form either on the austenite grain boundaries (PF(G)) or inside the austenite grains (intragranular polygonal ferrite, PF(I)). The former consists of allotriomorphs which grow in thickness in a direction perpendicular to the austenite grain boundary [2,8,9,10]. The latter is composed of large equi-axed ferrite grains which are not associated with the austenite grain boundaries. PF forms mainly when the cooling rate or alloy content is low.

2.2.2.2 Acicular Ferrite (AF)

Acicular ferrite is characterized by fine nonaligned ferrite grains which nucleate entirely within the austenite grains. According to reference 2, it is characterized by an aspect ratio (length/width) between 3/1 to 10/1 and a lath thickness of a few microns. According to reference 14, acicular ferrite laths have an aspect ratio between 2/1 and 4/1 with an average width of 1 to 3 microns. Most authors agree that acicular ferrite is associated with a high impact resistance due to the large number of high angle boundaries in the crack path.

2.2.2.3 Ferrite with a Second Phase(FS)

FS is present in two forms. The first has an aligned second phase and is referred to by Abson and Dolby as FS(A). The second has a nonaligned second phase(FS(NA)). FS(A) can be further subdivided into either Widmanstatten ferrite or bainite[10,12].

1 - Widmanstatten ferrite is a laminar structure which grows into the interior of the grains from the austenite grain boundaries[13] or from allotriomorphs [2,8]. The formation of this ferrite is favoured by a large undercooling and a large austenite grain size. The aspect ratio of this phase is usually between 10/1 to 20/1[2].

2 - Bainite formation depends principally upon the cooling rate and composition of the weld metal and often resembles Widmanstatten ferrite in the optical microscope[8]. It can often only be identified by transmission electron microscopy. Bainite has higher dislocation densities than Widmanstatten ferrite and has slight disorientation of the laths. For this reason Abson and Dolby [9,10] as well as many other authors do not try to differentiate Widmanstatten ferrite and bainite. Both are considered to be FS(A).

Nonaligned second phase ferrite, (FA(NA)), completely surrounds the microconstituents or regions of acicular ferrite[10].

2.2.2.4 Ferrite Carbide Aggregates (FC)

FC are regions of mixed ferrite and pearlite and/or interphase carbides[10]. This phase forms near the end of the $\gamma \rightarrow \alpha$ transformation in the austenite regions rich in carbon which form because of carbon rejection from the ferrite during the earlier stages of transformation.

2.2.2.5 Other constituents

Small regions of martensite and/or retained austenite can form in the carbon rich regions but their volume fractions are usually small due to the low carbon contents in microalloyed steels.

2.2.3 Sequence of Formation of the Weld Metal Microstructures

A schematic diagram illustrating the sequence of formation of weld metal microstructures is presented in Figure 2.2. This diagram is only a general representation of the transformation process and can be greatly modified by changes in the chemical composition, welding conditions and the inclusion state in the weld metal, which in turn can have a pronounced influence on the nucleation of intragranular ferrite and the $\gamma \rightarrow \alpha$ transformation temperature (via the austenite grain size).

Choi and Hill [15 in 13] have suggested that for C-Mn and C-Mn-Mo weld metal, the temperature of formation of the various phases are:

(i) Primary ferrite, between 750 and 650°C

(ii) Widmanstatten ferrite, between 750 and 650°C

(iii) Acicular ferrite, below 650°C

(iv) Bainite, below 500°C

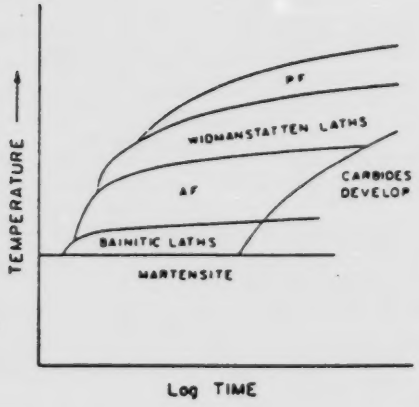

FIGURE 2.2 CONTINUOUS COOLING CURVE ILLUSTRATING THE SEQUENCE OF FORMATION OF THE WELD METAL MICROSTRUCTURES[6]

Pacey and co-workers[6] used GTAW to remelt their C-Mn-Mo welds and analyze the order of formation of the transformation products. This is presented in Figure 2.2. They found that acicular ferrite forms in the 590 to the 650°C range whereas bainite forms only at 550°C and below. Bainite formed only when the Ti level was high enough to delay the austenite to ferrite transformation[6,8]. Bainite could only be formed in weld metal of high hardenability and/or with high cooling rates[8].

The transformation sequence is illustrated in Figure 2.3[8]. When the factors that control the transformation (mentioned at the beginning of this section) favour a high transformation temperature, primary and Widmanstatten ferrite are the dominate microstructural components(Figure 2.3(a)) whereas low transformation temperatures (550°C) give rise to bainite formation (Figure 2.3(c)). Acicular ferrite is formed at intermediate transformation temperatures where the formation of Widmanstatten ferrite is suppressed and the bainite transformation has not yet begun (Figure 2.3(b)).

2.3 TOUGHNESS OF THE AS-DEPOSITED WELD METAL

2.3.1 Effect of Microstructure

There is general agreement amongst researchers that acicular ferrite is the weld metal microstructural constituent that has the best resistance to cleavage fracture initiation and propagation. The fine grain size and high angle boundaries between the individual grains are effective barriers to crack propagation since the cleavage cracks must continuously reinitiate for fracture to occur[16]. This results in a much higher energy for crack growth than in either the coarser PF or FS microstructures. This has been confirmed by the observations of fracture surfaces by Tweed and Knott[17 in 18] and McRobie and

Knott[18 in 16]. They found that cleavage failure occurred preferentially in the PF(G) structures.

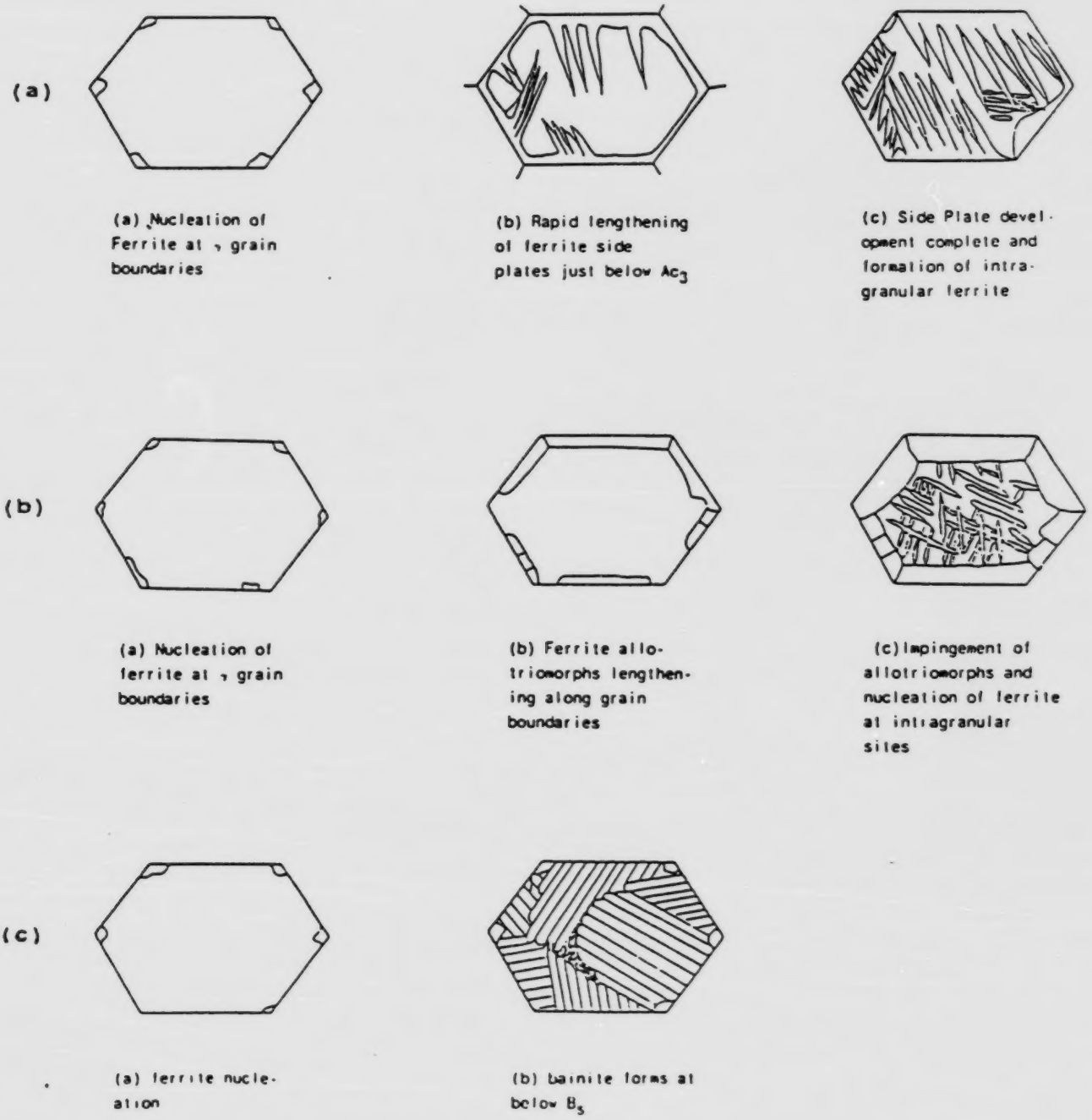
(a)
(a) Nucleation of Ferrite at γ grain boundaries
(b) Rapid lengthening of ferrite side plates just below Ac_3
(c) Side Plate development complete and formation of intragranular ferrite
(b)
(a) Nucleation of ferrite at γ grain boundaries
(b) Ferrite allotriomorphs lengthening along grain boundaries
(c) Impingement of allotriomorphs and nucleation of ferrite at intragranular sites
(c)
(a) ferrite nucleation
(b) bainite forms at below B_s

FIGURE 2.3 TRANSFORMATION SEQUENCE FOR VARIOUS WELD METAL MICROSTRUCTURES[8]

(A) POLYGONAL AND SIDE PLATE FERRITE (B) ACICULAR FERRITE

(C) BAINITE.

The toughness characteristics of the weld metal is therefore closely related to the size of the PF(G) network and the properties of the acicular ferrite[3]. The improvement in toughness and the reduction in the impact transition temperature has been associated with [19,20] :

(i) the size of the PF(G) veins

(ii) general refinement of the PF(G) and AF constituents

(iii) a reduction in the quantity of FC (ferrite-carbide) regions

The optimal microstructure depends upon the welding conditions and chemical composition which influence:

(i) the austenite grain size

(ii) inclusion size and distribution which are related to the austenite grain size

(iii)hardenability.

2.3.2 Effect of Austenite Grain Size

The austenite grain size affects both the ferrite start temperature and intergranular nucleation of proeutectoid ferrite PF(G). An increase in grain size decreases the ferrite start temperature which favours the formation of acicular ferrite (AF) [3]. This was confirmed by Chuen[2] and Ferrante and Farrar[21] who showed that austenite grain sizes greater that 45 μm tended to promote the formation of acicular ferrite.

Increases in the austenite grain size decreases the surface/volume ratio of austenite grains which decreases the number of nucleation sites for PF(G)[2,22] and hence the volume fraction of PF(G). This is clearly shown in Figure 2.4. The decrease in PF(G) favours the formation of larger volume fractions of AF or bainite.

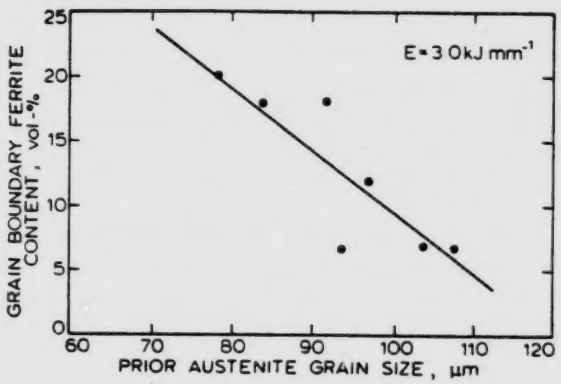

FIGURE 2.4 RELATIONSHIP BETWEEN PRIOR-AUSTENITE GRAIN SIZE AND QUANTITY OF GRAIN BOUNDARY FERRITE[22]

2.3.3 Influence of Cooling Rate

The cooling rate has an important effect on the austenite grain growth as well as the time for the various ferrite transformations. For this reason, the cooling rate is characterized by the time taken to cool from 1200 to 800 °C, $\Delta t(^{1200}_{800})$ and the time for cooling from 800 to 500°C, $\Delta t(^{800}_{500})$.

2.3.3.1 Influence of $\Delta t(^{1200}_{800})$

For a constant $\Delta t(^{800}_{500})$, Bonnet[3] found that increasing $\Delta t(^{1200}_{800})$, increased the austenite grain size which favoured the formation of intragranular transformation products to the expense of PF(G). This effect is illustrated in Figure 2.5.

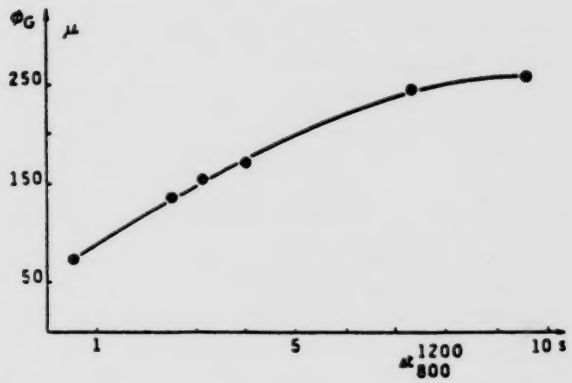

FIGURE 2.5 INFLUENCE OF $\Delta t(^{1200}_{800})$ ON AUSTENITE GRAIN SIZE[3]

2.3.3.2 Influence of $\Delta t(^{800}_{500})$

For similar compositions and austenite grain sizes, the dominate transformation products depends upon $\Delta t(^{800}_{500})$ [22] as follows:

(i) $\Delta t < 5$ sec gives mainly bainite and austenite

(ii) intermediate Δt values gives a mixture of FS (Widmanstatten ferrite), AF and PF.

(iii) high Δt values gives polygonal ferrite and pearlite

The relationship between $\Delta t(^{800}_{500})$, the percentage of AF and the Mn content is presented in Figure 2.6. The amount of AF decreases with increasing cooling times. The rate of cooling necessary for at least 50% acicular ferrite decreases with increasing Mn concentrations. For example, at 0.65% Mn levels, Δt must be less that 3 sec whereas at higher Mn levels (1.40%), this time is about 15 sec. A more detailed discussion of the effects of Mn will be presented in a later section.

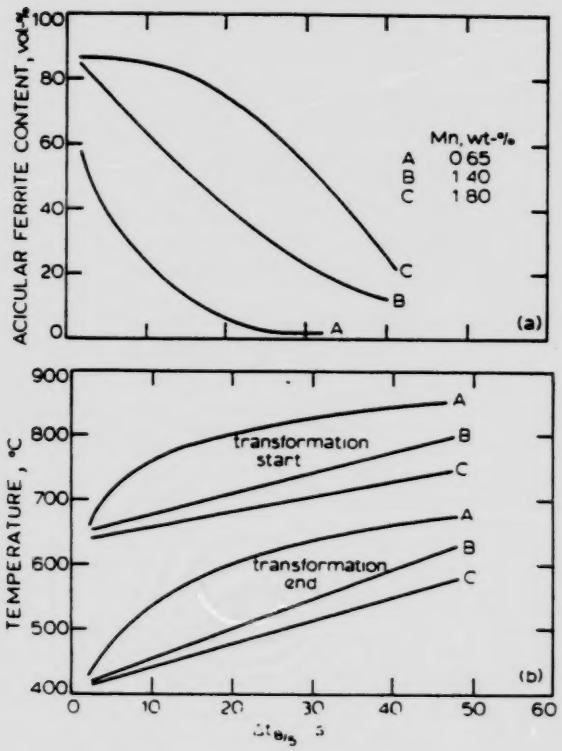

FIGURE 2.6 EFFECT OF $\Delta t(^{800}_{500})$ ON THE QUANTITY OF ACICULAR FERRITE AND THE AUSTENITE TO FERRITE TRANSFORMATION TEMPERATURES[22]

Bonnet[3] found the same relationship between Δt values and the amount of AF. For lower cooling rates, they found increased amounts of PF(G) and granular bainite (probably FS(NA) which forms at higher temperatures than AF). Lower cooling rates also increased the amount of carbides at the expense of M-A (martensite-austenite) microconstituents.

2.3.4. Effects of Alloy Additions

2.3.4.1 General Effects

Alloying additions have a multitude of effects on the microstructure of welds. They (i) modify the CCT(continuous cooling transformation) curves which changes the balance of the constituent phases during transformation, (ii) impart solid solution and/or precipitation strengthening and (iii) modify the chemical composition, size and distribution of inclusions which affects number of potential sites for intragranular nucleation of ferrite.

2.3.4.2 Carbon Equivalent

Many workers have used the carbon equivalent (C.E.) to evaluate the effects of various elements on the hardenability of alloys (higher values of C.E. give higher hardenability). The relationship between microstructure and C.E. according to Graville[23 in 2] is shown in Figure 2.7. This figure shows that for acicular ferrite to form, the value of C.E. must be between 0.25 and 0.43 with an optimal value near 0.4%. High alloy additions result in the replacement of AF with low temperature transformation products. The results of other researchers are similar [24,25 in 2].

The C.E. does not describe completely the effects of alloying elements on the transformation products since the individual effects of the elements are not always similar in nature and the effects of important alloying elements such as Ti, Al and O are ignored in the C.E.. Still, it is often a starting point for the design of filler materials for low alloy steel welds.

2.3.4.3 Carbon

Carbon affects more than the hardenability of steels. It has two opposing effects on the toughness of weld metal. Higher carbon contents decrease the rate of ferrite grain growth since the carbon must be rejected from the ferrite grains by diffusion. This refines the ferrite which improves the inherent toughness. However, higher carbon contents favour the formation of grain boundary carbides which are preferential sites for cleavage crack initiation and this decreases the low temperature fracture resistance. Hence, an optimal level of C exists for the maximum toughness. This level depends upon other factors which also control the weld metal microstructure.

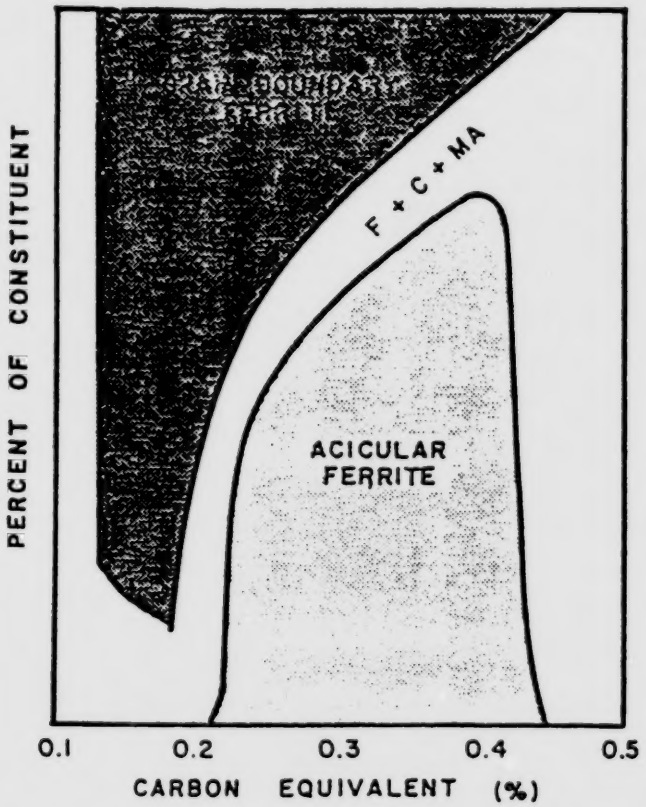

FIGURE 2.7 RELATIONSHIP BETWEEN CARBON EQUIVALENT AND THE PROPORTIONS OF MICROSTRUCTURAL COMPONENTS[23] in 2

Devillers et al[19] found the optimal level of C to be between 0.08 and 0.1 weight %. The relationship between the carbon content and various toughness measurements for their data is presented in Figure 2.8. Bonnet[3] found that the impact transition temperature decreased for increasing carbon levels above 0.06%, reaching an optimum level at 0.11%. Higher carbon levels than this were extremely detrimental to the impact properties. Evans [26 in 13] found also the optimal level to be in the 0.065 to 0.095% range, depending upon the Mn level. For all of these studies, it is not known if the oxygen levels were kept constant.

Low carbon levels (0.05 to 0.10%) are also required to reduce both the tendency for cold cracking due to hydrogen and for brittle crack initiation[13,22].

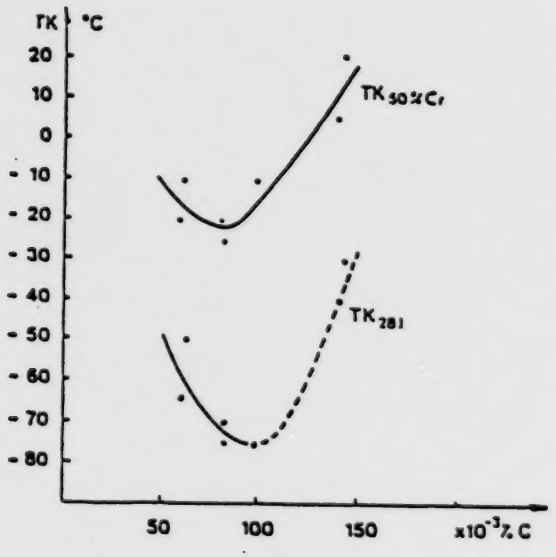

FIGURE 2.8 EFFECT OF CARBON CONCENTRATION ON IMPACT TRANSITION TEMPERATURES[19]

2.3.4.4. Manganese

Manganese effectively lowers the austenite to ferrite transformation temperature and hence promotes the formation of lower temperature transformation products such as acicular ferrite and bainite. It was found from a study of C-Mn welds that optimum toughness was achieved for Mn levels greater than 1%[13]. Bonnet[3] found decreasing impact transition temperatures for increasing Mn levels up to 1.1%. Evans[27 in 3] and Yoshimiri[28 in 3] found the optimum Mn levels to be 1.5 and 1.0% respectively. Other authors have found optimum Mn levels approaching 1.8%[13]. In general, for Mn levels above these values, the upper shelf energy decreases and the impact transition increases.

The evolution of the microstructure as a function of Mn level is illustrated in Figure 2.9. With increasing Mn levels above 0.5%, acicular ferrite begins to form and replaces initially the FS constituents and then the PF phase. Evans [26] in a review of the literature, noted that acicular ferrite becomes finer and replaces the PF with increasing Mn levels. Similar results were observed by other workers [13] except that a decrease in the FS in their steels was also observed.

2.3.4.5. Silicon

Contrary to Mn, Si is considered to be detrimental to the toughness even for small concentrations because it favours the formation of martensite-austentite islands as well as increases the yield strength[29,30 in 22]. However, in weld metal, Si seems to favour the formation of acicular ferrite for levels less than 0.5%. As will be seen in the following sections, Si is found mainly in the inclusions and plays an important role in the nucleation of acicular ferrite. Also, Si levels that are too low degrade the performance of the electrodes during the welding process.

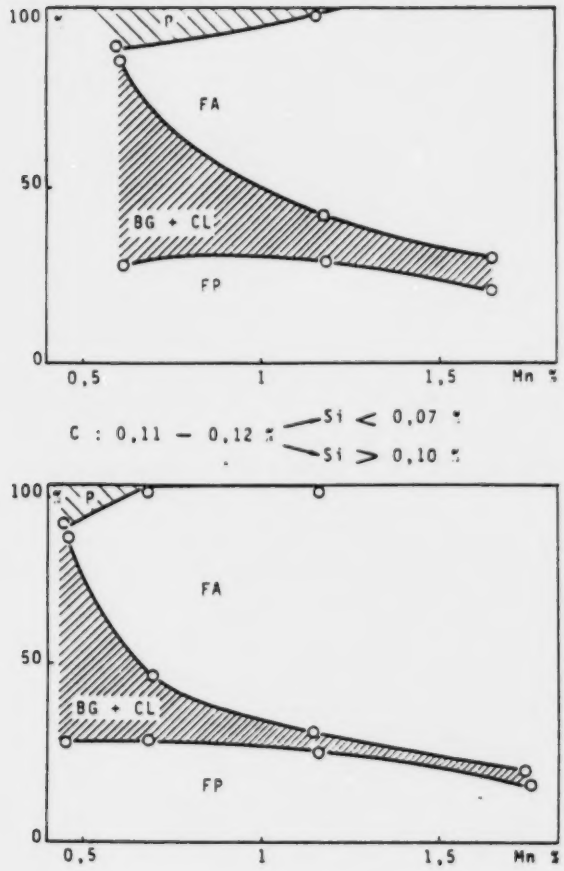

FIGURE 2.9 EFFECT OF MANGANESE CONCENTRATION ON MICROSTRUCTURAL DEVELOPMENT

Bonnet[3] showed that Si additions in 0.11%C-1.1%Mn welds decreased the impact transition temperatures when raised from 0.06 to 0.17%. Higher levels than this (0.30%) increased the transition temperature.

Many researchers have found that under certain welding conditions, moderate additions of Si can have a beneficial effect on weld metal microstructure[13]. Normally, Si additions of between 0.2 and 0.5% will give a greater

proportion of acicular ferrite. It appears that additions below these levels will result in either low oxygen levels and/or high Al concentrations. For Si over 0.5%, the reverse is true with respect to the oxygen and aluminium concentrations.

2.3.4.6 Titanium and Boron

It is now well established that small additions of Ti is very beneficial with respect to both the microstructure and toughness[13]. Bonnet and Charpentier[31] have shown that at least 0.004% of Ti is necessary for the nucleation of acicular ferrite in C-Mn submerged arc welds. Devillers et al[19,20] showed that 0.002% was sufficient to clearly improve the toughness. The optimum levels of Ti depends also on the welding parameters and the concentrations of the other alloying elements. Oxygen, Al, and Mo play a particularly important role in this regard[13]. Pacey, Kayali and Kerr [6] achieved the optimal quantities of acicular ferrite for Ti additions of between 0.02 and 0.04% (CO_2 shielded welds). For submerged arc welds, several authors in Reference 13 found that the optimum value of Ti was between 0.015 and 0.04%.

The beneficial role of Ti on the microstructure is linked mainly to the reduction in the free nitrogen levels in the welds(N reacts with Ti to form nitrides) and the preferred nucleation of acicular ferrite at inclusions containing Ti[2,13,19,20]. The deterioration of impact resistance for Ti levels over 0.04% is due to the lowering of the ferrite transformation temperature by the Ti in solid solution and the subsequent transformation to a lower toughness bainite[6]. Figure 2.10 presents the influence of Ti on the microstructure of the weld metal in C-Mn and C-Mn-Mo steels[6,31]. Nakano etal[32 in 13] studied the combined effects Al and Ti. They found that the optimum level of Ti

decreases for increasing Al levels, which by their chemical analysis was shown to be due to the high affinity of Al with oxygen and Ti with N.

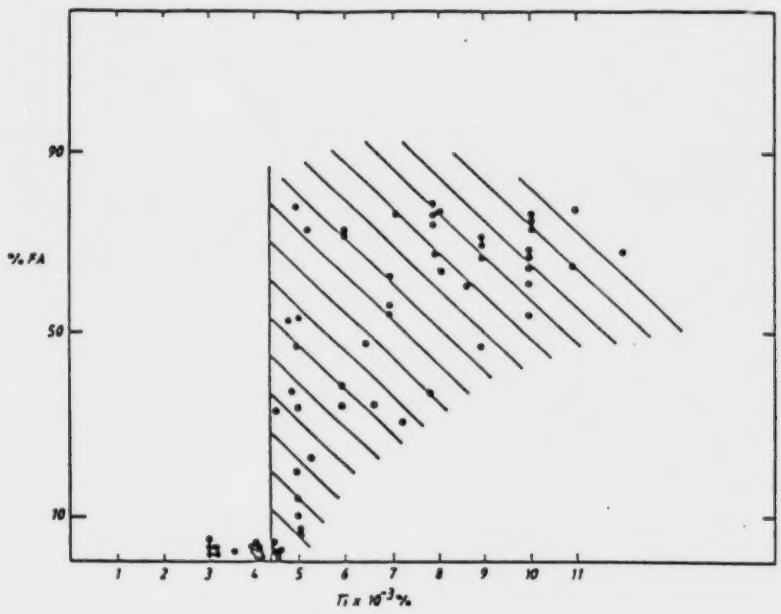

a) after Ref. 31

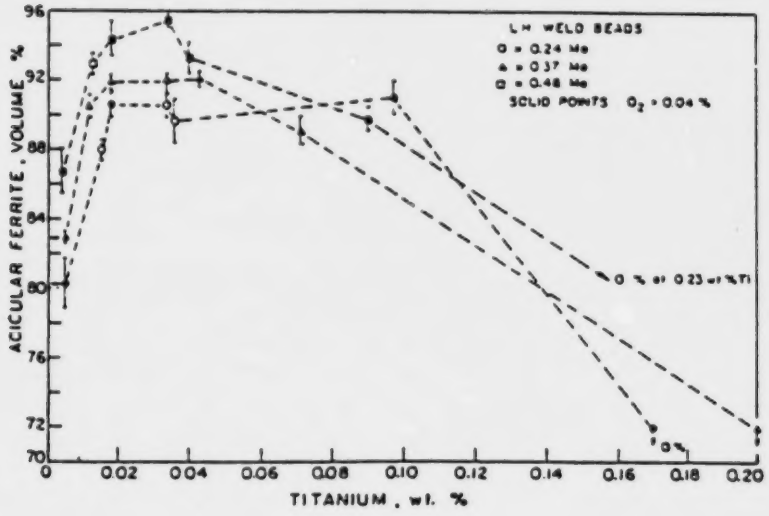

b) after Ref.6.

FIGURE 2.10 EFFECT OF TI LEVEL ON THE QUANTITY OF ACICULAR FERRITE

Boron, when in the presence of Ti, plays a very important role in the type of the transformation product. The optimum level of B is between 20 to 30 ppm or maybe even higher according to some researchers[in 13]. Boron diffuses rapidly to the austenite grain boundaries and delays or eliminates the nucleation of PF(G)[2-7,13,19-20,33]. Boron, to be effective, must be free and not combined with N. Ti and/or Al are important since they can tie up the N and thereby protect the boron. Mori et al[34,35 in 13], have suggested that Ti protects the boron from oxygen by forming TiO and that B then combines with N to reduce the free N levels. This reduced free N level will improve the impact resistance. Figure 2.11 illustrates the possible mechanisms by which Ti and B influences the microstructure according to References 34 and 35 in Reference 13

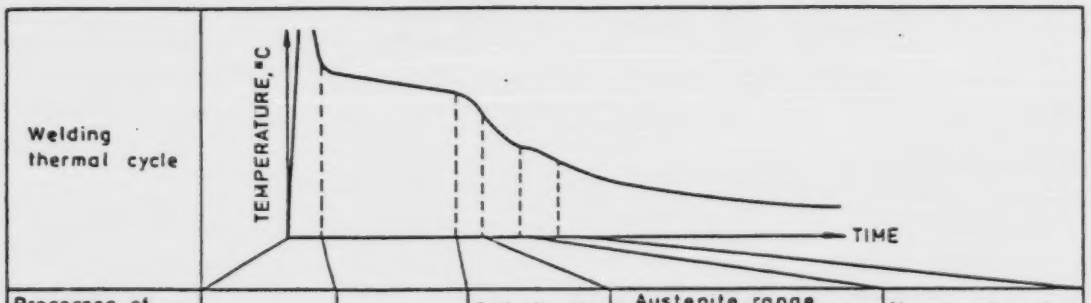

Processes of formation of weld metal	Arc column	Molten pool	Solidification range	Austenite range: High temperature range	Austenite range: Low temperature range	γ—α transformation range
Phases (Temperature range or cooling rate)	Liquid (2500—2300°C)	Liquid (1800—1600°C)	Liquid—δ.γ (1530—1450°C)	γ (10^2—10 Ks^{-1})	γ (~10 Ks^{-1})	γ + α (10 - 1, Ks^{-1})
Role of Ti	(TiO_2—Ti)		Protection of B from oxygen by forming TiO		Protection of B from N	Promotion of intragranular nucleation of acicular ferrite by TiO
Role of B	(B_2O_3—B)			Formation of BN in interdendritic region	Retardation of nucleation of proeutectoid ferrite at γ grain boundaries	Making inter-and intragranular transformation temperatures close together
Effect on notch toughness improvement	Additions of Ti/B by reducing oxides			Decreasing "free N"		Refining and homogenizing microstructure

FIGURE 2.11 MECHANISM BY WHICH TITANIUM AND BORON INFLUENCE WELD METAL TOUGHNESS AND MICROSTRUCTURE[34,35 in 13]

2.3.4.7. Oxygen

Due to its very low solubility in iron and its large affinity for reducing elements such as Al,Si,Mn,Ti etc., oxygen is the principal agent in the formation of inclusions in welds[2]. The volume fraction of inclusions and the inclusion density (i.e. number of inclusions per unit area on a polished surface) are related directly to concentrations of oxygen and sulphur in the weld metal. Figure 2.12 illustrates the relationships between the volume fraction of inclusions, the oxygen level and the combined O and S concentrations (Chuen[2]). An increase in oxygen and sulphur concentrations increase the volume fraction of inclusions. A similar trend holds for the inclusion densities. It should be noted that the inclusion density is related to the average inclusion size which in turn depends upon the level of the reducing elements, the flux, the welding conditions etc.... For this reason, it is possible to have, for the same oxygen and sulphur contents, different inclusion densities.

The oxygen level in the weld metal depends upon (i) the flux and its basicity, (ii) the welding parameters and (iii) the composition of the welding rod.

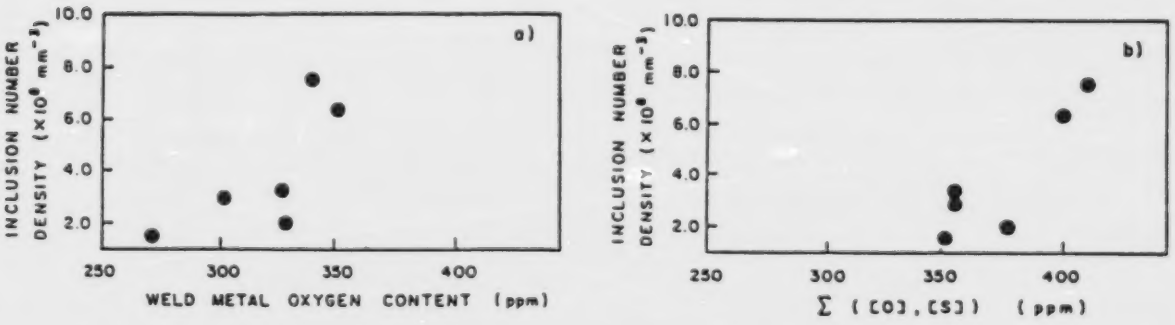

FIGURE 2.12 RELATIONS BETWEEN INCLUSION VOLUME FRACTION AND a) O CONTENT AND b) SUM OF O AND S CONTENTS[2]

Many researchers have found that the oxygen level affects the microstructure and toughness of weld metal[2,13,19,21]. They all found an optimum level of O that gives a maximum of acicular ferrite and a minimum in the impact transition temperature. Deviller etal[19,20] found that this optimum level was about 500 ppm(Figure 2-13) for submerged arc welding whereas others[2,14] have found the optimum concentration to be between 200 and 500 ppm. This value depends upon the amount of reducing elements and the concentration of S which determine both the final composition and the size distribution of the inclusions. Ti has an pronounced effect on the optimum O level. Increased Ti additions reduce the amount O necessary[13].

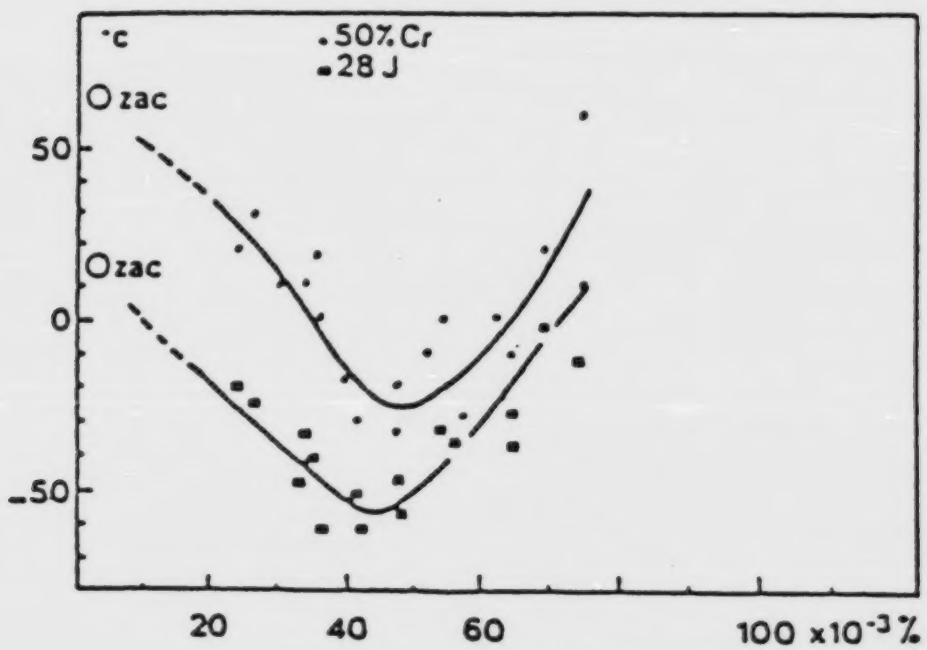

FIGURE 2.13 EFFECT OF O LEVEL ON TRANSITION TEMPERATURES OF WELD METAL[19]

Figure 2-14 presents the influence of the oxygen level on the continuous cooling transformation diagrams (CTT) for different levels of oxygen according to the work of Abson, Dolby and Hart [36 in ref. 2]. Three different types of transformation occurred, depending upon the O level, namely:

1- **Low O** Intragranular nucleation is almost nonexistent due to the small number of inclusions which also leads to large austenite grain sizes which in turn reduces the amount of PF(G) but increases the amount of FS(A) and bainite.

2- **Medium O** Sufficient sites for the intragranular nucleation of acicular ferrite exist and the number of intergranular inclusions is not too high; alloying an austenite grain size which is sufficiently large to prevent excessive quantities of PF(G) to form.

3- **High O** The high number and volume fraction of inclusions prevent austenite grain growth, increasing the number of austenite grain boundaries per unit volume which, in turn, increases the austenite to ferrite transformation temperature and increases the quantity of the higher temperature transformation products such as PF(G) and FS(A).

Barritte, Ricks and Howell[37] obtained similar results to those mentioned above with respect to the effects of oxygen level on the microstructural development. According to them, the small austenite grains due to high oxygen levels have the following effects. They:

1- increase the available sites for intergranular nucleation of ferrite

2- decrease the time available for AF grain growth since the amount of austenite to transform decreases

3- increase the PF(G) transformation temperature

4- result in a faster enrichment of the remaining austenite due to the suppression of the intragranular ferrite formation.

They suggest that the austenite grain size must be large but have a sufficient number of inclusions to nucleate acicular ferrite.

For submerged arc welding, the oxygen levels should be between 0.02 and 0.06%. Values outside this range will usually result in poor impact toughness. It is suggested that the oxygen level be kept as low as possible within this range as long as there is no deterioration in the microstructure[14].

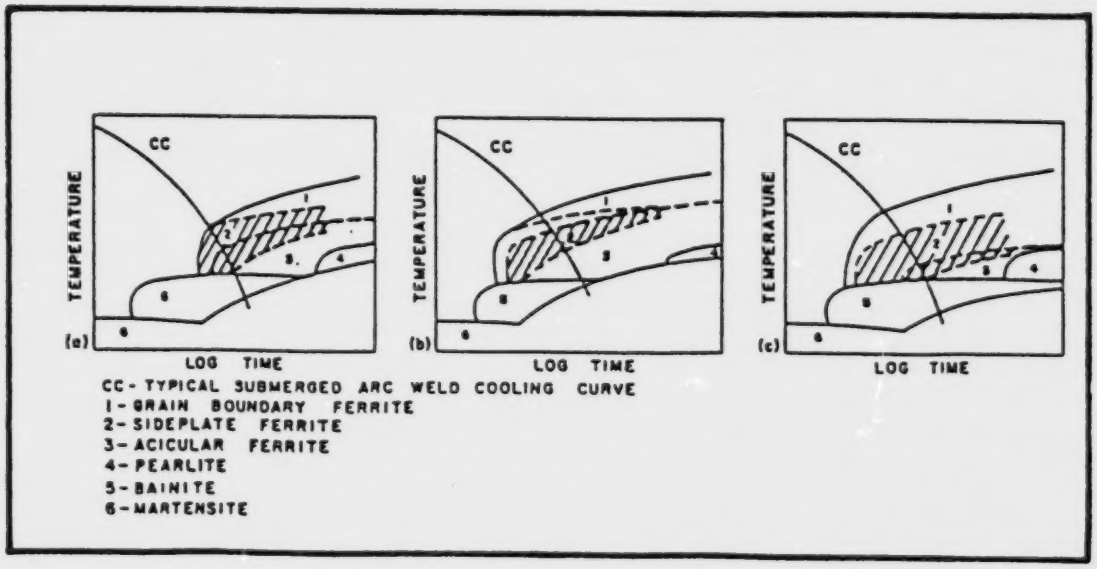

FIGURE 2.14 SCHEMATIC DIAGRAM OF THE EFFECT OF O CONTENT ON CONTINUOUS COOLING CURVES (a) LOW O (b) MEDIUM (c) HIGH[36 in 2

2.3.4.8 Aluminium

The influence of Al on the microstructure and the toughness is linked to the level of oxygen and Ti in the weld. As was mentioned in 2.2.4.6., an increase in Al decreases the optimum level of Ti necessary. Also, Al combines preferentially with oxygen as was shown by Terashima and Hart[38 in ref.12] who studied the effects of the $[\%Al]/[\%O]^2$ ratio on the average inclusion diameter and density. For values of this ratio equal to 28, they found the lowest impact transition temperature. Above this value, the average inclusion size increases rapidly which decreases the inclusion density and therefore the number of sites for acicular ferrite nucleation. This will be discussed in greater detail in a later section.

2.3.4.9 Sulphur

Like oxygen, sulphur is a major contributor to the formation of inclusions in weld metal. Most of the workers who have studied the effect of S on the toughness of welds have found that S decreases the upper shelf energy but does not have much effect on the transition temperature[13]. Some researchers have found that S does affect the transition temperature[13]. Evans attributed this deleterious effect of S on the transition temperature to a MnS rich layer on the surface of the inclusions which prevents the formation of acicular ferrite at the intragranular inclusions[39 in ref 13]. The effect of S on the microstructure will be presented in later sections.

In general, the levels of S in welds is kept as low as possible to ensure good impact resistance[13].

2.3.4.10. **Nitrogen**

Nitrogen has many effects in steels[40], namely:

1 - solid solution: causes distortion of the lattice which decreases toughness

2 - precipitation strengthening: forms carbonitrides or nitrides of Ti, Nb or V at temperatures between 400 and 700°C which generally reduce the toughness. This effect is not important in the melt zone due to relatively short time available during transformation for precipitation.

3 - segregation at defects: diffuses to defects such as dislocations which reduce their mobility (strain ageing).

With increasing N levels, the toughness of weld metal usually decreases. The addition of Ti,Nb,V or B can modify this trend.

Bonnet and Angeli[40] stated that when combined only with Ti, N had little effect on the amount of acicular ferrite present(50 to 150 ppm). When combined with Ti and B, however, N seems to have a negative effect, since it combines with B and reduces the amount of free B that can retard the formation of PF(G). Mori et al[34,35 in 13] postulated that the precipitation of boron nitride increases the toughness by reducing the free N level.

The small effect of N, when in presence with Ti, can possibly be explained by the decrease in aging of the steels[19] and by the precipitation of TiN which is favourable for the germination of acicular ferrite according to many authors[2,13,19,20].

2.3.4.11. Other Elements

Other elements can also affect the toughness of weld metal in C-Mn steels[3,6,7,13,22]. Mo, Cu and Ni have beneficial effects on the microstructural development and toughness of welds. Mo increases the temperature range during which acicular ferrite can form as well as decreases the γ -> α transformation temperature[6,22]. Cu and Ni affect the ferrite transformation in a way similar to Mn[22].

Nb and V have varying effects. When the γ->α transformation temperature is high, Nb and V cause a marked decrease in the toughness due to precipitation of carbides, nitrides or carbonitrides[22].

Phosphorus decreases the toughness through solid solution hardening which increases the transition temperature[13]. It does not appear to affect the average inclusion size.

Calcium when present in the flux, reacts strongly with S and oxygen thereby reducing the concentrations of these elements in the weld metal. The improved toughness due to Ca additions may be linked to the reduction in the quantity of inclusions (improved upper shelf) and the refining of the microstructure which can increase the resistance to cleavage fracture[13].

2.4. ROLE OF INCLUSIONS

2.4.1. General Effects

Due to the rapid solidification rates during welding, there is a higher density of inclusions (from 10^7 to 10^9 inclusions per mm^2) in weld metal than in conventional cast steel. The average inclusion diameter is smaller, being in the 0.1 to 3 μm range [2].

The higher density of inclusions can have a pronounced effect on the toughness of the weld metal, especially in the upper shelf region. The inclusions are stress concentrators which can accelerate microvoid growth and coalescence thereby reducing the energy necessary for ductile fracture. They can also affect the type and nature of the microstructure thereby modifying indirectly the resistance to cleavage fracture [17 in 13]. The results of fractographic studies have shown that large inclusions (> 1 μm) can initiate cleavage fracture directly[Ref 17 in 13]. Inclusions, therefore play an important role in the determination of both the toughness and microstructure of welds.

2.4.2. Influence of Inclusions Size and Distribution

2.4.2.1 Optimum Size and Distribution

To determine the optimum levels of inclusions, it is important to consider the effects of inclusions on (i) ferrite nucleation and (ii) austenite grain growth. The latter will modify the amount of intragranular nucleation of ferrite and the austenite to ferrite transformation temperature.

These two effects are linked to two different inclusion sizes. Zener [2] developed a relation between the volume fraction, f, and critical diameter of inclusions, d_{cr} to the austenite grain size, D_L.

$$d_{cr} = 3 f D_L / 2 \quad ...[2.1]$$

The critical diameter is that above which the inclusions cannot effectively block the austenite grain growth. During cooling, the austenite grains will grow until they are effectively stopped by the inclusions with a diameter inferior to d_{cr}. The resulting austenite grain size is directly proportional

to the average size and therefore inversely proportional to the density of inclusions for a given volume fraction. Higher volume fractions will naturally favour smaller austenite grain sizes but the effect may be reduced if the average size of the inclusions is larger.

To maximize the amount of acicular ferrite , it is important to have a sufficient number of intragranular sites for ferrite nucleation, a large austenite grain size to reduce the quantity of PF(G) and the inclusions must have a minimum size as is presented in detail in the next section. Based on this analysis, the optimum microstructure with respect to acicular ferrite formation will have a moderate volume fraction of large inclusions. However, this microstructure may not have the best toughness due to the effects of large inclusions on the fracture resistance. This underlines the difficulty in determining the optimum volume fraction and size distribution of inclusions for the best toughness in weld metal.

2.4.2.2 Influence of Size Distribution

Chuen [2] observed two types of inclusion size distributions, near-normal and log-normal. These are illustrated in Figure 2.15. The near-normal type distribution was associated with a high volume fraction of acicular ferrite and a large average inclusion size. This agrees with the results of Cochrane, Ward, and Keville [24 in 2] who found that the regions of high volume fraction of acicular ferrite did not have many fine inclusions.

Chuen related the austenite grain size to the density of intergranular inclusions and the percentage of acicular ferrite to the density of intragranular inclusions (Figures 2.16 and 2.17). From these results, Chuen made the three following conclusions:

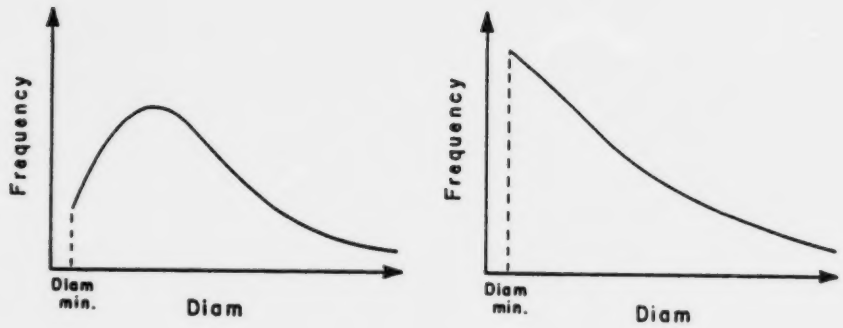

(a) NEAR NORMAL (b) LOG-NORMAL

FIGURE 2.15 TWO TYPES OF PARTICLE DISTRIBUTIONS OBSERVED BY CHUEN[2]

1 - A high density of **intragranular** inclusions (n_b) does not ensure a high percentage of acicular ferrite. If a high n_b is associated with a high number of **intergranular** inclusions, the austenite grain size will tend to be lower, favouring the formation of proeutectoid and side plate ferrite at higher transformation temperatures, leaving little untransformed austenite to form acicular ferrite.

2 - A sufficiently large austenite grain size, an optimum volume fraction and distribution (spacing) of intragranular inclusions is necessary for the formation of a fine acicular ferrite.

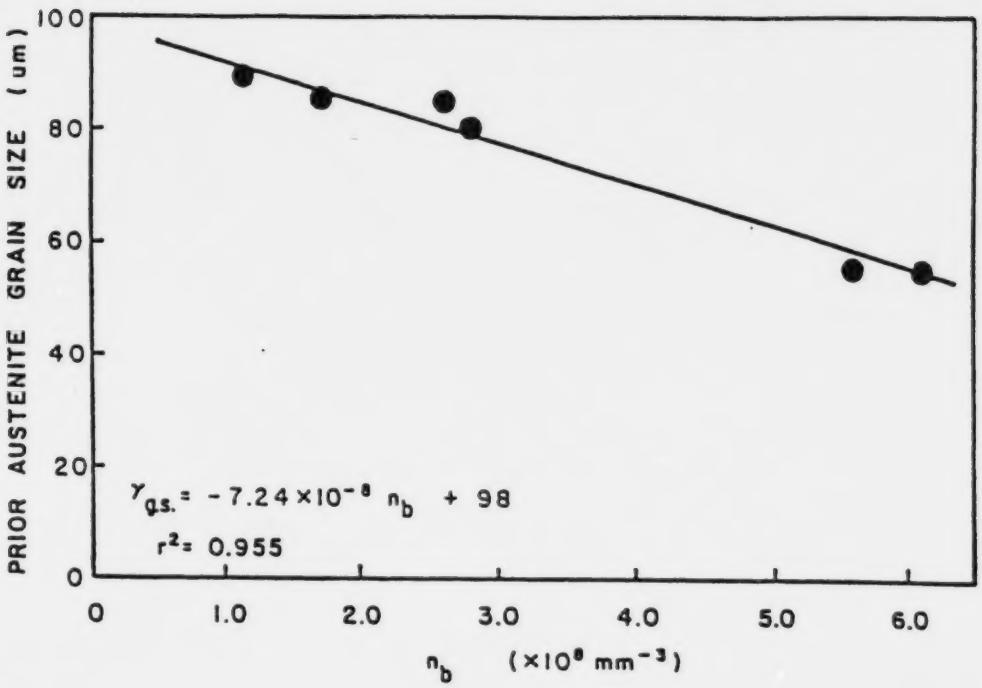

FIGURE 2.16 INFLUENCE OF INTERGRANUALAR INCLUSION DENSITY ON AUSTENITE GRAIN SIZE[2].

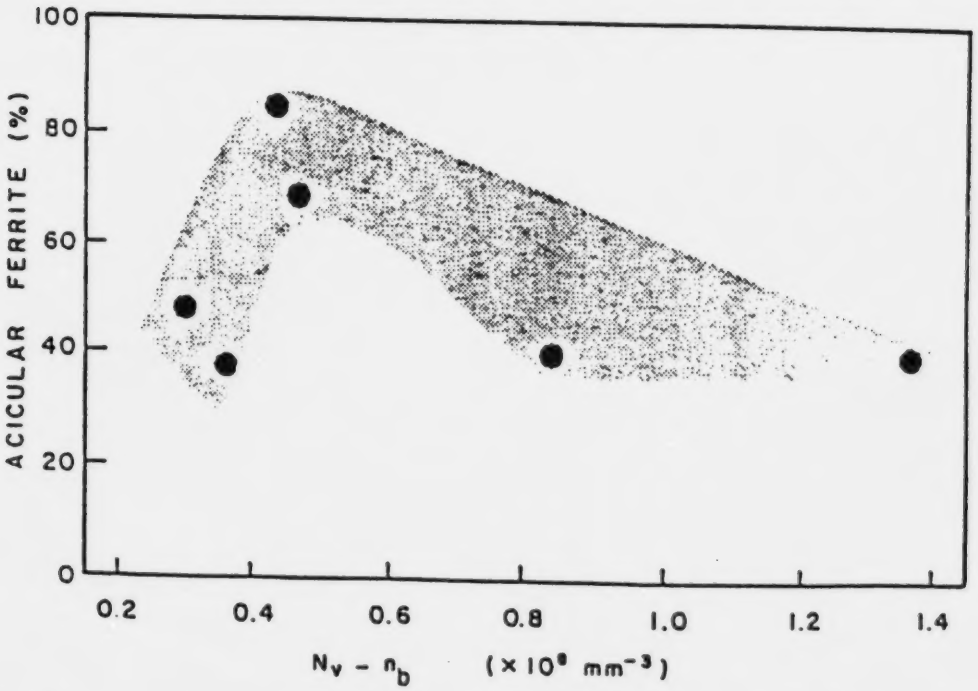

FIGURE 2.17 INFLUENCE OF INTRAGRANUALAR INCLUSION DENSITY ON QUANTITY OF ACICULAR FERRITE[2]

3 - A low density of both intergranular and intragranular inclusions gives large austenite grain sizes and an insufficient number of potential nucleation sites which leads to the formation of bainite instead of acicular ferrite.

If the volume fraction is sufficient, the near-normal distribution of inclusions is better able to give the right balance of inclusion sizes, since this distribution has a larger number of large inclusions and fewer number of small inclusions than the log-normal size distribution.

2.4.2.3. Effect of Oxygen Levels on Average Inclusion Size

Ferrante and Farrar[21] and Cochrane, Ward and Keville[24] according to Reference 2, have shown that the average inclusion diameter increases when the oxygen level increases whereas Chuen [2] found the opposite trend. This, however, may be due to the difference in minimum size of inclusion considered. Generally, only inclusions greater than 0.1 μm are considered but Chuen also measured inclusions down to 0.07 μm in diameter. To compare his results with the literature, Chuen used the data for inclusions greater than 0.1μm only and found trends similar to other researchers. This indicates that higher oxygen levels increases dramatically the number of fine inclusions (diameter less than 0.1 μm).

2.4.2.4. Effect of the Flux on the Inclusion Size

The size and composition of inclusions depends mainly on type of flux used. Fluxes rich in Si or that are acidic(i.e. rutile based) tend to give larger manganese silicates or manganese sulfides than do basic fluxes. This is explained by the decreased ability of the acidic fluxes to reduce the oxygen and sulphur levels and thereby giving larger inclusions due to the excess of

these elements. This would be expected since the total number of inclusions are about the same for basic and acid fluxes.

2.4.3. Influence of Chemical Composition of the Inclusions

2.4.3.1. General Trends

Even though an optimal size distribution of inclusions seems to be a prerequisite for the formation of a high volume fraction of acicular ferrite, other factors may also be necessary. The chemical composition also plays an important role in the intragranular nucleation of ferrite. A modification of the chemical composition of the inclusions due to changes in the composition of the flux and/or welding rod as well as the welding conditions will also result in a change in the size and distribution of inclusions[13,19,20,22].

Pargeter[41 in 2] showed that Mn and Si type inclusions are associated with PF(G) and FS(A) whereas inclusions with Al tend to form AF. Cochrane, Ward and Kerville[24] and Sagesse et al[42] according to Reference 2 showed that inclusions rich in Al or Al_2O_3 favour a high percentage of acicular ferrite. This is in conflict with Devillers et al [19,20] who showed that Al rich inclusions do not favour AF. They found that AF was favoured by the presence of manganese-aluminium-silicates that were not covered by a Cu-S rich layer. The absence of this layer was found to be associated with the presence of Ti.

The results of microanalysis of inclusions have shown the presence of Al, Mn, Si, Cu, S and Ti, the relative proportion of each depending upon the composition of the weld metal deposit[2,4,19,20,43,44,45].

2.4.3.2. Effect of Aluminium

Even in spite of the controversy concerning the role of Al rich inclusions on the nucleation of acicular ferrite, Al plays a very important role in the deoxidation of the weld metal and hence the ultimate chemical composition of the inclusions. According to many studies, Devillers [19,20] and Terashima et al [38 in 22] in particular, Al plays a beneficial role on the nucleation of intragranular ferrite as long as it is not in the form of Al rich inclusions.

Figure 2.18 illustrates the effects of the Al concentrations on the transition temperature from the work of Terashima and Hart[38in 22]. This clearly shows that both low and high levels of Al are detrimental to the toughness. The best transition temperatures in the study of Devillers et al [20] were for Al levels between 0.014 and 0.018 weight percent for Ti levels above 0.002% (Figure 2.19). This concurs well with Figure 2.18.

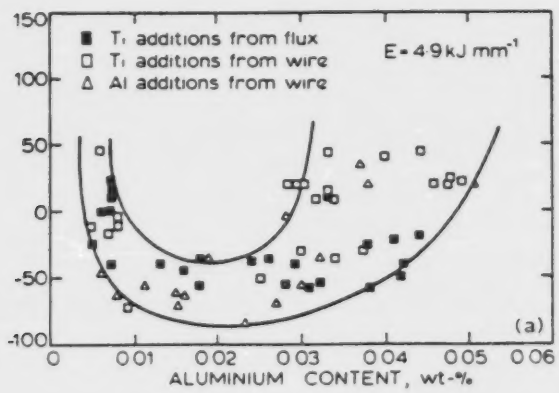

FIGURE 2.18 INFLUENCE OF AL CONTENT ON THE TRANSITION TEMPERATURE OF WELD METAL IN Si-Mn-Al-Ti[22]Data from Terashima and Hart[38]

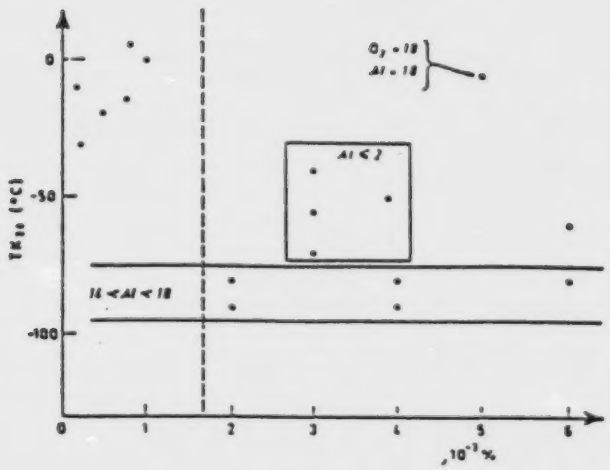

FIGURE 2.19 VARIATION OF THE TRANSITION TEMPERATURE AS A FUNCTION OF Ti AND Al LEVELS AFTER DEVILLERS et al [20]

Figure 2.20(a) shows the relationship between the transition temperature and the $[\%Al]/[\%O]^2$ ratio according to the data of Terashima and Hart[38 in 22]. The optimum condition is for a value of 28 which corresponds to the condition where there is a maximum of Al containing inclusions as is shown in Figure 2.20(b). These are manganese silico-aluminates. Below a ratio of 28, the Al content is too low to give a sufficient number of Al containing inclusions whereas above 28 the precipitation of Al_2O_3 leads to agglomeration of the inclusions which greatly increases the average inclusion size but also reduces the inclusion density[22].

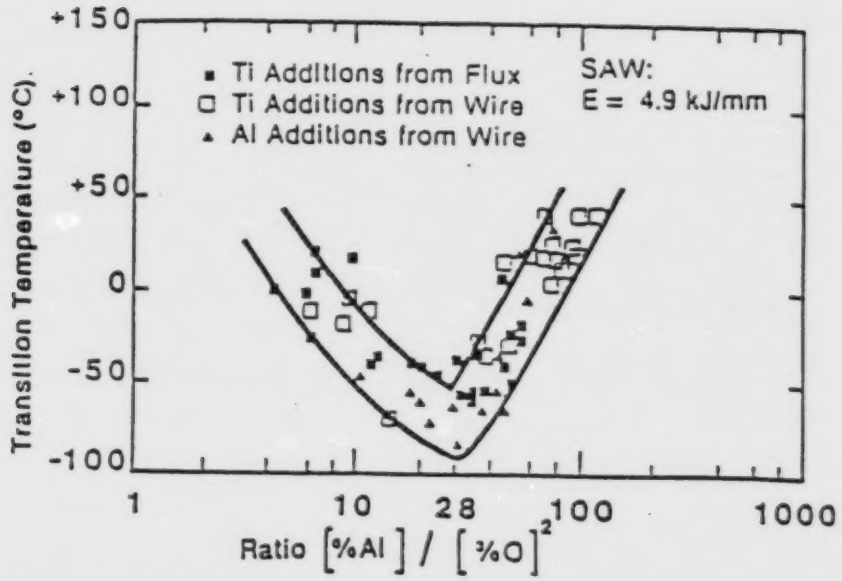

(a)

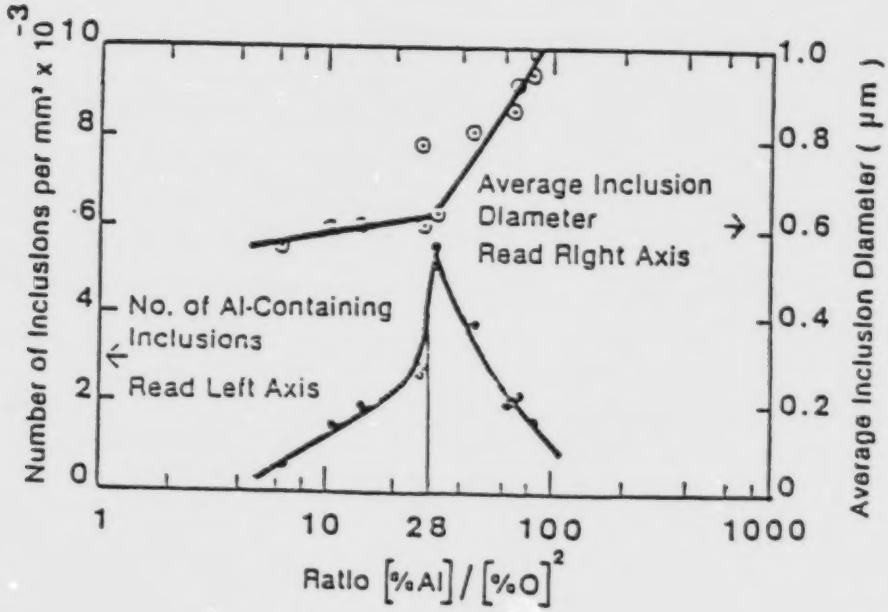

(b)

FIGURE 2.20 RELATION BETWEEN THE $[\%Al]/[\%O]^2$ RATIO AND (a) TRANSITION TEMPERATURE AND (b) AVERAGE INCLUSION DIAMETER AFTER THE DATA OF TERASKIMA AND HART[38 in 22]

Grong and Matlock[22] found that for the data of Devillers et al[19], the compositions with the best toughness had $[\%Al]/[\%O]^2$ ratios very close to the value of 28 suggested by Terashima and Hart[38] as can be seen in Figure 2.21. This suggests that there is an optimal amount of oxygen for a given level of Al that will give the precipitation of an optimal number of Al rich inclusions.

According to thermodynamic calculations by Devillers et al[19,20], for different levels of oxygen and Al, the inclusions should be mainly aluminium-manganese silicates for the optimal oxygen content. These thermodynamic studies agree well with the microanalysis of inclusions done by both Devillers et al[19] and Terashima and Hart[38]. The beneficial effect of this type of inclusion as compared with Al_2O_3 on the intragranular nucleation of ferrite appears to be linked to the differences in the thermal expansion coefficient as will be shown in section 2.5.2.

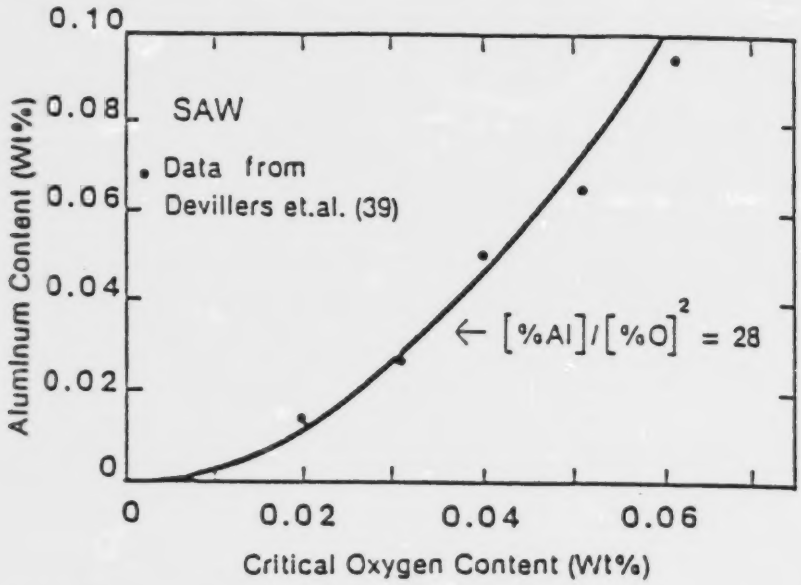

FIGURE 2.21 OPTIMUM O CONTENT (LOWEST TRANSITION TEMPERATURE) FOR A GIVEN Al CONTENT ACCORDING TO RESULTS OF DEVILLERS[19] AND TERASHIMA AND HART[38 in 22 p. 12].

2.4.3.3. Influence of Ti

The Ti has a powerful effect on the proportion of acicular ferrite as can be seen in Figures 2.10(a) and 2.19. Figure 2.22, which was taken from the work of Bonnet and Charpentier[31], shows the quantity of acicular ferrite as a function of the carbon equivalent for Ti levels above and below 0.0045%. This agrees with Figure 2.10(a) which shows that a minimum level of Ti is necessary for the formation of acicular ferrite[5].

The presence of Ti in inclusions, for Ti levels in the weld metal above 0.002%[19,20], is also associated with the disappearance of the Cu-S layer on the inclusions. Devillers[19,20] has shown that when this layer is present, the microstructures tend to have poor impact toughness.

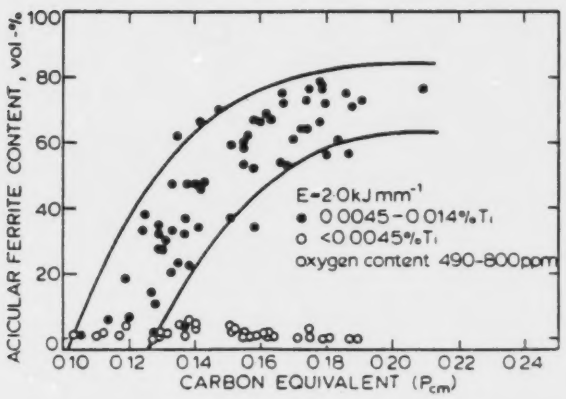

FIGURE 2.22 ROLE OF Ti ON ACICULAR FERRITE CONTENT FOR SMALL Al ADDITIONS AS A FUNCTION OF CARBON EQUIVALENT (ρ_{CM}). DATA OF BONNET et al [31]). REF.22.

Other researchers[19,20 in 2] have suggested that the beneficial effect of Ti is due to the formation of a titanium oxide or nitride which due to the coherence of its lattice with that of that of ferrite, favours the epitaxial growth of acicular ferrite. This has not yet been verified and will be discussed in greater detail in the following sections.

2.4.3.4 Microanalysis of Inclusions

The results of the microanalysis of inclusions in Mn-Si high-strength low-alloy steels shows that Al, Mn, Si, Ti, S and Cu are usually present but with widely varying proportions which depend upon the chemistry of the weld metal[2,4,13,19,20,43-45]. These results also show the heterogeneous nature of the inclusions, that is, they are usually made-up of many distinct phases. Figure 2.23 illustrates the heterogeneous nature of the inclusions and the corresponding X-ray analysis[44].

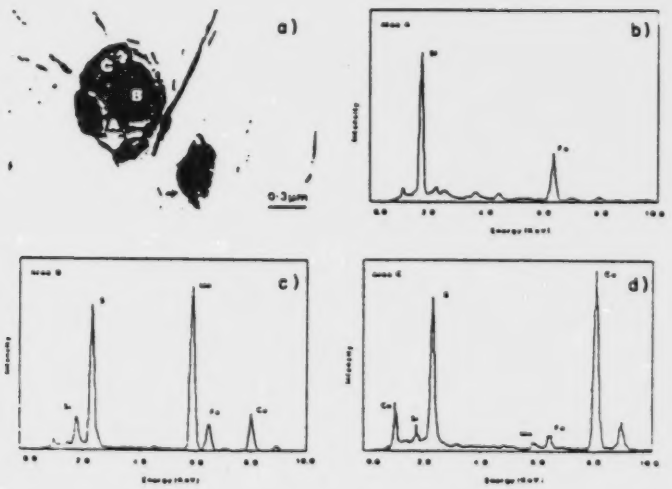

FIGURE 2.23 HETEROGENEOUS NATURE OF TWO INCLUSIONS ON CARBON REPLICAS (a) MICROGRAPH OF PARTICLE, (b),(c) AND (d) XRAY SPECTRA FROM VARIOUS REGIONS[44]

It is evident from this Figure that a phase rich in Cu and S exists as has been suggested by many researchers[4,19,20]. Kayali et al[43], Fisher et al[46 in 44]], and Court et al [44] have also observed manganese-copper sulfides which usually only partially surround the inclusions. It has been suggested that the copper sulfide layers form when the Cu levels exceed 0.05% in the weld metal and that oxides or silicates act as a nucleus for the precipitation of the copper sulfide layer[44].

Dowling, Corbett and Kerr[4] have also found phases rich in Cu-S, and Mn-S. The Cu-S phase was associated with the formation of a bainitic microstructure from which they concluded that the presence of this layer was detrimental to the formation of acicular ferrite. It should be noted that high Ti levels of about 0.2% existed in their weld metal. Kayali et al[43] found that under certain conditions, the layers of copper sulfides on the inclusions could act as sites for the nucleation of acicular ferrite.

These workers found other phases in the inclusions, namely:

1- Al rich

2- Ti rich

3- Al and Mn rich

Only the last two types were at least partially identified. The phase rich in Ti corresponds to either TiN, TiO or TiC (it was impossible to analyze the light elements). The Al-Mn rich phase corresponds to $MnAl_2O_4$[4]. It appears that the last compound was associated with the formation of acicular ferrite. The Ti rich phase was not necessary for the formation of acicular ferrite.

Figure 2.24 gives the influence of the Ti level of the weld metal on the composition of the inclusions. It should be noted that the highest percentage of acicular ferrite is for the two lowest Ti levels[43].

Chuen[2] found at least 12 different major types of inclusions during his microanalysis of inclusions on extraction replicas. A number of the inclusion types contained significant quantities of Fe which depends upon the quantity of reducing elements in the weld metal. The iron is the last element to react with O and hence high levels of iron in inclusions indicates that the deoxidation was insufficient in the liquid weld metal due to a lack of sufficient reducing elements. High Fe levels in inclusions favoured a coarser microstructure[2].

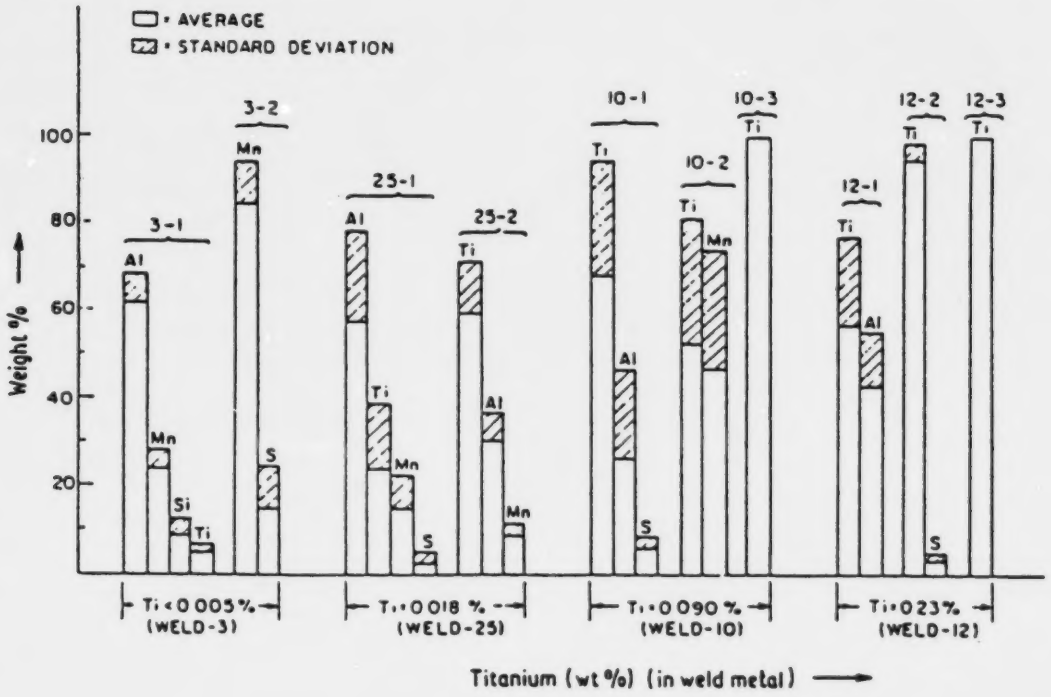

FIGURE 2.24 EFFECT OF Ti CONCENTRATIONS ON THE CHEMICAL COMPOSITION OF INCLUSIONS[43]

2.5 MECHANISMS FOR THE NUCLEATION OF ACICULAR FERRITE

2.5.1 Nucleation Thermodynamics

There have been many mechanisms suggested by which acicular ferrite can nucleate on intragranular inclusions. Thermodynamically, the heterogeneous nucleation of ferrite on the austenite grain boundaries or intragranular inclusions is always favoured over homogeneous nucleation as can be seen from Figure 2.25[47 in 2]. The austenite grain boundaries are the preferred sites for heterogeneous nucleation. However, for increasing inclusion radius, the barrier for nucleation at inclusions approaches that for the grain boundary. This analysis does not take into account the effects of stress concentrations caused by differences in the thermal expansion coefficients of the inclusions and austenite or possible epitaxal relationships between the inclusion surface and the ferrite which can decrease the nucleation barrier. These aspects will be discussed in the following sections.

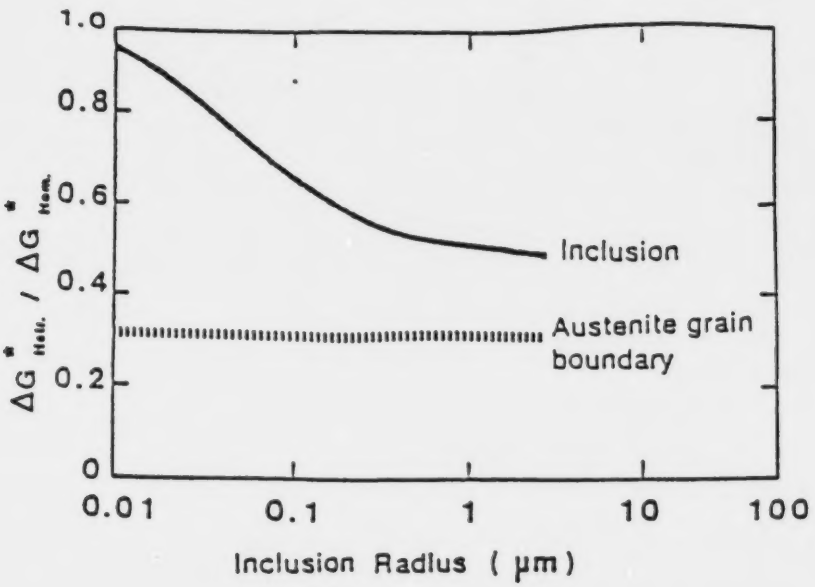

FIGURE 2.25 RATIO OF SURFACE ENERGY OF INCLUSIONS AND THE AUSTENITE GRAIN BOUNDARIES TO THE ENERGY OF HOMOGENEOUS NUCLEATION [47 in 2]

2.5.2 Epitaxial Relationships between Inclusions and Ferrite

Certain types of oxides can be semi-coherent with the ferrite matrix[19,20] which suggests that epitaxy may favour the nucleation of ferrite at the iron-inclusion interface.

Ito and Nakanishi[28], Kowkah et al [48] and Kanazawa et al[49] according to reference 2 have suggested that Ti can react with N to form TiN (a_o = 4.25) which favours ferrite nucleation but this could not be verified since N could not be detected with conventional energy dispersive X-ray spectrometers. Other results, however, do not show significant changes in the weld microstructures with increasing Ti levels (slight increase in the proportion of PF(G)). Some Japanese workers, according to reference 19, have proposed that TiO with a lattice parameter of 4.18 can favour expitaxial nucleation.

Dowling et al [4] have identified a F.C.C. phase in inclusions with a lattice parameter of 4.4 . They were not able to determine if this was TiO, TiN or TiC (a_o = 4.36) since the inclusion was too thick for analysis of the light elements by Electron Energy Loss Spectroscopy (EELS). They also identified a phase rich in Al and Mn as being $MnAl_2O_4$, a spinodal structure with a lattice parameter of 8.3 . They were unable to determine by diffraction the orientation relationships between the inclusions and the acicular ferrite. They noted, however, that certain planes of the inclusions were nearly parallel to that of the ferrite[4]. They also concluded that the Ti rich phase was not necessary for the nucleation of acicular ferrite since it was not found in a structure that was 100% acicular ferrite. This contradicts the results of other researchers who have made links between the formation of acicular ferrite with the crystallographic relationships of the ferrite and Ti rich phase. Devillers et al [19,20] have shown that a Ti rich phase is necessary for the

nucleation of acicular ferrite since it prevents the formation of a sulphur coating rich in Cu on the inclusions which tends to inhibit the formation of AF. This will be expanded upon in the following sections.

2.5.3. Strain Induced Nucleation

The large differences in the thermal expansion coefficients that exists between certain inclusion types and austenite can lead to large stress concentrations at the inclusion-austentite interface during cooling which induces localized plastic deformation of the austenite. The increase in dislocation density results in a reduced barrier to ferrite nucleation[2,19].

The thermal expansion coefficients for various inclusion types are shown in Figure 2.26. $(MnO)_2$, $(Al_2O_3)_2$ and $(SiO_2)_5$ have expansions coefficients about 10 times less than that of austenite and lower than those of other inclusion types. Devillers et al [19,20] have shown that the formation of acicular ferrite is favoured most by these inclusions. The presence, however, of a sulphur envelope rich in Cu on the surface of the inclusion has been shown to reduce the tendency for the formation of acicular ferrite. This has been ascribed to the higher thermal expansion coefficient of the Cu-S phase which is closer to that of the austenite[19,20].

Chuen [2] calculated the deformation associated with differences in thermal expansion coefficients between the inclusion and the matrix using a ball in an elastic hole model[50]. He assumed that the inclusion was a non-deformable sphere and all the strain energy was within the iron matrix. He found that the energy of differential contraction accounted for only 0.5% of the free energy of transformation. His conclusions were the following:

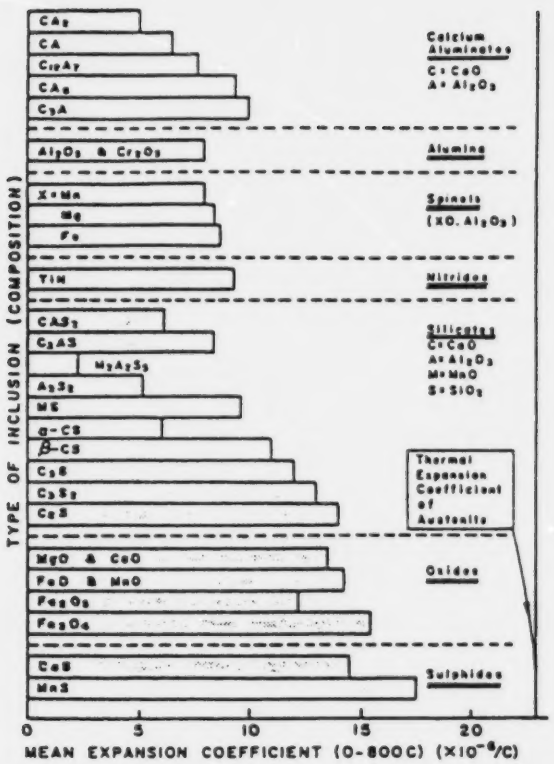

FIGURE 2.26 THERMAL COEFFICIENTS OF EXPANSION FOR VARIOUS PHASES (VALUE FOR AUSTENITE 23×10^{-6} / °C) [21]

(i) The ball in elastic hole is too simplistic to be considered in the case of phase transformations since this phase change will generate other forms of distortion energy far greater than those due to differential thermal contraction and that the elastic constants in the matrix are anisotropic.

(ii) The energy of thermal contraction is insignificant in the nucleation process.

Furthermore, this model does not take into account the possibility of plastic deformation in the austenite which generates dislocations near the inclusions which can favour acicular ferrite formation.

2.5.4. Nucleation on an Inert Substrate

According to Dowling, Corbett and Kerr [4] and other authors in Reference 2, inclusions can act as an inert substrate according to the classical theory of heterogeneous nucleation. The nucleation of acicular ferrite is favoured by a high surface energy of the inclusion-austenite interface which will lower the ferrite nucleation energy barrier. Also, according to Dowling et al[4] the heterogeneous nature of the surface of the inclusions (see section 2.4.2.4) can explain why a single inclusion can nucelate more than one ferrite grain as they observed for 70% of the inclusions they analysed.

2.5.5. Localized Variation in the Composition of the Matrix Near the Inclusions

The effects of microsegregation of elements near inclusions on the nucleation of ferrite (i.e. changes in the local hardenability, lattice distortion, and increase in defect concentration) was discussed by Devillers et al [19,20]. Efforts to reveal the presence of microsegregation by microanalysis were not successful. Also, reheating at 900 to 1200 ^{o}C for several hours to eliminate microsegregation had no effect on the subsequent formation of acicular ferrite for normal cooling conditions encountered during welding[19,20].

CHAPTER 3

EXPERIMENTAL TECHNIQUES

3.1 WELD METAL PREPARATION

3.1.1 Composition of the Weld Metal

3.1.1.1 Technique of Chemical Analysis

The composition of the weld metal was measured by spectrochemical analysis on a Jarrel Hash Atom Comp instrument. The concentrations of O and N were determined on a Leco TC-136 analyser.

3.1.1.2 Compositions of the Weld Metal Studied

In this report, two types of weld metal deposits have been studied: (i) standard test plate with small as-deposited weld metal zones and (ii) experimental welds with a very large and deep final pass. The reasons why these types of welds were studied will be discussed in the next Section. Tables 3.1 and 3.2 presents the chemical composition of the weld metal deposits along with the specimen codification for the standard industrial and experimental welds.

3.1.2. Electrode Fabrication

The welding electrodes were produced by extrusion, then baked at 450°C. The basic formula of the electrodes remained constant except for variations in specific alloying elements and impurities.

TABLE 3.1

CHEMICAL COMPOSITION OF STANDARD TEST PLATE WELDS WITH SMALL AS-DEPOSITED ZONES

Sample name	C	Mn	Si	Ti	Al	Ca	Cu	Cr	Ni	Mo	P	S	(1) O	(2) N
TiL	0.05	1.46	0.37	0.002	<0.02	---	0.04	0.03	0.03	<0.01	0.010	0.010	414	81
TiM	0.05	1.68	0.52	0.007	<0.02	---	0.03	0.03	0.04	0.01	0.012	0.010	293	102
TiH	0.05	1.47	0.52	0.034	<0.02	---	0.02	0.04	0.03	0.02	0.009	0.012	(2)	(2)
SM	0.05	1.46	0.48	0.007	<0.02	---	0.03	0.03	0.03	<0.01	0.012	0.014	382	62
SH	0.04	1.71	0.45	0.007	<0.02	---	0.03	---	0.03	0.01	0.008	0.037	437	88
TiCa	0.06	1.54	0.48	0.010	<0.02	---	0.02	0.03	0.02	<0.01	0.008	0.010	292	141
TiAl	0.05	1.71	0.70	0.017	0.03	---	0.03	0.03	0.02	<0.01	0.009	0.011	421	77

1 Oxygen and nitrogen concentration given in ppm

2 Oxygen and nitrogen concentration not obtained for TiH

TABLE 3.2

CHEMICAL COMPOSITION OF EXPERIMENTAL TEST PLATE WELDS WITH LARGE AS-DEPOSITED ZONE

Sample name	C	Mn	Si	Ti	Al	Ca	Cu	Cr	Ni	Mo	P	S	O*	N*
TiL	0.05	1.31	0.23	0.002	<0.02	---	0.04	0.04	0.04	<0.01	0.011	0.011	405	196
TiM	0.05	1.36	0.28	0.005	<0.02	0.001	0.03	0.03	0.04	0.015	0.013	0.011	384	209
TiH	0.05	1.34	0.34	0.02	<0.02	---	0.03	0.04	0.04	0.03	0.008	0.011	231	267
SM	0.05	1.38	0.36	0.005	<0.02	0.002	0.03	0.03	0.04	<0.01	0.014	0.013	337	122
SH	0.05	1.47	0.26	0.005	<0.02	0.001	0.03	0.03	0.03	<0.01	0.010	0.036	385	279
TiCa	0.07	1.36	0.33	0.008	<0.02	0.002	0.02	0.04	0.02	<0.01	0.009	0.010	271	191
TiAl	0.05	1.47	0.47	0.011	0.02	0.001	0.02	0.03	0.03	<0.01	0.011	0.012	416	212

* Oxygen and nitrogen concentrations given in ppm

3.1.3 Welding Techniques

During this study, all welds were done with SMAW process. Two kinds of welding test plates were used. The first consisted of a standard CSA W48 plate which was welded with several low energy passes and a heat input energy of ≈15 kJ/cm. From each plate, 15 Charpy specimens were cut. Figure 3.1 shows the test assembly as well as the orientation and dimensions of the standard Charpy specimens.

The second kind of test plate was designed in order to have the maximum as-deposited weld metal thickness. The standard Charpy specimens machined from these test plates were composed almost completely of metal from the last pass. This was achieved by a modified welding procedure. The technique consisted of first filling a standard CSA W48 type test plate with several passes of a filler material identical in composition to that of the final pass weld metal. A groove was machined in the filler material in order to accept the final pass (See Figure 3-2(a)). The last pass was done with a high heat input (>100kJ/cm) in order to have a weld metal deposit thickness of between 6 and 8 mm. However, due to the limited length of the electrodes, only about 25 mm of weld could be produced per electrode. Thus, over the 400 mm length of the test piece, there were a series of as-deposited weld metal regions separated by thin regions of reheated metal(See Figure 3-2(b)). In order to have the reheated regions as perpendicular to the surface of the weld material as possible, the test plate was inclined slightly. The welding parameters and the thermal cycle for the two types of test pieces are presented in Table 3.3.

DETAILS OF TEST ASSEMBLY

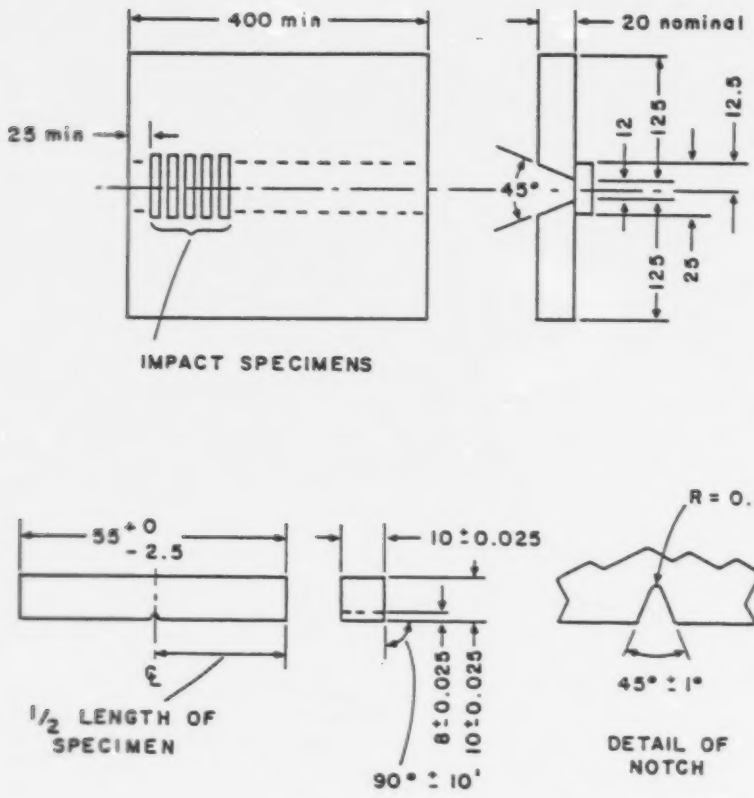

FIGURE 3.1 DETAILS OF WELD TEST ASSEMBLY AND STANDARD CHARPY SPECIMENS

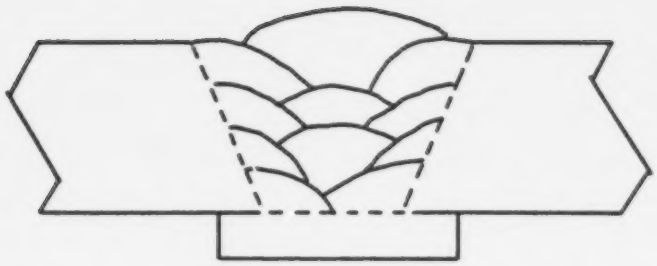

TRANSVERSE SECTION

(First deposit)

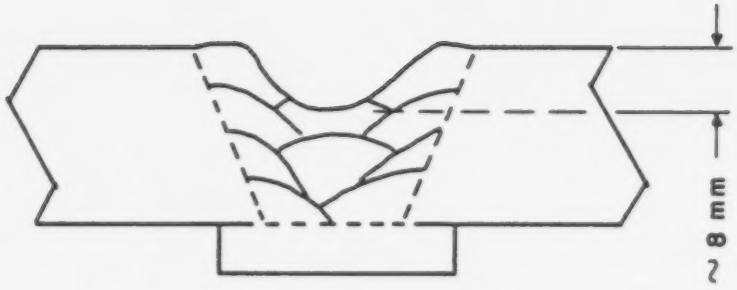

TRANSVERSE SECTION

(Machined)

FIGURE 3.2 DETAILS OF THE PREPARATION OF THE MODIFIED TEST PLATE

TABLE 3.3

WELDING PARAMETERS AND THERMAL CYCLE FOR WELD SPECIMENS

	FILLER PASS AND LAST PASS FOR STANDARD WELDS	LAST PASS FOR EXPERIMENTAL WELDS
AMPERAGE, A*	175	225
VOLTAGE, V	24-26	24-26
HEAT INPUT, kJ/cm	15	>100
COOLING TIME, seconds		
800 TO 500 °C**	≈10	25-30
INTERPASS TEMPERATURE, °C	150±15	---

* Current source Miller 300S, electrode diameter 4 mm.

** Temperatures of weld zone were measured with a WRe 5% -WRe 26% thermocouple dipped into the liquid metal immediately after extinction of the arc.

Two types of Charpy specimens were used to evaluated the toughness of the as-deposited weld metal in the second test plate. About 6 to 7 standard Charpy specimens (See Figure 3.1) as well as 6 to 7 5x5 mm sub-size (See Figure 3.3) Charpy specimens were machined from the 400 mm total length of the weld. The specimens were oriented as is shown in Figure 3.4.

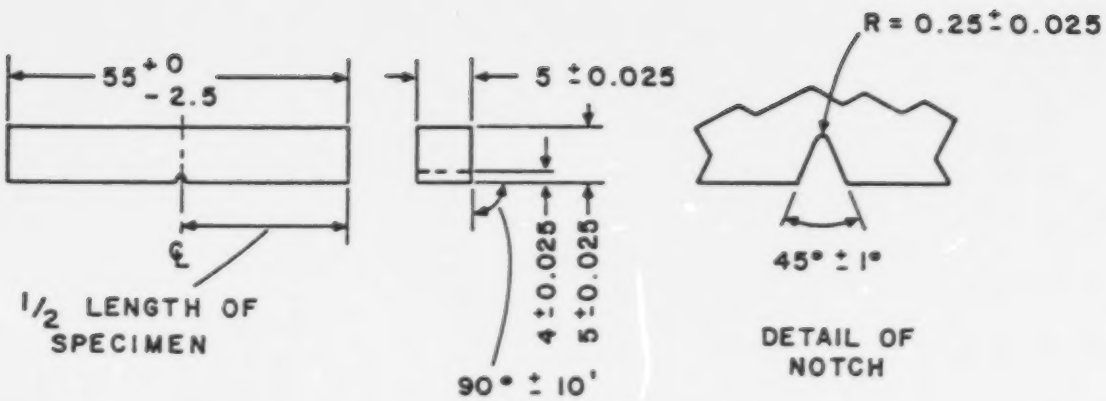

FIGURE 3.3 DETAILS OF SUB-SIZED CHARPY SPECIMEN (5x5 mm)

Sub-size Specimen

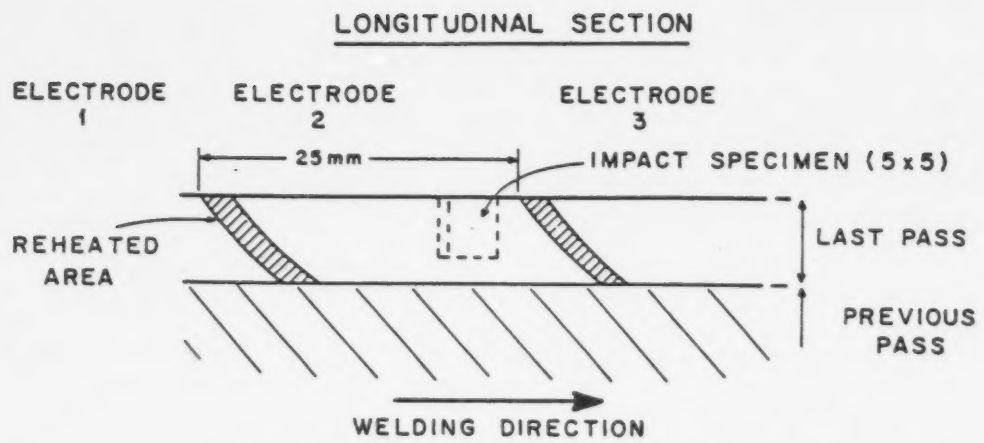

Full Size Specimen

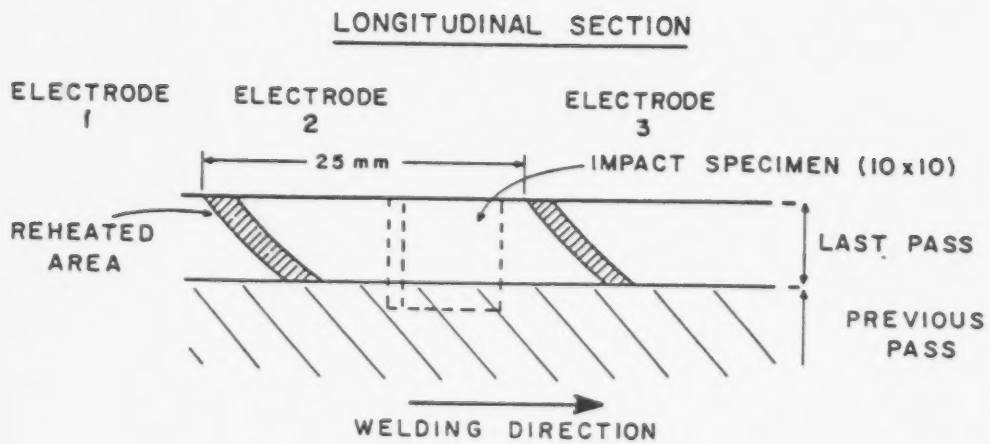

FIGURE 3.4 LOCATION OF CHARPY SPECIMENS IN THE MODIFIED WELD TEST PLATE

The V-notch was oriented in the welding direction. Previous results showed an important reduction of impact values if the V-notch was oriented perpendicular to the welding direction since the crack propagated easily in the proeutectoid ferrite decorating the prior-austenite grain boundaries.

These welding conditions were used for all weld metal chemistries. The vertical-up technique could not be used because it did not give the required last pass thickness.

To eliminate the effect of variability of chemical composition, the microstructural and inclusion analysis were done on exactly the same areas from which the spectrochemical analysis were taken which allowed the direct correlation of chemical composition to the microstructure and inclusion composition.

3.2 TOUGHNESS EVALUATION OF WELD METAL DEPOSITS

3.2.1 Experimental Procedure

Charpy V-notch instrumented impact tests were used to evaluate from the load-time traces, the general yield and maximum loads as well as the controlling fracture modes.

All impact tests were performed on a Tinuis Olsen model 74 impact tester. The load exerted by the tup on the specimen was measured using strain gauges attached to the special tup that was supplied by Dynatup. The load signal was first amplified by a Dynatup model 500 instrumented impact system and then was subsequently recorded on a Nicolet Model Explorer III digital oscilloscope equipped with floppy disk mass storage.

The Charpy testing was done according to the ASTM E23 standard. Prior to impact testing, the specimens were cooled for at least 15 minutes in an agitated methanol bath which was maintained within 0.3 degrees C of the desired test temperature by the addition of liquid nitrogen. The specimen was removed from the bath with thongs designed for the purpose and fractured within 5 seconds.

3.2.2 Types of As-Deposited Weld Metal Studied

Two types of welds were studied: (i) standard multi-pass welds with a small as-deposited weld metal zone and (ii) experimental welds with a very large and deep final pass from which Charpy specimens could be machined to give specimens that were almost completely as-deposited weld metal. The Charpy tests from the standard tests were used to evaluate the overall toughness of the as-deposited, heat-affected and remelted weld metal zones whereas the specimens from the experimental welds, hitherto referred to as large pass, were used to characterize the effect of as-deposited weld metal microstructure on the impact behaviour.

Two types of Charpy specimens were used to characterize the toughness in the large pass welds.

1- 5x5x55 mm sub-size V-notch specimens

2- 10x10x55 mm standard V-notch specimens

Only the second type was used for the standard welds. All Charpy specimens were machined with the longitudinal axis perpendicular to the direction of welding with the notch in the through-thickness direction as is indicated in Figure 3.1.

Since in the large pass welds, the maximum depth of as-deposited weld metal is 8 mm, it is necessary to use the 5x5 specimens in order to be able to compare the effects the various weld metal compositions and microstructures on the weld toughness uniquely. These results, however, cannot be compared directly with data from the literature taken from standard Charpy specimens due to differences in specimen size. For this reason, standard size Charpy tests were also performed. Even though the fracture region consisted of 80% as-deposited weld-metal in the standard specimens, these data are representative of the large pass toughness since the zone of maximum stress concentration in the center of the V-notch is well within the as-deposited weld metal.

To decrease the effects of inertial peaks and vibrations on the load-time traces for the 10x10 specimens, the maximum impact velocity for this machine was not used. The maximum impact velocity was used, however, in the 5x5 specimens in order to give a deformation rate at the notch root similar to that of the standard Charpy specimen.

3.2.3 Data Reduction

A typical load-time trace for ductile-brittle fracture of an instrumented Charpy test is presented in Figure 3.5. Many stages of deformation are present, namely, (A) crack initiation, (B) ductile crack propagation, (C) brittle crack propagation and (D) shear lip propagation.

The load-time traces were transferred to a computer and the various stages were delineated manually. The energy for each of the regions was determined by numerical integration of the load-time curve. Since, the initial velocity of the tup and the mass of the hammer is known, by conservation of energy the instantaneous velocity, v_i of the tup can be calculated for any time

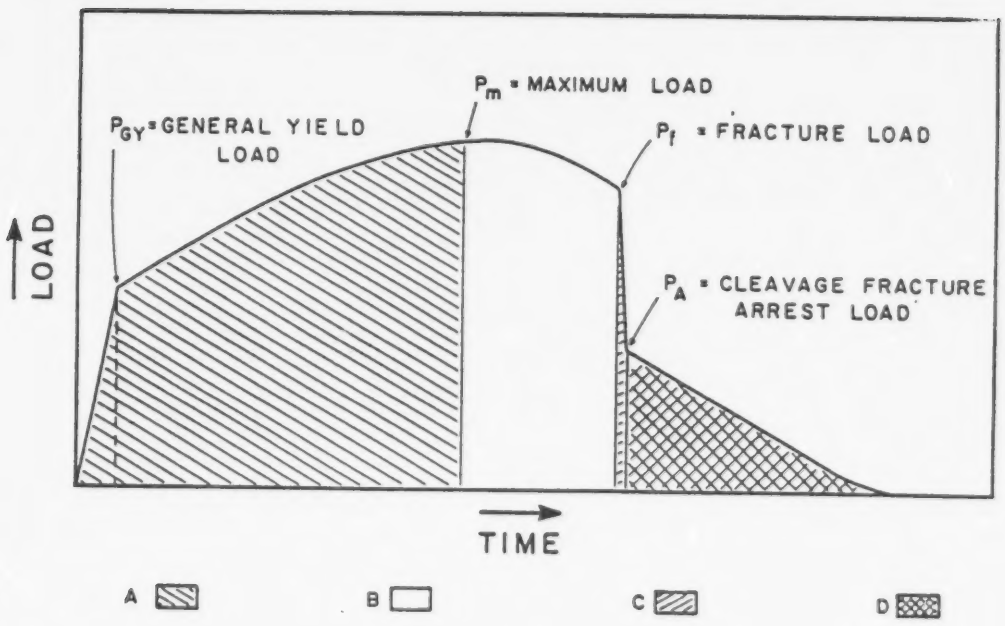

FIGURE 3.5 TYPICAL LOAD-TIME TRACE AND ASSOCIATED ENERGIES FOR AN IMPACT TEST (a) crack initiation, (b) ductile crack propagation, (c) brittle crack propagation, (d) shear lip propagation.

t during the test since the energy lost by the tup is equal to the energy required to fracture the Charpy specimen. The total absorbed energy, E_t at any time t is given in a general form by equation 3.1 where v_i is the instantaneous velocity. This energy was divided amongst the various stages of crack initiation and propagation.

$$E_t = \int_0^t F v_i \delta t \quad \ldots\ldots\ldots [3.1]$$

E_t = total energy at time t
F = instantaneous load
v_i = instantaneous velocity of the tup

The load-deflection curves were also calculated based on the relationships in equation 3.1. The load at the beginning of gross plastic deformation or general yielding can be used to estimate the dynamic yield stress of the material[51]. For the standard Charpy specimen:

$$\sigma_{YD} = 0.052 \times P_{GY}, \text{ MPa}$$

σ_{YD} = general yield strength

P_{GY} = general yield load, N

3.2.4 Fractography

The fracture surfaces of selected Charpy specimens were observed in a JEOL 840 or a JEOL T20 scanning electron microscope operating at 12 to 25 kV. Selected Charpy specimens were sectioned at an oblique angle along the centerline of the Charpy fracture surface perpendicular to the notch root. The

fracture surface had been previously coated with Microstop lacquer for both mechanical and chemical protection. The specimens were then mounted in lucite so that the surface of the specimen exposed by the sectioning procedure could be polished. The specimen was then polished and etched by standard metallographic procedures. By this oblique sectioning technique, the relationship between the tracture morphology and microstructure could be more easily determined.

3.3 MICROSCOPIC EXAMINATION

3.3.1 Regions Examined

All analyses of the microstructure and inclusion distributions in the as-deposited metal in the large pass welds were done on polished surfaces. These surfaces were perpendicular to the welding direction and the weld surface and were located at a distance of 4 mm from the weld surface. Since similar regions are examined for each of the weld metal compositions, it possible to determine the effects of composition on the microstructure and inclusion makeup.

3.3.2 Metallographic Examination

The area fraction of the various microstructural constituents were determined by point count methods on photographs obtained by scanning electron microscopy (Magnification 420X) on samples which had been polished and etched with 3% Nital. Inverse images were used to give photographs which resemble those that can be obtained by optical microscopy but with a much higher resolution. It was much easier to distinguish grain boundaries and other constituents by this technique. The classification of the various constituents was done according to a recent classification scheme by Abson and Dolby[10]. The

terminology used throughout this report is presented in Table 3.4.

Since the austenite grains in the region of metallographic examination are elongated, the austenite grain size was measured by dividing the length of the austenite grain boundaries (L_γ) by the total surface area analyzed (A_A). The ratio L_γ/A_A gives a better bases for comparison of the welds with differing sizes and morphologies of austenite grains. The prior-austenite grain boundaries are usually easy to detect since they are decorated with PF(G).

3.3.3 Quantitative Inclusion Analysis

The inclusion size, shape and approximate chemical composition of the inclusions was determined on specimens polished using a 1 μm diamond compound. Observations and measurements were done using the JEOL 840 scanning electron microscope equipped with the Tracor-Northern TN-2000 energy dispersive X-ray spectrometer. The classification of the inclusions was done using a modified form of the Particle Recognition and Classification programme (PRC) supplied by Tracor-Northern.

TABLE 3.4

Weld Metal Microstructural Classification

LABEL	CONSTITUENT MAKE-UP
PF(G)	ferrite veins or polygonal grains formed on the austenite grain boundaries
PF(I)	polygonal ferrite grains formed within prior austenite grains
AF	small nonaligned ferrite grains formed within prior austenite grain boundaries: - usually has a high aspect ratio
FS(NA)	ferrite with a non aligned second phase
FS(A)	ferrite with an aligned second phase
FC	ferrite carbide aggregates with either carbides or pearlite
M	martensitic colonies that are larger than the microconstituent phases

The inclusions can be differentiated from the matrix by variations in the backscattered electron signal level. Since the inclusions are lighter than the matrix, the inverse signal was used so that the inclusions will have a higher video signal level than the matrix. For the PRC programme, a window of analysis was selected so that the lower threshold was just above the level of the matrix. This adjustment was critical since the small inclusions could be lost due to the small difference in contrast between them and the matrix. The upper threshold was left at its default value.

The PRC programme sweeps the electron beam across the specimen until the resultant video signal level exceeds the lower threshold. The center of the particle is then located. The size, area and shape factor of the inclusion is measured by tracing a series of eight diameters through the center of the particle. At this point, a X-ray spectrum is obtained from the center of the inclusion and the intensities of selected peaks are recorded along with the size information of the particle. The particles are then classed according to chemical classifications that had been previously determined by a preliminary analysis. This process is repeated for the entire field of view. Multiple fields can also be measured during the analysis of a specimen.

For all samples, constant experimental conditions were maintained (see Table 3.5) in order to be able to compare the results from one sample to another since the relative peak heights of the various elements can change with operating conditions. The inclusion characterization included measurements of (i) average diameter, (ii) shape factor, (iii) size distribution, (iv) volume fraction, (v)number of inclusions per unit area and (vi) the relative concentrations of elements.

In order to have good statistics and an accurate evaluation of the size distribution, a minimum of about 400 particles was measured for each specimen to ensure that the area fraction of the largest inclusion was less than 1% of the total area of all inclusions.

TABLE 3.5

Experimental Conditions

Voltage (KeV)	15
Magnification	8000X
Beam Current (A)	0.7×10^{-9}
Working Distance (mm)	15
Dead Time %	25
X-ray Analysis time (sec)	15

CHAPTER FOUR

EXPERIMENTAL RESULTS

4.1 MICROSTRUCTURAL ANALYSIS OF LARGE FINAL PASS AS-DEPOSITED WELDS

4.1.1 Quantitative Microstructural Analysis

Table 4.1 presents the results of a quantitative microstructural analysis of the high heat input as-deposited weld metal of the 7 experimental compositions. These can be subdivided in three distinct series, namely:

1- Varying Ti concentrations

Low Ti (TiL) Medium Ti (TiM) High Ti (TiH)

2- Varying S concentrations

Low S (TiM) Medium S (SM) High S (SH)

3- Additions of Strong Deoxidizing Agents

No Additions (TiM) Ca additions (Ti-Ca) Al additions (Ti-Al)

It should be noted that TiM is part of both the Ti and S series.

4.1.2 Effect of Ti on Microstructure

An increase in the Ti concentrations from 0.002% (TiL) to 0.005 % (TiM) increases dramatically the proportion of acicular ferrite which increases from 8.4 to 48.1 %. Figures 4.1 and 4.2 presents typical optical microstructures for these welds. TiL is composed mainly of ferrite with a second phase (FS(NA) and FS(A)) whereas TiM in addition to the increase in AF, has much thicker PF(G) veins along the prior austenite grain boundaries. The increase in the proportion of these two constituents is at the expense of FS(NA) + FS(A) which decreases from 76.6 % for TiL to 19.2% for TiM.

TABLE 4.1

RESULTS OF QUANTITATIVE MICROSTRUCTURAL ANALYSIS

Weld deposit	Austenite Grain size S/L (mm)	CONSTITUENTS (%)				
		PF(G)	PF(I)	AF	FS(NA)	FS(A)
TiL Ti=0.002%	---	5.1	9.5	8.4	42.0	35.0
TiM Ti=0.005%	35.2	22.3	10.0	48.1	11.3	7.9
TiH Ti=0.02%	43.0	13.6	1.4	77.6	6.1	1.1
TiM S=0.011%	35.2	22.3	10.0	48.1	11.3	7.9
SM S=0.013%	84.6	16.4	5.8	58.0	9.9	9.6
SH S=0.036%	51.6	16.9	8.3	64.6	4.2	5.8
Ti-Ca	111.9	6.6	3.0	84.8	3.4	1.9
Ti-Al	46.4	9.9	3.6	60.6	18.3	7.4

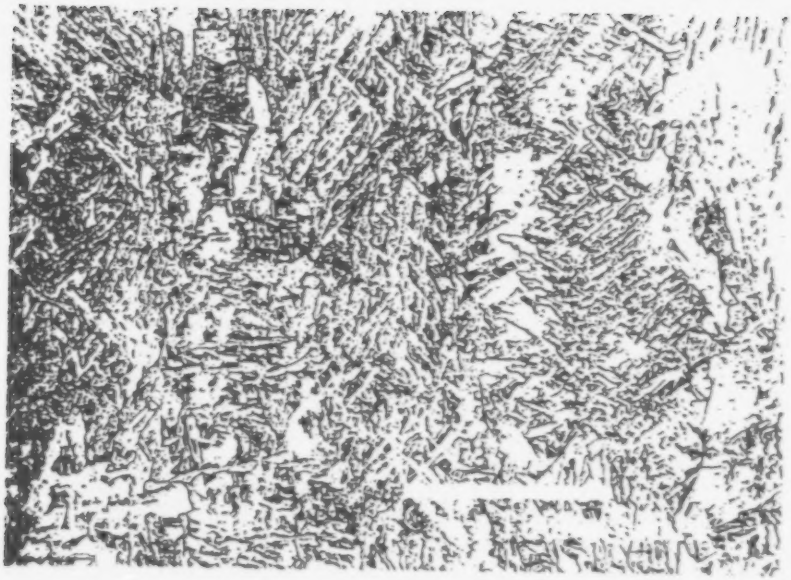

FIGURE 4.1 Typical Microstructure for TiL Weld

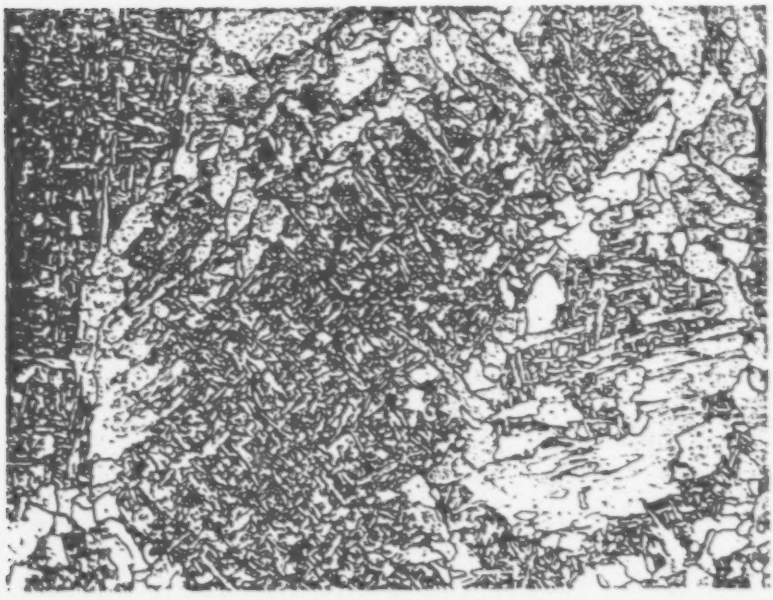

FIGURE 4.2 Typical Microstructure for TiM

The typical optical microstructure for TiH (0.02% Ti) is presented in Figure 4.3. There is a high proportion of AF in this weld (77.6%) even though the prior austenite grain size is only slightly larger than that for TiM. The proportion of FS(NA), FS(A) and PF(G) is less than in TiM. The decrease in PF(G) is due to thinner polygonal ferrite veins since the prior austenite grain sizes are similar in the two cases.

4.1.3 Effect of S on Microstructure

The increase in the concentration of S in the weld metal is linked to an increase in the proportion of acicular ferrite as can be seen in Table 4.1 for the welds TiM (0.011% S), SM(0.013% S) and SH(0.036% S). Typical optical microstructures for the SM and SH welds are presented in Figures 4.4 and 4.5 (See Figure 4.2 for TiM). High S levels (SH) decreases the PF(G) grain size and the width of the PF(G) veins as compared to the TiM and SM welds. The AF is also much finer in the SH. Since TiM and SM have almost identical chemical compositions (See Table 3.1), the increase in PF(G) in TiM can be related to the smaller prior austenite grain size in this weld which increases the grain boundaries on which PF(G) can form. The increase in PF(G) in TiM is to the detriment of AF since the proportion of FS remains almost constant in the two welds.

4.1.4 Effect of Ca and Al additions on Microstructure

Calcium added as a deoxidant increases the proportion of AF in the weld metal even though Ca was not retained in the weld metal to any great extent (0.002 %). Ca increases the Ti level from 0.005% (TiM) to 0.008% (Ti-Ca) with an accompanying increase in the proportion of AF from 48.1 to 84.8% which is higher than the value of 77.6% found for TiH (0.02% Ti) weld.

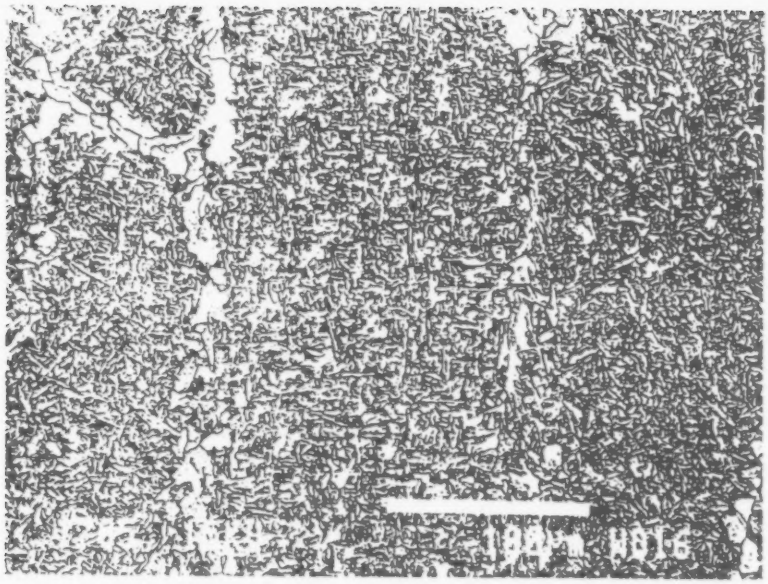

FIGURE 4.3 Typical Microstructure for TiH Weld

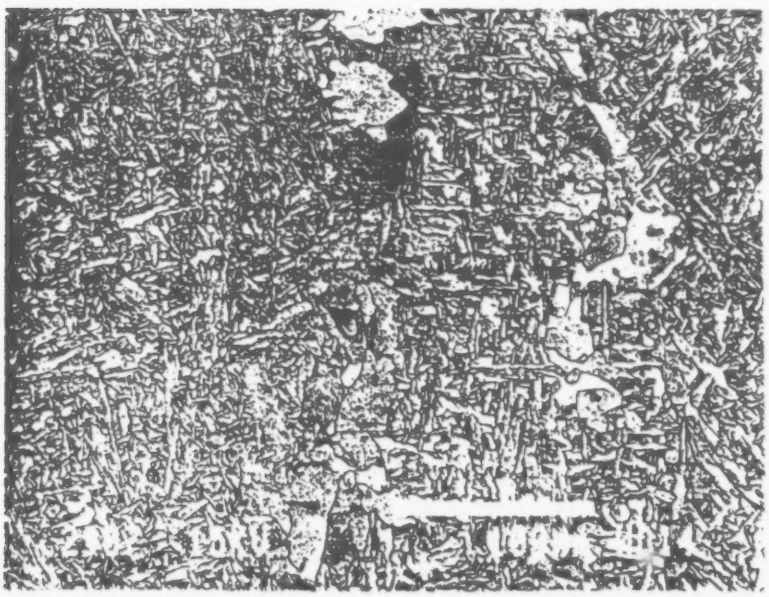

FIGURE 4.4 Typical Microstructure for SH Weld

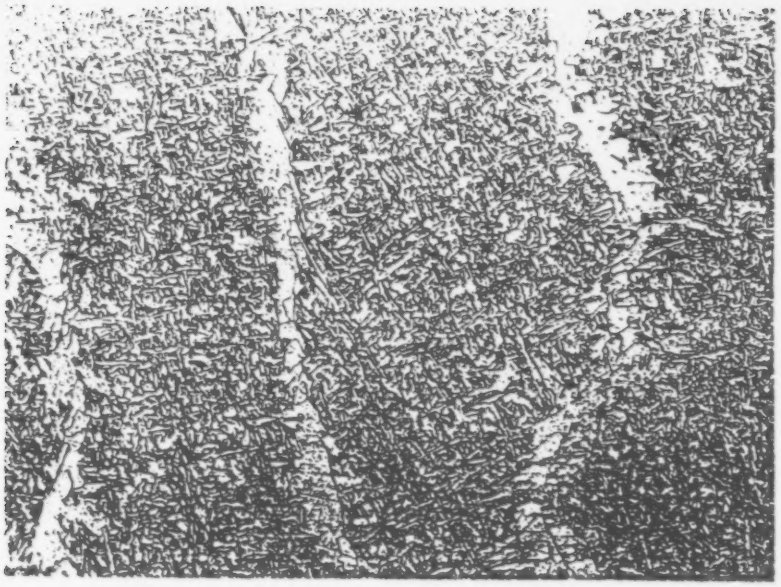

FIGURE 4.5 Typical Microstructure for SH Weld

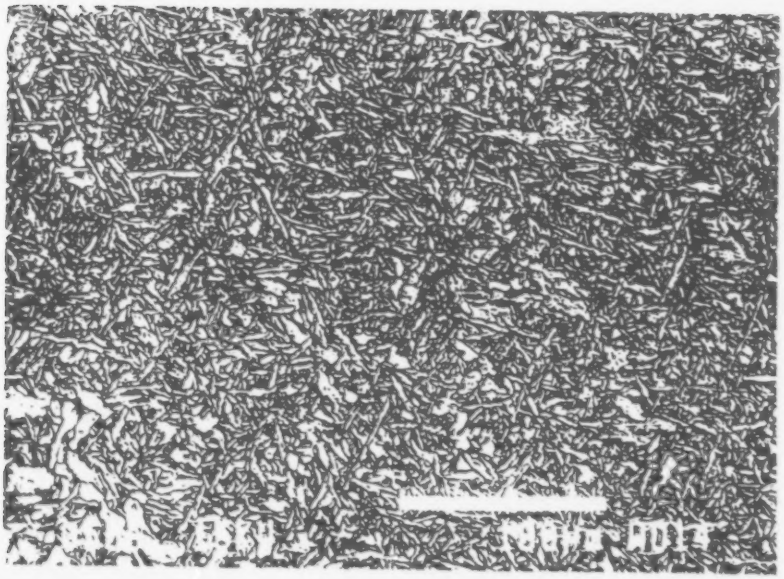

FIGURE 4.6 Typical Microstructure for Ti-Ca Weld.

For the Ti-Ca weld, the acicular ferrite is relatively coarse whereas the PG(F) is somewhat finer as can be seen by comparing Figure 4.6 and Figure 4.2. Comparing the results for the TiM, SM and Ti-Ca welds (similar chemistries except for the Ti levels), it can seen that the proportion of AF increases with increasing prior austenite grain sizes as expected.

The representative optical microstructure for the Ti-Al weld is presented in Figure 4.7. This weld, which has a high proportion of AF (60.6%), has a large amount of FS(A) + FS(NA) when compared to most of the other welds. This weld is characterized by a fairly high level of Ti (0.012 %), the presence of Al and by higher levels of Mn and Si(1.47 Mn and 0.47% Si as compared to about 1.36% Mn and 0.30% Si for the other welds).

4.2 INCLUSION ANALYSES OF EXPERIMENTAL AS-DEPOSITED LARGE PASS WELDS

4.2.1 Inclusion Size Distributions

4.2.1.1 General Aspects

Figures 4.8 to 4.10 present histograms of the size distributions for the three series of experimental welds. Table 4.2 is a summary of the principal characteristics of these distributions. The detailed effects of the alloying elements on the inclusions size distributions are presented in the following sections.

4.2.1.2 Effect of Ti on Inclusion Size Distributions

For all three levels of Ti studied, the size distributions are of the log-normal type. The distributions were very similar, especially with regards to TiL and TiH were the mean diameters are 0.42 and 0.41 um respectively. TiM has a smaller mean diameter of 0.35 μm. There appears to be little effect of the Ti level on the inclusion size distributions. Only the TiL weld had inclusions over 1.5 um (6.3×10^3 inclusions/cm^2). The changes in

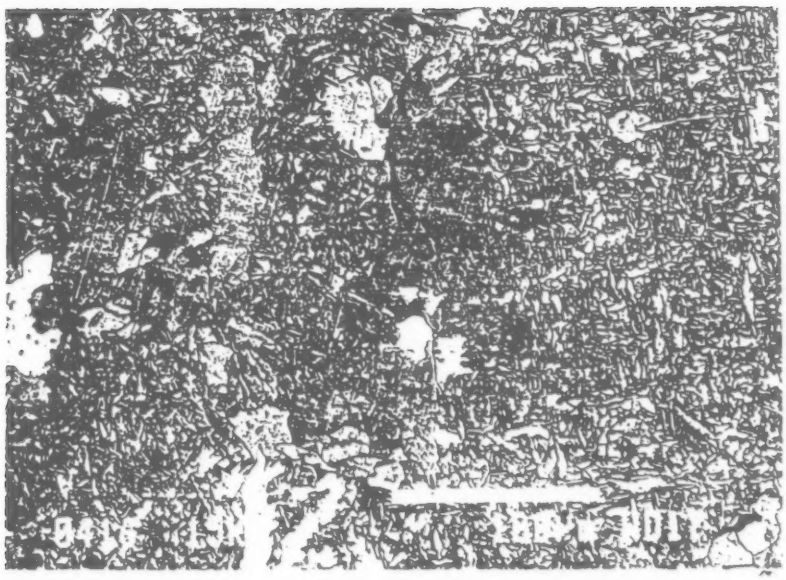

FIGURE 4.7 Typical Optical Microstructure for Ti-Al Weld

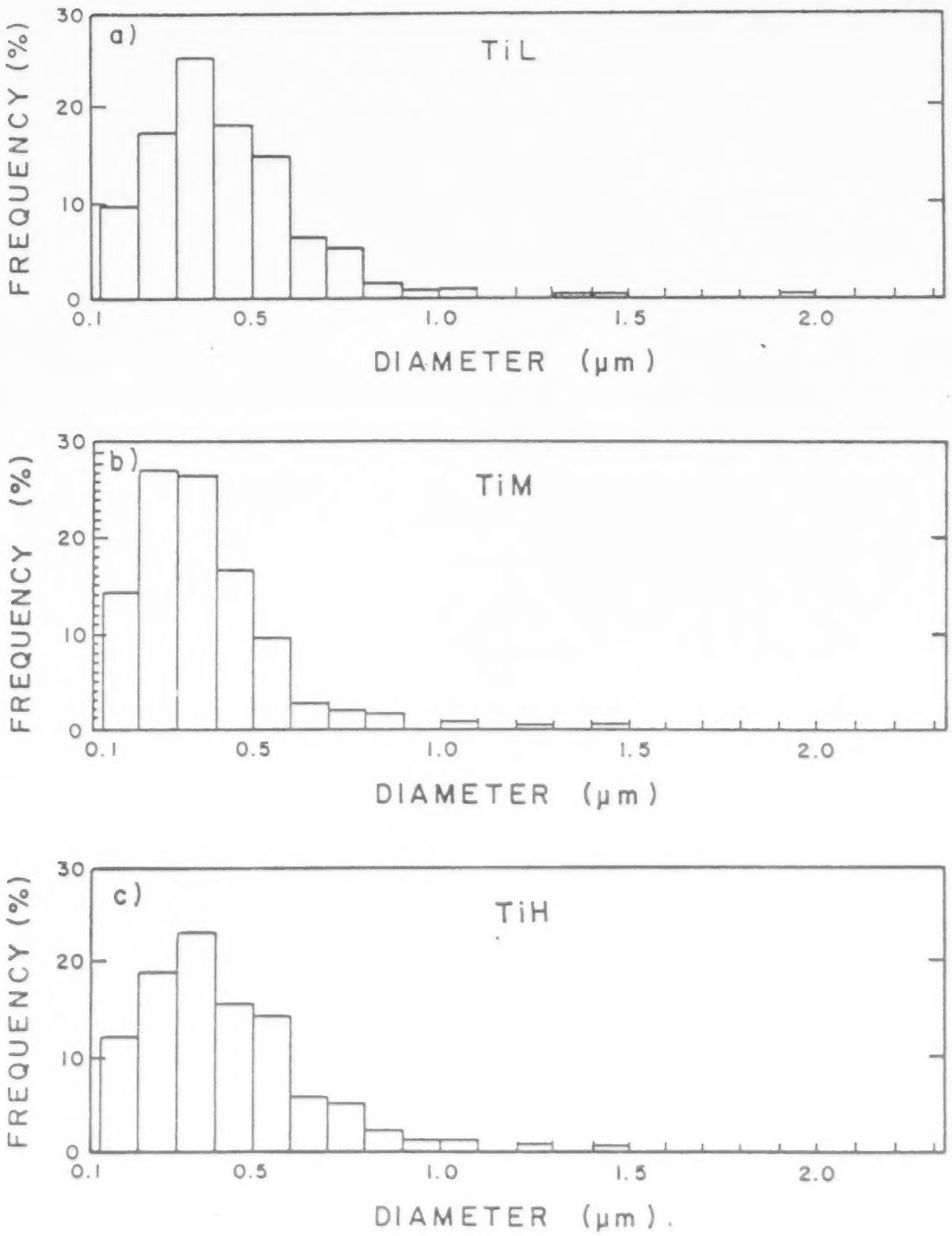

FIGURE 4.8 Inclusion Size Distributions for TiL, TiM and TiH Welds

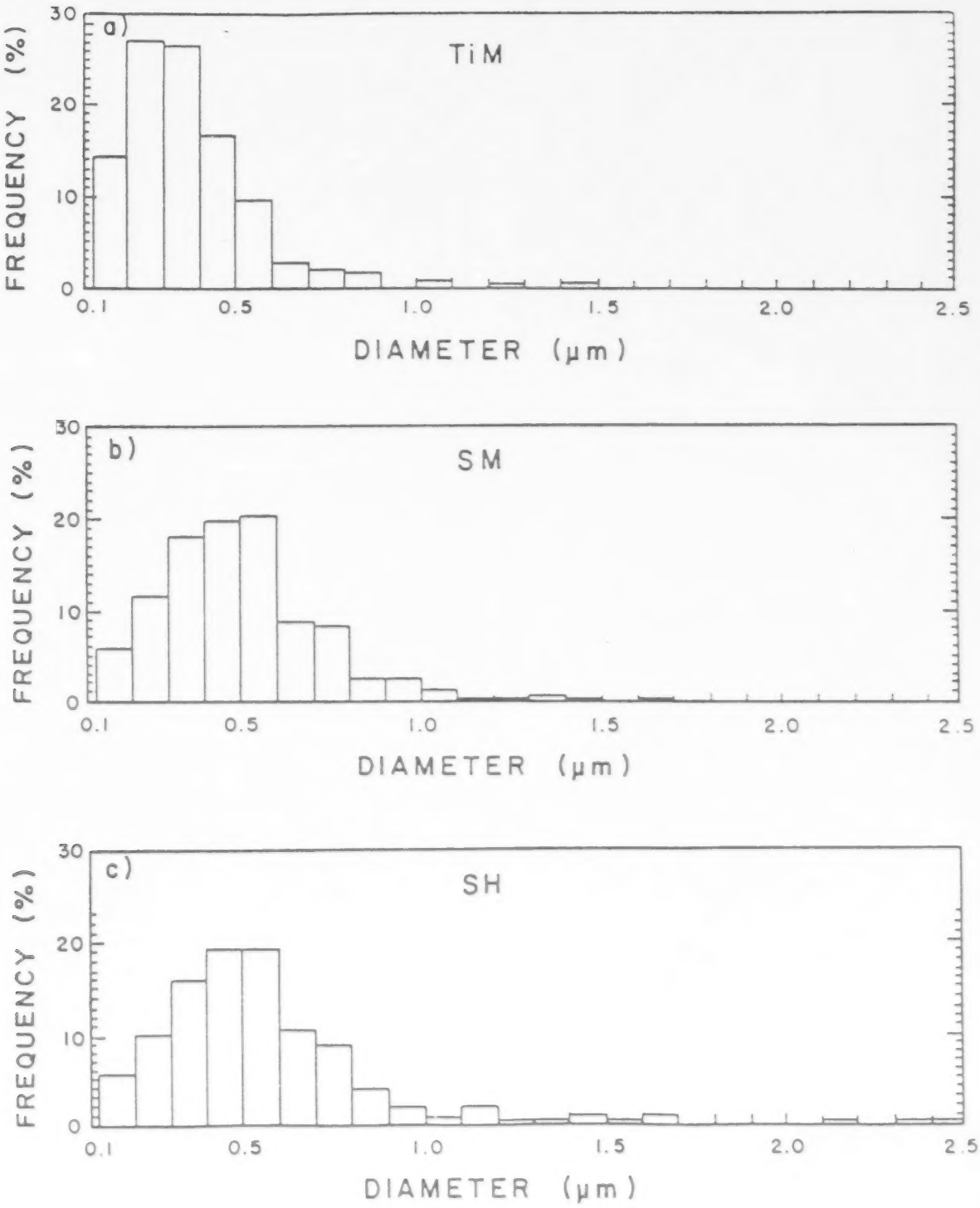

FIGURE 4.9 Inclusion Size Distributions for TiM, SM and SH Welds

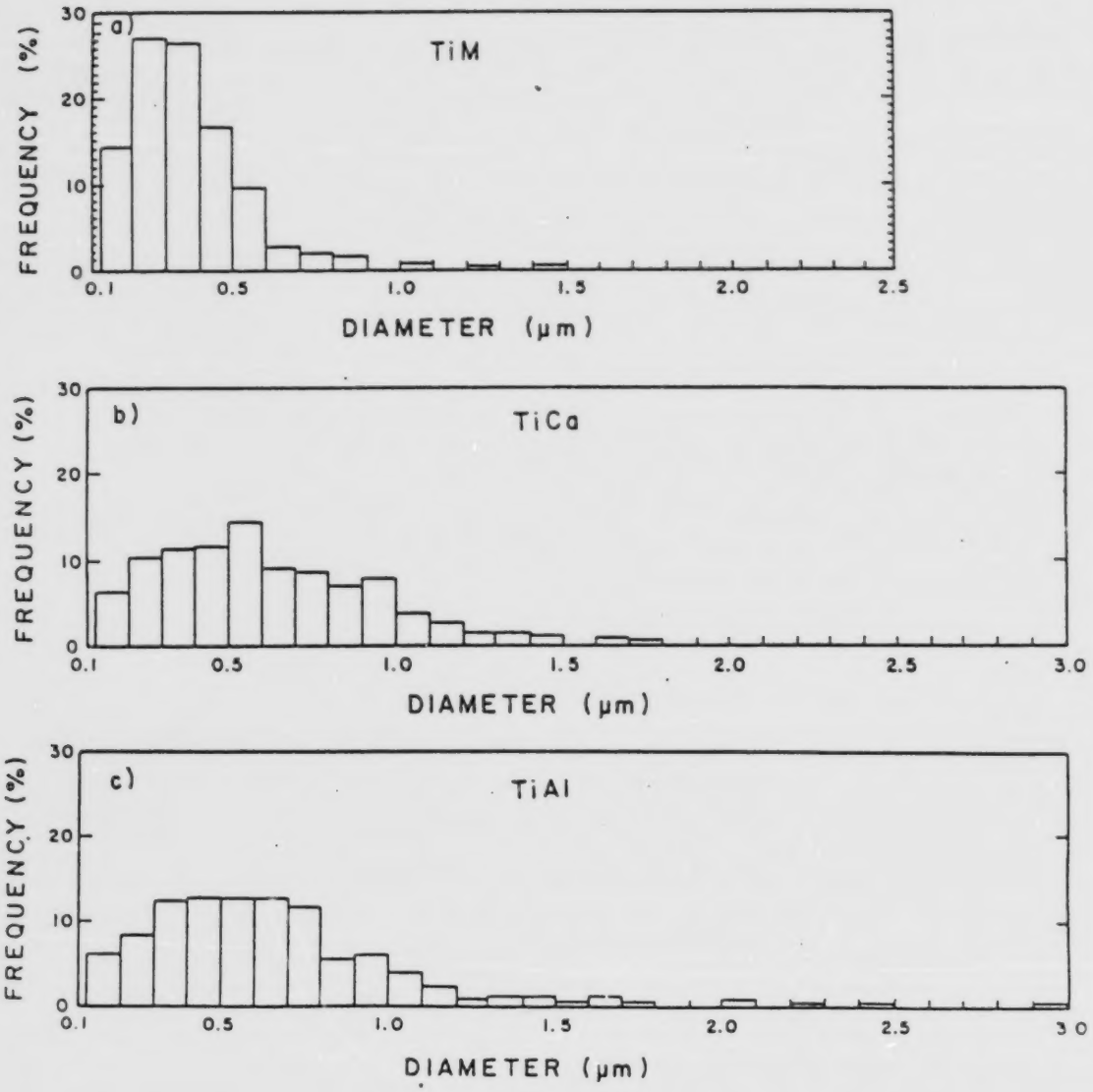

FIGURE 4.10 Inclusion Size Distributions for TiM, Ti-Ca and Ti-AL

TABLE 4.2

EFFECTS OF COMPOSITION ON INCLUSION SIZE DISTRIBUTIONS

Weld deposit	Mean diameter (μm)	Median diameter (μm)	Volume fraction fv (%)	INCLUSION DENSITY NA ($X10^5$ cm^{-2})		
				NA TOTAL	Diam. >1.0μm	Diam. >1.5μm
TiL	0.42	0.39	0.36	21.11	0.380	0.063
TiM	0.35	0.33	0.32	25.82	0.284	0
TiH	0.41	0.37	0.23	13.46	0.282	0
TiM	0.35	0.33	0.32	25.82	0.284	0
SM	0.49	0.47	0.33	14.22	0.469	0.043
SH	0.54	0.50	0.61	20.05	0.982	0.361
Ti-Ca	0.61	0.57	0.26	7.03	0.814	0.070
Ti-Al	0.64	0.58	0.37	8.29	1.04	0.31

inclusion volume fraction and inclusion densities are related to the O content as will be shown in section 4.2.1.5.

4.2.1.3 Effect of S on Inclusion Size Distribution

With increasing S levels the log-normal inclusion size distributions described in the preceding section become increasingly skewed to larger sizes and can be more accurately described by a normal size distribution, especially for the case of SH. As a result, the mean and median inclusion diameters as well as the frequency of larger inclusions increases with increasing S levels. The density of inclusions over 1.5 um increases from 0 for TiM to $3.6 \times 10^4/cm^2$ for the highest S level.

4.2.1.4 Effect of Ca and Al additions on Inclusion Size Distributions

Both Ca and Al additions in the flux of the welding electrode result in a normal inclusion size distributions as compared to the log-normal distribution found for the base composition, TiM. These distributions have higher average mean diameters, 0.61 um for Ti-Ca and 0.64 um for Ti-Al. The use of Al as an deoxidant causes the formation of a great number of large inclusions between 1.5 and 3.0 um (NA>1.5 of $31 \times 10^3 cm^{-2}$) whereas the majority of large inclusions for Ti-Ca lies between 1.5 and 1.8 um (NA>1.5: $7 \times 10^3 cm^{-2}$).

4.2.1.5 Effect of O plus S on Volume Fraction of Inclusions

Figure 4.11 presents the relationship between the volume fraction of inclusions and the sum of the S and O contents in the weld metal. The volume fraction of inclusions is linearly dependant upon the [O+S] concentrations as would be expected from the fact that these two elements are the main inclusion forming agents.

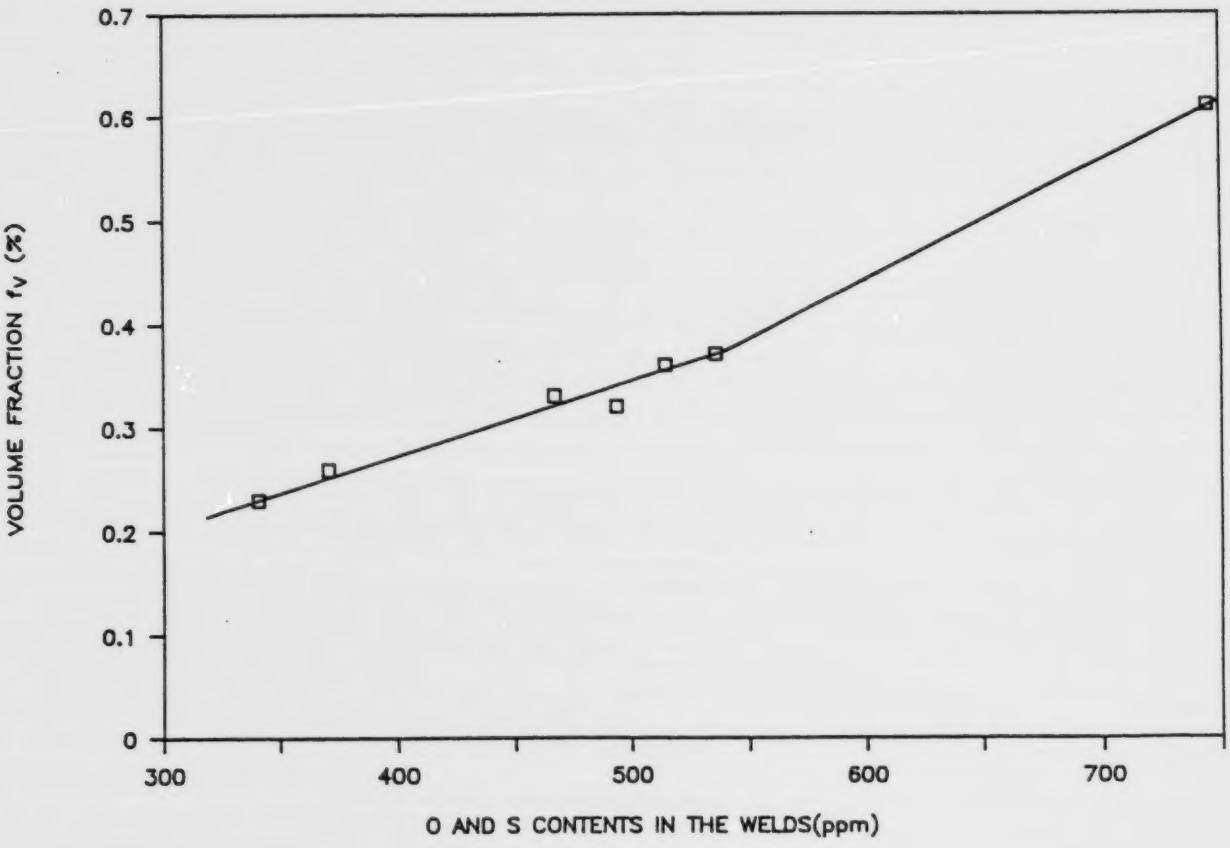

FIGURE 4.11 Relationship between [O+S] and Volume Fraction of Inclusions

4.2.2 Chemical Composition of Inclusions

4.2.2.1 General Aspects

Table 4.3 presents the average relative intensities (i.e. average of number of X-rays for a particular element divided by the total counts for all the elements in the inclusion) for the different series. Al, Si, S, Ca, Ti and Mn were found in varying amounts in the inclusions. Figures 4.12 to 4.18 illustrate the variation in the relative intensity with inclusion diameter for each of the constituent elements for all of the experimental welds. The trends will be discussed in greater detail in the following sections.

4.2.2.2 Effect of Ti on Chemical Composition of Inclusions

The relative intensity of Ti in the inclusions increases with increasing Ti concentration within the weld which is to be expected due to the high affinity of Ti for oxygen. There is no significant amount of Ti in the inclusions of TiL since the measured average relative concentration of 0.4% is below the dectectability of the spectrometer for the counting times used. For 0.005 wt% Ti in the weld, TiM, there is about 4.6% relative intensity and for 0.02% Ti (TiH) there is 46.3% Ti in the inclusions. Figure 4.19 shows the relative intensity of Ti measured in the inclusions as a function of the Ti level in the weld deposit for all the experimental compositions studied. Clearly, the amount of Ti in the inclusions is linearly related to the amount of Ti in the weld deposits but it should be noted that a minimum amount of Ti (0.004%) is required in the weld before Ti is detected in the inclusions.

If the relative intensity of an element in the inclusion is taken as a measure of the total amount of an element in the inclusions, then total content of a given element in the inclusions can be estimated from the following relationship:

TABLE 4.3

AVERAGE RELATIVE INTENSITY OF THE X-RAY PEAKS FOR THE PRINCIPAL ELEMENTS FOUND IN THE INCLUSIONS

Weld deposit	RELATIVE INTENSITY (%)					
	Al	Si	S	Ti	Mn	Ca
TiL	0	26.1	8.9	0.4	64.6	0
TiM	0	23.6	9.5	4.6	62.0	0
TiH	0	7.4	6.4	46.3	39.9	0
TiM	0	23.6	9.5	4.6	62.0	0
SM	0	21.8	15.3	4.1	58.6	0
SH	0	10.4	30.0	2.0	57.6	0
Ti-Ca	0	23.2	7.9	9.8	57.6	1.6
Ti-Al	15.2	19.3	6.0	12.3	47.0	0

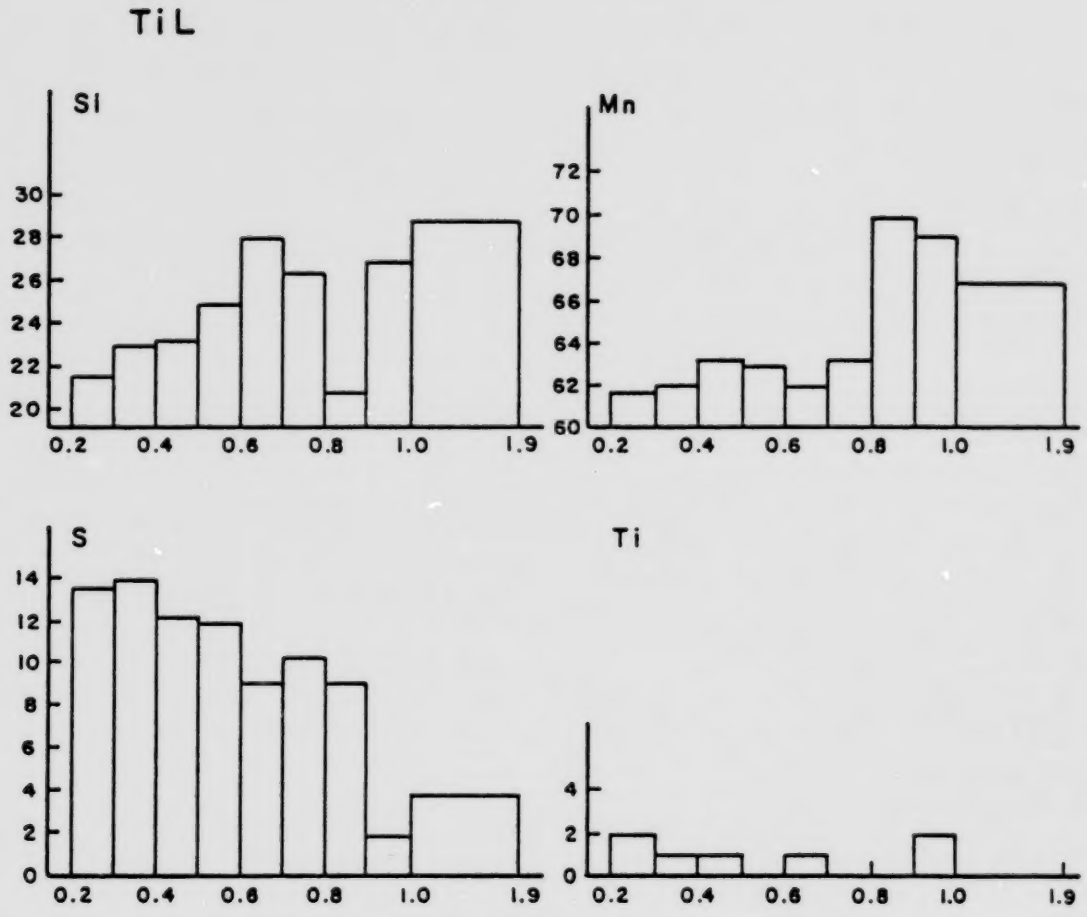

FIGURE 4.12 Relative Intensity of the Major Elements as a Function of Inclusion Diameter for TiL

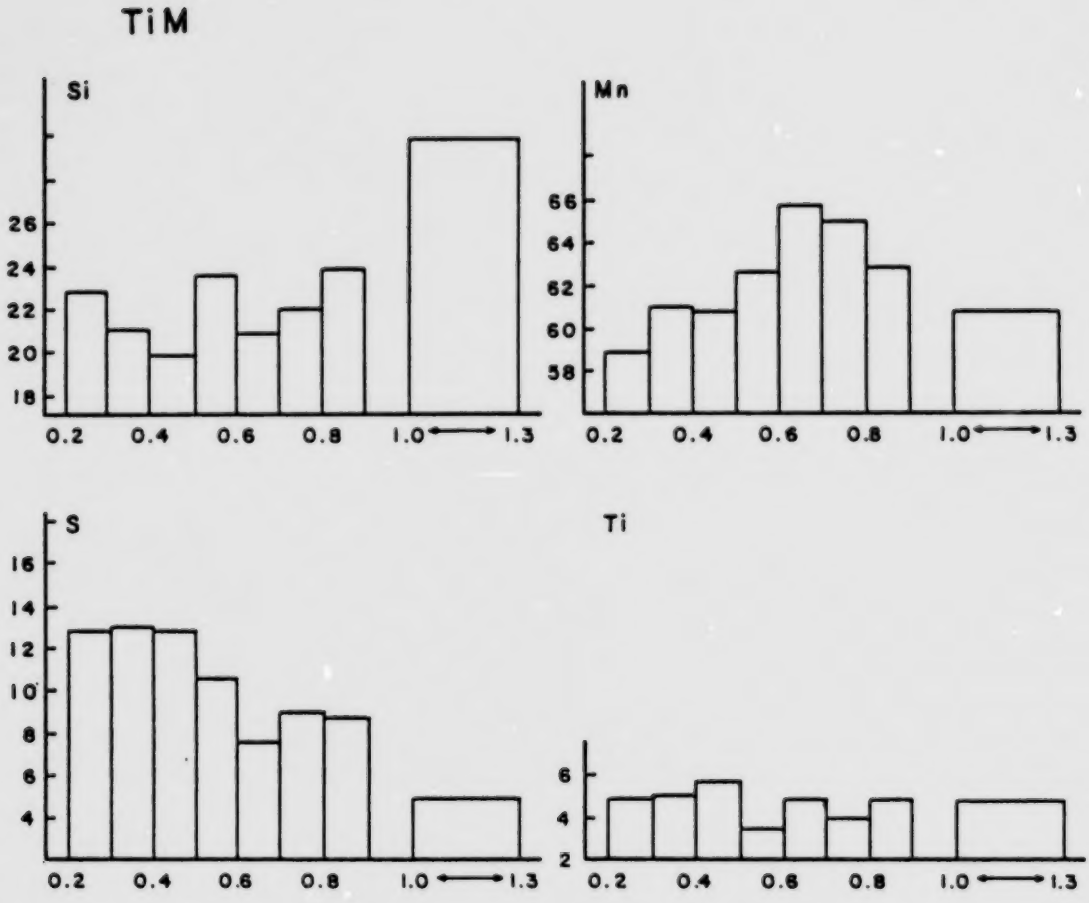

FIGURE 4.13 Relative Intensity of the Major Elements as a Function of Inclusion Diameter for TiM

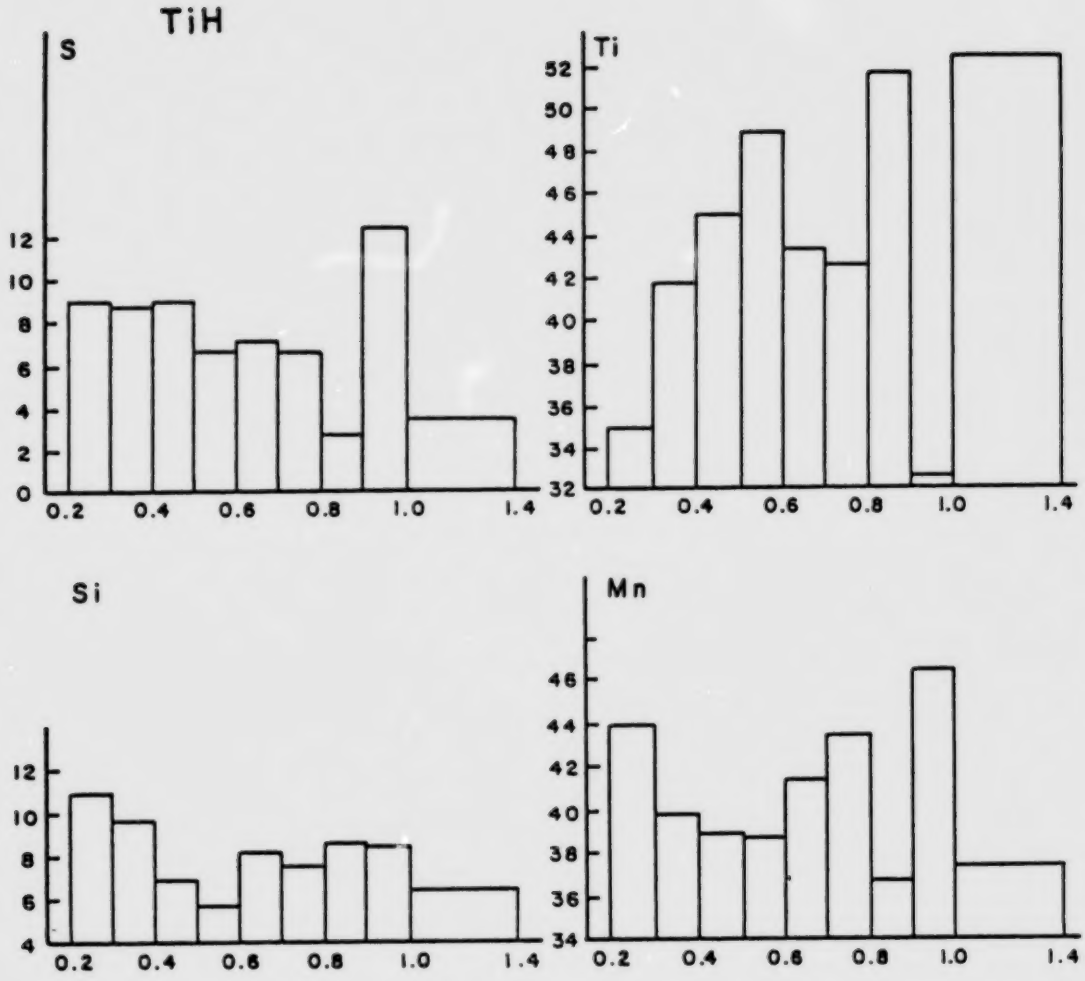

FIGURE 4.14 Relative Intensity of the Major Elements as a Function of Inclusion Diameter for TiH

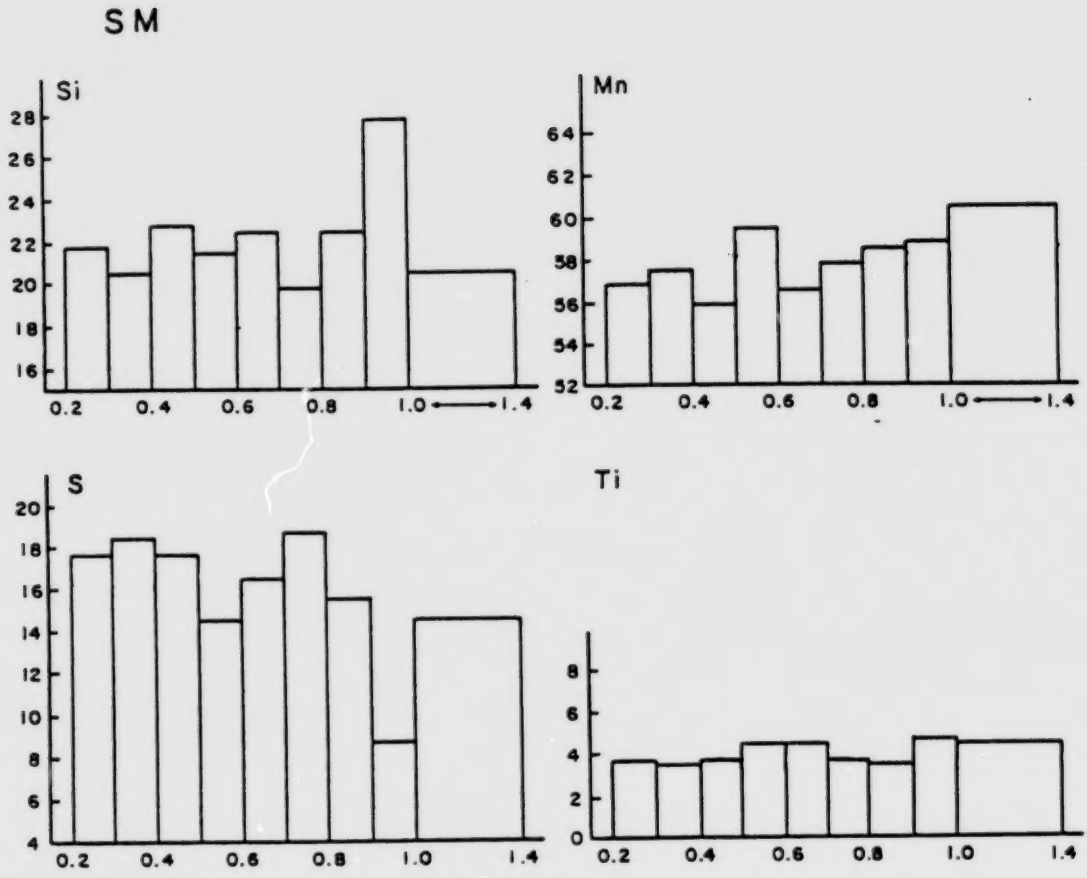

FIGURE 4.15 Relative Intensity of the Major Elements as a Function of Inclusion Diameter for SM

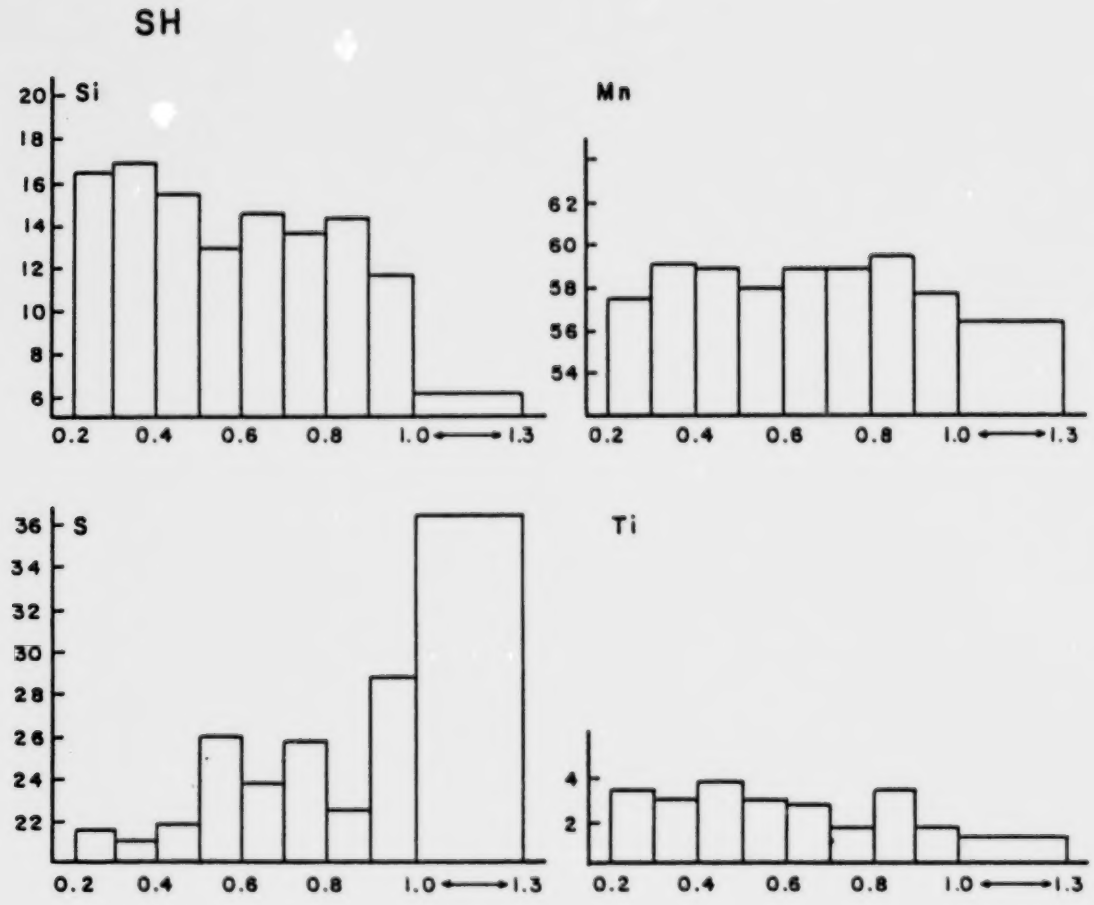

FIGURE 4.16 Relative Intensity of the Major Elements as a Function of Inclusion Diameter for SH

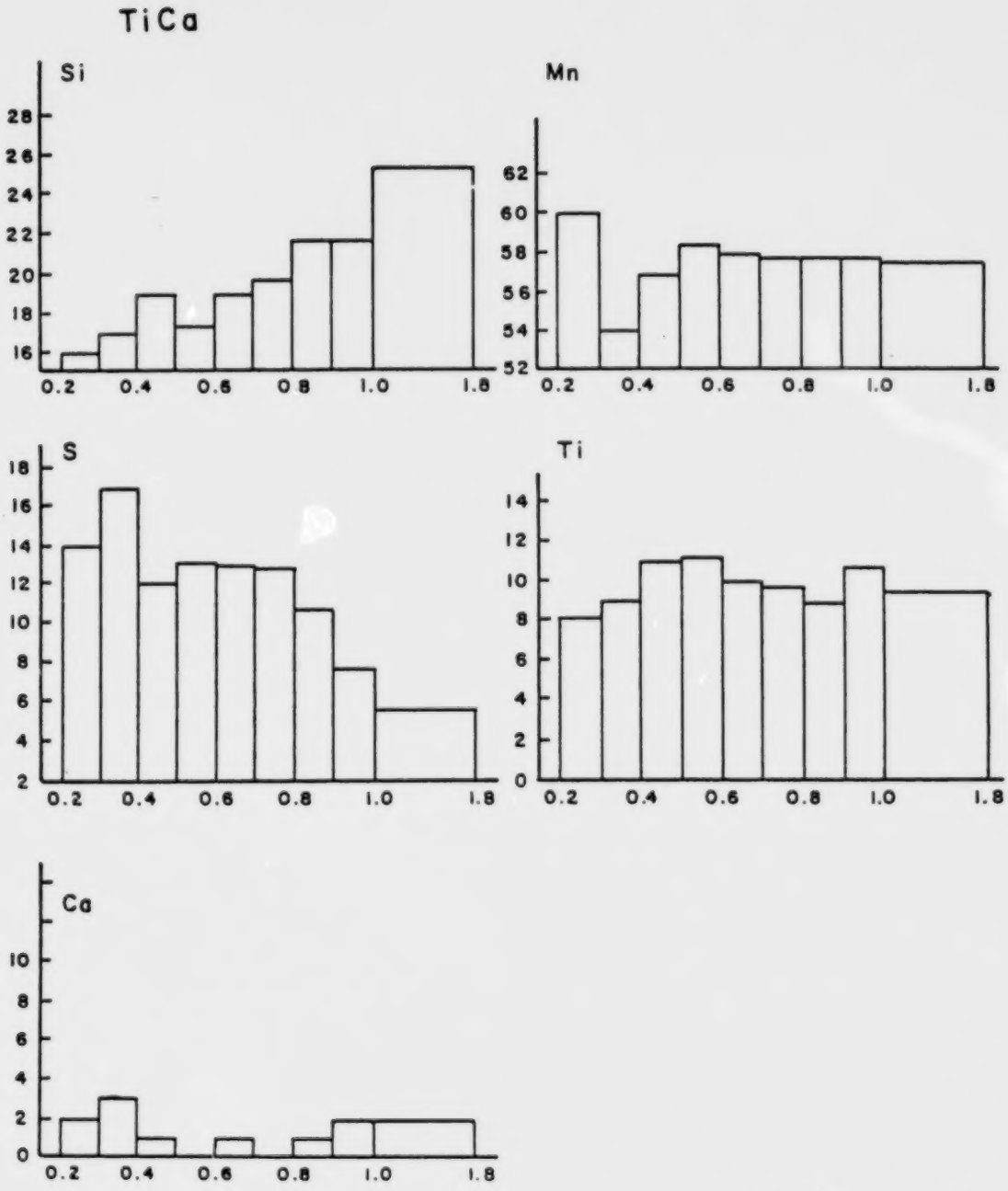

FIGURE 4.17 Relative Intensity of the Major Elements as a Function of Inclusion Diameter for Ti-Ca

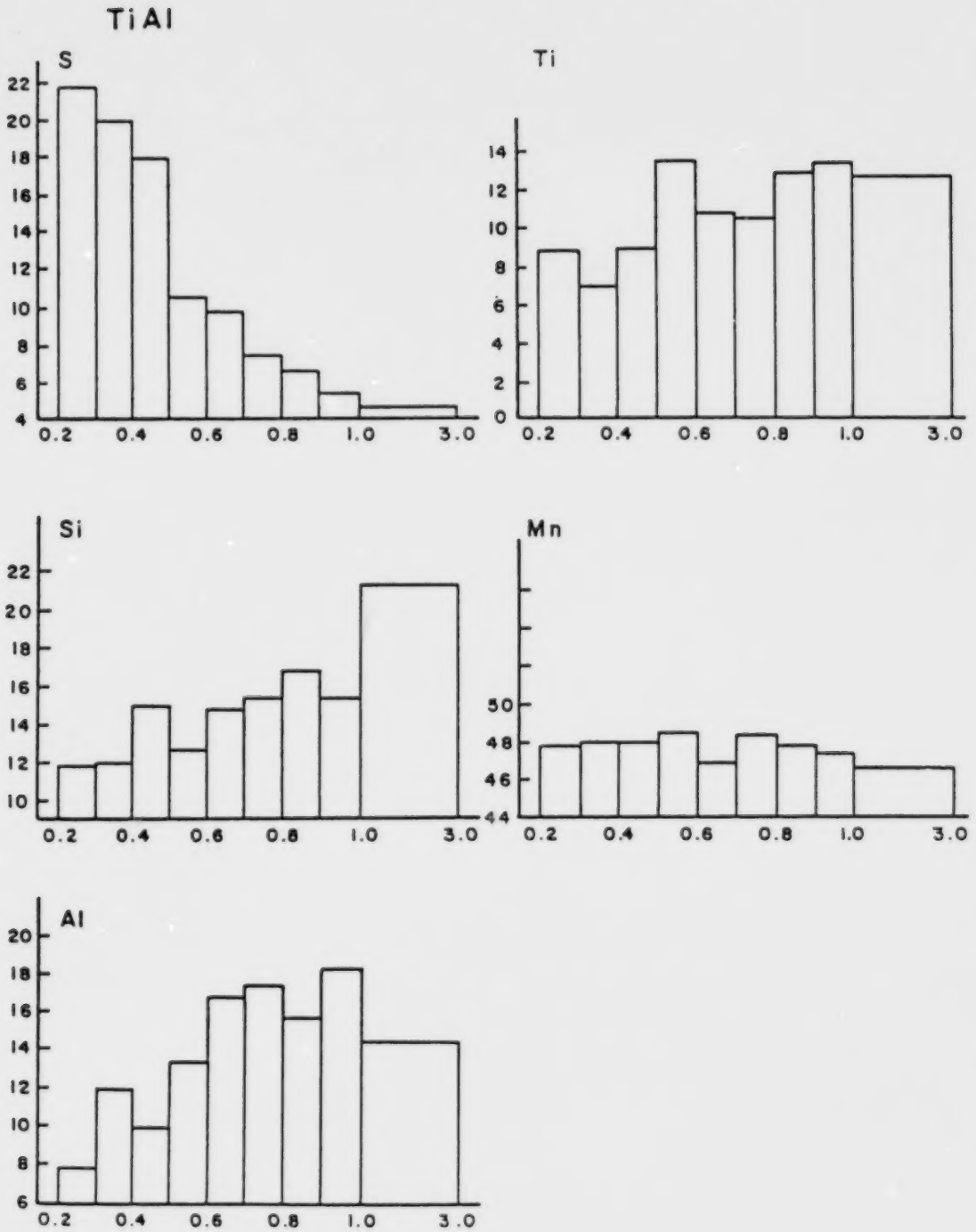

FIGURE 4.18 Relative Intensity of the Major Elements as a Function of Inclusion Diameter for Ti-Al

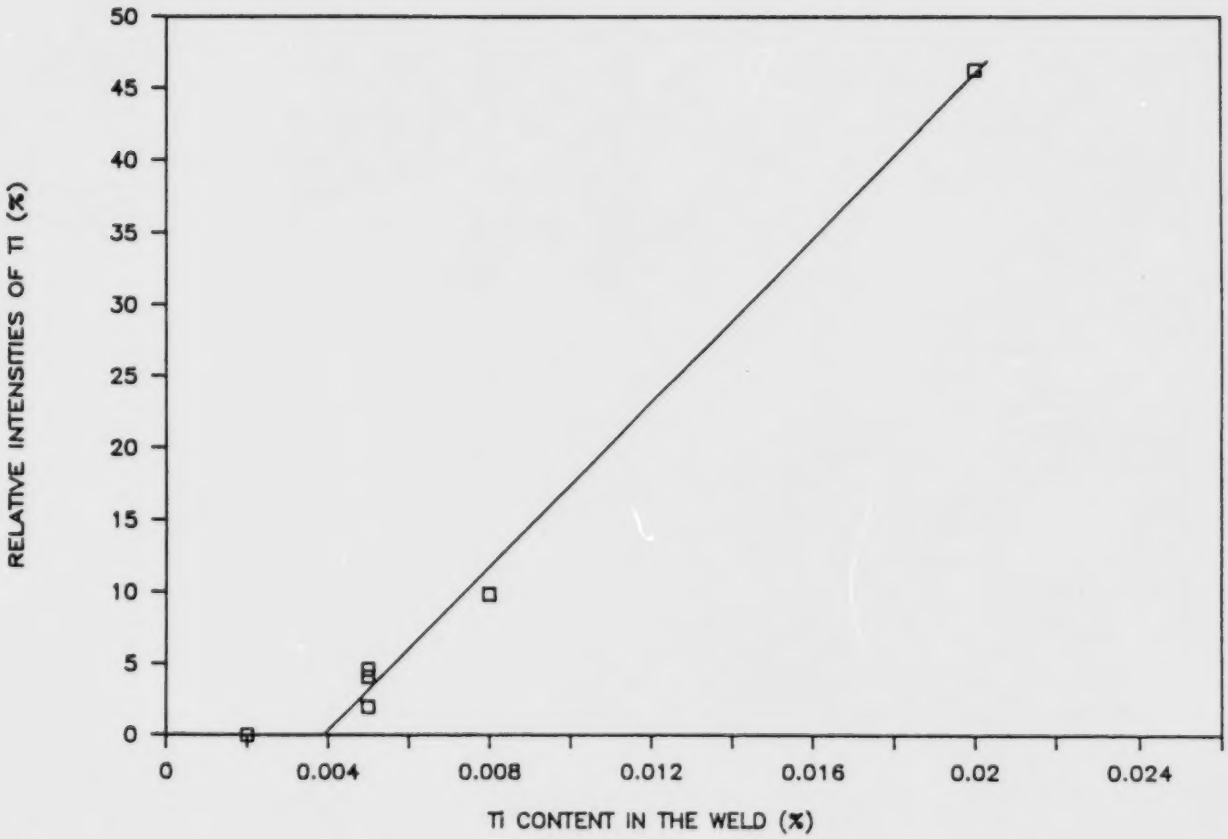

FIGURE 4.19 Relative Intensity of Ti in Inclusions as a Function of Ti Content of the Weld Metal

$$m_x = I_x \times f_v$$

where m_x = estimation of the total content of element x contained in the inclusions

I_x = average relative intensity of element x in the inclusions

f_v = volume fraction of inclusions in weld

m_x can not be considered to give the exact amount of an element in the inclusions since the O,N and C levels cannot be measured with an energy dispersive X-ray spectrometer that has a Be window. In addition, no corrections for the variations in atomic number, fluorescence or absorption were performed. The changes in m_x, however, will still reflect changes in the total amount of an element in the inclusions, since I_x, will increase with increasing concentrations of an element.

Figure 4.20 shows the changes in m_{Ti}, m_S, m_{Si} and m_{Mn} in the inclusions for the TiL, TiM, TiH and Ti-Ca welds for which the chemical compositions of the base metal are similar. The increase in Ti in the inclusions (i.e. m_{Ti}) due to the increase in the concentration of Ti in the base metal) is at the detriment of the concentrations of the other elements in the inclusions, principally manganese and silicon.

Due to the fact that Ti, Mn and Si have a very high affinity for oxygen, changes in the total amounts of these elements in the inclusions will reflect changes in the amounts of the oxides of these elements in the inclusions. An increase in Ti will mean an increase in the quantity of titanium oxides present but with a corresponding decrease in the amount of manganese and silicon oxides in the inclusions. More of the later elements will therefore remain in solid solution for a given total amount in the weld deposits.

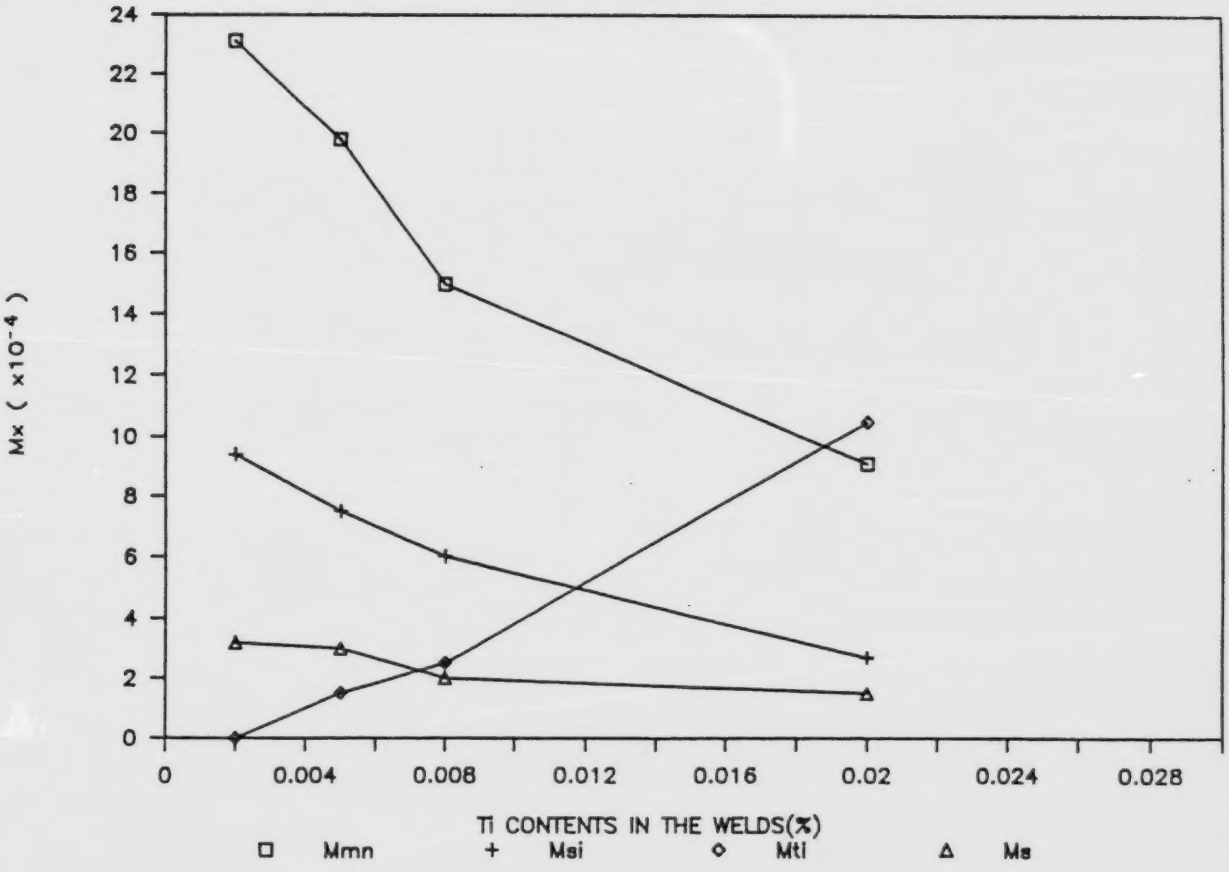

FIGURE 4.20 Calculated Total Contents of Ti, S, Si and Mn in the Inclusions as a Function of Ti Content of the Weld

It is difficult to determine clear trends from the histograms of the chemical composition as a function of the inclusion diameter for the three specimens, TiL, TiM and TiH (See Figures 4.12-4.14). It appears, however, that an increase in diameter of the inclusion is associated with a decrease in the relative intensities of S. For the welds TiL and TiM, the amount of Ti is constant whereas the amount of Mn and Si fluctuates with inclusion diameter. For TiH, the amount of Ti increases with the diameter whereas the amount of Si and Mn fluctuates. The quantity of Ti in the inclusions is inversely proportional to the quantity of Mn and S. The lowest Ti levels (0.9 to 1.0 um) is obtained for high levels of Mn and S. This trend indicates that the quantity of the inclusions rich in Ti not only limits the amount of Mn and Si oxides but are also closely linked to the quantity of MnS in the inclusions.

4.2.2.3 Effect of S on Chemical Composition of Inclusions

Since S and O are the principal inclusion forming elements, increases in the S level in the weld metal is associated with an increase in the S content of the inclusions. The relative intensity of S increases from 9.5% for TiM(S=0.011%) to 15.3% for SM (S=0.013%) and to 30% for SH (S=0.036%). This significant increase in the S level in the inclusions with only a slight increase in the S level between TiM and SM can be accounted for partially by a decrease in the total O content in the weld metal for SM (337 ppm as compared to 384) which will decrease the amount of oxides present and therefore increase the relative proportion of S.

Figure 4.21 illustrates the relative changes in the total mass of the elements in the inclusions as represented by m_x (see equation 4.1) as a function of the concentration of S in the weld metal. An increase in the concentration of S in the as-deposited weld metal increases the total amount of S in the inclusions whereas the amounts of Ti and Si remain almost constant.

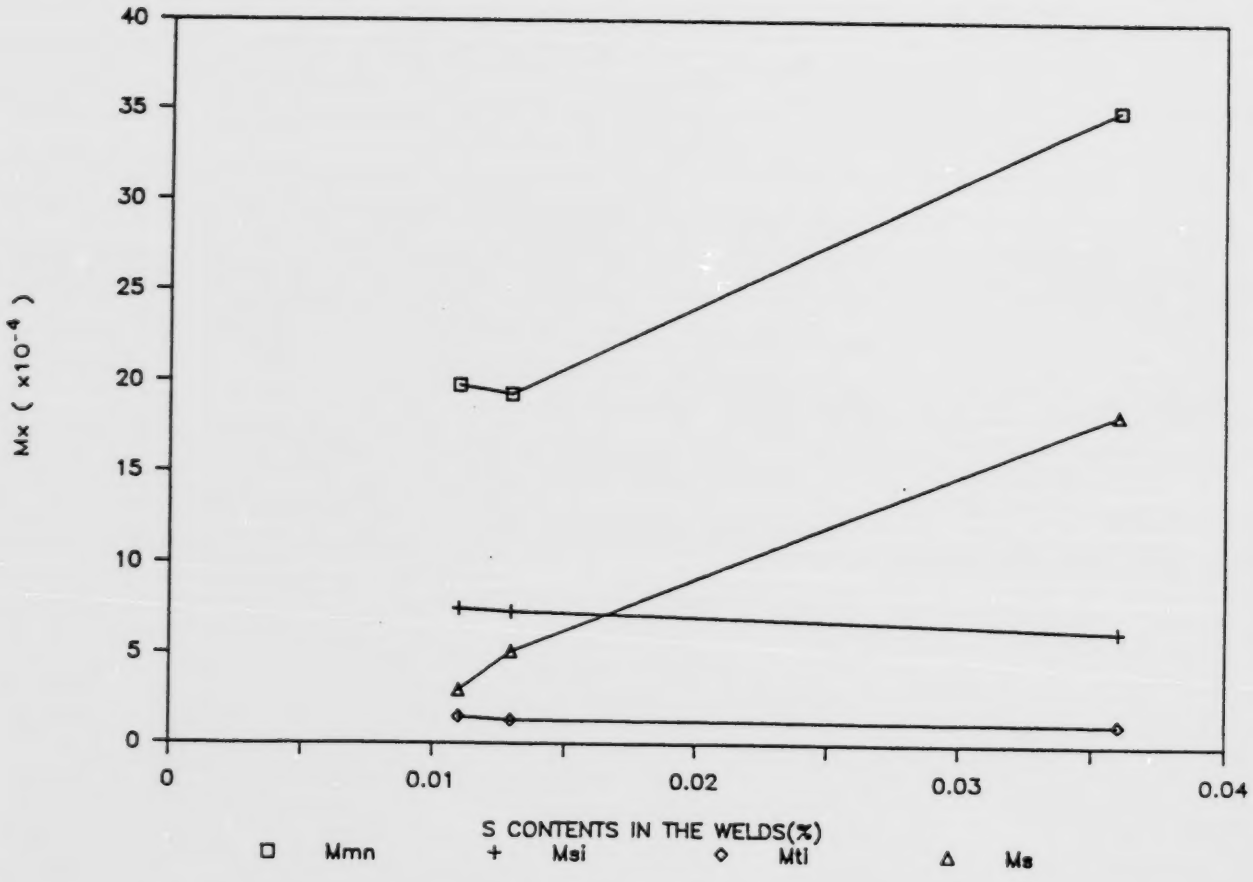

FIGURE 4.21 Calculated Total Contents of Ti, S, Si and Mn in the Inclusions as a Function of S content of the Weld

The Mn level in the inclusions increases with large increases in the S level (i.e. SH as compared to SM or TiM). There is an abnormality in this trend when comparing TiM to SM. For a slight increase in S of 0.002% there is a corresponding decrease in the total Mn content of the inclusions. This can be at least partially explained by the decrease in the total O content from 384 ppm for the TiM weld to 337 ppm for the SM weld which will decrease the amount of Mn oxides present in the inclusions and increase the relative proportion of S. This will result in a decrease in the total amount of Mn present in the inclusions.

Figure 4.21 shows that the increase in the S concentration is associated with an increase in the MnS content and does not affect the quantity of Ti, Mn and Si oxides present. The oxide volume fraction is related directly to the total O content.

The relative S content of the inclusions in TiM tends to decrease with increasing inclusion diameter whereas the reverse is observed for the high S containing weld, SH. In the first case, the Ti and Si levels decrease with increasing S levels whereas the Mn level remains about constant. For the SM weld, the relative intensities of S, Mn, Ti and Si fluctuate as a function of the inclusion diameter.

4.2.2.4 Effect of Al and Ca on Chemical Composition of Inclusions

Even though Ca was used as a deoxidizing agent, there is no measurable levels of Ca found in the weld metal and only 1.3 relative % in the inclusions. Ca, however, facilitates the transfer of Ti to the weld metal which results in the increase of Ti in the inclusions(9.8%) as compared to the welds TiM and SM(4.6 and 4.1 % Ti respectively). As is shown in Section 4.2.2.2, an increase in Ti in the inclusions is to the detriment of Mn and Si

oxides (See Figure 4.20).

The use of Al in the electrode Ti-Al improves the transfer of Ti to the weld metal (0.012%) and also increases the oxygen content of the weld metal (416 ppm). An increase in Ti in the weld deposit normally decreases the oxygen content. The inclusions in the Ti-Al weld are characterized by significant quantities of Al(15.12%) and higher levels of Ti (12.3%) than are found in the non-Al containing welds of the same composition. These increases in Al and Ti are at the expense of the Mn and Si contents. The S level remains about constant.

A summary of the effects of chemical composition of the weld metal on the inclusion chemistries is presented in Figure 4.22.

4.2.2.5. Heterogeneous Nature of the Inclusions

Inclusions were extracted from the SM weld using carbon extraction replicas and observed in the Scanning Electron Microscope (SEM). The relative intensities of the X-ray peaks as measured by the Energy Dispersive Spectrometer are as follows: I_{Si} = 21.8%, I_S=15.3%, I_{Ti}=4.1%, I_{Mn}= 58.6%. Multiple distinct phases were observed in most of the inclusions. This is in accordance with the results of many other researchers[2,4,19,20,43,44,46] who found that inclusions in weld metal tend to be heterogeneous (See Section 2.4.2.4).

Figure 4.23(a) shows a typical inclusion found on the extraction replica. Several distinct phases (regions 1,2, 3) can be observed in the inclusion. Figures 4.23 (b-d) are the X-ray spectra for these regions. The central region (1) which appears to be the nucleous of the inclusion contains mainly Si and Mn with smaller quantities of S and Ti. The two outer regions are chemically different than the center as is clearly shown by the spectra from region

2 and 3. Region 2 is richer in Ti whereas region 3 is richer in S with a small peak of Cu which was not found in the other regions. It should be noted that during a spot analysis on a particular region within the inclusion, X-rays will also be produced to some extent from the other regions of the sample due to beam broading effects. Hence, the spectra for the outer regions of the inclusion will also contain X-rays from the central region. Thus region 2 is associated with a Ti rich phases (probably an oxide) whereas region 3 is S rich (MnS and/or Cu).

These results show that several distinct phases can form around a central nucleus which in this case is probably a S or Mn oxide. It is interesting to note that the Ti rich phase is located at the outside of the inclusion. This is the general case for the SM weld, that is to say, the central region of the inclusion is rich in Si and Mn whereas the Ti rich phase occurs at the surface of the inclusion.

4.3 TOUGHNESS OF THE EXPERIMENTAL WELDS

4.3.1. As-deposited Weld Metal

4.3.1.1. Results of Charpy Impact Tests

Tables 4.4 to 4.6 present the results of the standard Charpy tests the titanium, sulphur and strong desoxiding series respectively for all the large last pass welds. These results are presented in graphical form in Figures 4.24, 4.25 and 4.26. Table 4.7 summarizes the impact toughness characteristics of the seven compositions studied. Table 4.8 presents the results for the 5x5 Charpy specimens for the electrodes with varying Ti concentrations. The variation in toughness values for these sub-size specimens from one composition to another is less than is the case for the full-size specimens which is due to the limited ability of a smaller specimen to provide plastic constraint at the notch root. Hence, this test piece failed mainly by plane

stress and not plane strain. The results for the 5x5 specimens follow similar trends to those of the full size specimens, hence, only full size tests were performed for the other series.

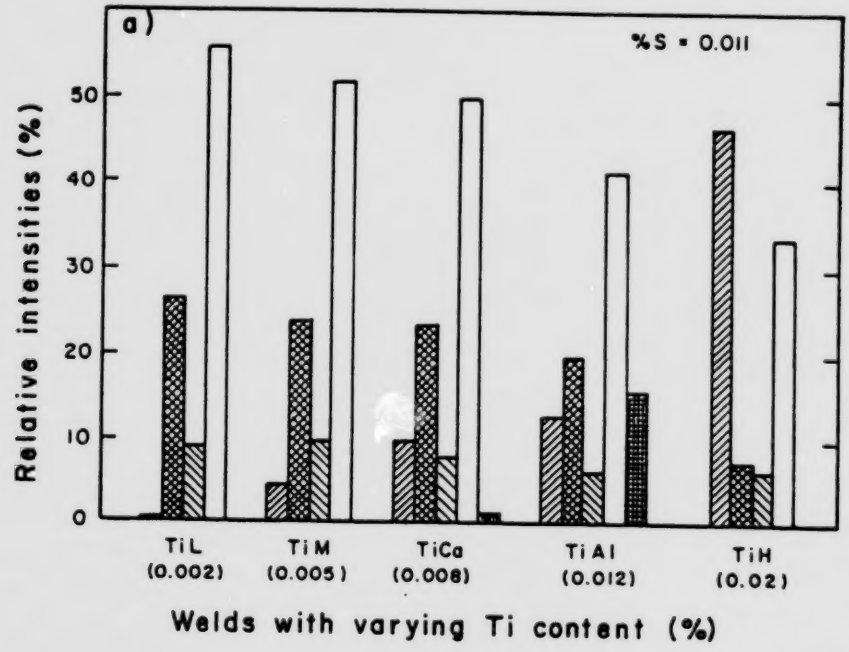

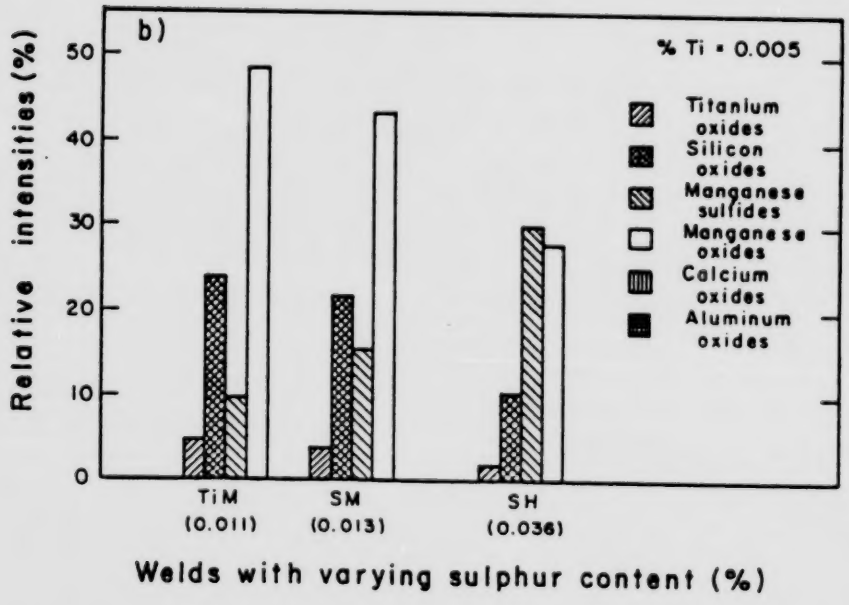

FIGURE 4.22 SUMMARY OF THE EFFECTS OF WELD METAL COMPOSITION ON THE INCLUSION CHEMISTRY

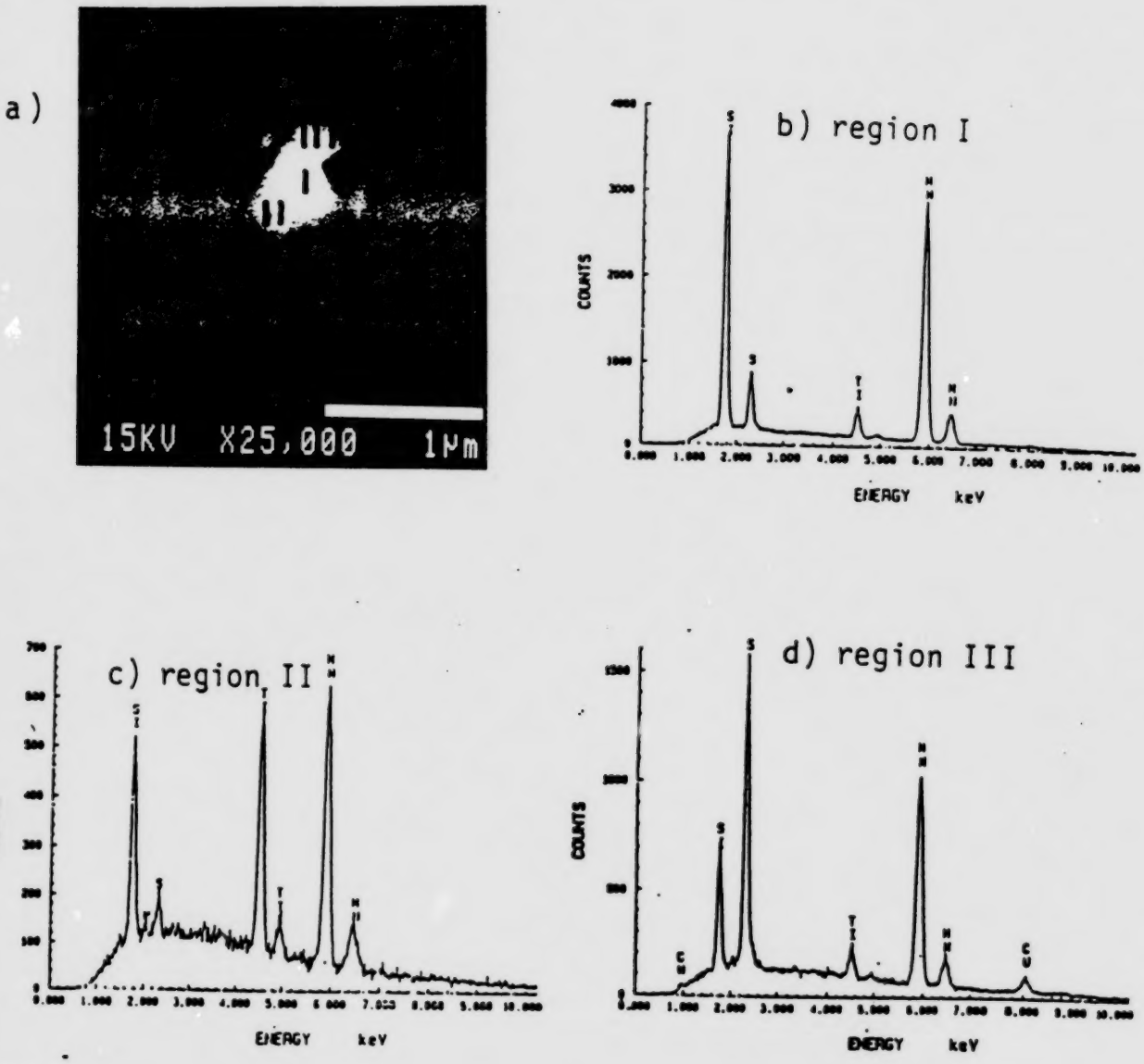

FIGURE 4.23 Typical Inclusion of SM Weld which shows the Heterogenious Nature of Inclusions. (a) Micrograph of the Inclusion. (b), (c) and (d) Energy Dispersive X-ray Spectra from Regions I, II and III.

TABLE 4.4

RESULTS OF CHARPY TESTS FOR EXPERIMENTAL TEST PLATES

(LARGE AS-DEPOSITED ZONE) WITH VARYING TI CONCENTRETIONS

Sample name	T(°C)	ABSORBED ENERGY Kv (J/cm^2)					Kv average (J/cm^2)
TiL	+23.0	112	161	---	---	---	136.5
	+ 5.0	57	60	89	107	---	78
	- 5.0	22	39	67	67	71	53
	-10.0	25	52	69	---	---	46
	-20.0	30	39	44	---	---	38
TiM	- 0	150	155	202	---	---	169
	-20.0	110	133	---	---	---	122
	-25.0	14	54	112	147	---	82
	-30.0	15	45	62	76	---	50
	-40.0	20	23	82	87	---	53
TiH	+23.0	118	---	---	---	---	118
	0.0	83	87	99	---	---	90
	-10.0	47	52	78	87	---	66
	-20.0	33	66	72	72	---	61
	-30.0	24	33	34	---	---	30
	-40.0	17	23	27	---	---	22

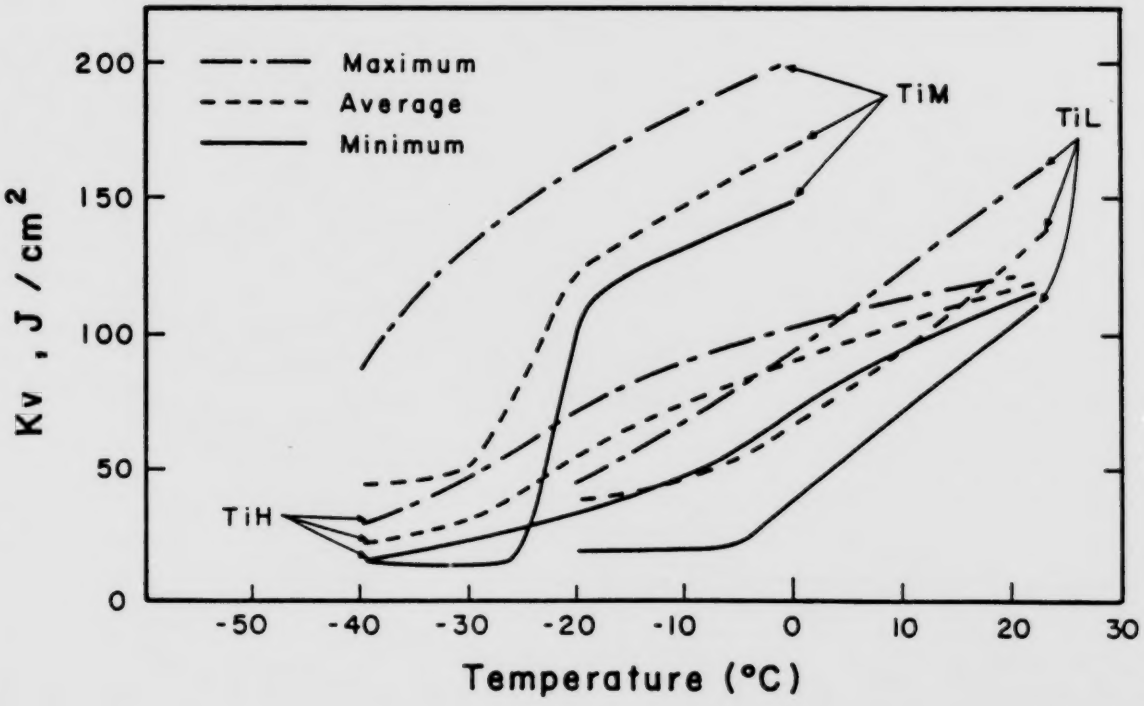

FIGURE 4.24 Impact Transition Curve for Experimental test plates (Large As-deposited Zone) with varying Ti additions.

TABLE 4.5

RESULTS OF CHARPY TESTS FOR EXPERIMENTAL TEST PLATES

(LARGE AS-DEPOSITED ZONE) WITH VARYING S CONCENTRATIONS

Sample name	T(°C)	ABSORBED ENERGY Kv (J/cm^2)					Kv average (J/cm^2)
TiM	0.0	150	155	202	---	---	169
	-20.0	110	133	---	---	---	122
	-25.0	14	54	112	147	---	82
	-30.0	15	45	62	76	---	50
	-40.0	20	23	82	87	---	53
SM	0.0	168	---	---	---	---	168
	-20.0	101	128	---	---	---	114.5
	-30.0	97	103	128	128	---	114
	-35.0	23	57	69	72	146	73
	-40.0	18	32	50	71	---	40
	-50.0	13	13	27	---	---	18
SH	+15.0	81	82	85	---	---	83
	0.0	51	65	76	---	---	64
	-15.0	39	50	52	---	---	49
	-30.0	23	34	35	44	---	40
	-40.0	8	13	18	---	---	13

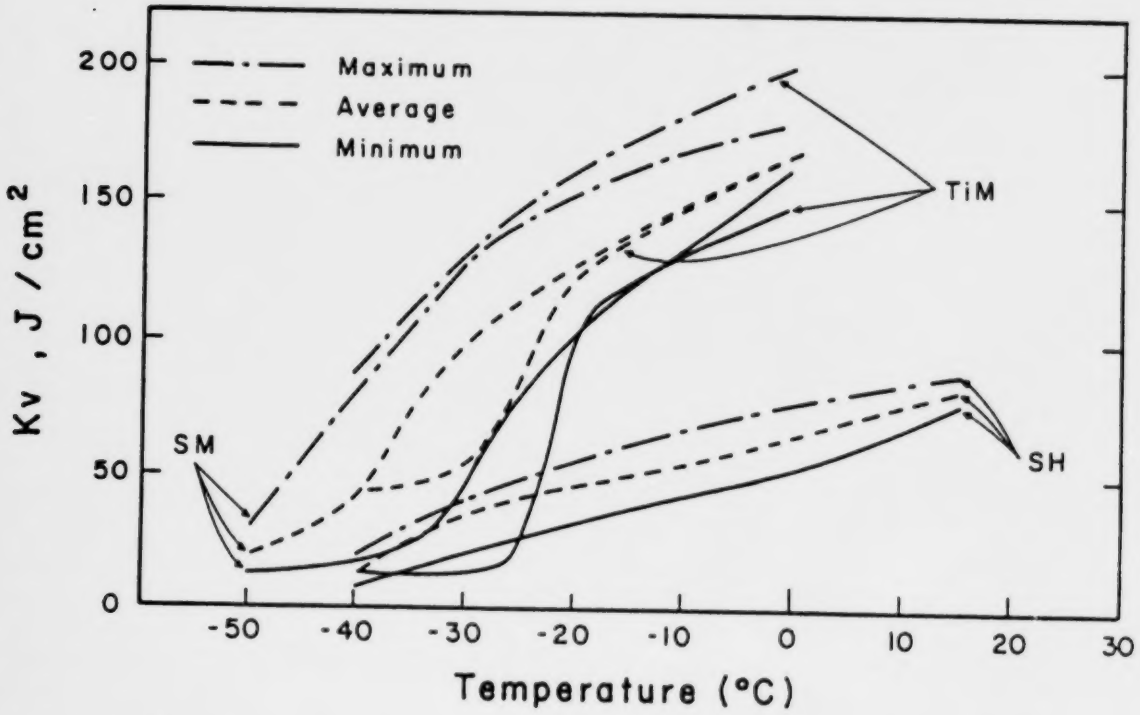

FIGURE 4.25 Impact Transition Curves for Experimental test Plates (Large As-deposited Zone) with Varying Sulphur Additions.

TABLE 4.6

RESULTS OF CHARPY TESTS FOR EXPERIMENTAL TEST PLATES

Sample name	Ti (°C)	ABSORBED ENERGY Kv (J/cm²)					Kv average (J/cm²)
Ti-Ca	0.0	97	123	137	---	---	119
	-20.0	60	67	79	---	---	69
	-25.0	30	59	66	67	86	62
	-30.0	32	71	94	109	---	77
	-40.0	15	16	24	---	---	18
Ti-Al	+23.0	112	115	---	---	---	113.5
	+10.0	45	53	57	---	---	52
	0.0	46	53	60	---	---	53
	-10.0	50	54	60	---	---	55
	-20.0	23	30	41	52	---	37
	-30.0	21	31	---	---	---	26
	-40.0	20	34	---	---	---	27

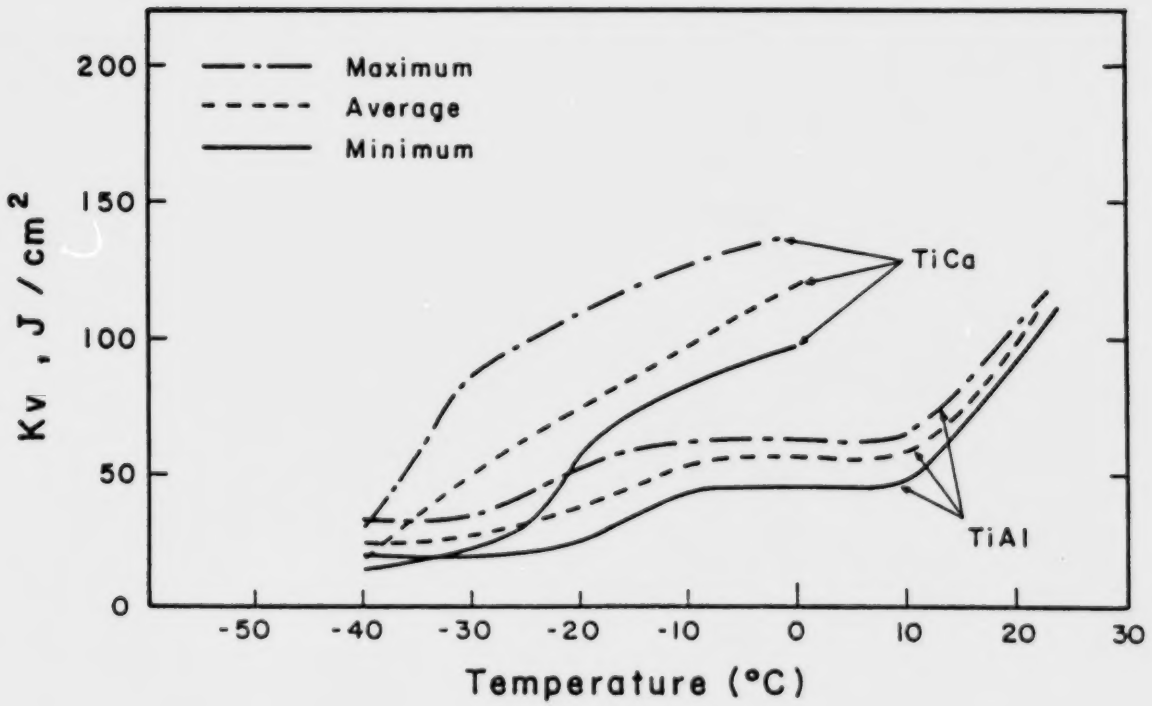

FIGURE 4.26 Impact Transitions Curves for Experimental Test Plates (Large As-deposited Zone) with Ca or Al additions.

TABLE 4.7

RESULTS OF FULL SIZE CHARPY TESTS FOR THE EXPERIMENTAL TEST PLATES

Weld deposits	TRANSITION TEMPERATURE (Tt)			Kv average at 0 °C
	Minimum	Maximum	Average	
TiL	-18	+3	-7	66
TiM	---	-23	-32	166
TiH	-28	-8	-21	90
TiM	---	-23	-32	169
SM	-45	-30	-38	168
SH	-35	-2	-15	64
Ti-Ca	-36	-21	-29	119
Ti-Al	-21	+11	-11	54

TABLE 4.8

RESULTS OF 5x5 CHARPY TESTS FOR EXPERIMENTAL TEST PLATES

WITH VARYING Ti CONCENTRATIONS

Sample name	temperature (°C)	Absorbed Energy Kv (J/cm^2)				Kv average (J/cm^2)
Til	+20	107	---	---	---	107
	0	65	78	90	---	78
	-5	52	72	77	---	67
	-10	13	58	62	64	49
	-20	11	23	67	68	42
SM	+20	107	121	---	---	114
	0	114	---	---	---	114
	-20	75	90	113	---	93
	-30	92	92	94	---	93
	-40	77	78	88	---	81
	-50	62	75	80	---	72
	-60	35	50	68	---	51
TiH	+20	97	---	---	---	97
	0	79	86	94	---	86
	-10	60	70	82	---	71
	-15	47	72	78	---	66
	-20	57	67	72	---	65
	-30	13	34	60	77	46

4.3.1.2. Effect of Ti on Toughness

An increase in the Ti concentration from 0.002 to 0.005% decreased dramatically the transition temperature based on a 50 J/cm^2 criteria (T_{50}) from -7 to -32 C. For still higher levels of Ti of 0.02%, T_{50} increases to -21°C. This, however, is lower than the T_{50} for TiL.

The impact transition is more sharply defined in the TiM sample as compared with the TiL or TiH welds. The lower bound energy increases from 14 J/cm^2 to about 110 J/cm^2 for this weld for a temperature increase of only about 5°C(-25°C to -20°C). By contrast, a similar change in energy level occurs for temperature increases of about 30°C for the TiL (-5 to +25°C) and for 65°C for TiH(-40 to +25°C). This behavior is related partially to differences in the upper shelf energy between the samples (lower energies will decrease the Charpy transition slope) but is also closely tied to the influence of microstructure on the strength and fracture behavior as will be discussed in chapter 5.

4.3.1.3. Effect of S on Toughness

The welds with the two lowest levels of S (0.011% for TiM and 0.013% for SM) have very similar impact transition characteristics, that is, a high upper shelf energy of about 150 to 200 J/cm^2, a transition temperature below -30°C and a high Charpy transition slope. This may be expected due to the almost identical chemical compositions of the two welds. The SM weld has slightly better toughness properties(i.e. lower transition temperatures) due mainly to a decrease in the dispersion of the energy values for temperatures within the impact transition range. The role of nitrogen on this dispersion of impact energies will be discussed in Section 4.3.1.5..

An increase in S to 0.036% leads to a marked deterioration in the impact properties of the weld metal. The upper shelf energy decreases to a value below 100 J/cm^2 and T_{50} increases to a value near -15°C. The slope of the impact transition curve also decreases dramatically. The lower shelf energy and the high transition temperature can be explained, at least partially, by the detrimental effect of the large volume fraction of large inclusions (f_v = 0.61% with 9.8×10^4 inclusions /cm^2 greater than 1 μm in diameter) on the fracture mode.

4.3.1.4. Effect of Ca and Al on Toughness

The Ti-Ca weld (Ti= 0.008%) has a transition temperature, T_{50} of -29°C which is similar to the TiM and SM welds. This weld, however, has a lower upper shelf energy and a lower Charpy transition slope than the TiM and SM welds.

The addition of Al to the flux causes a deterioration in the impact properties which can be related to the large number of large inclusions in this weld metal. The ductile to brittle transition occurs in two stages. The impact energies which are over 100 J/cm^2 above 20°C decrease to an intermediate shelf value of near 50 J/cm^2 for temperatures between 10 and -10 °C. Below this temperature range, there is a further decrease in impact energy until the lower shelf is reached. This two stage ductile to brittle transition behavior is related to changes in the fracture mode as will be shown by the load-displacement curves from the instrumented impact tests presented in Section 4.3.2.3..

4.3.1.5. Effect of Nitrogen on Toughness

The effects of changes in the total nitrogen content of individual Charpy specimens on the total absorbed energy was determined by measuring the N

content for selected Charpy specimens within the impact transition region where the variability in toughness is most marked. The level of N content in ppm is indicated beside the data points for the impact transition curve of TiM(Figure 4.27). Without exception, the specimens with the lower N content (about 100 ppm) have much higher toughness than specimens with higher N contents(about 200 ppm) for the same test temperature. These results underline the importance of a careful control of the N content in order to ensure good impact properties of these welds.

4.3.2. Instrumented Impact Tests of the As-Deposited Weld Metal

4.3.2.1 Introduction

The total absorbed energy for a Charpy test does not give a complete picture concerning the effects of microstructure on the impact resistance. The impact transition depends also on the cleavage fracture resistance, the basic ductility of the material as well as the dynamic yield strength. These are unknown quantities for conventional Charpy testing but by recording the load applied to the Charpy specimen as a function of time during the test, mechanical resistance of the material can be estimated. Hence, through the use of instrumented impact tests, a much more detailed analysis of the fracture behaviour of weld metal is possible. This technique can be used to evaluate the effects of changes in the as deposited weld metal microstructure and composition on the impact properties thereby permiting the development of new electrode compositions on a more rational basis. In the following sections, the strength and deformation characteristics as was determined by instrumented impact tests will be presented.

4.3.2.2. Effect of Ti

Figure 4.28 presents the load-temperature diagrams for the TiL, TiM and TiH welds. In general, both the general yield and maximum loads increase

with increasing Ti content in the weld metal which indicates an overall strengthening of the matrix due to Ti. This can be due to a refinement in the microstructure due to increasing quantities of acicular ferrite but can also be the result of precipitation strengthening during the relatively long cooling times which result from the high heat input.

This marked increase in strength is illustrated in Figure 4.29 which are the load-displacement traces for impact tests for the three weld specimens tested at 0°C. The increase in Ti concentration increases the mechanical resistance of the Charpy specimen but at the same time decreases the displacement needed to reach the maximum load. For comparison purposes, the maximum load can be considered to be the point of unstable crack growth. This is not strictly true since it has been found that crack initiation may have already occurred before the maximum load had been reached[52]. However, the displacement to maximum load can still give an indication of the ductility of the metal under dynamic conditions. For the case of TiH, the higher strength results in a decrease in the overall ductility of the specimen which is a trend commonly observed for steels, especially those that have been precipitation strengthened[53]. The higher strength of the TiH weld may also account for the increase in the impact transition temperature observed for this material. The TiL specimen has smaller displacements to maximum load than the TiM weld for the highest test temperatures. The reasons for this will be discussed in Chapter 5.

4.3.2.3. Effect of S

Figure 4.30 presents the load-temperature diagrams for the weld as a function of the S content. Increasing S content has no effect on the general yield load as would be expected since S in not a strengthening agent. The maximum load for the SH weld is less than that for the lower S welds for

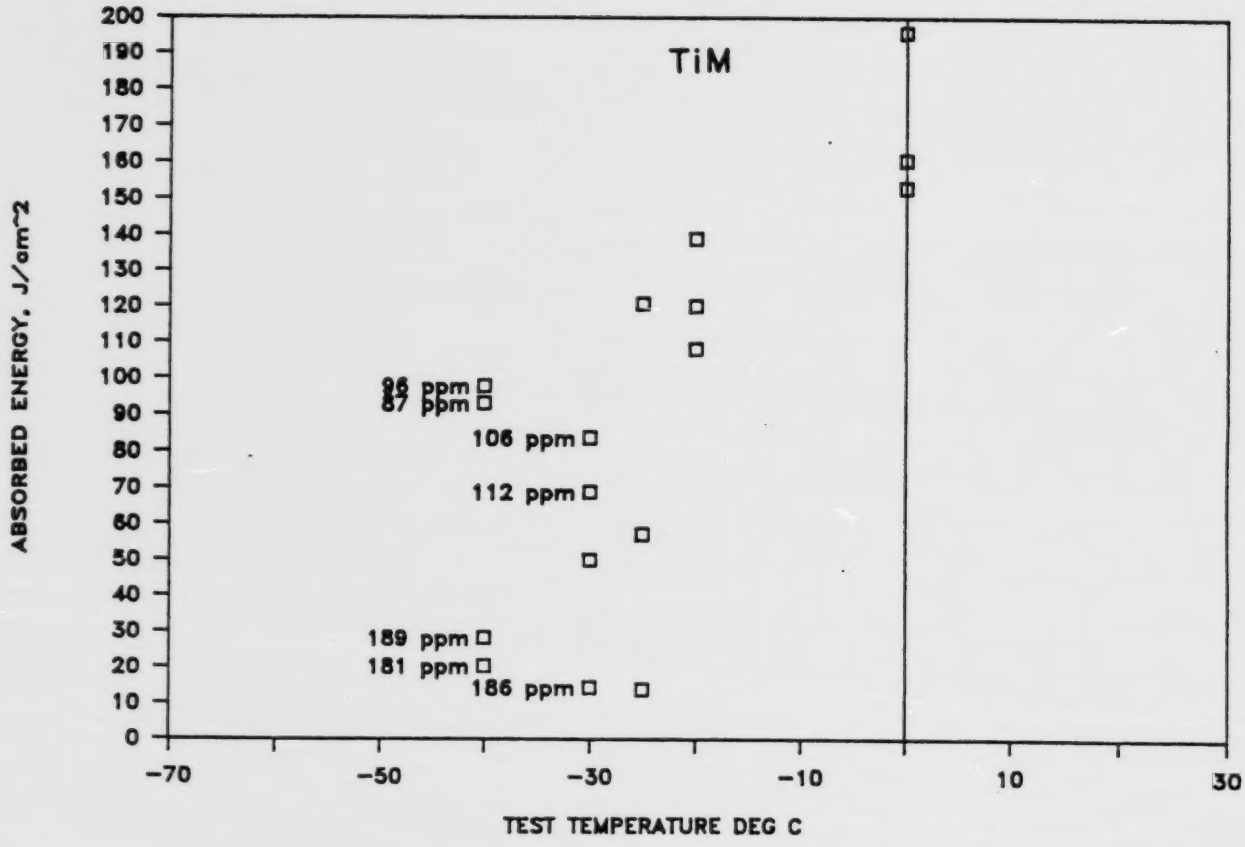

FIGURE 4.27 Effect of N on Impact Energy for TiM Weld

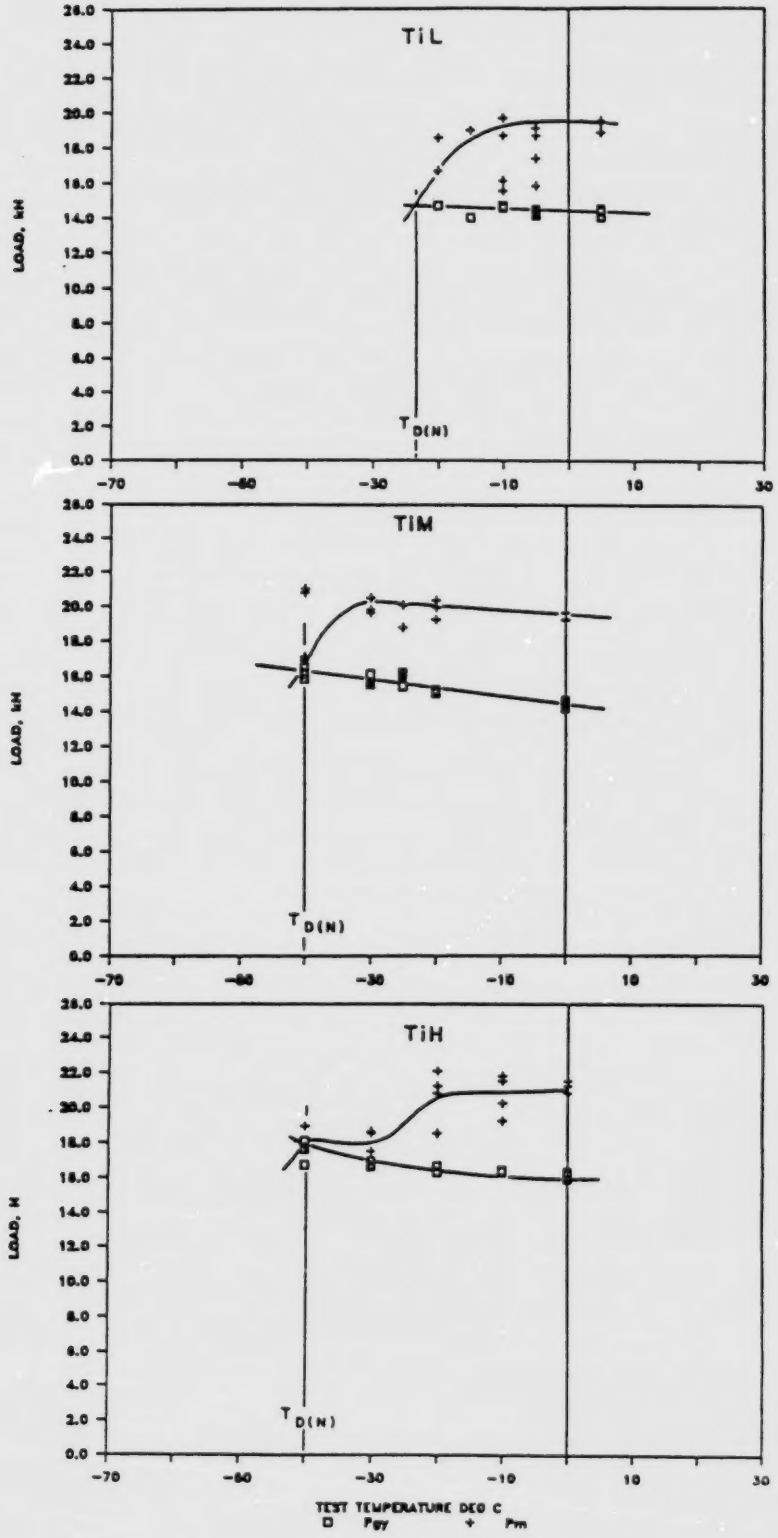

FIGURE 4.28 Load-Temperature Diagrams for TiL, TiM and TiH Welds.

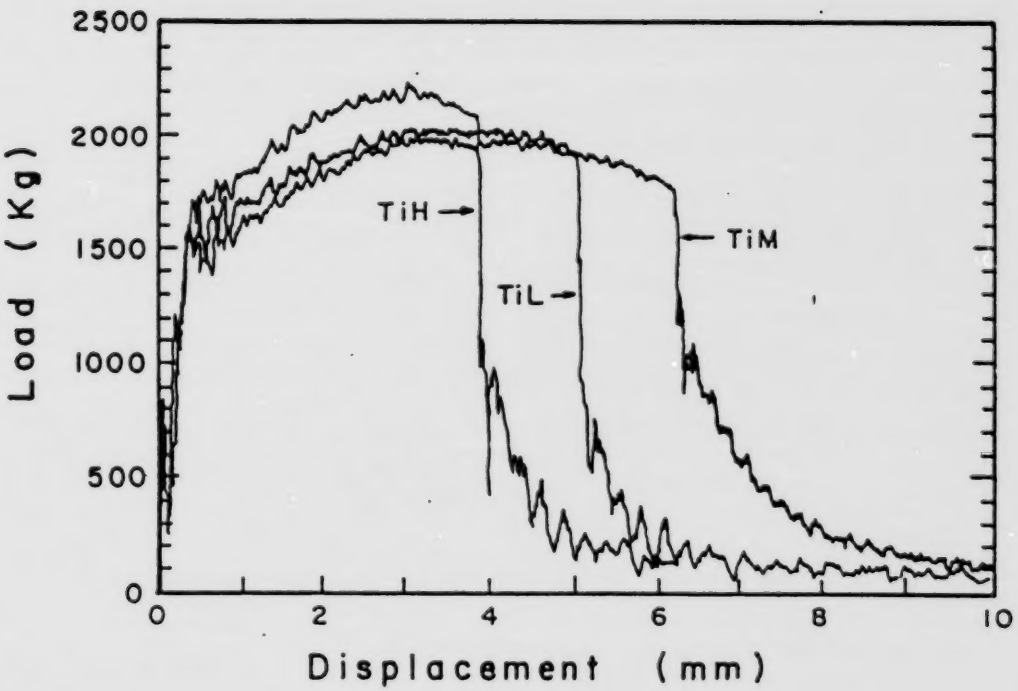

FIGURE 4.29 Load-Displacement Curves for TiL, TiM and TiH Welds Tested at 0 °C.

temperatures within the impact transition region. This can be attributed to a decrease in ductility of the Charpy specimen due to an increase in the volume fraction of large MnS inclusions, which favour the onset of unstable fracture. This effect can be clearly seen by comparing the load-displacement curves for the instrumented impact tests of the TiM and SH welds which were tested at 0°C as is shown in Figure 4.31. Whereas, the TiM sample requires more than 6 mm of displacement to induce the initiation of fast cleavage fracture, the SH specimen requires only slightly more than 2 mm. Since the total energy is related to the area under the load-displacement curve, the early initiation of cleavage fracture will greatly reduce the total absorbed energy.

4.3.2.4. Effects of Ca and Al

Ca additions to the flux increases the quantity of acicular ferrite and the amount of Ti present in the weld metal. These changes are reflected by an increase in the overall strength, an increase in impact transition temperature and a decrease in the ductility of the Charpy specimen. The increased strength is shown in Figure 4.32 which is a comparison of the load-temperature curves for the Ti-Ca and Ti-M welds. The decrease in overall ductility is shown in Figure 4.33 which is a comparison of the load-displacement curves for samples of these two welds tested at 0°C. Note the increase in strength and the decrease in displacement to maximum load for the Ti-Ca weld. These trends are similar to the series of welds with increasing Ti levels which suggest that the increase in Ti in the Ti-Ca weld may be in part responsible for the change in the impact properties.

Al, however, when added to the flux tends to form large Al_2O_3 inclusions in the weld metal as was seen in section (4.2.2.4). This is accompanied by an increase in the Ti level in the weld as well as an increase in the transition temperature. Contrary to the other welds with increased Ti

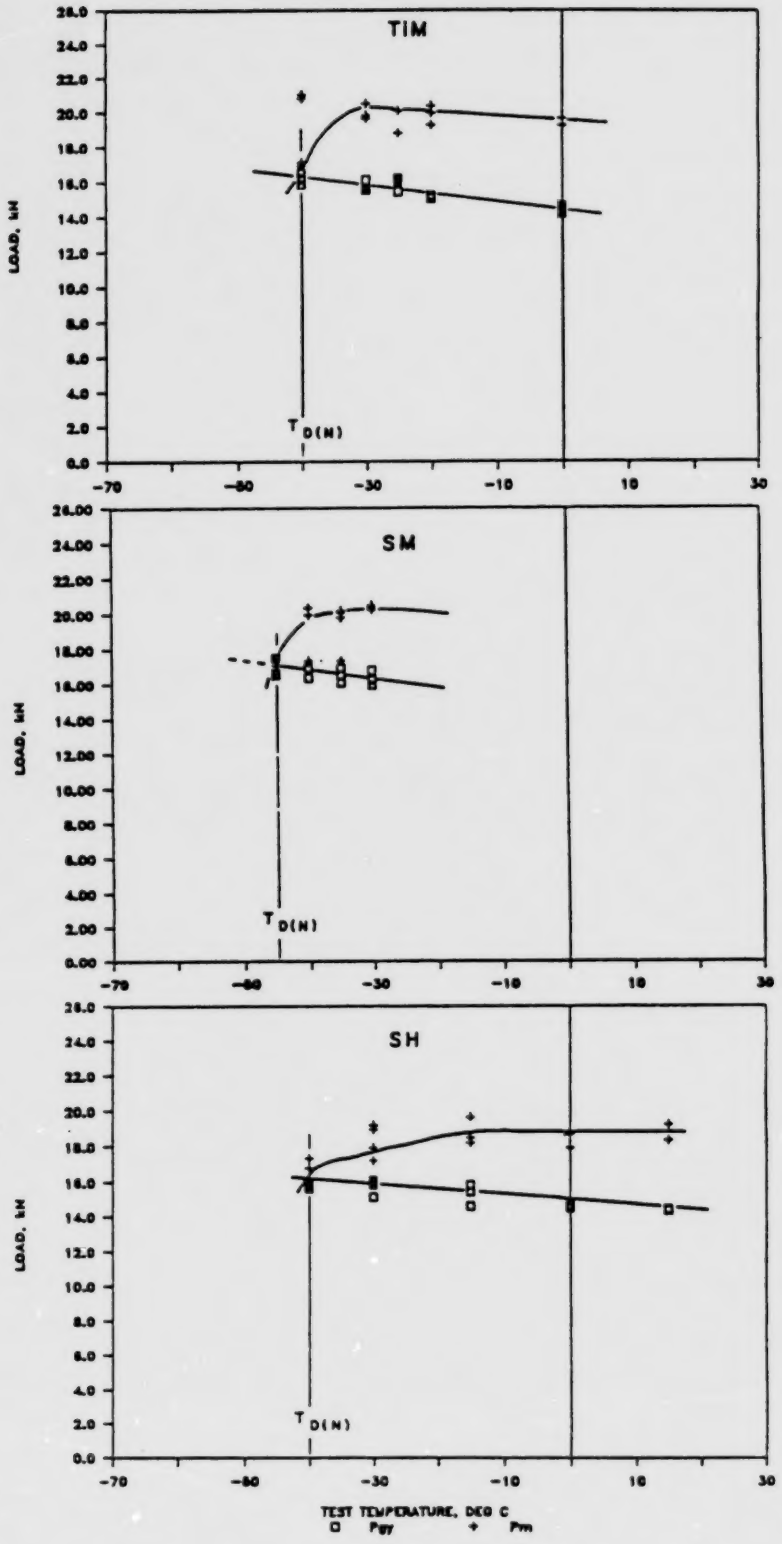

FIGURE 4.30 Load-Temperature Diagrams for TiM, SM and SH Welds.

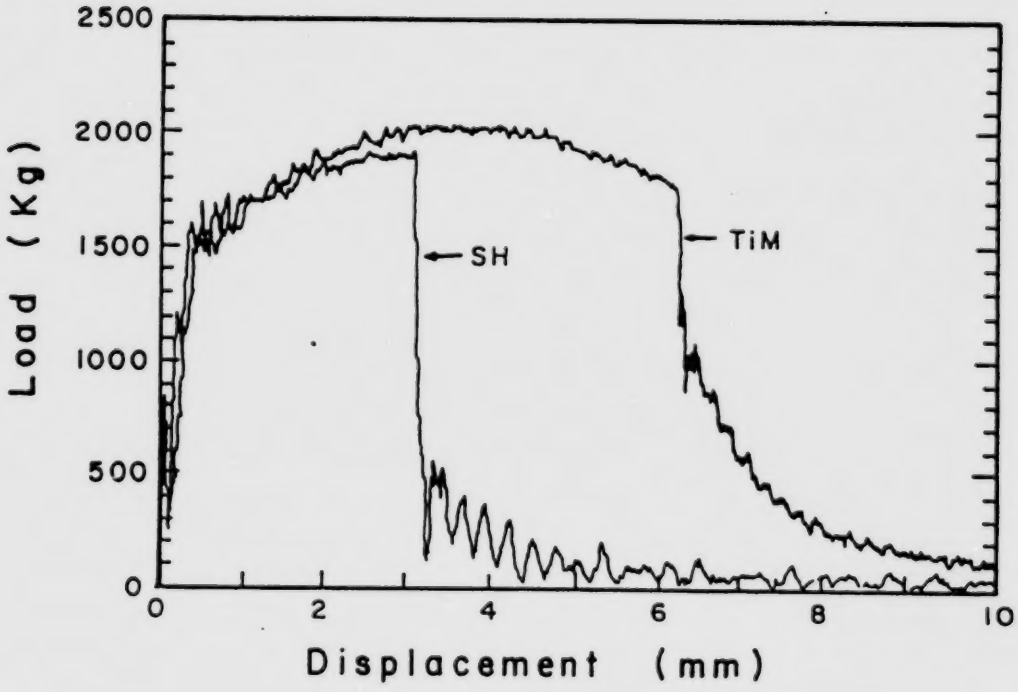

FIGURE 4.31 Load-Displacement Curves for TiM, SM and SH Welds.

Tested at 0 °C.

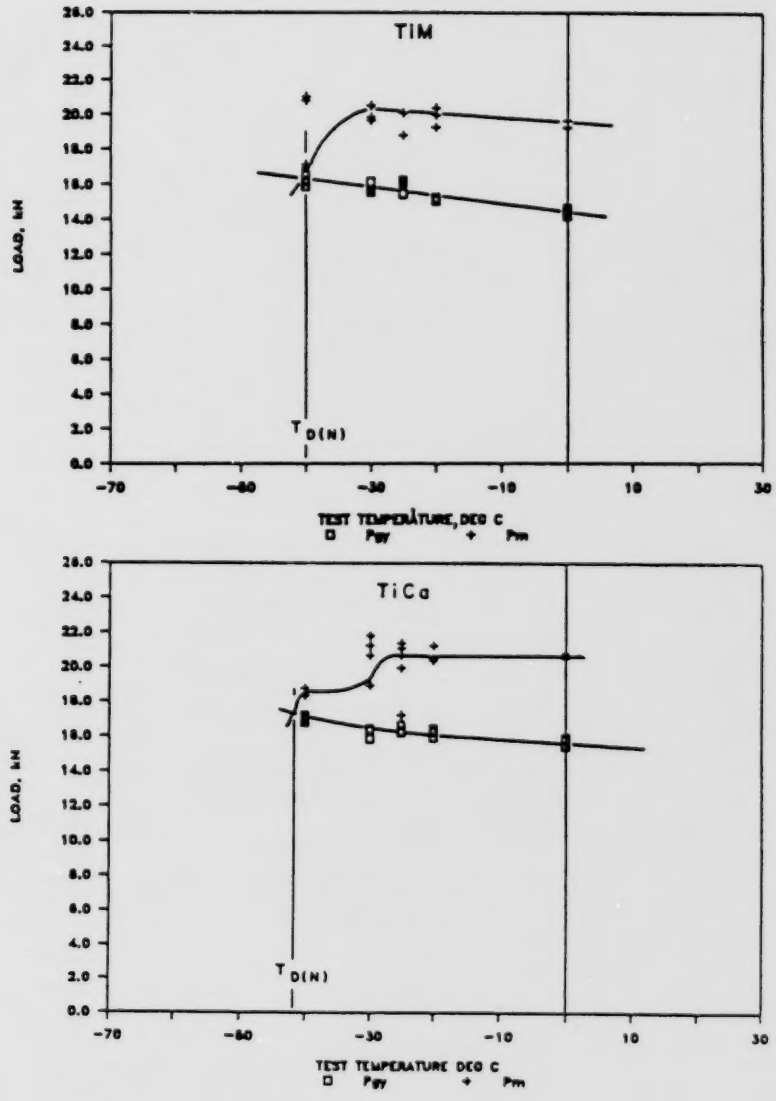

FIGURE 4.32 Load-Temperature Diagrams for TiM and TiCa Welds.

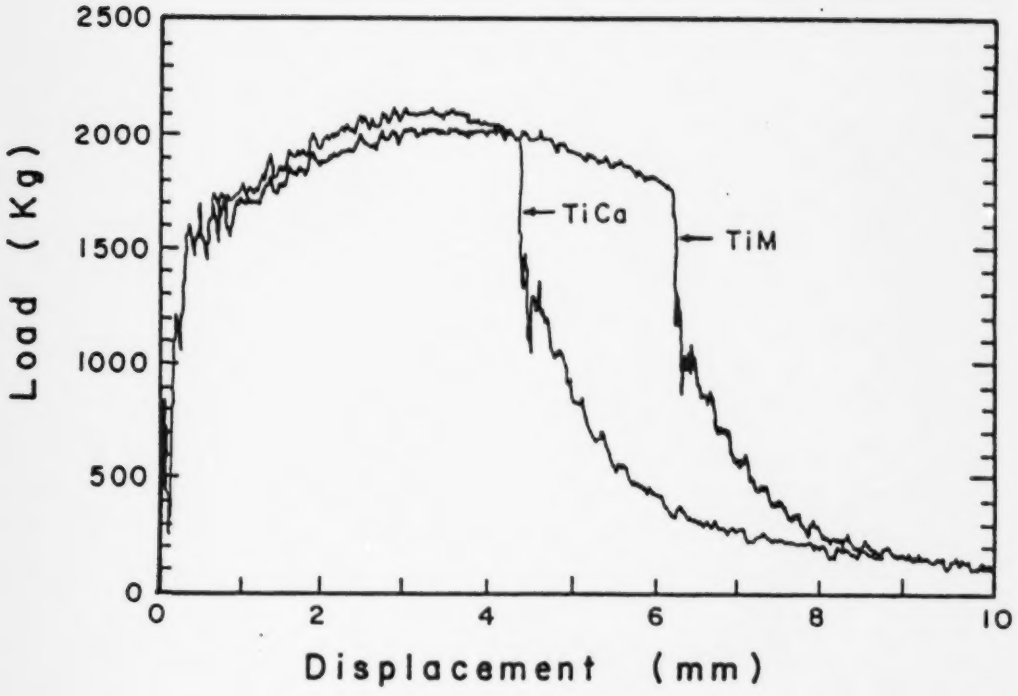

FIGURE 4.33 Load-Displacement Diagrams for TiM and TiCa Welds Tested at 0 °C

content, there is an apparent decrease in the general yield load for the Al containing weld as compared to the TiM weld. This trend can be seen in Figure 4.34 which is a comparison of the load-temperature diagrams for the Ti-Al and TiM welds. However, the load-displacement curves (Figure 4.35) for impact samples of these two welds at 0°C show that there is premature crack initiation occurring in the Ti-Al weld. This accounts for the greatly reduced impact resistance of the Ti-Al weld in the intermediate shelf region. This premature cracking below the notch root relaxes the triaxial stress state thereby reducing the load necessary for general yielding. Thus, the general yield loads measured for the Ti-Al specimen are not likely to give an accurate estimation of the strength of this material. This abnormal fracture behaviour is related to the presence of the large inclusions in this weld.

4.3.2.5 Cleavage Fracture Resistance of As-deposited Weld Metal

The nill ductility transition temperature, $T_{D(N)}$, is the temperature at which the fracture load, P_F, is equal to the general yield load, P_{GY}. The critical cleavage fracture stress, σ^*_F, is 2.18 times the general dynamic yield stress due to stress concentrations of the V-notch. The dynamic yield stress can be calculated directly from the measured general yield load by equation 3.2. If no work hardening the notch root occurs Cutler [54] found that based on strain-rate sensitivity tests of several HSLA steels, the dynamic yield stress is underestimated by about 25% for acicular ferrite HSLA steels using equation 3.2. Hence, to have a more relatistic estimate of the fracture resistance for the present study, all dynamic yield strengths were increased by 25% before a calculation of σ^*_F was performed.

The results of this analysis is presented in Table 4.9. The TiL specimen (8% AF) has to lowest resistance to cleavage fracture, 2100 MPa wheras the two specimens with high AF contents have the highest cleavage

TABLE 4.9

DYNAMIC YIELD AND FRACTURE PROPERTIES OF EXPERIMENTAL TEST PLATES (LARGE AS-DEPOSITED ZONE)

Weld Sample	T_{DN} (°C)	P_{GY} at T_{DN} (N)	σ_F^* estimated (MPa)	σ_{YD} estimated (MPa)
TiL	≈ -25	15000	2125	975
TiM	≈ -40	16800	2380	1092
TiH	≈ -42	18000	2550	1170
SM	≈ -45	17000	2408	1105
SH	≈ -40	16400	2323	1066
TiCa	≈ -45	17700	2508	1155
TiAl	≈ -40	15600	2210	1014

fracture resistance of about 2500MPa. The other specimens with intermediate quantities of AF have intermediate values of cleavage fracture strength. These results highlight the beneficial effects of acicular ferrite on the clevage fracture resistance of weld metal.

The σ^*_F value for the Ti-Ca weld should not be compared with those of the other welds since premature crack initiation was observed in this specimen and the true dynamic yield strength could not be measured. The σ^*_F value of 2400 MPa will be less than the true cleavage fracture strength.

The $T_{D(N)}$ temperatures varied little with weld metal composition except for the TiL specimen which contained little AF. Comparing the TiM and TiH welds, there is a increase in strength of the TiH weld but this is compensated for by an increase in the cleavage fracture resistance which results in little change in $T_{D(N)}$. The microstructure changes responsible for the increased strength are also increasing the cleavage resistance. This interesting result will be discussed in Chapter 5.

4.3.3. Fractographic Studies

4.3.3.1. General Trends

The quantity of the various microstructural constituent phases plays an important role on the fracture behaviour. In general, the FS and PF(G) phases are more prone to cleavage fracture than is the AF as will be seen in Sections 4.3.3.2.. This results in fracture surfaces with a blocky appearance (large cleavage facets, the coarseness of which is determined by the distance between the PF(G) and FS phases). As the quantity of these phases decrease, the size and number of cleavage facets on the fracture surface decreases. The AF regions usually failed by ductile tearing or quasi-cleavage fracture. Large inclusions in the SH welds were found to promote cleavage fracture.

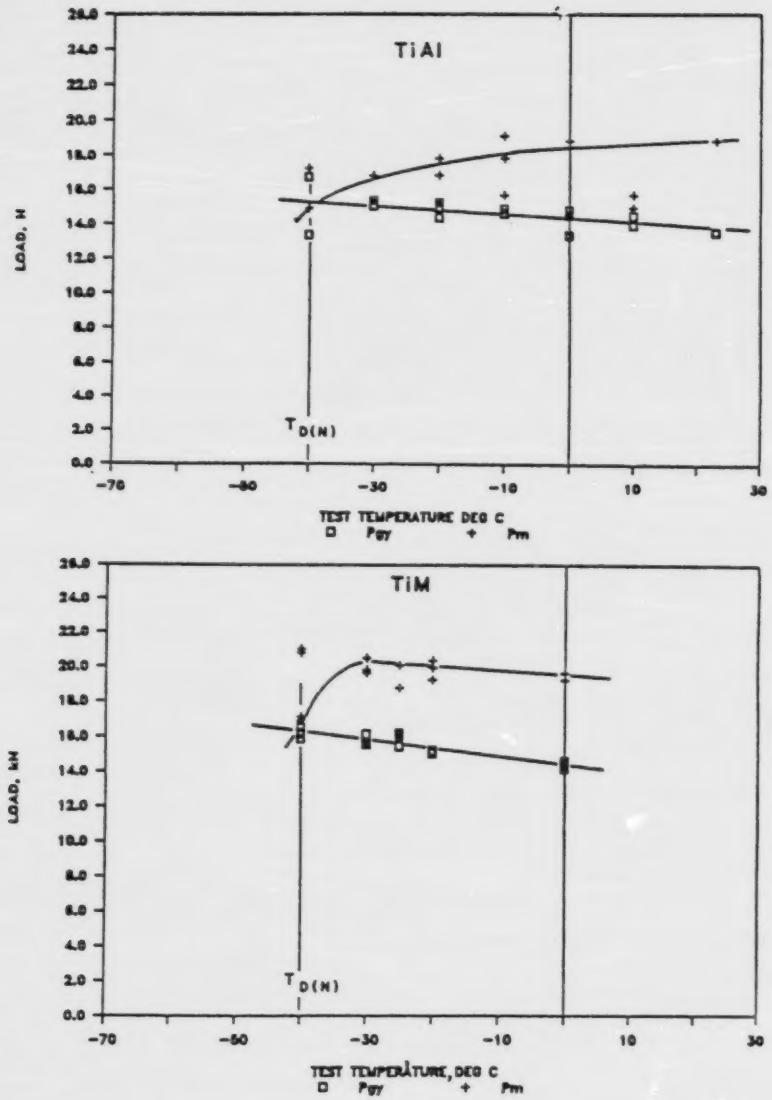

FIGURE 4.34 Load-Temperature Diagrams for TiM and TiAl Welds.

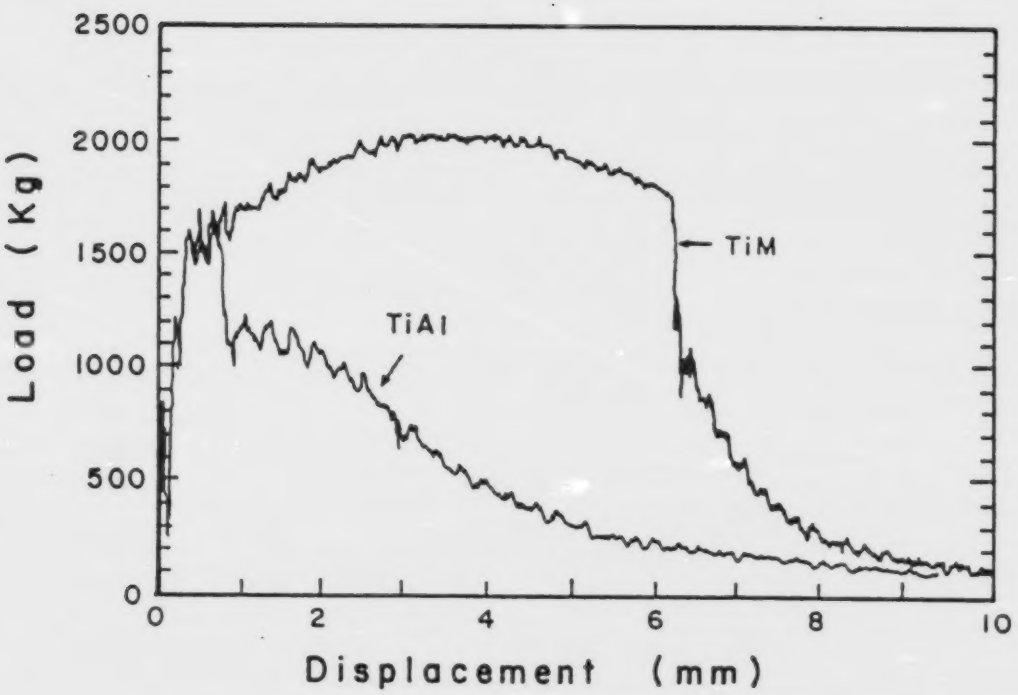

FIGURE 4.35 Load-Displacement Curves for TiM and TiAl Welds Tested at 0 C

4.3.3.2. Effect of Ti

The specimen with the low Ti content, TiL, is composed of 42.0% FS(NA) and 35.0% FS(A). This structure has a poor cleavage fracture resistance since there are few high angle boundaries to deflect the cleavage cracks and the large martensite-austenite constituent phases on the lath boundaries are preferential sites for cleavage crack nucleation. The effective grain size controlling cleavage fracture is large for this type of microstructure as is illustrated in Figure 4.36(a) which is a fractograph of a Charpy specimen tested at -30°C. Note the large size of the cleavage facets. An oblique section of the same specimen, Figure 4.36(b), reveals that the FS(A) structure is largely responsible for the large cleavage facets. The main crack can be seen traversing completely a region of FS(A) without a significant deviation in the crack direction over a distance of about 100 μm(arrow in Figure 4.36(b)). It should be noted that the cleavage crack is almost invariably at 45 degrees to the aligned martensite-austenite microconstituent in the FS(A) phase which shows that cleavage fracture occurs on specific crystallographic orientations.

An increase in the Ti level in the TiM weld, results in an increase in the percentage of AF and an improvement in the toughness. This is a result of the increased resistance of the AF structure to cleavage crack initiation and propagation as was measured in Section 4.3.2.5 which results in a decrease in the effective grain size controlling cleavage fracture since a large proportion of the FS microstructure in TiL is replaced by AF in TiM.

These trends are illustrated in Figure 4.37 which are representative fractographs and oblique sections taken from the TiM weld which was tested at -30°C. Long cleavage facets oriented in the direction of the prior austenite grain boundaries are separated by regions of ductile tearing (Figure 4.37(a)). Oblique sections (See Figure 4.37(b)) show many non-propagating

cleavage microcracks just below the fracture surface. They are associated with the PF(G) and FS regions of the sample. Almost no microcracks are found in the AF regions. Extensive plastic deformation occurs in the AF during the propagation of the main fracture (Figure 4.37(c)) requiring significant energy.

Further increases in the Ti level in TiH, increases the proportion of AF. There is, however, no improvement in the impact resistance. Figure 4.38 presents a fractograph and an oblique section of a specimen of this weld tested at -30^{o}C. The number and size of the cleavage facets is smaller in this specimen than it is for the TiM specimen. Considerable ductile tearing can be observed between the cleavage facets as can be seen in Figure 4.38(a). Oblique sections (Figure 4.38(b)) reveal that the non-propagating microcracks are limited to the FS(A) and PF(G) microstructures. The microcracks are shorter that in TiM due to the narrower PF(G) and FS phases along the prior-austenite grain boundaries. Few microcracks can be observed in the AF. Failure of the AF occurred by shear since numerous micro- voids can be observed just below the main fracture surface. These microvoids presumably are formed around inclusions or the martensite-austenite microconstituent phases.

a

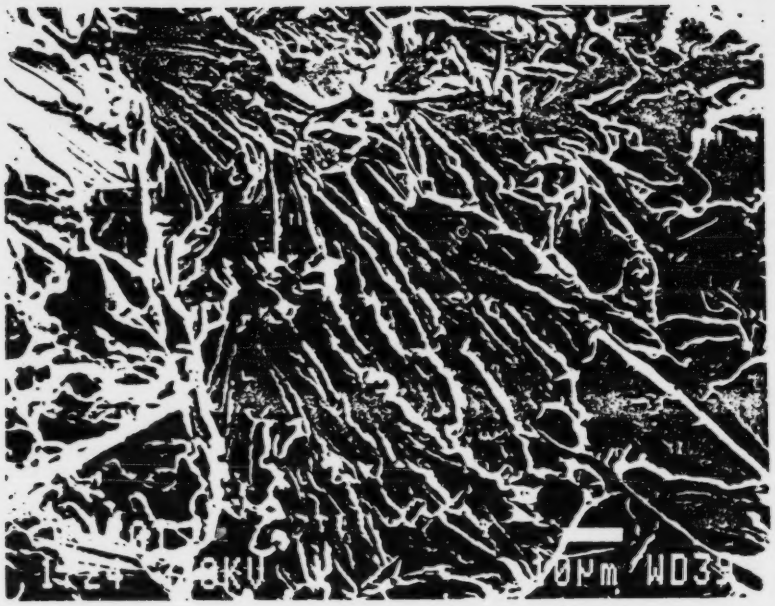

b

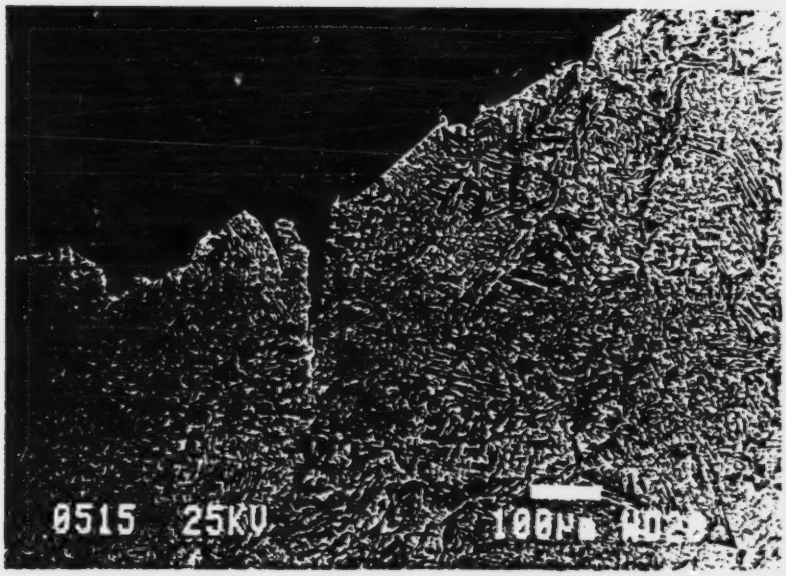

FIGURE 4.36 Fractograph and Oblique Sections of TiL Weld Impact Tested at -30 °C. (a) Fractograph (b) Oblique Section

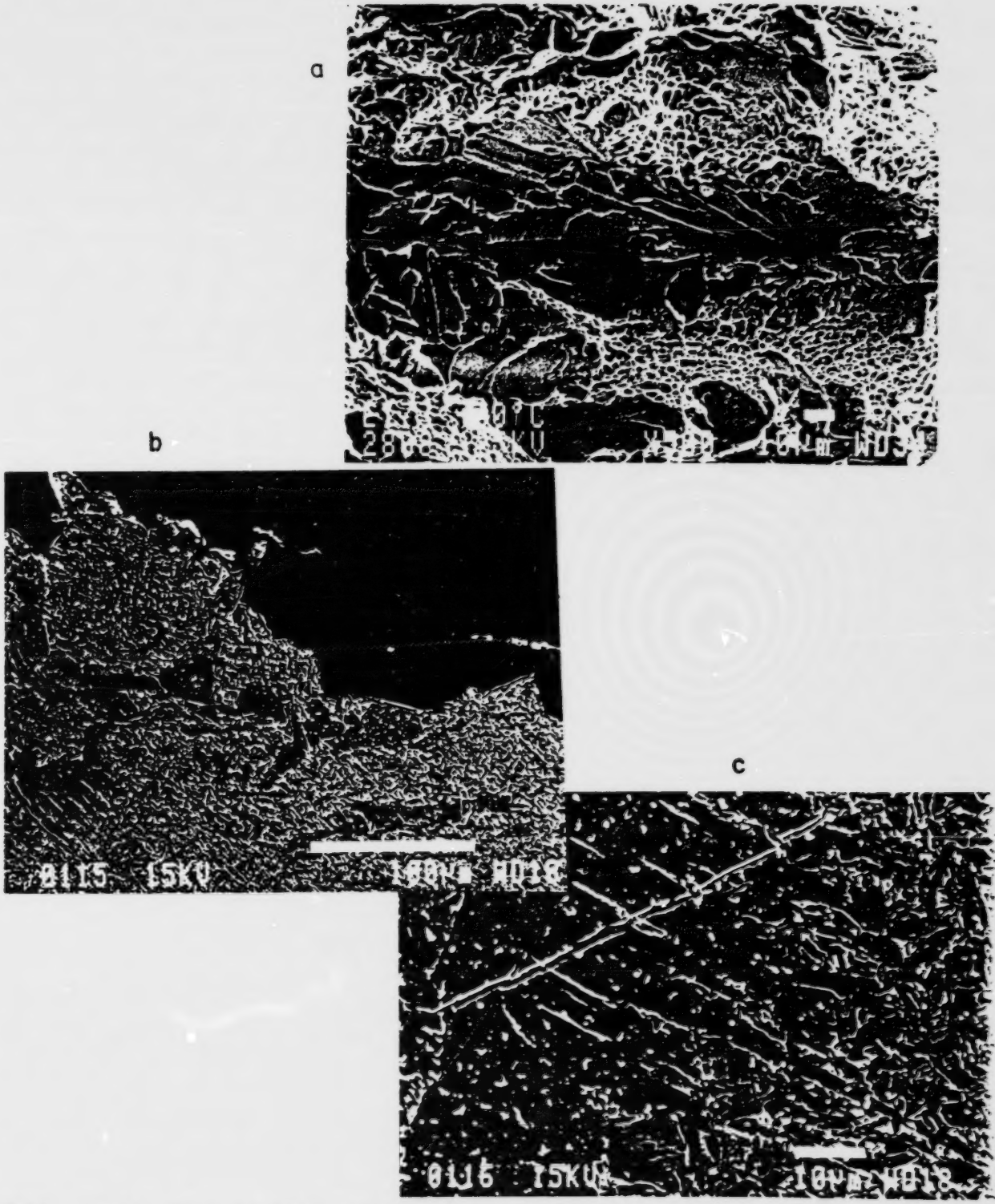

FIGURE 4.37 Fractograph and Oblique Section of TiM Weld Impact Tested at -30 °C. (a) Fractograph (b) and (c) Oblique Sections

a

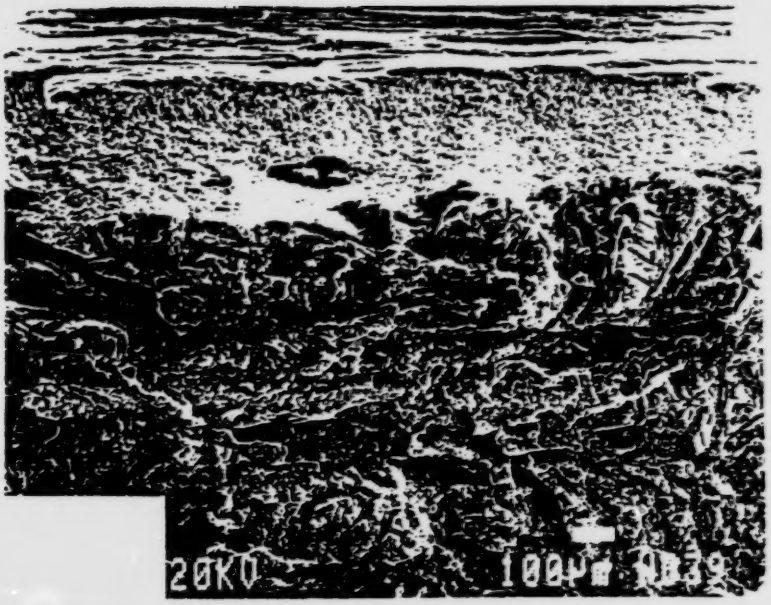

b

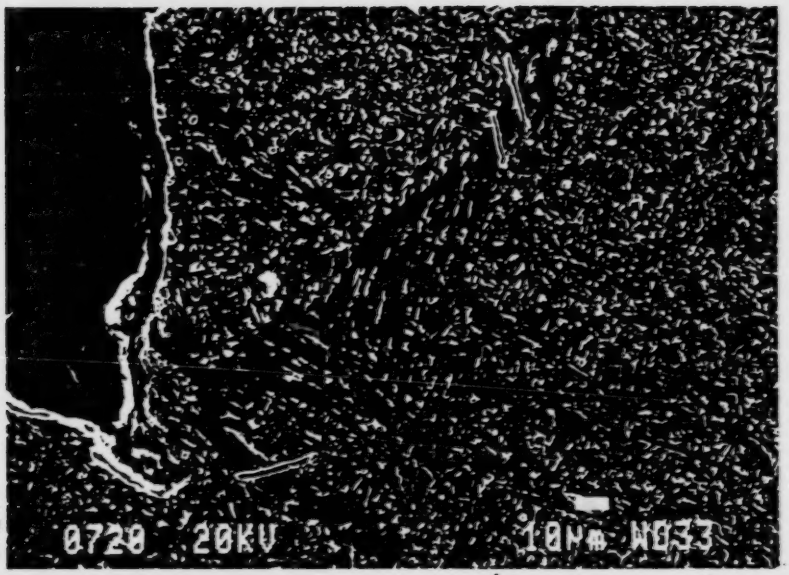

FIGURE 4.38 Fractograph and Oblique Section of TiH Weld Impact Tested at -30 °C. (a) Fractograph (b) Oblique Section

4.3.3.3. Effect of S

The fracture characteristics of the low S weld TiM was discussed in Section 4.3.3.2. The medium S specimen SM has similar fracture characteristics to those of TiM.

By contrast, many more cleavage facets are observed for the high S specimen, SH. Many smaller secondary cleavage cracks were observed between the large cleavage facets as is shown in Figure 4.39(a). Cleavage failure was initiated often at large MnS inclusions (See Figure 4.39(b)). Oblique sections show that contrary to the lower S containing weld, numerous microcracks also form in the region of AF. These microcracks, however tend to be shorter, presumably due to the small effective grain size of the AF grains. These short microcracks were seen to initiate at large MnS inclusion, as is illustrated in Figure 4.39(c).

4.3.3.4. Effect of Ca and Al

The addition of Ca increases the volume fraction of large inclusions as well as increases the strength. These factors, alone, would be expected to decrease dramatically the toughness but this is not the case for the Ti-Ca weld. The 50 J/cm^2 transition temperature only increases 5 $^{\circ}$C from that of TiM. The large proportion of AF in this weld improves the fracture resistance. (σ^*_F = 2500 MPa).

As was the case with the other welds, cleavage fracture occurred in the PF(G) and FS microstructures (Figure 4.40 (a)). The proportation of the fracture surface occupied by large cleavage facets decreases from that for TiM which contains less AF. Cleavage fracture also occurred in the AF regions of the weld, but it was much more difficult as is indicated by Figure 4.40 (b) which shows a mixed mode fracture, small cleavage facets are separated by

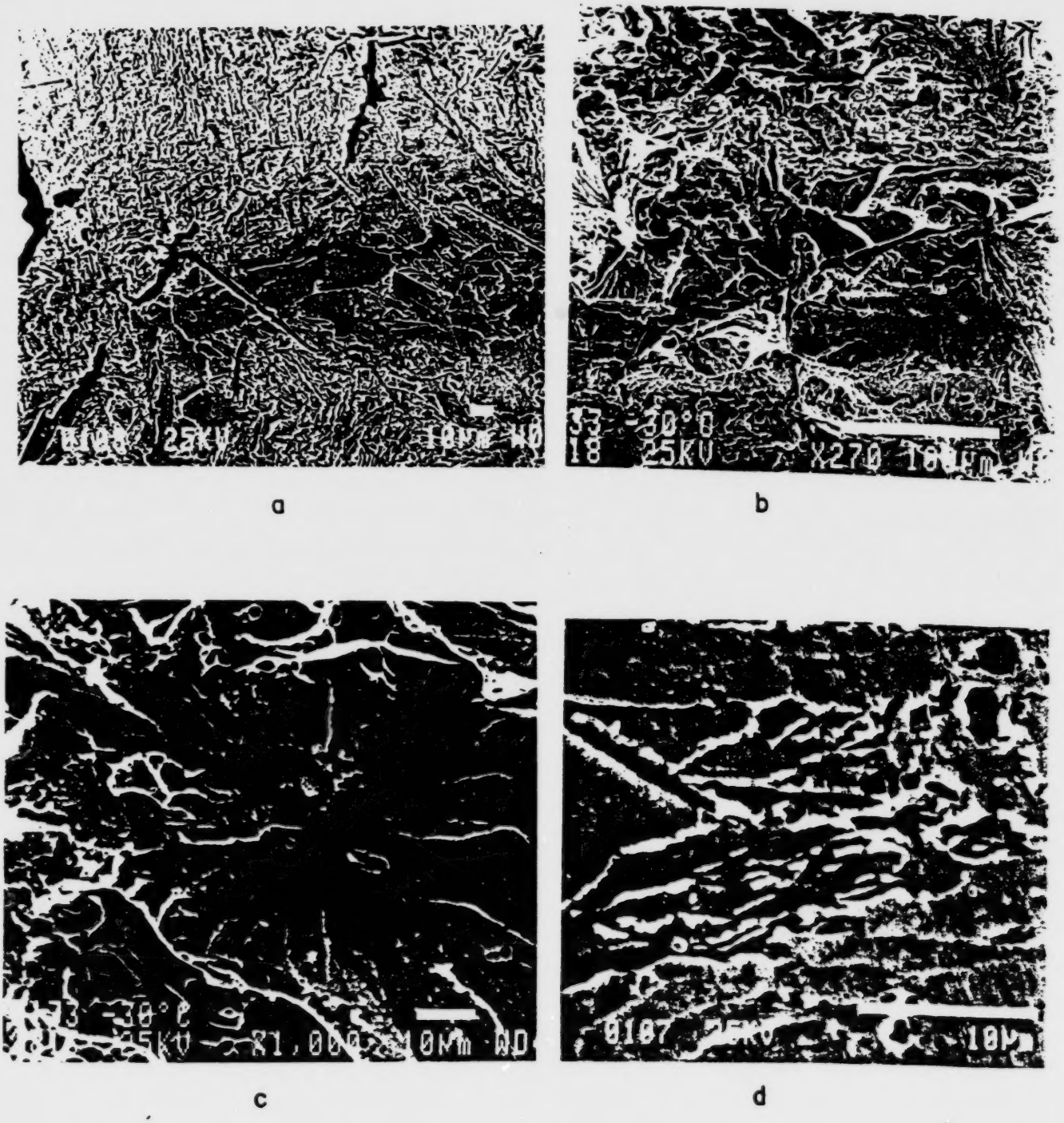

FIGURE 4.39 Fractograph and Oblique Section of SH Weld Impact Tested at -30 °C. (a) and (b) Fractographs (b) and (d) Oblique Sections.

ductile tear ridges or regions of microvoids. Many short non-propagating cleavage microcracks are found in the AF structure just beneath the main fracture surface as is shown in Figure 4.40(b). These formed presumably due to the presence of many larger inclusions. As a result, fractographs in the AF regions of the main fracture, exhibit a quasi-cleavage type fracture as is shown in Figure 4.40(c). Small cleavage facets were sometimes sean to initiate at cracked inclusions (See arrows in 4.40(c)). These results suggest that the AF has a small effective grain size and hence an inherent resistance to cleavage fracture and can better resist the detrimental effects of larger inclusions on the toughness.

For the Ti-Al weld, the load-displacement traces of the instrumented impact tests show that there is premature fracture initiation for temperatures in the impact transition region. Fractographic studies of a Charpy impact specimen show that fracture initiation occurs by ductile shear at the notch root as is shown in Figure 4.41(a). The fracture propagates mainly by a quasi-cleavage mechanism with considerable tearing between the small cleavage facets as is shown in Figure 4.41(b). Significant shear lips were observed on the sides of fracture Charpy specimen which accounts for the high post fracture energies of the Ti-Al weld.

4.3.3.5. Effect of Nitrogen

Increased nitrogen levels of about 100 ppm from ≈ 100 ppm to 200 ppm for the TiM weld tested at -30 C decreased the total absorbed energy by 75 J/cm^2. Fractographic evidence indicates that this is due in part to a decreased cleavage fracture resistance of AF with high N levels. Comparing figure 4.37 and 4.42(a) which is a specimen with low N levels with figure 4.42(b) and (c) which is a specimen with high N levels the following conclusions can be drawn. For the weld with low N, cleavage fracture is confined to

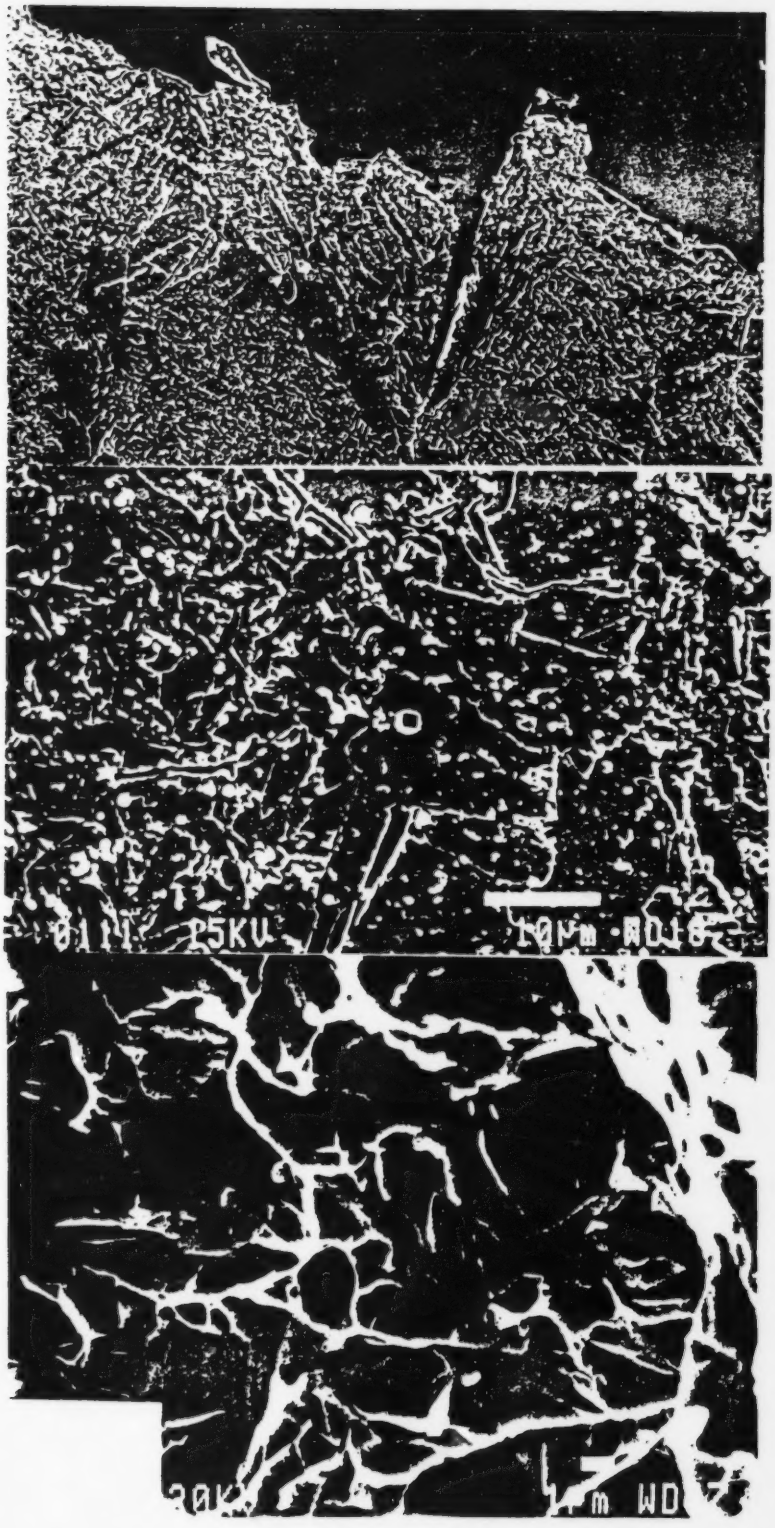

FIGURE 4.40 Fractograph and Oblique Sections of TiCa Weld Impact Tested at -30 °C. (a) and (b) Oblique Sections (c) Fractograph

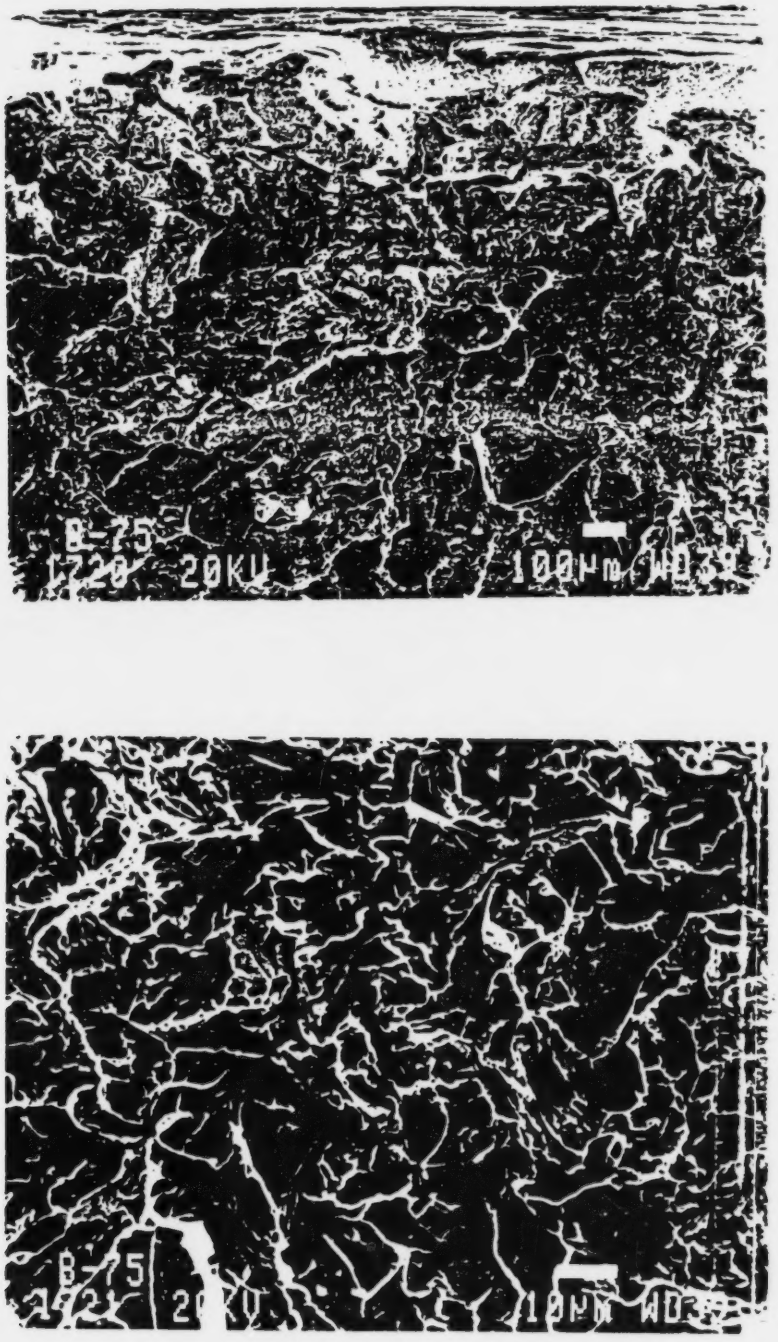

FIGURE 4.41 Fractographs of TiAl Weld Tested at 0 °C.

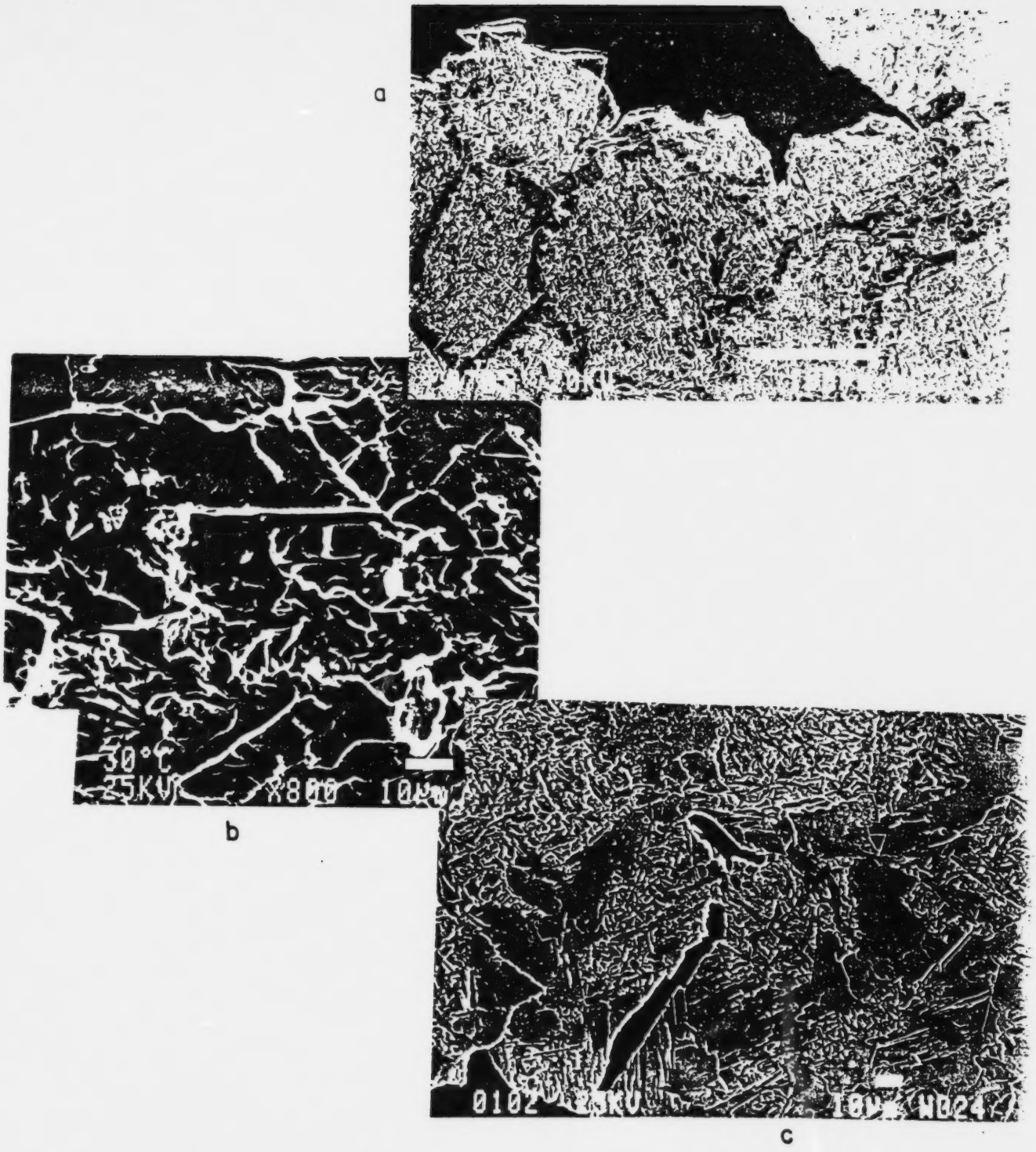

FIGURE 4.42 Fractograph and Oblique Sections of TiM Welds with Low and High Levels of N, Impact Tested at -30 °C. (a) Oblique Section of Low N Weld (b) and (c) Fractograph and Oblique Section of High N Weld.

the PF(G) and FS phases. Almost no cracking of the AF occurs (figure 4.42(a)). For the high N weld, extensive cracking of the AF phase was also observed. A region of AF fails by quasi-cleavage fracture with extensive secondary cracking also occuring (figure 4.42(b)). Many non-propogating cleavage microcracks occur in the AF regions although they tend to be blunted (figure 4.42(c)). These results indicate that higher levels of N decrease the cleavage fracture resistance of the AF although the AF remains more resistant than the PF(G) or FS phases since extensive blunting of the cleavage microcracks occurs in the AF. The significance of these important observations to the impact fracture resistance of weld metal will be discussed in Chapter 5.

4.3.4. Toughness of Standard CSA Welds

Tables 4.9 to 4.11 and Figures 4.43 to 4.45 present the data for the toughness tests as well as the impact transition curves for the standard CSA test welds for the three series studied. Electrodes identical to those used for the large pass welds were used for these welds. Table 4.12 summarizes the minimum, maximum and average 50 J/cm^2 transition temperatures.

There is a decrease in the impact transition temperature for the standard welds as compared with the large pass welds which is due, in part, to the almost total lack of as-deposited weld metal in the fracture path in the standard weld. The final pass thickness, being only a few millimeters, limits the effect of the as-deposited weld metal on crack propagation to one side of the Charpy specimen. The region of the Charpy specimen where fracture initiation occurs is composed entirely of reheated metal which has a much finer structure and hence a higher resistance to cleavage fracture.

Changes in Ti, S, Ca and Al contents of the electrodes or flux also had an effect on the concentration of the other elements, notably Mn and Si.

For this reason it is difficult to assess the effects of these alloy elements on the weld metal properties. Nevertheless, the electrodes which gave the best toughness for the large last pass welds also gave the best toughness in the standard CSA welds. It should be noted, however, for the standard welds, the welds with the lowest S , TiM, has better impact resistance than the SM weld. The reverse was observed for the large pass experimental weld. For the serie with varying Ti level, TiM gave the best impact resistance for the two types of welds. Overall, the best impact resistance is obtained for the TiM standard weld. Impact transition temperatures of less than -65 °C were obtained for this electrode which meets one of the objectives of this study.

TABLE 4.10

RESULTS OF CHARPY TESTS FOR STANDARD TEST PLATES

FROM ELECTRODES WITH VARYING TI ADDITIONS

Sample name	T(°C).	ABSORBED ENERGY Kv (J/cm^2)					Kv average (J/cm^2)
TiL	-30.0	166	---	---	---	---	166
	-40.0	68	124	143	---	---	112
	-50.0	25	54	94	117	123	83
	-60.0	30	42	96	---	---	56
TiM	-40.0	164	168	181	---	---	171
	-50.0	133	147	166	---	---	149
	-60.0	89	97	110	111	---	102
	-70.0	50	99	---	---	---	74.5
	-75.0	16	24	---	---	---	20
TiH	0	149	---	---	---	---	149
	-20.0	80	89	95	---	---	88
	-40.0	56	60	63	---	---	60
	-50.0	39	44	63	---	---	49

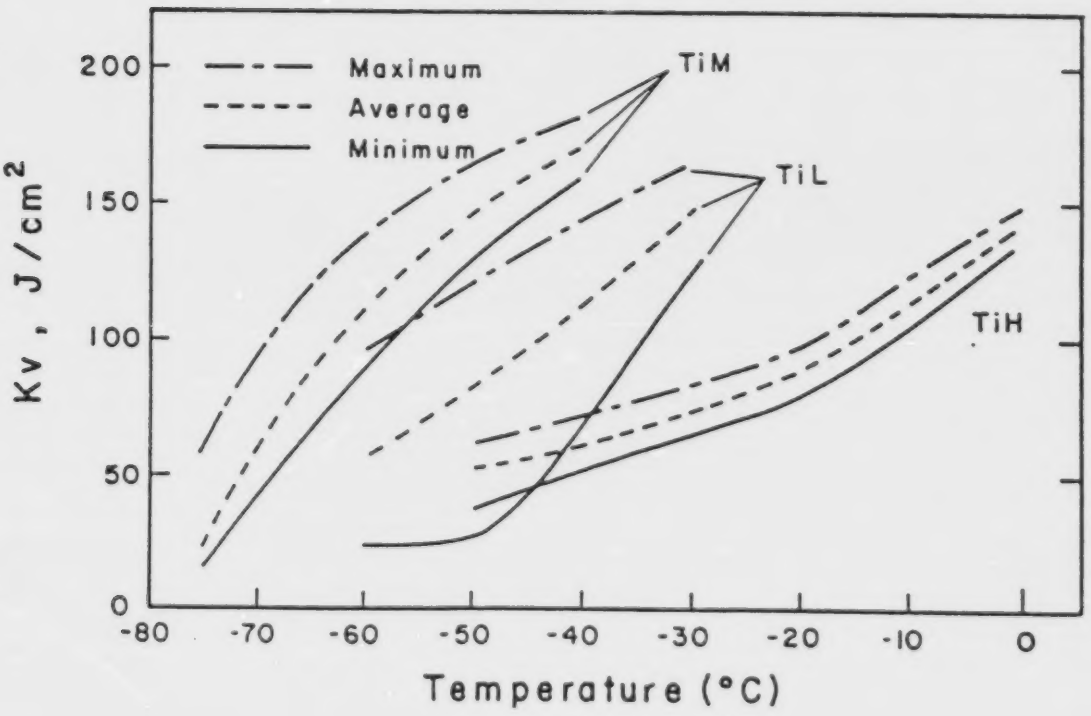

FIGURE 4.43 Impact Transition Curves for Standard Test Plates from Electrodes with Varying Ti Additions.

TABLE 4.11

RESULTS OF CHARPY TESTS FOR STANDARD TEST PLATES

FROM ELECTRODES WITH VARYING SULPHUR ADDITIONS

Sample name	T(°C)	ABSORBED ENERGY Kv (J/cm^2)					Kv average (J/cm^2)
TiM	-40.0	164	168	181	---	---	171
	-50.0	133	147	166	---	---	149
	-60.0	89	97	110	111	---	102
	-70.0	50	99	---	---	---	74.5
	-75.0	16	24	---	---	---	20
SM	-30.0	180	---	---	---	---	180
	-40.0	104	147	158	---	---	136
	-50.0	96	111	146	---	---	118
	-60.0	60	86	97	---	---	81
	-70.0	27	50	50	---	---	39
SH	-20.0	97	106	107	---	---	103
	-30.0	81	81	97	---	---	86
	-40.0	78	78	90	---	---	82
	-50.0	32	37	55	---	---	41
	-60.0	19	21	34	---	---	25

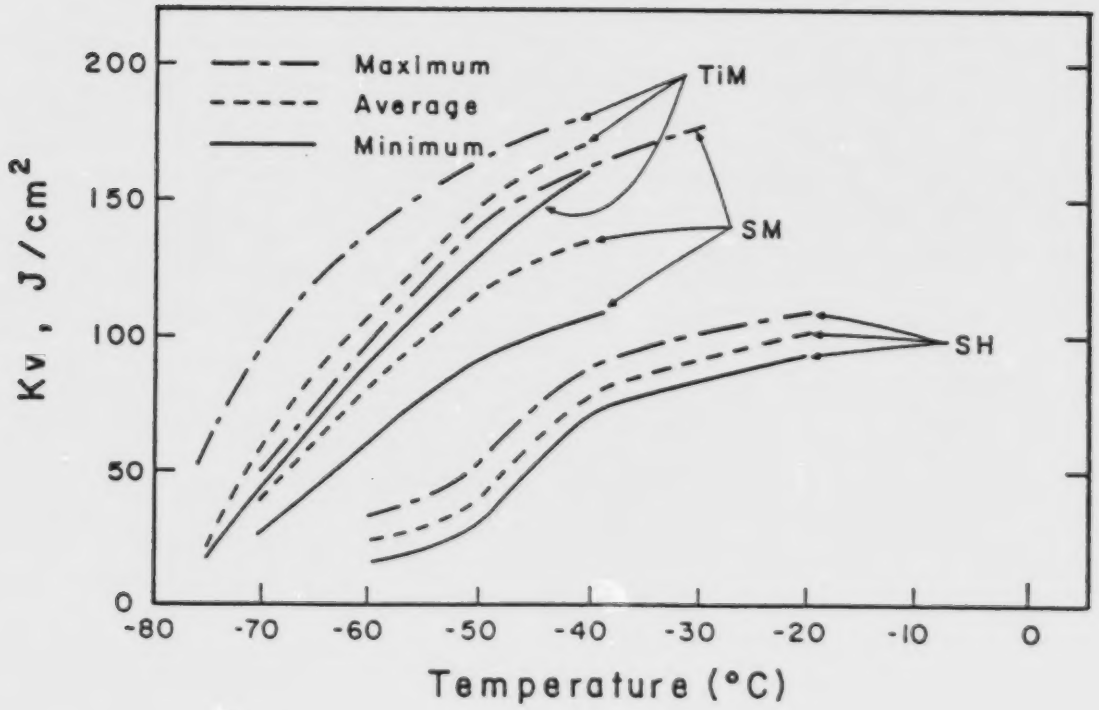

FIGURE 4.44 Impact Transition Curves for Standard Test Plates from Electrodes with Varying sulphur additions.

TABLE 4.12

RESULTS OF CHARPY TESTS FOR STANDARD TEST PLATES

FROM ELECTRODES WITH CA AND AL ADDITIONS

Sample name	T(°C)	ABSORBED ENERGY Kv (J/cm^2)					Kv average (J/cm^2)
Ti-Ca	-30.0	128	137	148	---	---	138
	-40.0	99	124	135	---	---	119
	-50.0	62	81	102	---	---	82
	-60.0	54	69	84	---	---	69
Ti-Al	-25.0	94	99	105	---	---	99
	-40.0	60	68	72	---	---	67
	-50.0	29	35	41	---	---	35
	-60.0	25	30	34	---	---	26

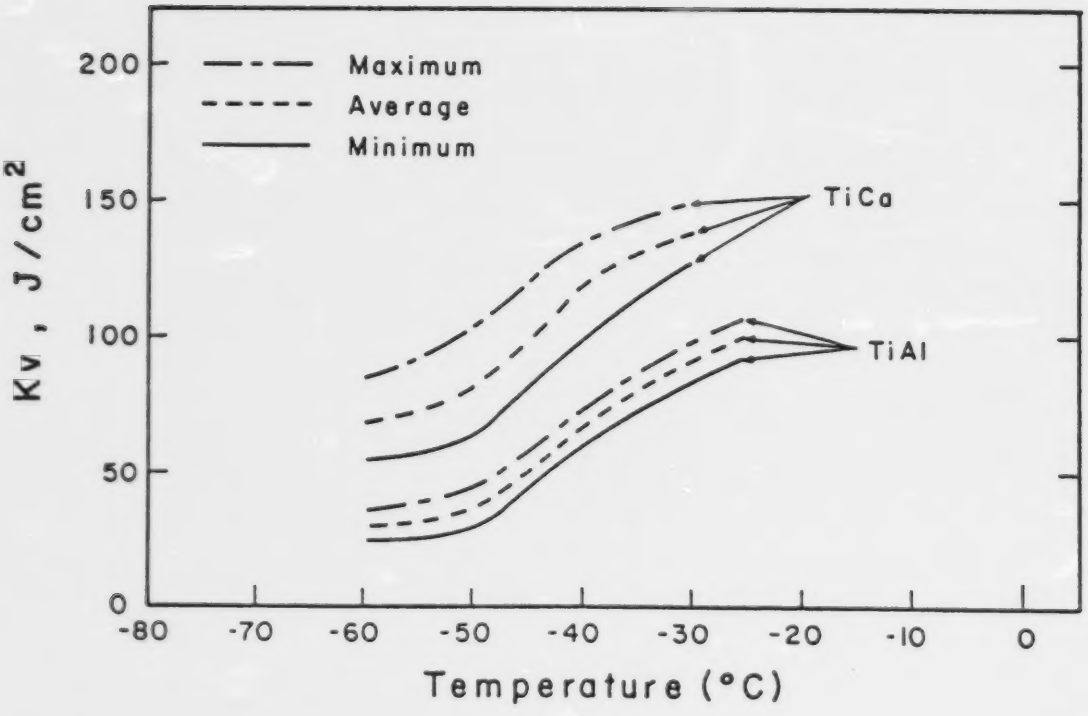

FIGURE 4.45 Impact Transition Curves for Standard Test Plates from Electrodes with Ca or Al Additions.

TABLE 4.13

TRANSITION TEMPERATURES FOR THE STANDARD TEST PLATES

Sample name	TRANSITION TEMPERATURE		
	Minimum	Maximum	Average
TiL	---	-43	-62
TiM	---	-68	-72
TiH	---	-42	-50
TiM	---	-68	-72
SM	-70	-63	-67
SH	-51	-45	-47
Ti-Ca	---	---	---
Ti-Al	-47	-43	-45

CHAPTER 5

DISCUSSION

5.1 ROLE OF INCLUSIONS ON THE DEVELOPMENT OF THE WELD METAL MICROSTRUCTURE

5.1.1. Effect of Inclusion Chemistry

5.1.1.1. Effect of Ti

The microstructural analysis revealed that amongst the elements that can be contained in the inclusions(i.e. Al,Si,S,Ti,Mn and Ca), Ti is required for the formation of acicular ferrite. Figure 5.1 shows clearly that inclusions have not played an active role in the formation of the TiL(0.002%Ti) microstructure which contains mainly ferrite with a second phase(FS) and primary ferrite(PF(G)). The average Ti concentration of the inclusions in this weld is below the detection limits of the energy dispersive X-ray spectrometer. The Ti concentration is so low in these inclusions that it can be considered to be negligible. By contrast, Figure 5.2 shows that for the TiM weld(0.005%Ti), the inclusions are preferential sites for the nucleation of AF grains. The inclusions in the TiM weld contain about 4.6%Ti relative to the other elements detected in the inclusions. Figures 5.3 to 5.5 illustrate other examples of the nucleation of AF at inclusions for the other experimental weld chemistries. In all cases except TiL, the inclusions contain significant quantities of Ti and the weld metal contains significant proportions of AF. This is illustrated in Figure 5.6 which gives the relationship between the relative intensity of Ti in the inclusions and the proportion of AF in the weld for all the experimental chemistries.

FIGURE 5.1 Micrograph Showing that the Inclusions of TiL Weld have not Played an Active Role on the Microstructure.

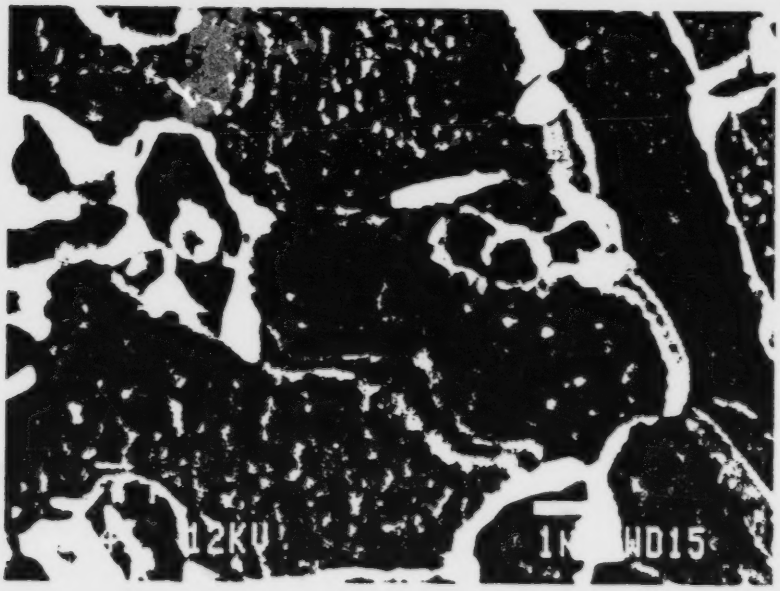

FIGURE 5.2 Micrograph Showing that the Inclusions of TiH Weld are Preferential Sites for the Nucleation of Acicular Ferrite

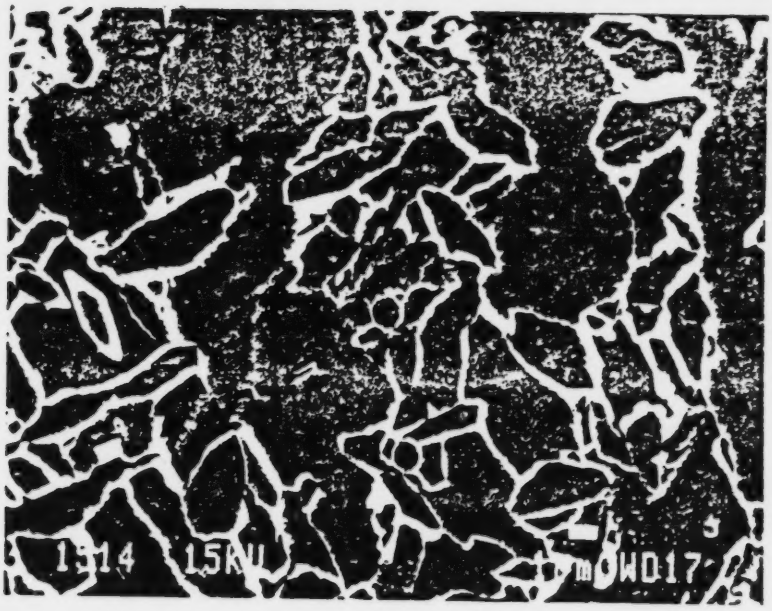

FIGURE 5.3 Nucleation of Acicular Ferrite at Inclusions for SM Weld

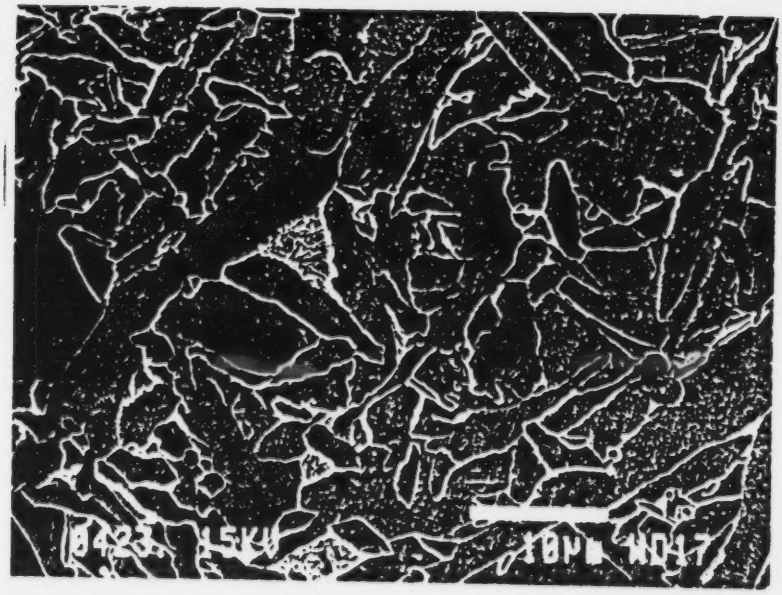

FIGURE 5.4 Nucleation of Acicular Ferrite at Inclusions for Ti-Al Weld

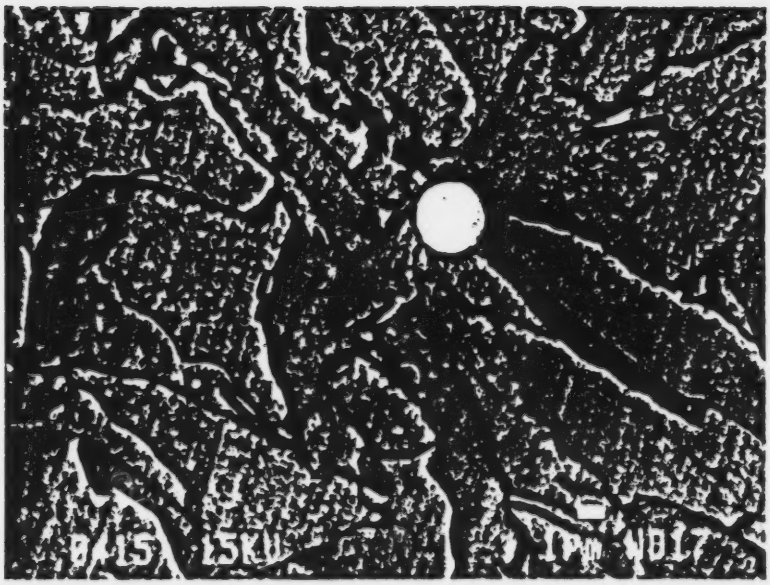

FIGURE 5.5 Nucleation of AF at Inclusions for Ti-Al Weld

On the other hand, observations and Energy Dispersive X-ray micro-analyses of inclusions on extraction replicas of the SM weld as well as on polished surfaces previously etched with Nital showed the heterogeneous nature of the inclusions and the presence of Ti rich phases. This and the observation that Ti rich phases in inclusions can be associated with the nucleation of acicular ferrite suggest a possible mechanism by which Ti rich phases can act to nucleate AF. This mechanism is discussed in detail in Section 5.1.2.2.

5.1.1.2. Effect of S and Deoxidizing Agents, Ca and Al

It was shown that Ti plays an important role in the nucleation of AF in the welds with varying Ti levels. This is confirmed by the data for the other experimental welds which shows that the presence of Ti in the inclusions is always linked to the formation of significant quantities of AF. Moreover, this effect does not depend on the other elements constituting the inclusions for the range of relative intensities observed (Si:7.4 to 26.1%, S:6.0 to 30.0%, Mn:39.9 to 64.6%, Al:0 to 15.2%).

On the other hand, it appears that an increase in the levels of S in the inclusions is associated with an increase in the proportion of AF for the series of welds with varying S contents. This is illustrated in Figure 5.7. This result may be misleading, however, given the significant quantities of Ti present in the inclusions in all the three welds. Ti was shown to favour the formation of AF in the previous section. If the results for the TiL and TiM welds which have similar quantities of S but different levels of Ti, 0.002% and 0.005% respectively, are compared it can be seen that the inclusions in TiL do not favour the nucleation of AF since they do not contain Ti. This is in spite of the fact that the relative intensities of S in the inclusions of TiL is similar to that of TiM(TiL=8.9% S, TiM=9.5%S). This shows that the nucleation of AF is not related to the S rich phases but to those of Ti. It appears

that the increase in the proportion of AF with the increased S level as is illustrated in Figure 5.7, is not directly related to the chemical makeup of the inclusion, that is, an increase in S rich phases but is simply related to the increased volume fraction of large inclusions with increased S concentrations in the weld metal. The effect of inclusion size on the formation of AF will be discussed in detail in Section 5.1.2.2.

The results for the Ti-Ca and the Ti-Al welds show that the use of powerful deoxidizing agents change the particle size distributions of the inclusions but do not prevent the formation of the Ti rich phases in the inclusions. These deoxidants actually favour an increased transfer of Ti to the weld metal and hence the inclusions. The presence of Ti rich phases in the inclusions for these two welds favours the formation of high levels of AF, 84.6% for TiCa and 60.4% for Ti-Al.

5.1.1.3. Comparison with Results of Other Workers

The important role of Ti on the development of AF agrees with the results of many workers[2,19,20,34,35]. It is clear from the present results, that a minimum quantity of Ti is required for the nucleation of acicular ferrite and that this minimum lies between 20 and 50 ppm. This agrees with the results of Devillers et al[19,20] and Bonnet et al[31] who found that the lower threshold value was about 40 ppm. Given that a minimum threshold concentration of Ti in the weld metal is required for the appearance of Ti rich phase in the inclusions (and thus of acicular ferrite), this value can be estimated by extrapolating figure 4.19 which gives the variation of the relative intensity of Ti in the inclusions as a function of the Ti content of the weld. This minimum level can be estimated to be about 39 ppm which agrees very well with the results of the other workers mentioned above.

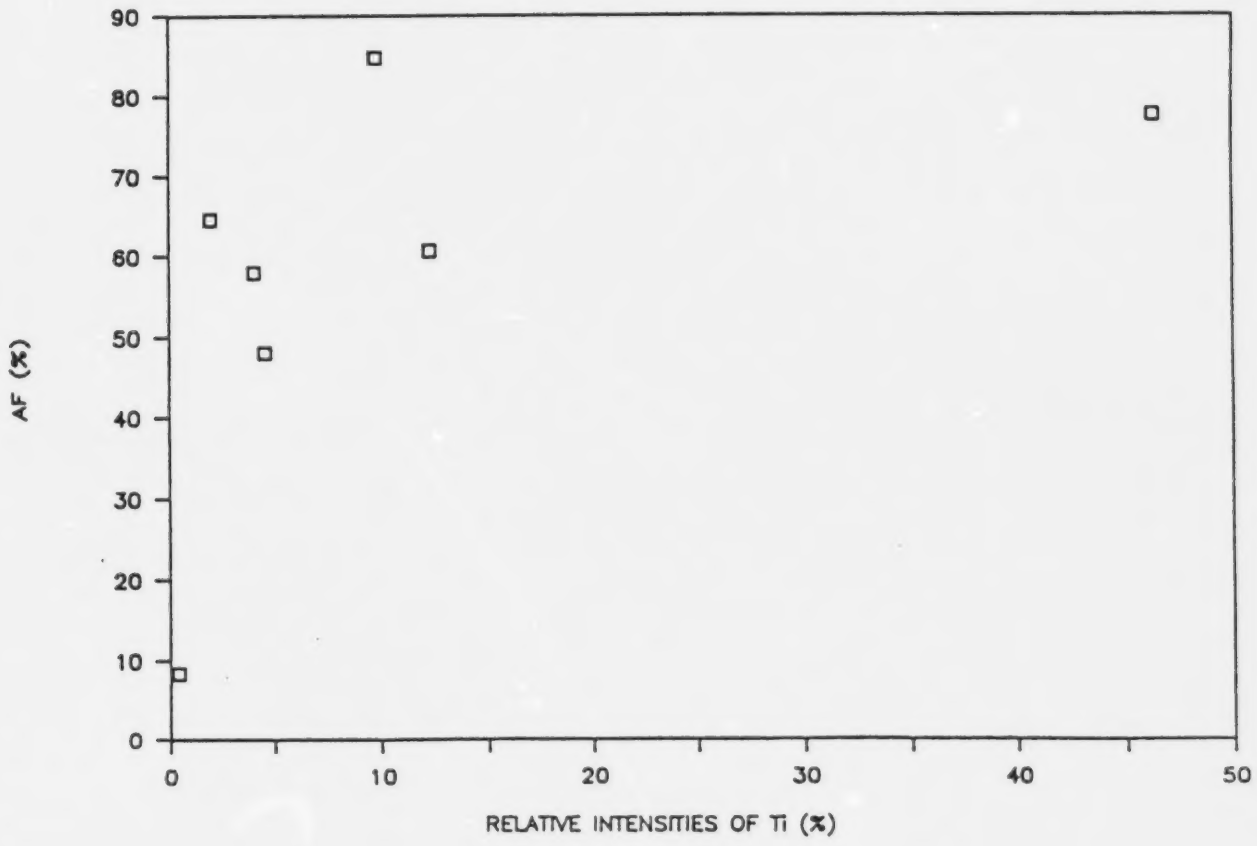

FIGURE 5.6 Proportion of AF in the Weld as a Function of the Relative Intensity of Ti in the Inclusions

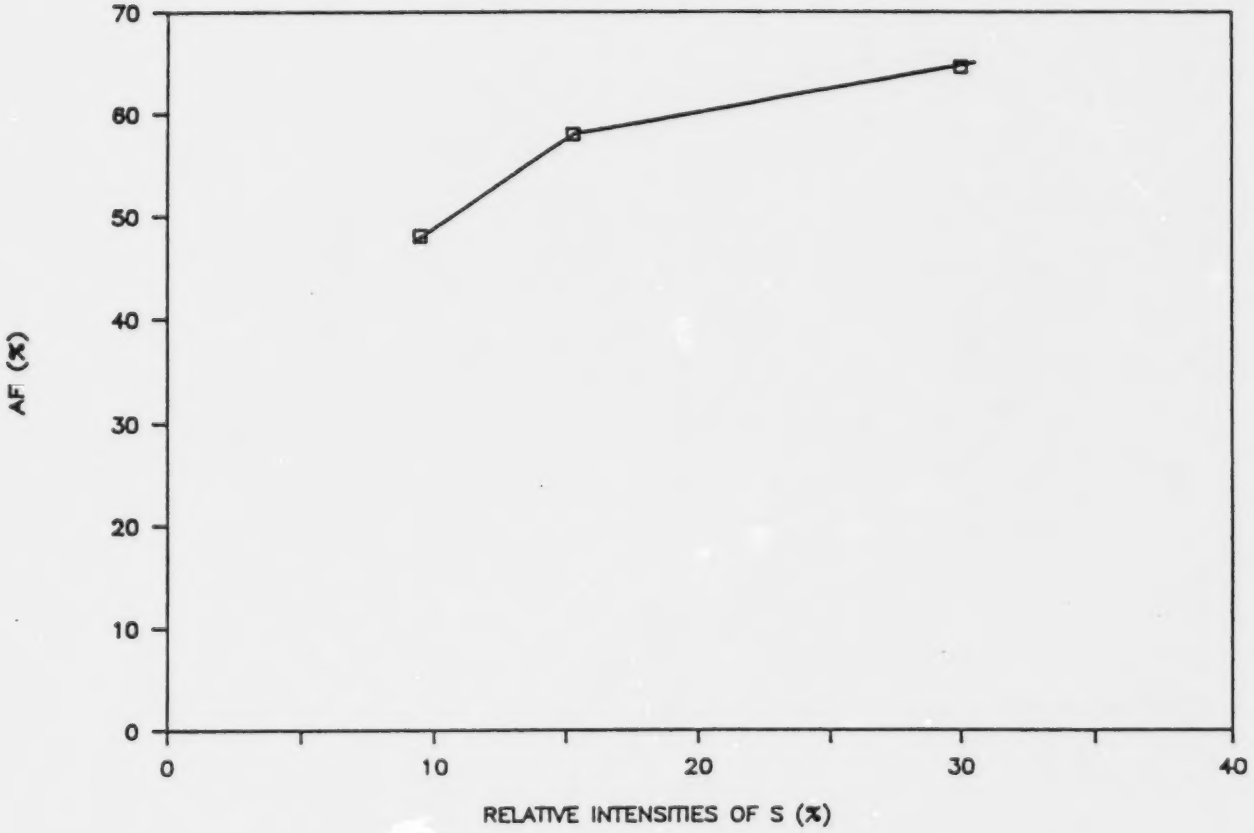

FIGURE 5.7 Proportion of AF in the Weld with Varying Sulphur Content as a Function of the Relative Intensity of S in the Inclusions.

The detailed mechanisms by which the Ti rich phases induce the nucleation of acicular ferrite will be discussed in detail in Section 5.1.2.2.

5.1.2. Effect of the Inclusion Size, Density and Distribution

5.1.2.1. Effect of Austenite Grain Size

During cooling of the as-deposited weld metal, the microstructure undergoes a number of transformations that are described in Section 2.2.1. The final austenite grain size depends upon the cooling conditions and the density of inclusions that can block effectively the austenite grain growth. Figure 5.8 illustrates the austenite grain size (represented by the ratio of total surface analyzed to the total length of the austenite grain boundaries) as a function of the inclusion density for the TiM, TiH, SM, SH, Ti-Ca and Ti-Al welds (Since the austenite grain boundaries of the TiL weld were not decorated with PF(G), it was impossible to evaluate this ratio for this weld). There is a good correlation for the welds that have intermediate levels of Ti, that is, TiM, SM, SH (0.005% Ti) and TiCa (0.008% Ti). This shows clearly that these inclusions can retard austenite grain growth as was observed by Chuen[2].

The TiH and TiAl welds, however, have much finer austenite grain sizes than would be expected if only the inclusion density is considered. These observations can possibly be explained in the following manner. These welds have high levels of nitrogen and elements that have a high affinity for nitrogen, namely Al and Ti. For the TiH weld, which contains 200 ppm of Ti (the Al content is very low), the small austenite grain size can be explained by the precipitation of fine TiN which retards austenite grain growth. This effect is additive to that of the inclusions.

For the Ti-Al weld, there is a larger discrepancy between the S/L ratio measured and the S/L ratio expected from the inclusions density. This is in spite of the lower Ti content which would decrease the precipitation of TiN. However, this weld is characterized by high Al contents of 0.02% Al which can have two effects. First, the high affinity of Al for O can prevent the formation of Ti oxides which can increase the quantity of Ti available for precipitation as nitrides. Second, AlN can precipitate directly. The precipitation of AlN occurs at about 900°C [55] which means that this precipitation will have little effect on the austenite grain size. Austenite grains form below 1500°C and grow mainly at temperatures well above 900°C. Furthermore, L'Ecuyer et al[56] have shown that the precipitation of AlN does not occur for low levels of Ti ($\leq$50 ppm). The Ti combines preferentially with nitrogen in this case. It would then seem that the precipitation of Ti nitrides in the Ti-Al specimen also explains the small austenite grain size. Al protects Ti from the O which favours increased Ti nitride precipitation which exceeds that of the TiH weld even though the later has a higher level of Ti.

Observations on extraction replicas in the transmission electron microscope of the precipitation occurring in these welds has not yet been performed. However, based on the work of L'Ecuyer et al[56] who found the precipitation of Ti nitrides in microalloyed steels for Ti (< 50 ppm) and nitrogen ($\approx$ 60 ppm) levels which are much less than in the Ti-Ca or Ti-Al welds, it can be expected that extensive Ti nitride precipitation will also occur in the welds with powerful deoxidizing agents.

The precipitation of fine nitrides results in an increase in strength of the matrix. This was observed for TiH on the force-displacement curves that were calculated from the load-time traces recorded during the instrumented impact tests. This weld has higher general yield and maximum

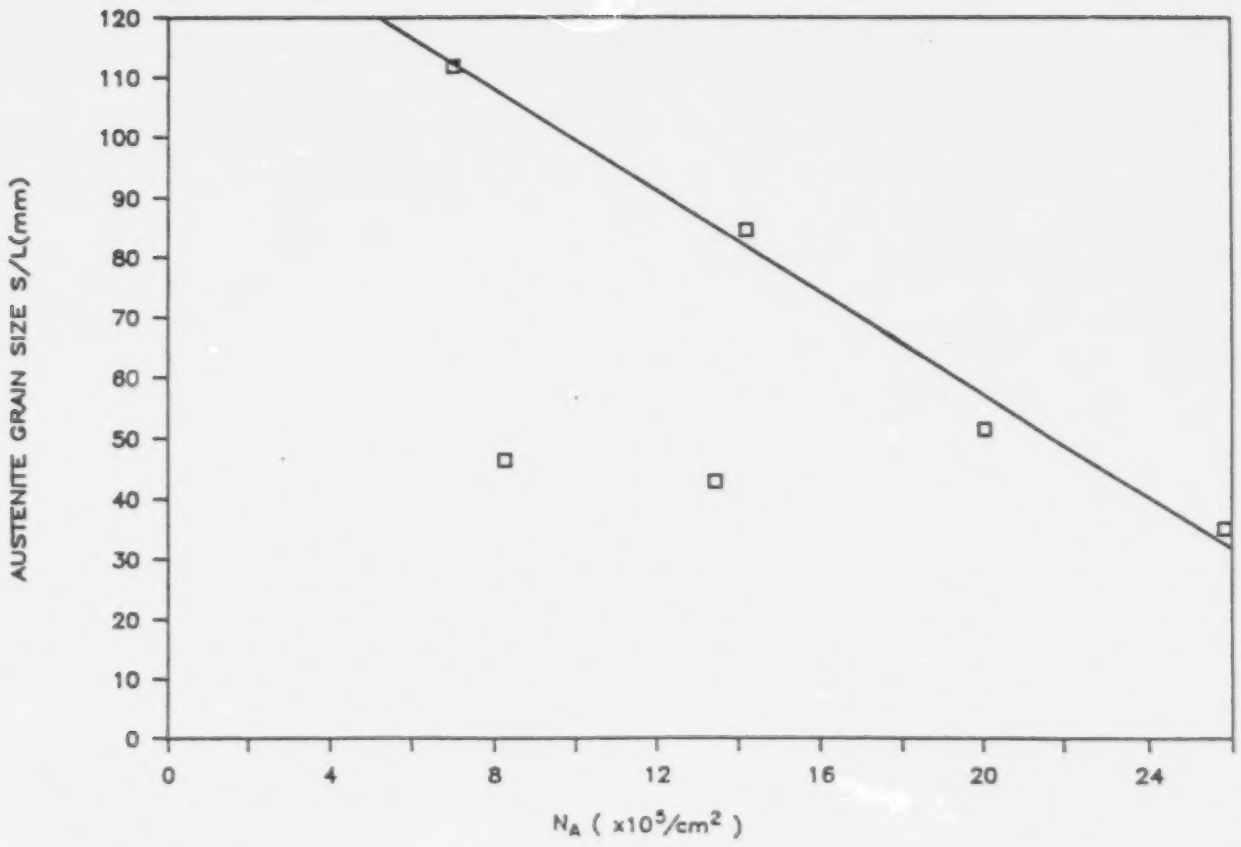

FIGURE 5.8 Austenite Grain Size (represented by the ratio S/L) as a Function of Inclusion Density (N_A) for the Welds except TiL.

loads than weld TiM as was presented in Section 4.3.2.2. An increased strength, however, was not observed in the instrumented Charpy tests for the Ti-Al weld. This is not, however, an indication that increased strengthening due to Ti nitride precipitation is not occurring. Abnormalities in the load-displacement curves of the instrumented impact test as was presented in Section 4.3.2.4, show that fracture initiation occurs before the general yield load is achieved and hence the apparent general yield load measured from the load-displacement traces will underestimate the true dynamic strength. Fractographic studies of the Charpy specimens (Section 4.3.3.4) have shown that fracture initiation is by a shear process which is favoured by the presence of the large Al_2O_3 inclusions and higher strengths(i.e. lower work hardening rates). These results, which will be discussed in greater detail in Section 5.2.5, indicate indirectly that extensive Ti nitride precipitation is occurring in the Ti-Al weld.

5.1.2.2. Nucleation of Acicular Ferrite

Even though it has been shown that a minimal amount of Ti in the inclusions is a requirement for the formation of AF, it is evident that the Ti level in the inclusions is not the only factor determining the proportion of AF present. This point is clearly shown in Figure 5.6 which presents the proportion of AF as a function of the relative intensity of Ti present in the inclusions. In addition to the level of alloying elements and the cooling rate which are assumed similar for all the welds, other factors influence the nucleation of AF. The inclusion density and size distribution as well as the austenite grain size will also influence the proportion of AF present.

Considering just those welds whose inclusions contain Ti in significant quantities, the proportion of AF was compared to the austenite grain size and inclusion density in Figures 5.9 and 5.10 respectively. Clearly, an

increase in the austenite grain size results in increased quantities of AF which is a result found in many previous studies[2,3,21,22,37]. The inclusion density, however, does not seem to have much effect. This last result is somewhat surprising, considering the anticipated role of inclusions and hence of their number on the nucleation of AF. It should be noted, however, that the proportion of AF is related to the austenite grain which is in turn related to the inclusion density which makes it difficult to evaluate the two effects separately. In the following discussion, an attempt is made to isolate the effect of the austenite grain size thereby allowing a determination of the true role of the inclusions on the nucleation of AF.

The austenite grain boundaries act as preferred sites for the nucleation of PF(G) and FS[2]. Small austenite grain sizes (S/L small) offer more sites for the nucleation of these phases than does large grain sizes(S/L large). The increased number of nucleation sites increases the amount of PF(G) and FS phases that forms during transformation thereby decreasing the amount of austenite that can transform to AF which in turn decreases the total number of inclusions that can act as sites for the nucleation of AF. The volume fraction of austenite available for the formation of acicular ferrite after PF(G) and FS phases have formed can be estimated from the following relationship.

$$F_\gamma = S_T - S_{PF-FS} / S_T \quad \ldots\ [5.1]$$

where: S_T = Total Surface Area and

S_{PF-FS} = Total Surface Area occupied by PF(G) and FS at grain boundaries.

The value of S_{PF-FS} is the volume of material in which the inclusions could not act as sites for the nucleation of AF since the effect of grain boundaries in nucleating PF(G) and FS dominated. These values cannot be estimated directly from the results of the quantitative microstructural analysis since the quan-

tity of FS measured contains portions of FS that occurs at intragranular locations.

For a large grain size the total area of S_{PF-FS} is $\approx$ Lt where L is the length of the austenite grain boundaries and t is the thickness of the PF(G) and FS phases on the prior-austenite grain boundaries. The value of t is a function of the cooling conditions which was assumed to be constant for all welds. Hence, an average value for t for all the welds of 0.025 mm was estimated from the micrographs.

It is then possible, knowing F_γ, to evaluate the efficiency of nucleation of AF by the ratio AF/F_γ which represents the volume fraction of austenite that transformed to AF. For example a factor of 1 indicates that all of the available austenite transformed into AF. A value of 0.5 indicates that only 50% of the austenite formed AF.

For the series of welds with varying S content, the quantity of Ti is constant in the weld metal (0.005%) and almost constant in the inclusions(the relative intensity of Ti is between 2 and 4.6%). It can be considered that the quantity of the Ti rich phase in the inclusions which is necessary for the nucleation of AF is almost constant for the three welds.

Figure 5.11 shows the relationship between the ratio AF/F_γ and the inclusion density for this series of welds. It is not possible to establish a direct relationship between the ratio AF/F_γ and the inclusion density. This is in spite of the fact that it was observed that these inclusions play a very important role in the nucleation of acicular ferrite. It follows that the total number of inclusions per unit volume (inclusion density) is not the only factor which influences the efficiency of the nucleation of AF for the series

with varying S content.

On the other hand, observations of the role of inclusions on the nucleation of AF in the scanning electron microscope indicated that the efficiency of the inclusions for the nucleation of AF increased with increasing inclusion diameter, that is to say, large inclusions are often associated with the formation of AF and the number of ferrite grains nucleated at the inclusions increased with increasing inclusion diameter (see Figure 5.3). Since the nucleation of AF occurs at the surface of the inclusions, it appears that the increased surface area of the large inclusions will offer more possible sites for the nucleation of AF and result in the large inclusions being more efficient than the small inclusions for the nucleation of AF.

Figure 5.12 is the relationship between the ratio AF/F_γ and the total number of inclusions N_A times the average surface area of the inclusions A_{inc} which is the total surface area of the inclusions $N_A x A_{inc}$. In this case there is a direct relationship between AF/F_γ and $(N_A x A_{inc})$, that is to say the ratio AF/F_γ increases with increasing values of $(N_A x A_{inc})$. This result shows the importance of these two factors on the efficiency for the formation of AF, namely the inclusion density which determines the total number of inclusions that could possibly nucleate AF and the inclusion size distribution which determines the average inclusion diameter and hence the efficiency of the individual inclusions for the nucleation of AF (large inclusions are more efficient since they have a larger surface area). The importance of these two factors is shown in the results for the TiM and SM welds. For these two cases, the efficiency factor is identical ($AF/F_\gamma = 0.65$). TiM has a high inclusion density ($25.8 \times 10^5/cm^2$) whereas SM has a low density of inclusions ($14.2 \times 10^5/cm^2$). On the other hand, the inclusions in the SM weld are on the average larger than those in the TiM weld which results in a total surface area

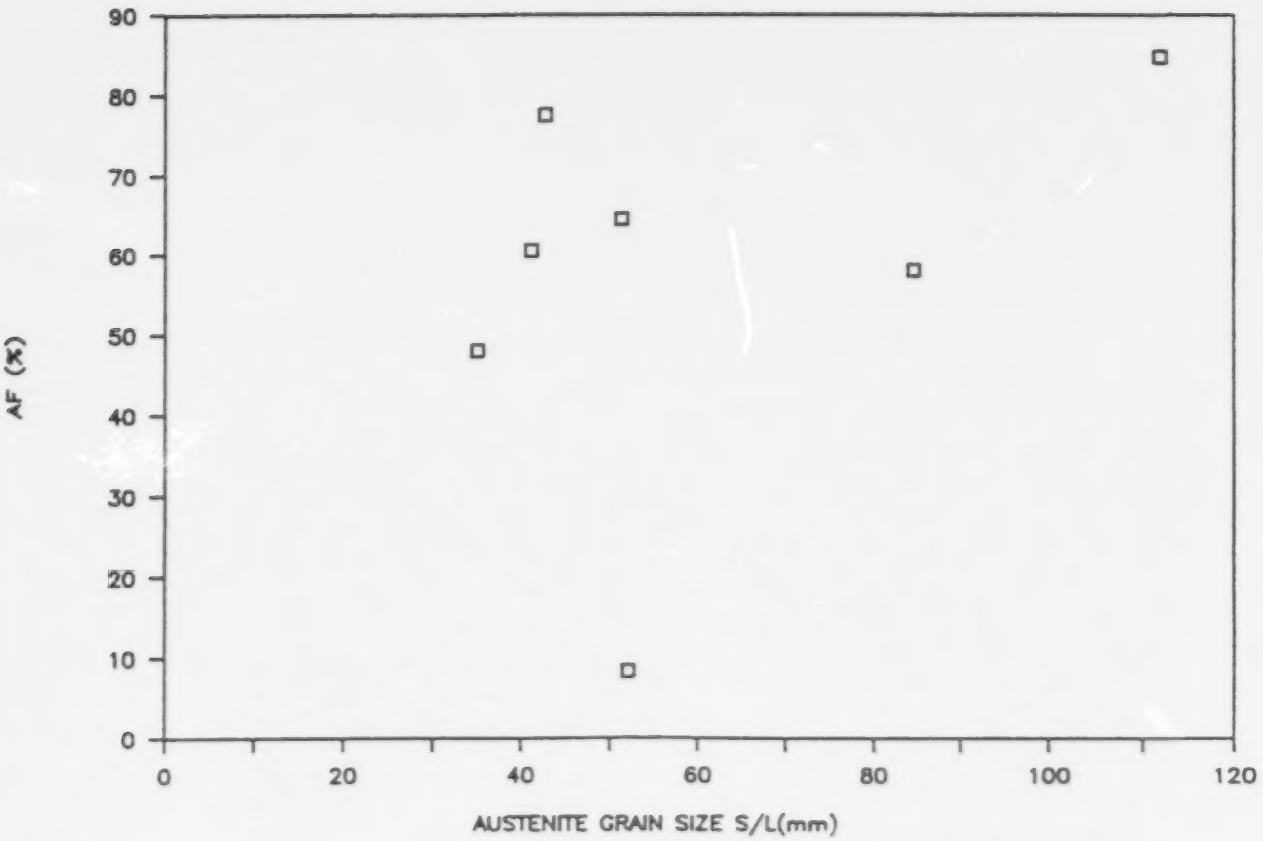

FIGURE 5.9 Proportion of AF as a Function of the Austenite Grain Size (S/L)

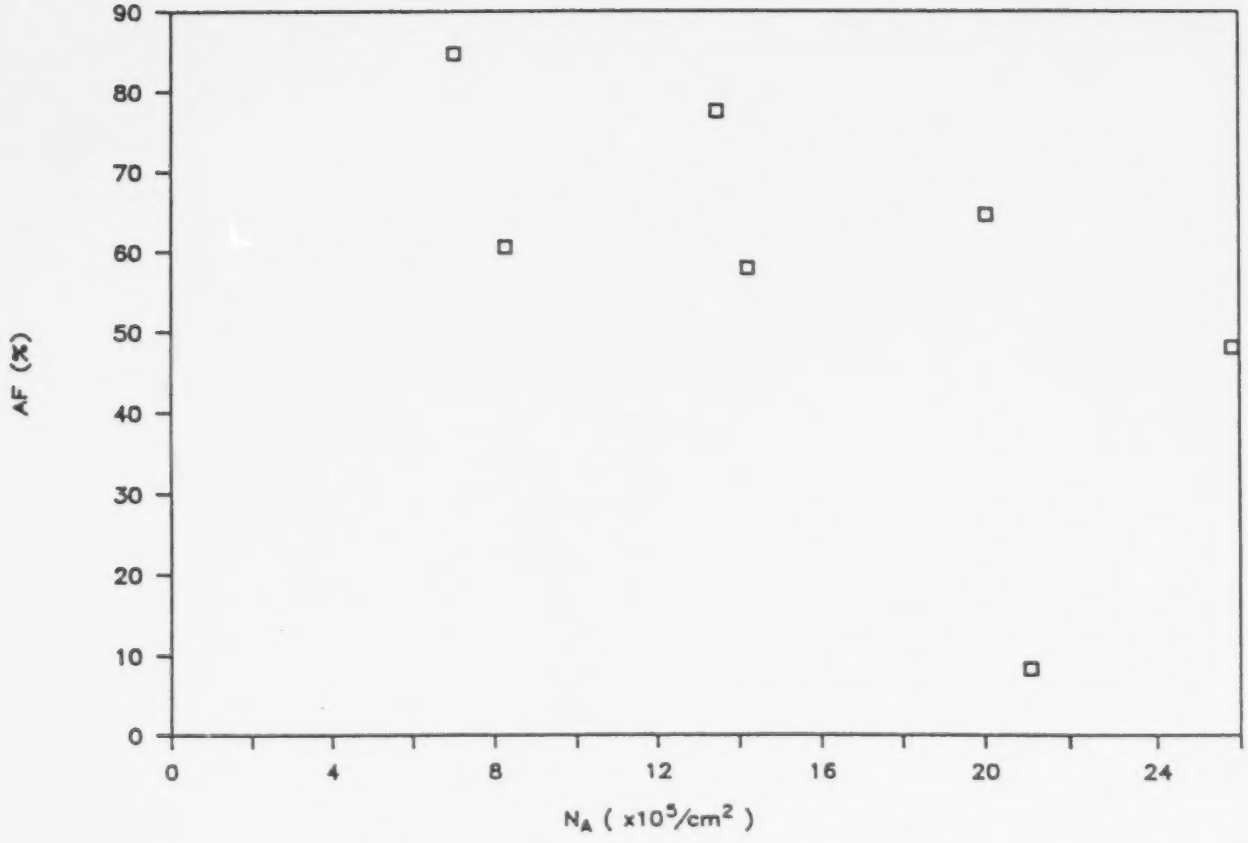

FIGURE 5.10 Proportion of AF as a Function of the Inclusion Density (N_A).

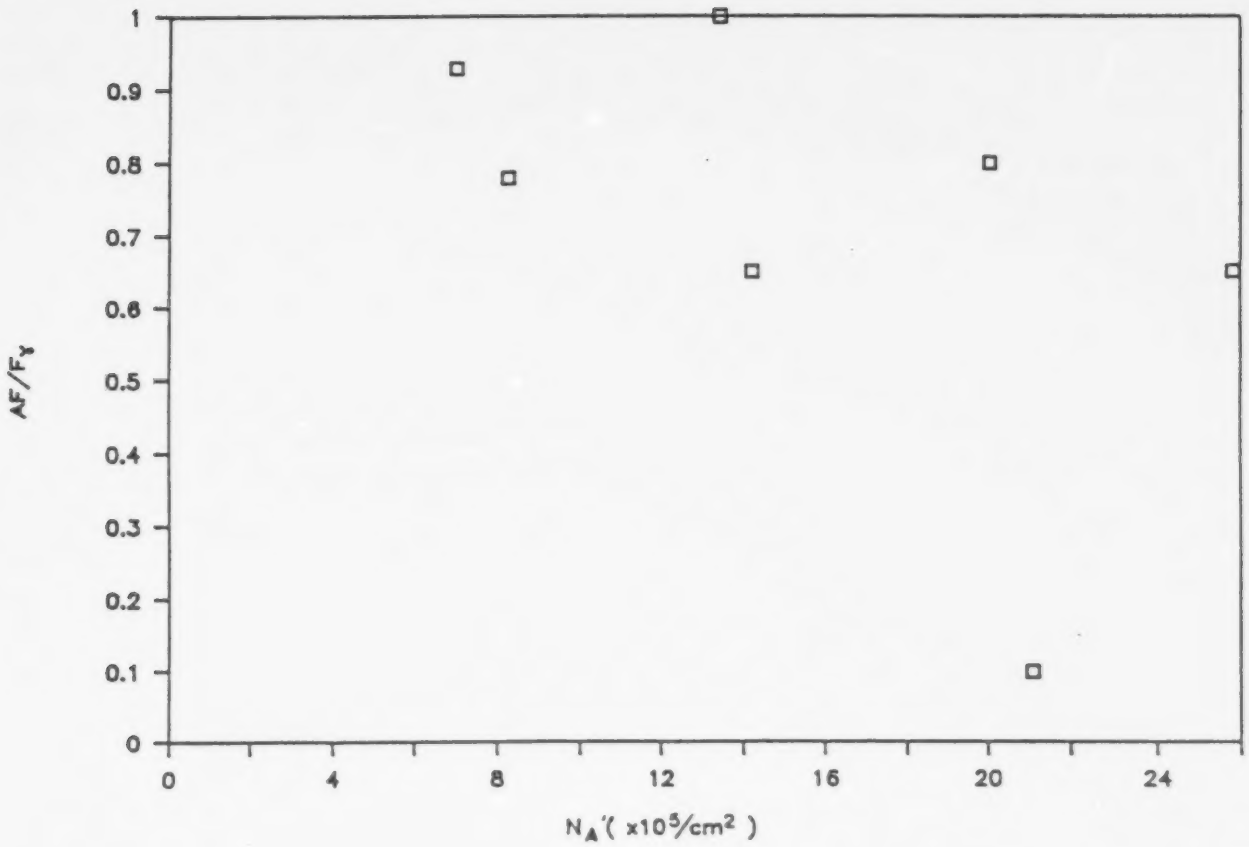

FIGURE 5.11 The ratio AF/F_γ as a Function of the Inclusion Density (N_A) for the Welds with Varying Sulphur Content.

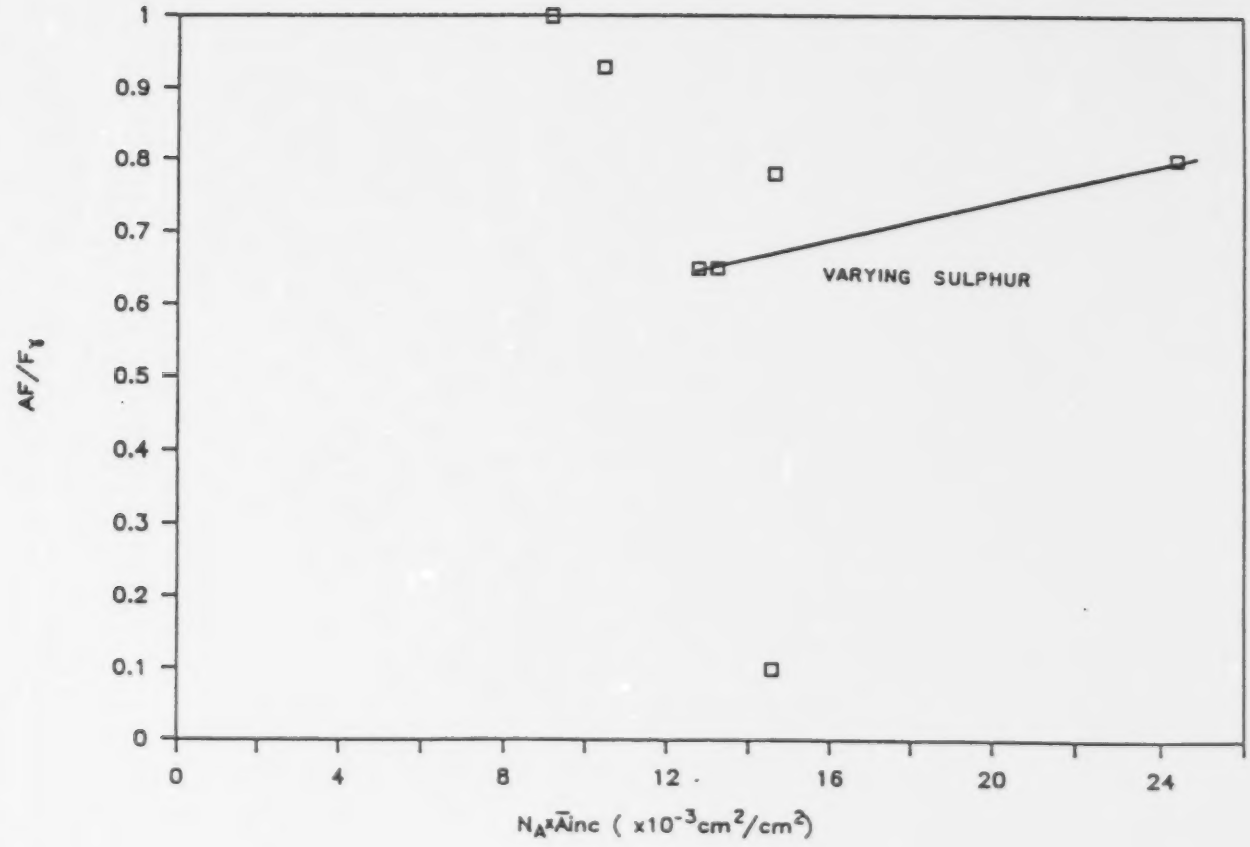

FIGURE 5.12 The ratio AF/Fγ as a Function of ($N_A x A_{inc}$).

of inclusions which is much higher than TiM(0.92 μm2 as compared to 0.48 μm^2). Both welds which have different distributions of inclusions have similar values of $(N_A x A_{inc})$.

Figure 5.12 also shows that it is impossible to establish a relationship between $(N_A x A_{inc})$ and AF/F_γ for the other welds. These welds are characterized by Ti contents which vary and are different than those of the series with varying levels of S. This indicates that in addition to the inclusion density and size distribution, the efficiency for the nucleation of AF is also related to the Ti content of the inclusions. For higher Ti contents in the inclusions the ratio AF/F_γ is greater for a given total inclusion surface area per unit volume than that established from the results for the welds with varying S content and less for the TiL weld which has no Ti in the inclusions. The following section discusses a proposed mechanism for the nucleation of AF at the Ti rich phase in the inclusions.

5.1.3. Proposed Mechanism for the Nucleation of Acicular Ferrite

5.1.3.1. Nucleation on the Ti rich Phase

The results show clearly that the nucleation of AF is associated with the following factors.

- The presence of titanium rich phases in the inclusions, which have been observed at the surface of the inclusions, is required for the nucleation of AF.
- The ratio AF/F_γ is related for the welds with varying S contents (and having similar relative intensities of Ti in the inclusions) to the inclusion density as well as the size distribution of the inclusions. The inclusion density determines the number of inclusions which can act as potential sites for nucleation and the size distribution of the inclusions determines the average surface area

of the inclusions which in turn determines the average efficiency of the inclusions for the nucleation of AF. The nucleation of AF appears to be a surface effect of the inclusions.

- The ratio AF/F_γ appears to be related for the other welds to the Ti content of the inclusions. This ratio increases with increasing Ti content of the inclusions.

Given the apparent importance of the Ti content of the inclusions, the average surface area of the inclusions and the presence of Ti rich phases on the surface of the inclusions (Section 4.2.2.5), it appears that the nucleation of AF occurs at the surface of the Ti rich phases. To verify this conclusion, it is necessary to estimate the total surface area of the Ti rich phases on the inclusions.

5.1.3.2. Estimation of the Surface Area of the Ti rich Phases

In order to estimate the specific surface area of the Ti rich phase several hypotheses were made. First, the average relative intensity of Ti in the inclusions was considered to be equal to the concentration of Ti in the inclusions. Second, the inclusions were considered to be perfectly round, the Ti rich phase forming a perfect cap on the surface of the inclusions. Figure 5.13 illustrates the shape of the Ti rich phase that was assumed and gives the expressions used to calculate the volume and the external area occupied by this phase.

The volume occupied by the Ti rich phase is

$$V_{Ti\ rich} = I_{Ti}\, V_{inc}\, \rho_{inc} / \rho_{Ti\ rich} \quad \ldots\ldots [5.2]$$

where I_{Ti} = relative intensity of Ti in the inclusion

V_{inc} = volume of the inclusion

ρ_{inc} = average density of the inclusion

$\rho_{Ti\ rich}$ = average density of the Ti rich phase

Assuming $\rho_{inc} = \rho_{Ti\ rich}$, we have

$$V_{Ti\ rich} = I_{Ti}\ V_{inc}$$

$$V_{Ti\ rich}/V_{inc} = I_{Ti}$$

The volume fraction of the Ti rich phase is equal to its concentration in the inclusion.

Knowing the volume of the inclusion and its Ti content, the value of h (which represent the height of the titanium rich cap as shown in figure 5.13) can be evaluated by an iterative process from the following equation.

$$1/3\ \pi\ h^3(3(d/2) - h) = I_{Ti}\ 4/3\ \pi\ (d/2)^3$$

From the value of h calculated for a known value of d and I_{Ti}, the specific surface area of the Ti rich phase occupying the surface of the inclusions can be calculated.

$$A_{Ti} = 2\pi(d/2)h\ /\ (4\pi(d/2)^2)$$

where A_{Ti}(%) is the fraction of the surface of the inclusion that is occupied by the Ti rich phase. Figure 5.14 illustrates the relationship between the relative intensity of Ti in the inclusion, I_{Ti}, and the percentage of the surface of the inclusion occupied by the Ti rich phase, A_{Ti}. A_{Ti} depends in a parabolic manner on I_{Ti} which means that small increments of I_{Ti} have much more

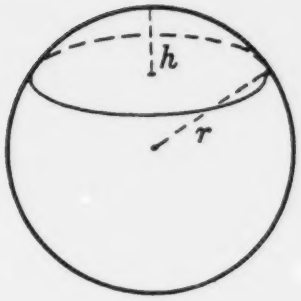

Volume (of the cap) = $1/3\pi h^2(3r-h)$

Surface Area = $2\pi rh$

where r = radius of the sphere

h = heigth of the cap

FIGURE 5.13 Schematic Illustrating the Spherical Cap which is the Form Assumed for the Ti-rich Phase Present in the Inclusions.

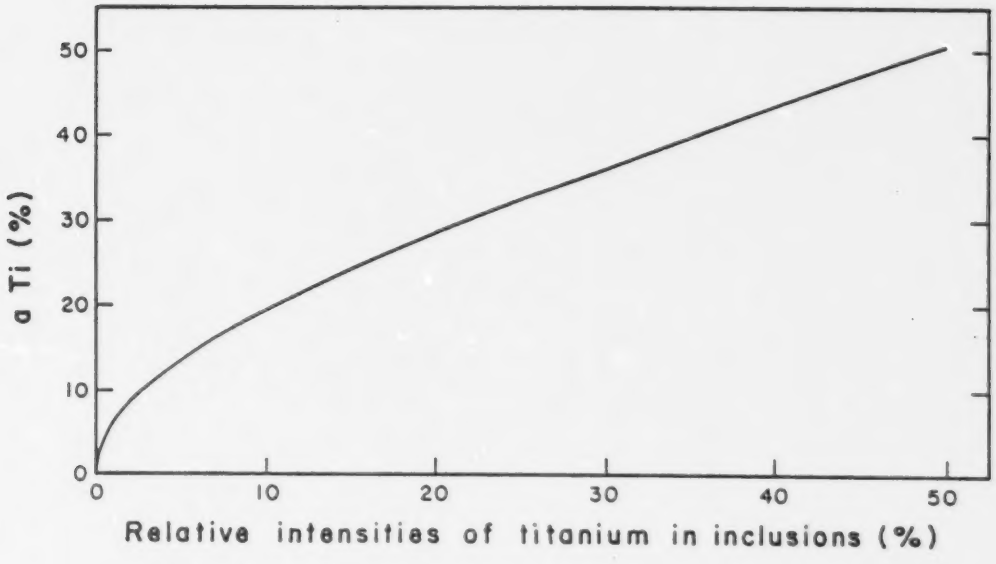

FIGURE 5.14 Percentage of the Inclusion Surface Area Occupied by the Ti-rich Phase as a Function of the Relative Intensity of Ti in the Inclusion.

effect on the total surface area of the Ti rich phase for small values of l_{Ti} than at large values of l_{Ti} which explains the rapid increase in the proportion of AF for small increments of Ti just above the threshold level.

For an inclusion of known diameter, d, the available surface of the Ti rich phase can be found from the following equation:

$$A_{Ti} = a_{Ti}(\%) \times A_{inc}$$

where ^{ATi} is the fraction of the total surface area of the inclusion occupied by the Ti rich phase and A_{inc} is the total surface area of the inclusion.

For a distribution of inclusion diameters, the average surface area of the Ti rich phase can be found from the following summation.

$$A_{Ti} = \Sigma\, a_{Ti}(\%) \times A_{inc}/n_i$$

$$A_{Ti} = (a_{Ti}/n_i)\, \Sigma\, A_{inc}$$

where n_i is the number of inclusions analyzed.

Table 5.1 gives the values of A_{Ti} measured for the welds TiL, TiM, TiH, SM, Ti-Ca and Ti-Al.

5.1.3.3. Relationship between the AF/F_γ and the Total Available Surface Area of Ti-rich Phase per unit Volume

Now that the average surface area of the Ti rich phase has been calculated, it is possible to calculate the total surface area of this phase per unit area of the weld metal by multiplying the average area A_{Ti} by the inclusion density, N_A. Figure 5.15 gives the relationship between the AF/F_γ

ratio and ($N_A x A_{T_i}$) for the welds TiL, TiM, TiH, SM, SH, TiCa and TiAl. If the point for the TiAl is eliminated due to its higher levels of Si and Mn (1.48% Mn and 0.47% Si compared to the 1.36% Mn and 0.30% Si averages for the other welds) there is a linear relationship between ($N_A x A_{T_i}$) and AF_γ for the other welds. It follows that the formation of AF is clearly related to the total surface area of the Ti rich phases per unit surface of austenite available for transformation. This relationship also shows that there exists a threshold value of ($N_A x A_{T_i}$) equal to $5.73 \times 10^{-4} cm^2/cm^2$ above which the AF/F_γ ratio becomes 1 and the total available volume of austenite transforms into AF. This is the reason why the weld TiH which has a value of ($N_A x A_{T_i}$) greater than the threshold ($11.09 \times 10^{-4} cm^2/cm^2$) has a value of a AF/F_γ ratio equal to 1.0

It is clear, based on Figure 5.15, that the nucleation of AF in the weld metal which has similar alloying additions and cooling cycles is associated with a Ti rich phase. The capacity of the inclusions to favour the formation of AF from austenite as is given by the AF/F_γ ratio, depends upon the total surface area of the Ti rich phase per unit volume of austenite ($N_A x A_{T_i}$). This indicates that in addition to the quantity of Ti in the inclusions which determines the volume of the Ti rich phase in the inclusions and hence the area fraction of the inclusion surface associated with this phase, the inclusion density and size distributions also play an important role. The inclusion density determines the number of sites from which AF can germinate. The size distribution of inclusions determines the average inclusion surface area and hence the surface area of the Ti rich phase.

Hence, for small Ti levels in the inclusions (TiL), the inclusion density and size distributions have little effect on the nucleation of AF given the insignificant surface area of the Ti rich phase which results in inclusions. By contrast, for slightly increased levels of Ti in the weld metal the

TABLE 5.1

SUMMARY OF THE PRINCIPAL VALUES USED IN THE CALCULATION OF $N_A x A_{Ti}$

	WELD DEPOSIT						
	TiI	TiM	TiH	SM	SH	TiCa	TiAl
Iti (%)	0.4	4.6	46.3	4.1	2.0	9.8	12.3
ati (%)	3.7	12.9	48.3	12.2	8.3	19.2	21.9
A_{inc} (μm^2)	0.6912	0.4956	0.6828	0.9324	1.2164	1.4892	1.769
A_{ti} (μm^2)	0.0256	0.0640	0.3296	0.1136	0.1008	0.2860	0.3876
N_A ($\times 10^5$ cm^{-2})	21.11	25.82	13.46	14.22	20.05	7.03	8.29
$N_A \times A_{ti}$ ($\times 10^{-4}$ cm^2/cm^2)	5.40	16.52	44.36	16.16	20.20	20.12	32.12
$AF/F\gamma$	0.10	0.65	1.0	0.65	0.80	0.93	0.70

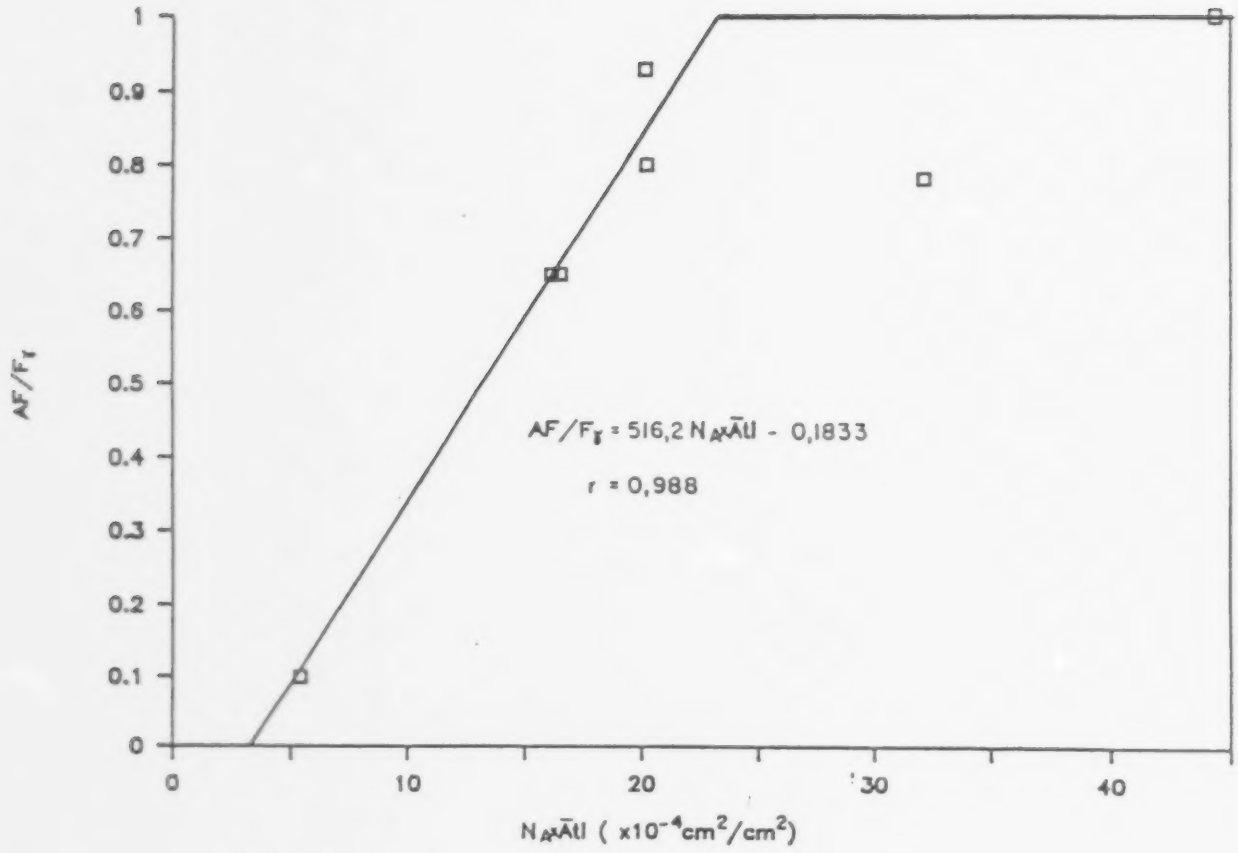

FIGURE 5.15 The Nucleation Effenciency Ratio, AF/F*, as a Function of $N_A x A_{Ti}$.

increased Ti contents in the inclusions makes them much more likely to nucleate AF and hence the density and size distributions will now influence the AF/F_γ ratio. The TiM, SM, SH and TiCa welds illustrate this effect. If the data for the inclusions from the SM and TiM welds are compared, the average surface area of the Ti rich phases in SM (A_{Ti} = 0.0284) is larger than that for TiM (A_{Ti} = 0.0160) which is due to the fact that larger inclusions are found in SM. Thus, the inclusions in SM will be more effective in nucleating AF in spite of similar Ti levels in the inclusions (4.1% for SM and 4.6% for TiM). On the other hand, the TiM weld has a higher density of inclusions than does SM which results in more possible nucleation sites. Globally, the two welds have ($N_A x A_{Ti}$) values that are very close together ($4.13 \times 10^{-4} cm^2/cm^2$ for TiM and $4.04 \times 10^{-4} cm^2/cm^2$ for SM) and AF/F_γ that are identical (0.65).

For the SH weld, the AF/F_γ ratio is higher that TiM and SM in spite of a decrease in the average Ti content of the inclusions (2% compared to about 4% for the others). There are many more large inclusions in the SH weld which results in a larger A_{Ti} value (0.0252 μm^2 compared to 0.0160 μm^2 for TiM). The inclusion density of $20.05 \times 10^5 / cm^{-2}$ is also higher. This results in a ($N_A x A_{Ti}$) value of 5.03×10^{-4} cm^2/cm^2 which is higher than the TiM and SM welds.

The TiCa weld has a high AF/F_γ ratio of 0.93. In spite of a low inclusion density ($7.03 \times 10^5 / cm^2$), the higher Ti content in the inclusions (9.8%) have a higher mean size (0.61 μm) which results in an A_{Ti} value of 0.0715. In this case, there are few potential sites for the nucleation of AF but those that exist are very effective due to the high Ti content. This results in a ($N_A x A_{Ti}$) value of 5.03×10^{-4} cm^2/cm^2 which is similar to that of SH.

For high levels of Ti such as is the case for TiH with 46.3% Ti in the inclusions, the inclusion density and average surface area become less important than was the case for lower Ti contents in the inclusions due to the large proportion of the surface area of the inclusions that is covered by the Ti rich phase. Hence, TiH has an average surface area of the Ti rich phase of $0.082\mu m^2$ which is higher than in the other welds (except for TiAl) in spite of a lowest total surface area of inclusions ($A_{inc} = 0.1707\ \mu m^2$). The inclusion density in the TiH weld is not very high and if only the total surface area is considered, TiH should give the lowest AF/F_γ value (see Figure 5.13). Hence, for inclusions with high proportions of the Ti rich phase, the size distribution and the necessity to have large inclusions in order to have a large area of the Ti rich phase becomes less important for the nucleation of AF than is the case for lower levels of Ti. An important consequence of this observation is that the total number of inclusions and/or the size distribution could be reduced without a reduction in the amount of AF and a possible improvement in toughness. As will be discussed later, however, a significant improvement in toughness is more likely to occur by reducing the amount of nitrogen or possibly the amount of Ti since the precipitation of Ti(C,N) appears to be detrimental to the toughness of the welds.

The AF/F_γ ratio depends directly on the $(N_A x A_{Ti})$ product. However, AF/F_γ cannot exceed 1 which corresponds to the complete transformation of the untransformed austenite into AF. In this study, a value of 1 is reached at a value of $(N_A x A_{Ti})$ of $5.73 \times 10^{-4} cm^2/cm^2$. For values of AF/F_γ over this, the volume fraction of AF depends upon the total volume of untransformed austenite which in turn depends upon the austenite grain size which is related directly to F_γ. For values less than $5.73 \times 10^{-4}\ cm^2/cm^2$, the proportion of AF depends upon the factors which influence the nucleation of AF such as the level of Ti in the inclusions and the density and size distribution of inclusions. For

values less than 5.73×10^{-4} c^{m2}/cm^2 the following regressions apply:

$$AF/F_\gamma = -0.1826 + 2065.3\ N_A x A_{Ti} \quad \ldots\ldots\ [5.1]$$

$$AF = (-0.1826 + 2065.3\ N_A x A_{Ti})\ F_\gamma \quad \ldots [5.2]$$

An excellent correlation coefficient of 0.988 was obtained for the equation 5.1.

5.1.3.4. Ti-Al Weld

Figure 5.15 clearly shows the role of Ti in the inclusions on the nucleation of AF which has been related to the surface area of the inclusions occupied by the Ti rich phase as was discussed in detail in the proceeding section. The AF/F_γ ratio is linearly related to $(N_A x A_{Ti})$ which is the total surface area of the Ti rich phase per unit surface area of weld metal, until a maximum value of 1 is reached. For higher $(N_A x A_{Ti})$ values, AF/F_γ remains constant at 1. This relationship applies for all the welds except TiAl which has a AF/F_γ ratio of 0.78 which is lower than the predicted value of 1 (for TiAl, $(N_A x A_{Ti})$ is equal to $8.03 \times 10^{-4} cm^2/cm^2$ which is greater than the threshold value of $5.73 \times 10^{-4} cm^2/cm^2$). This deviation from the predicted behaviour can be related to the two following factors.

1- The calculated value of F_γ for Ti-Al is too low resulting in an AF/F_γ ratio which is too high.

2- The surface area on the outside of the inclusions associated with the Ti rich phase has been over estimated since some of this phase may be contained within the inclusion which results in an $(N_A x A_{Ti})$ value which is too high.

During the γ to α transformation, the austenite grain bounderies are preferential sites for the nucleation of ferrite in the absence of boron[2,13] (See Figure 2.25). For constant cooling conditions and alloying additions, a certain volume of the austenite will transform at temperatures above that for the formation of AF into grain boundary allotriomorphs and Widmanstatten ferrite (FS(A))[2,3,8,13]. This volume of austenite cannot transform into AF and hence is represented by $1-F_\gamma$ and is directly proportional to the surface area per unit volume of the austenite grain boundaries and hence increases as the austenite grain size decreases. The value $1-F_\gamma$ depends upon the cooling conditions and alloying additions which affect the amount of ferrite grain growth and the ferrite transformation start temperature. These two factors are represented by the thickness of the ferrite phases which is represented by the value t (see Section 5.1.3.2.) and was measured for the welds with high values of ($N_A x A_{Ti}$), namely TiH, Ti-Ca and SH.

Even though this value of t measured for TiH, Ti-Ca and SH welds can be used for the TiL, TiM, TH, SM, SH and Ti-Ca welds, it is very likely that this value cannot be used for the Ti-Al weld which has higher levels of Si (0.47% as compared to 0.30% for the other welds). Si is a ferrite forming element which raises the ferrite start temperature which in turn favours increased PF(G) and FS growth before the beginning of the AF transformation and results in a higher value of t. The value of t used for Ti-Al is likely to be too small and hence the actual volume of untransformed austenite, F_γ, will be less than was assumed. This is supported by microstructural observations which show that the Ti-Al weld is characterized by thicker PF(G) and FS phases (Figure 4.7) than for the other welds (Figures 4.2 to 4.6).

The second possible reason for the low value of AF/F_γ is related to the hypothesis that the Ti rich phase occurs just as spherical caps on the

surface of the inclusions which was based on observations of the inclusions in the SM weld (Section 4.2.2.5.). Observations of the inclusions in the Ti-Al weld, however, seem to indicate that a certain proportion of the Ti can be found in the center of the Al rich inclusions. This is supported by the data for the chemical composition of the inclusions in the matrix which show that the relative intensity of Ti and Al increase with increasing inclusion diameter. Since the electron beam is situated in the center of the inclusions during the analysis, if the Ti rich phase is just on the surface of the inclusion then the proportion of the electron beam which excites this phase will decrease with increasing inclusion diameter due to absorption as a result of electron scattering. Hence for large Al rich inclusions, almost none of the surface layer of the inclusion will contribute to the Ti X-ray peak since the electrons will have insufficient energy to efficiently excite the Ti rich layer on the surface. An increase in the average Ti intensity with increasing inclusion diameter indicates that the Ti content in the center of the inclusion is significant.

This suggests that the surface area of the Ti rich phase on the surface of the inclusion, A_{Ti}, was over estimated since some of the Ti can be found inside the inclusion. This results in a value of $N_A x A_{Ti}$ which is higher that its true value.

The fact that the proportion of AF in the Ti-Al weld is less than would be expected from the data for the other welds can therefore be explained in part by a higher Si content in the weld metal and by the presence of a Ti rich phase inside as well as outside the Al rich inclusions.

5.1.3.5. Comparison of the Proposed Model with those of other Researchers

Even though Devillers et al [19,20] have mentioned that the presence of a Ti rich phase is necessary in order to have a high proportion of AF, they did not associate the nucleation of AF directly to this phase but instead proposed that differences in thermal expansion coefficients between the austenite and the inclusions rich in Si, Al and Mn. They proposed that the Ti rich phase prevented the formation of a layer which completely surrounds the inclusions rich in S and Cu which due to its thermal expansion coefficient very close to that of austenite would not favour the formation of AF.

The present results do not support this picture of the role of Ti on the nucleation of AF. Observations of the inclusions have shown that the surface of the inclusions is not covered by just one phase but is generally quite heterogeneous with several phases being present as can be seen in Figure 4.23. It was seen also that the Ti rich phases as well as a phase rich in S (with some Cu at times) can co-exist on the same inclusion. This indicates that the Ti rich phase cannot prevent the formation of a S rich phase which contains Cu.

The model of Devillers et al[19,20] is closely linked to the large difference in the thermal expansion coefficient of the Si, Al and Mn rich inclusions and that of austenite. If this is the case, even in the absence of Ti in the inclusions, these inclusions should be able to nucleate AF (a layer rich in S and Cu cannot completely surround the inclusion). Devillers et al[19,20] did not have nucleation of AF in weld metal with Ti contents of 0.002%. This agrees well with the data for the TiL weld (Ti = 0.002%) where no significant quantities of Ti are found in the inclusions and very little AF was

nucleated. The results of Devillers et al and the present study clearly indicate that the nucleation of AF is not related to the differences in thermal contraction coefficients but is instead related to the surface chemistry of the inclusions as has been shown in Section 5.1.3.3..

The present results illustrate the necessity for the presence of Ti on the surface of the inclusions for the nucleation of AF but appears to disagree with the observations of Dowling et al[4]. These researchers tried to identify the phases present in the inclusions by chemical analysis as well as by diffraction in the transmission electron microscope of inclusions on extraction replicas. They were not able to decide whether the Ti rich phase which they called "TiO" was TiO, TiC and TiN due to the similarity in the lattice constants and crystal structure of these phases and the impossibility to detect light elements with the microscope they were using. In light of their results these researchers concluded that "TiO" was not responsible for the nucleation of AF in the weld W2 which contained 84% AF.

The overall Ti content in the W2 weld was less than 0.005% as for the K6 and K8 welds. Micro-analysis of the inclusions of the last two welds (the results for the W2 weld were not given) showed that Ti was present in the inclusions (between 4 and 8%) for Ti levels below 0.005% indicating that it may be possible that Ti was present in the inclusions in the W2 weld. In addition, Kayali et al[43] found for the same electrode containing higher Mo contents that the inclusions in the weld contained about 4 wt % Ti which supports the hypothesis that Ti was also present in the inclusions in W2. The inability to identify the "TiO" phase in the W2 weld by these researchers may be due to a limited number of inclusions analyzed as well as the difficulty in determining on thick, multi-phased inclusions the presence of a particular phase which occurs in small quantities.

It can be concluded from the present study that a Ti rich phase on the surface of the inclusions is necessary for the extensive nucleation of AF in weld metal. Although several hypothesis concerning the role of Ti on the nucleation of AF have been suggested by other workers, their data do not appear to contradict the trends and conclusions of the present study. The data of Devillers et al[19,20] also support these conclusions.

5.2 MICROSTRUCTURE-TOUGHNESS RELATIONSHIPS FOR EXPERIMENTAL LARGE PASS WELDS

5.2.1. Introduction

The impact toughness as measured by a Charpy specimen is the result of a complex interaction of a multitude of factors which are related not only to the nature of the microstructure but also to the mechanics of the test. Fracture of ferritic steels may occur by cleavage fracture, ductile tearing or a combination of the two processes. Since the impact transition in ferritic steels is associated with the onset of cleavage fracture, a study of the factors that control brittle fracture will give insights into the means by which the low temperature impact resistance can be improved.

It has generally been recognized that the cleavage fracture resistance of ferritic steels is stress controlled, that is, a critical cleavage fracture stress must be exceeded over a microstructurally significant distance ahead of the notch tip for fracture to occur[57,58]. Cleavage fracture will not occur if the yield strength is sufficiently low to allow considerable plastic deformation before the critical cleavage fracture stress is attained due to the stress concentration of the notch root. Since the critical cleavage fracture stress, σ_F^* is almost temperature independent[59], increases in strength due to increased strain rates, microstructural changes or reductions in test temperatures will favour cleavage fracture[60]. The lowest transition temperatures, therefore, will occur for alloys with the highest σ_F^*/σ_y ratios.

The nature of the microstructure will also influence the low temperature fracture resistance. Increased alloying additions of Mn and Ni as well as reduced ferrite grain sizes increases the temperature dependence of the energy release rate for cleavage fracture thereby decreasing the ductile to

brittle transition temperature[61]. The packet size in lath microstructures(i.e. bainite, martensite or acicular ferrite) has been found to have an effect similar to that of the ferrite grain size, that is, smaller packet sizes increase the yield strength but lower the ductile to brittle transition temperature[62]. Additions of C and N were found to decrease the energy release rate for cleavage fracture over the whole low temperature range by a value proportional to the amount of these elements present[63]. These elements are therefore especially detrimental to low temperature cleavage fracture resistance. The detrimental effect of large inclusions on the toughness above the ductile to brittle transition temperature is well documented[63-64] but it is still not clear as to the role inclusions play in the cleavage fracture behaviour of low alloy steels. It has been reported that inclusion cracking can lead to cleavage crack nucleation[65,66] in weld metal but large inclusion volume fractions have also been found to decrease the impact transition temperature[63].

It is generally agreed that increased proportions of AF in the weld metal increases the cleavage fracture resistance and lowers the ductile to brittle transition temperature[67in13,16,18in16,17in18]. This increased fracture resistance has been attributed to the small effective grain size of AF which is due to the large number of high angle boundaries per unit volume which can effectively arrest the propagation of the cleavage microcracks. Constant reinitiation of the cleavage crack is required for fracture to occur which results in a higher energy fracture process than can be obtained in the relatively coarse PF(G) or FS microstructures[16].

Several models have been proposed concerning the beneficial role of AF on the cleavage fracture resistance. Dolby[67] proposed that the impact resistance is determined by competition between the volume fraction of 'tough'

AF, the strength increase due to the AF and the size of the grain boundary ferrite. High toughness is associated with a large volume fraction of a 'soft' phase or high volume fractions of 'tough' AF with little PF(G) present. Garland and Kirkwood[68] proposed that cleavage crack nucleation may occur at the M-A microphases whereas Tweed and Knott[65] proposed that strain localization in the PF(G) was responsible for plastic strain induced cracking of inclusions in the PF(G) which nucleates cleavage fracture. They argue that AF only plays a role by limiting plastic strain to the PF(G) regions.

In the initial portion of this discussion, several of the major factors that influence the formation of acicular ferrite in as-deposited weld metal have been identified. Although increased proportions of AF decrease the transition temperature, the reasons for this increased resistance to cleavage fracture has not been completely identified.

The following discussion will first examine the effects of changes of the proportion of AF and the inclusion density on the strength and cleavage fracture resistance for the data as a whole. The effects of Ti, S, Al, Ca and N on the fracture behaviour both above and below the impact transition temperature will then be discussed in detail. The discussion will conclude with a brief summary of the possible avenues that can be taken to improve further the impact resistance of weld metal.

5.2.2. General Trends

5.2.2.1. Effects of Acicular Ferrite

5.2.2.1.1. Effect on Dynamic Strength

Although many of the factors that favour the formation of AF in weld metal have been identified, there is still not a complete understanding of how AF affects the mechanical properties. Part of the difficulty is that weld

metal microstructures are heterogeneous with softer phases such as PF(G) or FS(A) intermixed with stronger AF phases in varying proportions. There are at present few models that describe the effects of multiple phases on the flow properties but using a number of reasonable assumptions, a simple law of mixtures can be used to describe the strengthening by AF.

The dynamic yield strength can be estimated from the general yield load as was described in 4.3.2.5. At the point of general yielding, there is a high triaxial stress state at the V-notch root and the deformation is mainly plain strain. The changes in the flow stress for a given temperature as a function of the proportion of AF should therefore be described by a model assuming plain strain conditions (i.e. the strain in the two heterogeneous phases is equal). Such a model, proposed by Dieter[69], follows:

$$\sigma_{avg} = f_1\sigma_1 + f_2\sigma_2 \quad \ldots\ldots [5.\ ]$$

where σ_{avg} is the average flow stress, f_1 is the volume fraction of phase 1, σ_1 is the flow stress of phase 1, f_2 is the volume fraction of phase 2 ($f_2 = 1-f_1$) and σ_2 is the flow stress for phase 2. This model predicts a linear relationship between the volume fraction of phase 1 and the resulting flow stress. The strengths of the phases 1 and 2 must remain constant as a function of the AF content for this relationship to hold.

To see if such a relationship can describe the present results, the dynamic yield strength at -30°C which was estimated from the load-temperature diagrams in Chapter 4, was plotted as a function of the AF content of the weld. The results are presented in Figure 5.16. The observed scatter in the estimated dynamic yield strength are also indicated on the plot. A linear rela-

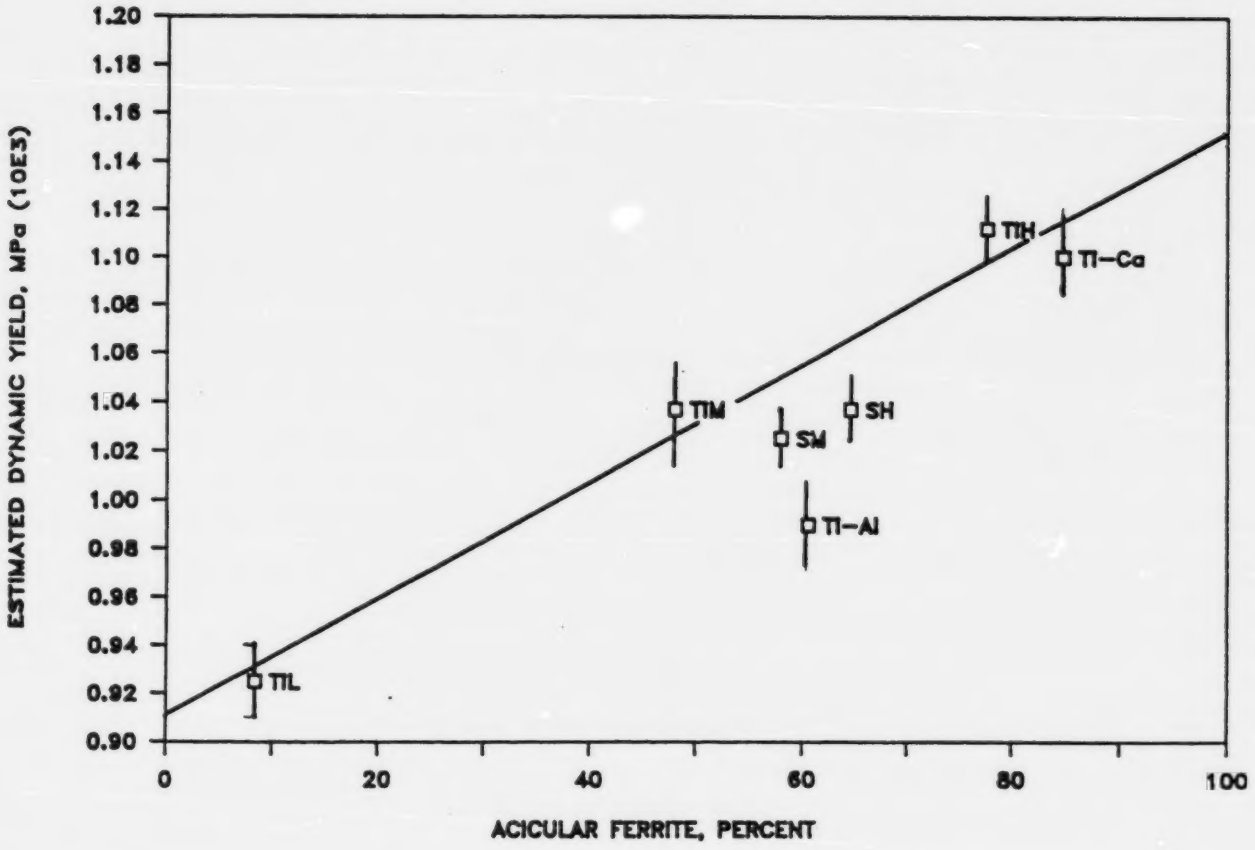

FIGURE 5.16. DYNAMIC YIELD STRENGTH AT -30°C AS A FUNCTION OF AF CONTENT

tionship between the dynamic yield strength and the proportion of AF describe within experimental error, the dynamic yield strengths of the TiL, TiM, TiH and Ti-Ca welds, all of which have similar S contents but different Ti levels. The microhardness of the AF and PF(G) phases were checked for these four specimens. The AF phase has nearly a constant hardness of 220 to 230 VPN whereas the PF(G) microstructures had a microhardness of about 190 to 200 VPN. Hence, the conditions for the Dieter model are satisfied, that is, constant strength of the hard and soft phases as well as near plain strain deformation.

The dynamic yield strength in MPa, σ_{YD}, for the four compositions can be described by the following regression equation and should be compared to the work of Tweed and Knott[17] and Widgery[70 in 17] who found similar trends for room temperature tensile tests for welds with compositions only slightly different from the experimental welds used in this study.

$$\sigma_{YD} = 909 + 2.43 \times (\% \text{ AF})$$

$$\sigma_Y = 389 + 1.52x(\% \text{ AF}) \quad \ldots\ldots\ldots \text{[Tweed and Knott]}$$

$$\sigma_Y = 390 + 1.69x(\% \text{ AF}) + 644(\text{wt\% Ti}) \ldots \text{[Widgery]}$$

The difference in the constants between the static and dynamic results is due to the temperature dependence of the yield strength and the strain rate sensitivity of the weld metal. The greater stress dependence of AF in the dynamic results is due in part to the increased strain rate sensitivity that has been observed in acicular ferrite steels as compared to polygonal ferrite HSLA steels[54]. This regression can be used as a basis from which the strength of the other specimens can be compared.

For the specimens with increasing S contents and inclusion volume fractions as well as increasing AF contents, namely TiM, SM and SH, there is no apparent strengthening due to the increased AF. The dynamic yield strength remains almost constant at 1040 MPa in spite of an increase in the AF content from about 48% to about 64%. Microhardness tests of the AF regions in the SH weld gave values of about 200 VPN which is lower than the value of 220 to 230 VPN measured for the TiM weld. The Dieter relationship will not therefore apply for the series of welds with increasing S contents. The expected strengthening due to the increased AF is compensated for by a reduction in the strength of the stronger phase and there is no increase in strength. This decrease in strength of the AF is not due to coarsening of the AF phases since qualitatively the regions of AF are fine in both the SH and TiM welds. Since the strength of acicular ferrite is determined to a great extent by the dislocation density[54,71 in 13] the decreased strength in the SH weld may be due to a decrease in the dislocation density of the AF regions. Transmission electron microscopy, however, is required to confirm this explanation.

The strength of Ti-Al as was estimated by the Charpy test should not be compared to the data of the other welds since it was shown that premature crack initiation occurred for this specimen. These results are included for comparison purposes only.

5.2.2.1.2. Effect on Cleavage Fracture Resistance

In order to be able to compare the effects of AF on the critical cleavage fracture stress, σ_F^*, welds with similar inclusion distributions and volume fractions but with different amounts of AF should be compared in order to eliminate any effects of inclusions on the fracture process. Fortunately, the series of welds with varying Ti levels, TiL, TiM and TiH meets this

requirement. The critical cleavage fracture stress for all the welds is plotted as a function of the AF content in Figure 5.17 but only the TiL, TiM and TiH welds were considered in a regression analysis. The results for the Ti-Al specimen are considered in this analysis since the fracture stress measured is for cleavage fracture although the initiation appears to be slightly premature and is caused by a shear mechanism. The critical cleavage fracture stress is only an apparent value for this weld. As was the case for the dynamic yield strength, there is a linear relationship between the percentage of AF and the critical cleavage fracture stress in MPa which is as follows.

$$\sigma_F^* = 2075 + 6.16(\% \text{ AF})$$

This equation predicts a critical cleavage fracture stress of about 2075 MPa for a ferritic matrix that does not contain AF which agrees well with values of 2030 to 2188 measured for several low carbon polygonal ferrite HSLA steels[54]. Microstructures that are nearly 100% AF will have σ_F^* values of nearly 2700 MPa which also agree favorably with the value of 2787 MPa measured for a fined-grained controlled rolled acicular ferrite pipeline steel[54].

These results indicate that a simple law of mixtures determines the fracture resistance of weld metal containing both PF(G) and FS phases along with significant proportions of AF. It should be noted that this regression takes into account only the effects of changes in the AF content and is based on an inclusion density for inclusions over 1μm of about $0.3 \times 10^5/cm^2$. The effects of changes in inclusion density on the critical cleavage fracture resistance will be determined in the following section.

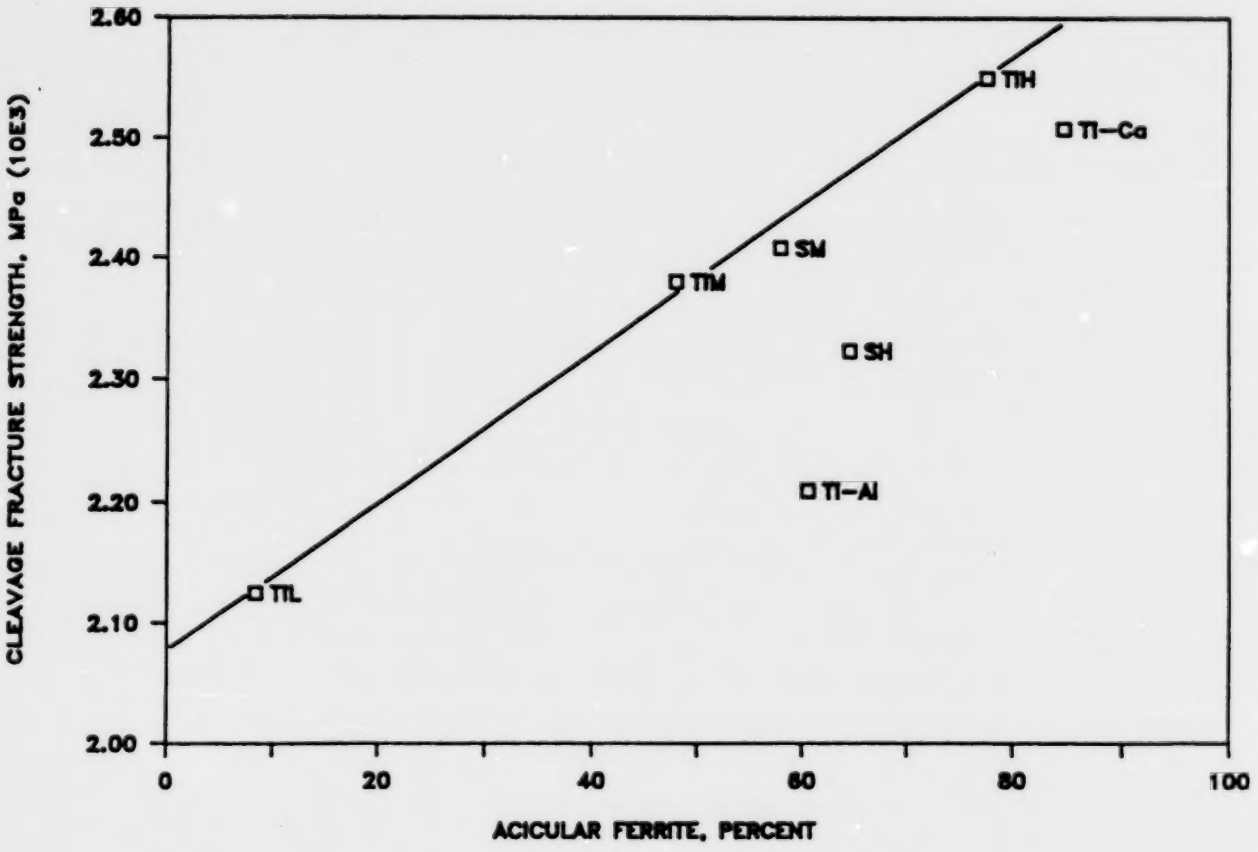

FIGURE 5.17 CRITICAL CLEAVAGE FRACTURE STRESS AS A FUNCTION OF AF CONTENT

5.2.2.2. Effect of Inclusion Density and Size on Critical Cleavage Fracture Stress

It should be noted that in Figure 5.17 that all of the weld samples with inclusion densities greater than that of the Ti series have lower σ_F^* values than is predicted for welds with that particular AF content. Increased densities of inclusions over 1μm decrease the critical cleavage fracture stress for the SM, SH, Ti-Ca and Ti-Al welds from the value that would be expected based on the regression developed in the previous section. This deviation in cleavage fracture strength is plotted as a function of the inclusion density over 1μm in Figure 5.18. There is a clear monotonic relationship between the increase in inclusion density for inclusions larger than 1 μm and the reduction in the critical cleavage fracture resistance. This result indicates that inclusions are playing an important role in the cleavage fracture process for the weld metals and reduce the cleavage fracture resistance. In the detailed discussion of the effects of each of the alloying elements, fractographic observations will be used to clarify the role of inclusions on the reduction of the cleavage fracture strength.

It is expected based on the work of Tweed and Knott[65] and Klassen et al[72] that the inclusion size as well as the inclusion density is also playing a role in the fracture process. Indeed, the welds with the larger inclusions have larger reductions in the cleavage fracture strength, the largest inclusions being found in the Ti-Al weld followed by SH and Ti-Ca. This trend is identical to that of the inclusion density. These larger inclusions will tend to accentuate the effects of increases in inclusion density and explain partially the large difference in fracture resistance of Ti-Al weld compared to the SH weld for only small increases in inclusion densities of inclusions larger than 1 μm($1.04 \times 10^5/cm^2$ for Ti-Al as compared to $0.982 \times 10^5/cm^2$ for SH).

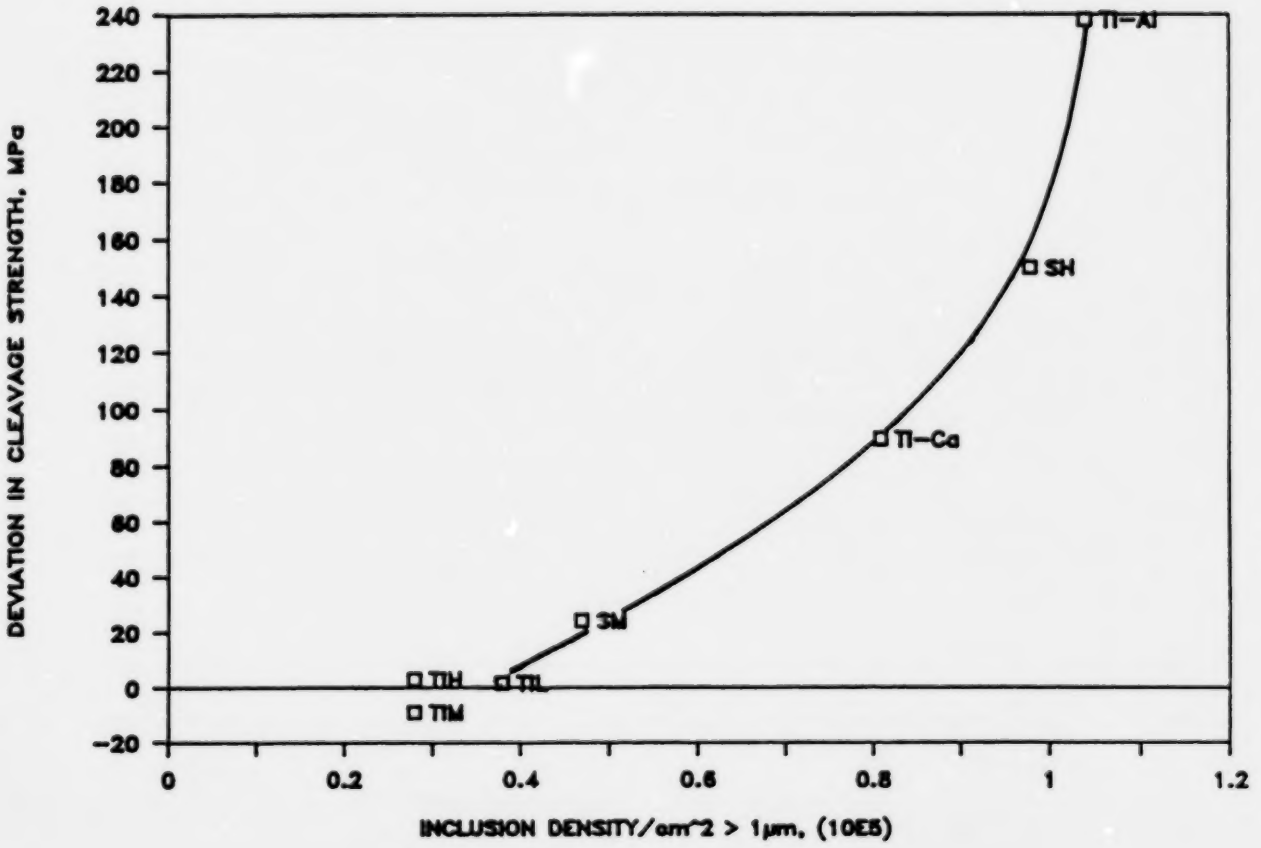

FIGURE 5.18 DEVIATION IN THE CRITICAL CLEAVAGE FRACTURE STRESS AS A FUNCTION OF THE INCLUSION DENSITY GREATER THAN 1μm

5.2.3 Effect of Ti on As-deposited Weld Metal Strength and Toughness

5.2.3.1. Effect on Strength

With increasing Ti levels, the microstructure passes from a predominantly coarse FS microstructure with large microconstituent particles to a predominantly fine AF microstructure with little FS and PF(G). The dynamic yield strength of the weld metal increases with increasing Ti content of the weld metal. This is shown in Figure 5.19 which presents the dynamic yield strength as estimated from the instrumented impact tests at -30°C of all the large pass welds as a function of the Ti concentration. The dynamic yield strength increases rapidly for increases of Ti in the weld metal from 0.002 to 0.008%, thereafter increasing little with increased Ti contents to 0.02%. Only the Ti-Al weld does not follow the trend of the other specimens, with an apparent dynamic yield strength considerably less than would be expected from the level of Ti. This is not surprising, however, since abnormal fracture initiation occurs and the true general yield load is not achieved as was discussed in Section 4.3.2.3..

There are two possible explanations for this increase in strength due to the increased Ti content. The addition of Ti causes grain refinement by increasing the amount of AF which increases the strength due to a Hall-Petch effect[73,74] and by increasing the dislocation density. Strengthening of the matrix by solid solution strengthening and/or the formation of Ti(C,N) is a second possible effect of increased Ti content[55,56]. This second mechanism is favoured for Ti:C ratios below the stoichiometric ratio of Ti carbides[75] which is the case for the present study. For precipitation strengthening to occur, however, Ti must not have already been tied-up by O or N in the inclusions.

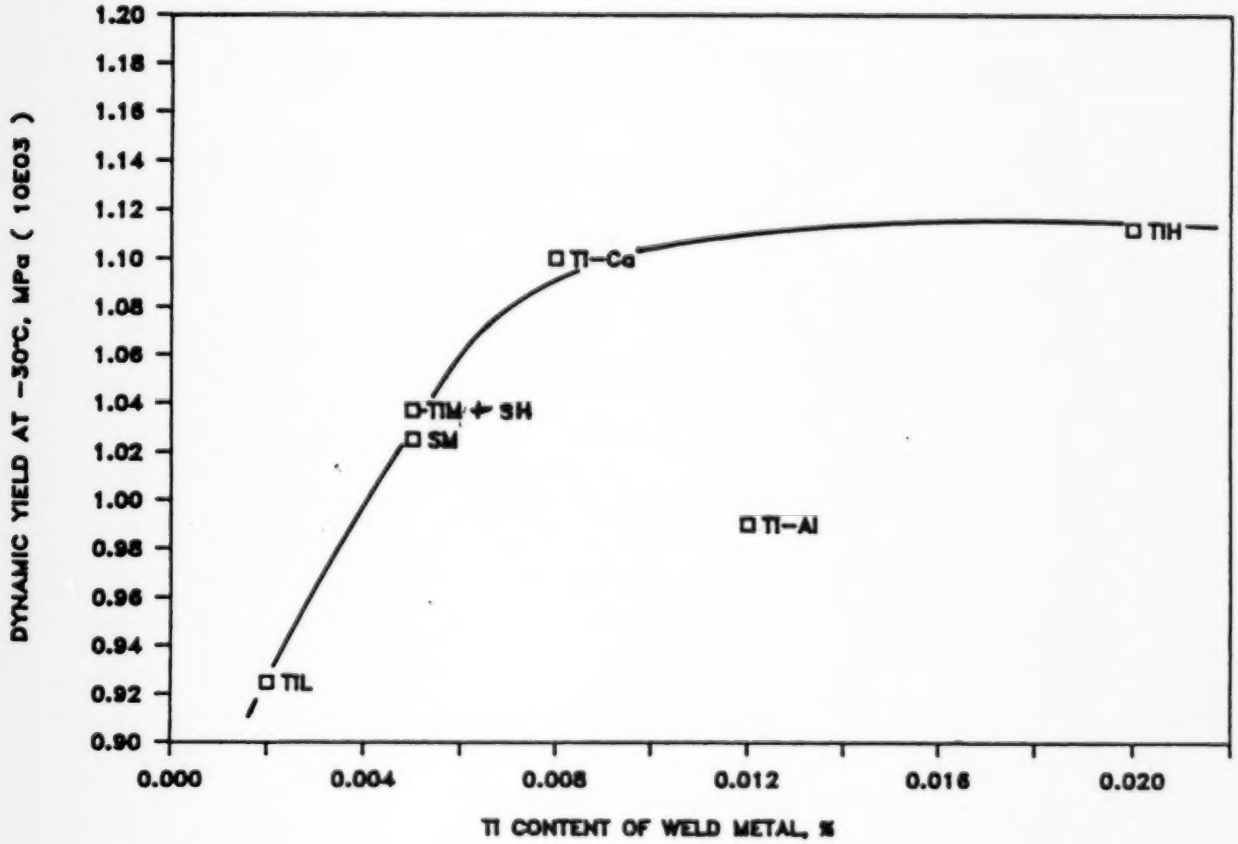

FIGURE 5.19 DYNAMIC YIELD STRENGTH AT -30°C AS A FUNCTION OF Ti CONTENT

The tendencies shown in Figure 5.19 are not consistent with precipitation strengthening being the major reason for the increase in the yield strength of the welds. If precipitation strengthening is occurring then further strength increases should be observed for changes in the Ti content above 0.008%. The increase in strength due to increased Ti contents parallels the increase in AF content of the welds as can be seen by comparing Figure 5.20 with Figure 5.19. Figure 5.20 is a plot of the percentage of AF as a function of the Ti weld metal content. As was concluded in 5.2.2.1.1, these results also confirm that the increased strength due to Ti is not due to increased precipitation strengthening. The effect of Ti is indirect, that is, it is related to its effect on the microstructural development of the weld metal as was discussed in 5.1. This picture of the role of Ti on strength is confirmed by the fact that the cleavage fracture stress increases with increasing Ti contents as was discussed in 5.2.2.2. This is attributed to the grain refinement of the increased proportion of AF. Grain refinement is the only strengthening mechanism that increases both the strength and the cleavage fracture resistance[63]. The fact that the cleavage fracture resistance increases in a linear manner with increased AF content and hence increased Ti content indicates that grain refinement is the dominant strengthening mechanism.

The results of Widgery[70 in 17] (see 5.2.2.1.1.) also supports the suggestion that Ti precipitation is not playing a significant role in the increased strength due to increased Ti contents. He found by multiple regression analysis that Ti increases strength directly by about 644 MPa per weight percent which is only about 2 percent of the observed effect of Ti on strength (29100 MPa per weight percent)in the initial portion of the curve in Figure 5.19.

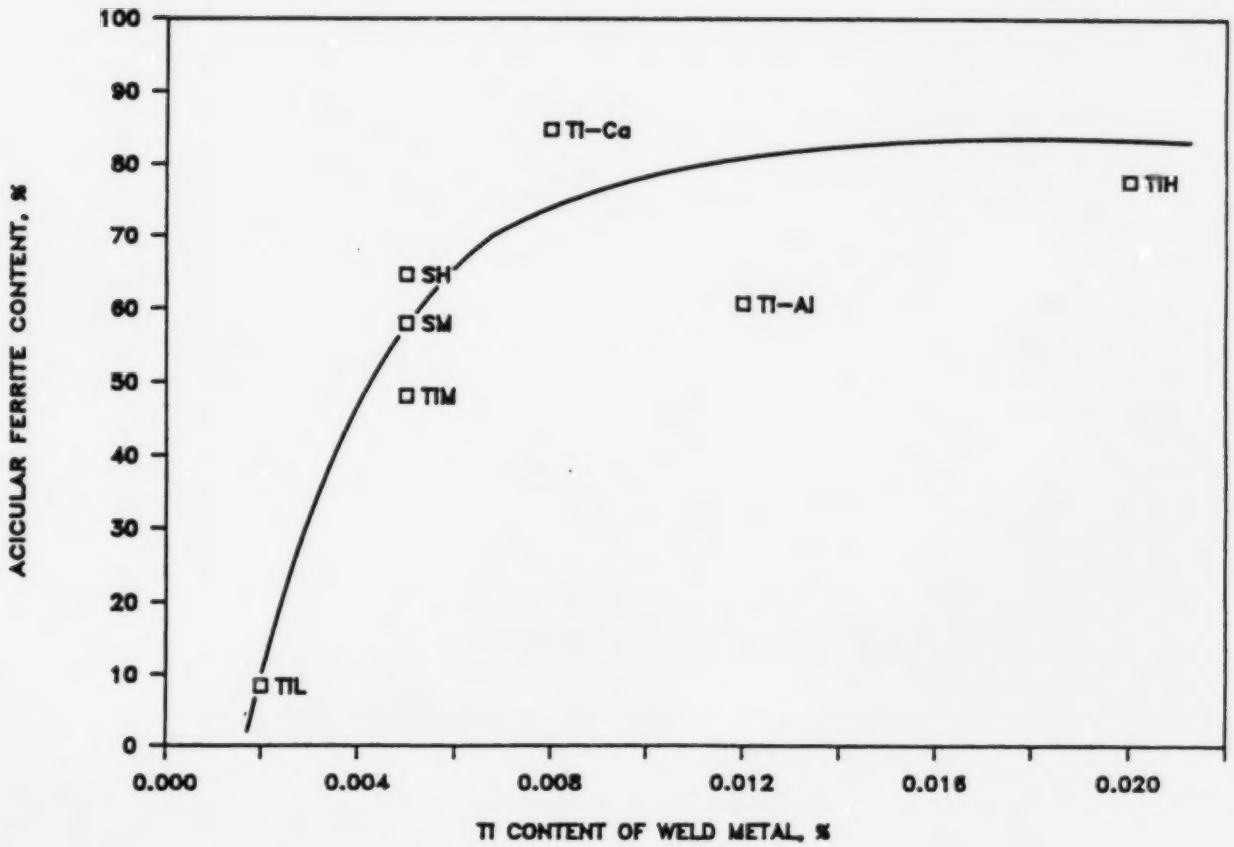

FIGURE 5.20 AF CONTENT IN THE WELD METAL AS A FUNCTION OF Ti CONTENT

5.2.3.2. Effect on Cleavage Fracture Resistance and T_t Temperature

As was seen in 5.2.2.1.2., the cleavage fracture resistance of the as-deposited weld metal is linearly dependent on the proportion of AF present for welds with varying Ti content. On the other hand, the increase in dynamic yield stress also directly dependent on the quantity of AF. The flow stress of the material is raised by the stress concentration factor of the notch root which is about 2.18 for Charpy specimens. Thus for increased low temperature cleavage fracture resistance, the value of σ_F^* must increase faster than 2.18 times the dynamic flow stress. Comparing the slopes of the regression for the critical cleavage fracture strength (Figure 5.17) and the dynamic yield strength (Figure 5.16) vs the AF content, the ratio is 6.16/2.4 =2.5 and is slightly greater than 2.18 which indicates improved impact resistance and lower transition temperatures for increased AF and hence Ti contents.

This analysis is strickly valid for the brittleness transition temperature ($T_{D(N)}$), only, and may not reflect the actual changes in transition temperatures based on an energy criteria such as the T_t temperature used in this study. The T_t temperature not only depends upon the $T_{D(N)}$ temperature but also upon the Charpy slope. For materials with similar $T_{D(N)}$ temperatures, the steel with the lower Charpy slope will have a higher T_t transition temperature even though the cleavage fracture resistance of the two steels is the same.

The Charpy slope is determined by the temperature interval over which the factors that control the initiation of cleavage fracture after significant plastic deformation are operative. If cleavage fracture can be initiated for temperatures well above the $T_{D(N)}$ temperature, the Charpy slope will be decreased since the total energy to fracture the Charpy specimen will be less than for a fully ductile fracture. High work-hardening rates raise the flow stress more rapidly with plastic strain and can raise the flow stress

above that for cleavage fracture at temperatures well above the $T_{D(N)}$[76]. Inclusions or carbides that crack will decrease the cleavage fracture resistance and hence less work hardening is required to raise the stress to a level so that cleavage fracture can occur. Inclusions or second phase particles can also nucleate voids which can sharpen the notch and induce cleavage fracture at temperatures above $T_{D(N)}$[77]. High Charpy slopes and low transition temperatures based on an energy criteria can be achieved for clean materials with low strengths.

The present results are a case in point. There appears to be a large influence of Ti on the impact transition temperature. For an increase in Ti from 0.002% (TiL) to 0.005% (TiM) there is a decrease in the transition temperature of about 25°C. It can be seen from Table 4.9 that the $T_{D(N)}$ temperature decreases only by about 15°C, the difference being due to differences in the impact behaviour in the transition region. The TiL specimen has a much lower Charpy transition slope than does the TiM specimen which is mainly due to a reduced ability of the TiL weld to resist plastically-induced cleavage fracture. It was observed that at temperatures 10°C above the $T_{D(N)}$ temperature, cleavage fracture could be induced by deflections of the Charpy test averaging less than 2 mm for the TiL weld whereas nearly 3 mm was required for the TiM weld. This increased deflection will greatly increase the energy absorbing capacity of the TiM weld and result in a faster ductile to brittle transition for the TiM weld and thus lower T_t temperatures.

There are a number of reasons why the TiL specimen has poorer impact resistance than TiM. There is a transition in the cleavage fracture behaviour of the TiM compared to the TiL weld. The coarse cleavage facets (more than 100μm in diameter, see 4.3.3.2.) associated with the FS(A) microstructure in the TiL weld are replaced by finer cleavage facets and regions of

ductile tearing in the TiM weld tested at the same temperature. Cleavage fracture is associated with PF(G) in TiM and not FS(A) as was the case for TiL. Since the PF(G) has a smaller effective grain size than FS(A), the fracture resistance is improved. The high angle boundaries in the PF(G) regions limit the slip distance so that dislocation pileup at obstacles is reduced. By contrast, cleavage facets were observed with sizes of over 100 μm in the TiL weld which indicates that only low angle boundaries separate the individual laths. This type of cleavage fracture will require only small energies to propagate. The aligned microconstituent phases in the FS(A) microstructure will also have less resistance to brittle failure. They are likely to be more effective barriers to dislocation motion since dislocations cannot slip around them as could be the case in the TiM weld where the microconstituents are more globular in the PF(G) structures. Also, the aligned microconstituents would be more susceptible to fiber loading which would also increase their likelihood of cracking at low strains[17]. This last effect will also reduce the ability of the TiL specimen to resist plastically induced cleavage fracture which will raise the transition temperature as was discussed above.

For the higher Ti levels in TiH, the microstructure is predominantly AF but there is an <u>increase</u> and not a <u>decrease</u> in the T_t impact transition temperature as would have been normally expected based on the improved cleavage fracture resistance of this weld. Two factors are responsible for this. First, the increased strength of the TiH specimen due to the increased AF content cancels any beneficial effect the increased critical cleavage fracture resistance has on the impact transition temperature with a net result that the $T_{D(N)}$ temperatures are not very different between the TiM and TiH welds (-40 and -42°C respectively). The T_t transition temperature is increased, however, since the TiH weld has a lower Charpy slope than TiM. The reduced slope for acicular ferrite steels has been observed elsewhere [54].

The ascribed beneficial effect of the AF may be in fact due to the elimination of the brittle FS phases as well as the reduction in the effective grain size of the PF(G) as compared to FS(A) when extensive PF(G) occurs. The section which follows, proposes a new model for the cleavage fracture process in weld metal. It is supported by observations of the fracture surface and oblique sections of the fractured Charpy specimens near the transition temperature.

5.2.3.3. Proposed Model for the Cleavage Fracture Process in Weld Metal Containing Significant Quantities of AF

Since there is no satisfactory model for the cleavage fracture for heterogeneous materials that contain a weak brittle phase and a strong tough phase as is the case for weld metal containing significant quantities of AF, the changes in the fracture resistance can be only described in qualitative terms. The recent model of Tweed and Knott[17] which was developed from Crack Opening Displacement Tests(COD) assumes that strain localization occurs in the softer phase due to its lower strength. This strain localization will result in cracking of inclusions and hence initiate cleavage fracture. This model, however, may not accurately describe the cleavage fracture process occurring in heterogeneous weld microstructure below the notch root in a Charpy specimen since near plain strain conditions exist and the AF and PF(G) or FS phases must undergo nearly equal strains.

It is proposed, that before cleavage fracture occurs below the notch root, the weld metal is subjected to near plain strain deformation, that is, all parts of the microstructure undergo nearly equal deformation. Due to the higher strength and work hardening rate of AF[54], there will be a stress differential between it and the PF(G) and FS phases. The PF(G) microstructure will not be expected to have strain localizations as was described by Tweed and

Knott except near the interface of the AF where some localized strain may occur to accommodate for the difference in stress levels between the PF(G) and AF phases. This stress differential and resulting localized strain at the AF-PF(G) or AF-FS interface may favour cleavage crack initiation in the coarser PF(G) phase or cleavage crack initiation by the cracking of inclusions or carbides in the regions adjacent to the stronger AF phase. The cleavage microcracks will propagate preferentially in the PF(G) or FS phases due to the larger effective grain size of these microstructures. The final fracture process will be the link-up of these microcracks and will occur predominantly in the PF(G) or FS regions of the weld. Cleavage fracture will be difficult in the AF due to the high critical cleavage fracture strength of the AF phase.

The fracture process will, therefore, be a balance between the amount of AF and the amount of PF(G) or FS phases. Increased proportions of AF will increase the total stress level and therefore the stress differential between the AF and PF(G) phases which will favour cleavage fracture initiation. On the other hand, increased proportions of AF will result in decreased proportions of PF(G) and FS present that can take part in the fracture process thereby increasing the fracture resistance since at least part of the final fracture process must take place in the tougher AF region of the weld. For high AF contents, the stress differential between the AF and PF(G) is high but the width of the grain boundary ferrite is narrow, so the link-up of the cleavage microcracks is difficult and the fracture process is controlled by the AF.

There is considerable fractographic evidence to support this picture of the fracture process from the results for the welds with varying Ti contents. For low Ti levels, the AF content is low and does not have a significant influence on the cleavage fracture resistance. In this case, the fracture process is controlled by the dominant phase which is FS. The reasons for

the poor impact resistance of this phase is described in the previous section. An increase in the proportion of AF reduces the amount of the 'brittle' phase present for fracture but increases the stress differential at the AF-PF(G) or AF-FS interface due to the general increase in stress level due to the increased proportion of AF. This will favour cleavage crack initiation and explains the increase in density of non-propagating microcracks as was observed in the TiM weld(see Section 4.3.3.2.) These microcracks are often associated with the AF interface (Figure 4.37(b)). This observation has also been reported by Tweed and Knott[17]. Since the PF(G) in the TiM has a smaller effective grain size, the link-up of these microcracks is more difficult with a resulting increase in fracture resistance. For high AF contents, the narrow width of the PF(G) phase limits the length of the microcracks that form at the AF interface (See Figure 4.38(b)). As a result, the amount of cleavage fracture in the PF(G) is reduced. This explains the reduction in the amount of cleavage facets observed on the fracture surface in Figure 4.38(a).

This model gives valuable new insights into the fracture process in heterogeneous weld metal and will be used to suggest new avenues for the possible increase in fracture resistance of weld metal in a later section.

5.2.3.4. Effect on Impact Resistance above the Impact Transition Temperature

The ductility and impact resistance at test temperatures near the upper shelf region is affected not only by the increased Ti contents but the microstructure as well. The TiM weld has higher displacements to maximum load (ductile fracture is assumed to begin at this point) than either TiL or TiH which results in the highest impact energy for this material. This effect can be partially explained by the relationship of microstructure to ductility. For the TiL weld, the relatively coarse FS microstructure with its relatively large

martensite-austenite constituent phases as well as its moderate inclusion density over 1.0 μm (0.28 x $10^5/cm^2$) will favour the onset of ductile fracture by microvoid growth and coalescence which nucleate at the large number of relatively large second phase particles (i.e. > 1μm). Although the volume fraction of inclusions is an important parameter in determining the strain to fracture, the size distribution of inclusions also plays a significant role, large inclusions being more favourable to strain localizations and unstable fracture.[72]. Microvoids have been shown to form around inclusions and carbides by interfacial decohesion. Iricibar et al[75] have shown that the particle size and location are very important on the nucleation of microvoids. Large inclusions on grain boundaries are the most favourable sites for void nucleation. It has been recognized that the ductile fracture process is inherently statistical in nature, the fracture path occurring in the weakest regions of the material[75]. In the case of TiL, the larger volume fraction of large inclusions and microconstituent phases will be expected to hasten the onset of ductile fracture thereby decreasing the total absorbed energy in the upper shelf region as compared to TiM.

In the TiH weld there are no inclusions over 1.5 μm and the microconstituent phases are very much finer in the AF regions so it would be expected that very high impact toughness and large displacements to fracture in the upper shelf region should result. This is, however, not the case. At the highest test temperatures, the TiH weld has the lowest absorbed energy of all the welds in the series with varying Ti content and has impact energies considerably less than the TiM weld. The higher strength of the TiH weld results in higher stresses in the notch root. AF has higher work hardening rates than PF(G) or FS but this cannot compensate for the higher stress levels and tensile instability will occur for small strains (i.e. displacements to maximum load). This decreases the area under the load-displacement curve and hence the total

absorbed energy for fracture to occur. This is evident when comparing the load-displacement traces of the TiH and the TiM weld specimens tested at 0°C (See Figure 4.29).

5.2.4 Effect of S on Toughness

The decrease in the upper shelf energy and of the displacement to fracture and the increased transition temperature of the SH as compared with the SM or TiM welds can be ascribed to the detrimental effect of the large MnS inclusions. It was shown in Section 5.2.2.2. that the increased density of large MnS inclusions decreases the critical cleavage fracture strength but this is accompanied by a reduction in the dynamic yield strength with the result that the $T_{D(N)}$ temperatures for the SH and TiM welds remain about constant at -40°C. There is, however, a marked increase in the T_t temperature for the SH weld (-15°C) as compared with the TiM weld (-32°C). This discrepancy is due to the low Charpy slope of SH as compared with TiM. The load displacement curves for the TiM and SH specimens tested at 0°C show that cleavage fracture occurs after displacements of 3 mm for the SH specimen whereas over 6 mm is required to initiate cleavage fracture in the TiM specimen. This premature cleavage fracture in SH reduces the area under the load-displacement curve. Larger differences in temperature between the $T_{D(N)}$ and T_t are required for the SH weld in order for the displacement to fracture to be sufficient to give energies of greater than 50 J/cm^2. Thus the lower Charpy slope for the SH weld increases the T_t temperature which is a result of the detrimental effect of the large inclusions on cleavage fracture initiation after plastic deformation.

Fractographic evidence shows that cleavage fracture is initiated near large inclusions in both the PF(G) and AF phases (see Figure 4.39(c)&(d)). This is contrary to the results of the Ti series of welds where non-propagating microcracks form exclusively in the PF(G) and FS phases. The main fracture

surface forms after considerable plastic deformation. A microvoid formed around the large MnS inclusion in Figure 4.39(c) and cleavage fracture occurred after strain hardening of the ferrite phase. The site of cleavage crack nucleation is several μm away from the inclusion surface. Hence, plastically induced cleavage fracture is relatively easy in the SH weld and accounts for the low Charpy slope and higher transition temperatures.

There is a detrimental effect of the large inclusions on the AF phases also since many non-propagating microcracks are observed near the large inclusions which was not observed in the TiM weld with lower S contents. This indicates that the cleavage fracture resistance of the AF is being reduced by the presence of large inclusions. This would be expected to have a large effect on the transition temperature since σ_f will be reduced in the AF phase but this detrimental effect is mitigated by lower than expected strength of the SH weld for the quantity of AF present and there is not a large shift in the $T_{D(N)}$ temperature.

5.2.5. Effect of Ca on Toughness

The addition of Ca as an deoxidant increased the proportion of AF dramatically. However, there is an increase in strength due to increased Ti levels as was discussed in Section 5.2.2.2.1. and there is an increase in the number of inclusions over 1μm ($0.81 \times 10^5/cm^2$ as compared to $0.28 \times 10^5/cm^2$ for the TiM). Both of these effects will have a tendency to increase the impact transition temperature. There is, however, a marked increase in the cleavage fracture resistance of Ti-Ca as compared to TiM (2508 MPa as compared to 2380 MPa) due to the increased AF content of the Ti-Ca weld which more than compensates for the increased strength with a net decrease in the $T_{D(N)}$ transition temperature to -45°C from -40°C for the TiM weld. The T_t transition temperature increases about 5°C, however, due to a reduced Charpy slope which can be

attributed to the effect of higher levels of AF and higer work-hardening rates as was discussed in Section 5.2.3.2.

The Ti-Ca weld has a critical cleavage fracture stress of 2508 MPa which is about 90 MPa less than would be expected for a weld with its AF content of about 84% (see section 5.2.2.1.2.). It appears that the increased density of inclusion over 1μm is related to this reduced cleavage fracture resistance. Fractographic studies have shown that several cracked inclusions in the AF region favours the nucleation of cleavage fracture thereby reducing the critical cleavage fracture stress (see arrows in Figure 4.40(c)). Smith[81] has proposed a model for cleavage fracture initiation caused by inclusion cracking.

$$\sigma_F = \pi/2 \left(\left(2 E \gamma_p \right)/\pi(1-\nu^2)a \right)^{0.5}$$

where σ_F is fracture stress, E = Young's Modulus for ferrite (200 GNm^{-2}), γ_p surface energy for ferrite (14 Jm^{-2}), v is Poissons ratio, and a is the radius of the cracked inclusion. The cracked inclusions in Figure 4.40(c) have a diameter of 1.5 μm which gives a cleavage fracture stress of about 2500 MPa which is identical to the value of the cleavage strength measured for this weld by instrumented impact tests. It is concluded that the fracture of these inclusions is controlling the cleavage fracture resistance of the AF phase and is responsible for the reduced cleavage fracture strength for this weld. Contrary to the TiH weld with similar AF contents, many non-propagating cleavage microcracks are observed on the oblique sections in the AF regions in the Ti-Ca which indicates that inclusions are favouring cleavage fracture. It should be noted that not all inclusions crack in this manner, several large inclusions can be observed in Figure 4.40(c) which have not cracked. Although identification of the chemical composition of these cracked inclusions has not

been performed. Tweed and Knott[65] have found that Ca rich inclusions are susceptible to fracture and it is assumed that a similar trend holds here.

It should be noted that the effect of inclusion cracking is a strong function of the inclusion diameter. If large Ca rich inclusions are present then the cleavage fracture resistance will be greatly decreased. For example an inclusion of 2μm will have a fracture resistance of about 2200 MPa. On the other hand, inclusions with a diameter less than 1.3 μm will have a fracture resistance greater than the maximum for AF and therefore will not contribute to cleavage crack nucleation. Fortunately, in the Ti-Ca weld there are very few inclusions above 1.5 μm which explains the high cleavage fracture resistance of this weld. If the maximum diameter of inclusion can be reduced to below 1.3 μm then the maximum cleavage fracture resistance for this microstructure can be obtained.

5.2.6. Effect of Al on Toughness

The presence of large Al_2O_3 inclusions has a detrimental effect on the impact resistance of the Charpy specimens for temperatures below 10°C. The load-displacement curves from the instrumented impact tests have shown that premature crack initiation occurs in this specimen. There were well defined regions of shear (Figure 4.41(a))that formed just below the root of the notch in the regions of high stress concentration and high hydrostatic stresses. Extensive void formation around the inclusions is favoured by the large inclusion size, high density of large inclusions and the high hydrostatic stresses[78]. The link-up of these voids by a shear process is favoured by low work hardening rates[78] and the presence of a dispersion of fine carbides.

As was stated in Section 5.1.2.1., it is possible that the precipitation of Ti(C,N) is occurring in this weld metal due to the presence of Al.

If this is the case, the fine dispersion of particles will favour the link-up of the voids that form around the large Al inclusions by localized shear. The increased precipitation strengthening will increase the strength and decrease the work hardening rate, both which favour localized shear fracture. This will result in the premature fracture initiation such as that which occurs in the Ti-Al weld. This detrimental effect of large Al rich inclusions on the impact properties has been reported by others[38].

5.2.7. Effect of Nitrogen on Toughness

It was shown in Section 4.3.1.5. that variations in the nitrogen levels has a marked effect on the variability of the toughness values in the impact transition region of the TiM weld, high nitrogen levels being associated with low impact resistance. There appears to be two distinct levels of N in the TiM welds, around 100 and 180 ppm. This fact can be used to estimate the absolute effect of N on the changes in the toughness values as well as the impact transition temperature and the critical cleavage fracture strength.

Figure 5.21 shows the toughness of the weld metal as a function of the N content for impact tests of the TiM weld at -30 and -40°C. There is a linear relationship between the N content and the toughness in J such that K_V = 162 -7630 J/(% N). The value of the slope is the same order of magnitude as the value of 10000 J/%N found in a study of shielded arc welds[79]. This high value shows that N is very detrimental to weld metal toughness.

There is scatter in the load-temperature diagram of the TiM weld which can also be related to the variation in the N content. Since there appears to be two distince levels of N for the TiM weld, two load-temperature diagrams can be constructed from the instrumented impact data, one with a N level of 100 ppm and the other with 180 ppm as is presented in Figure 5.22.

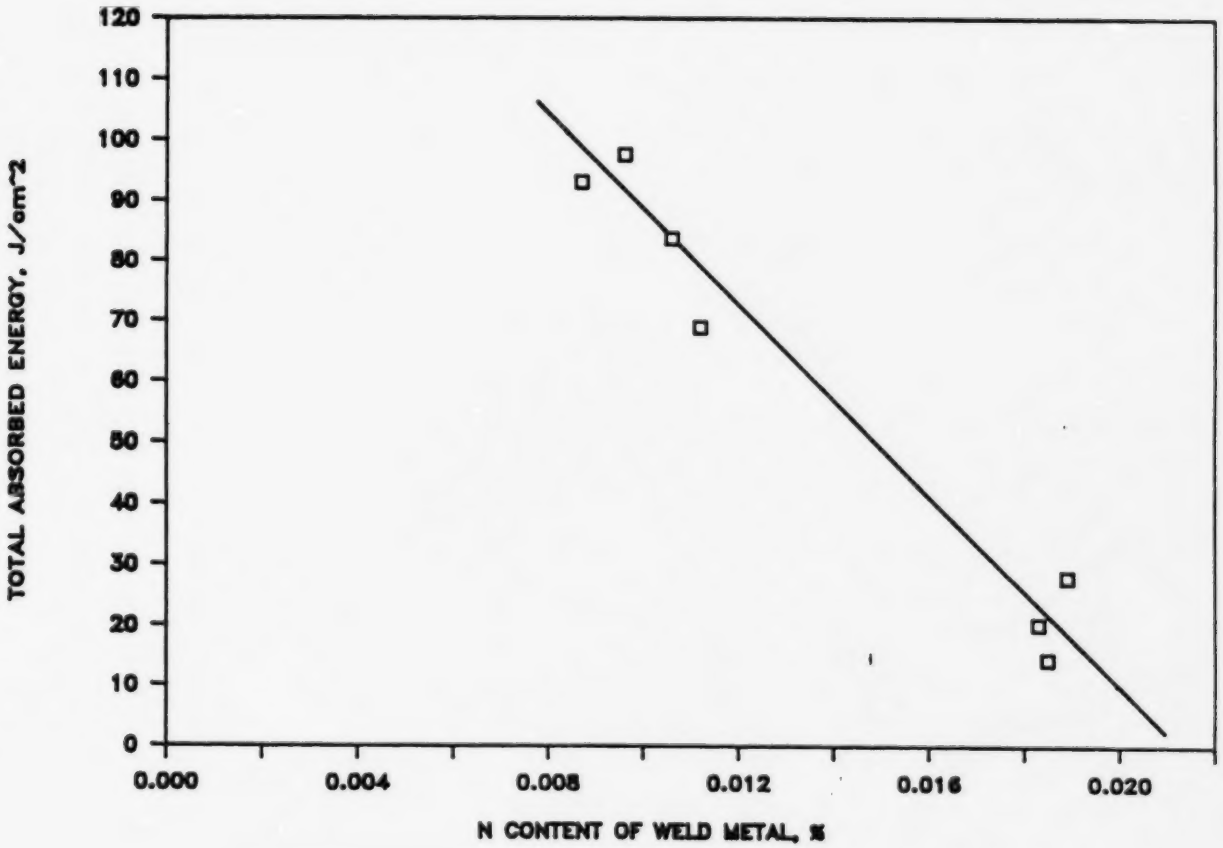

FIGURE 5.21 EFFECT OF N CONTENT ON ABSORBED ENERGY FOR CHARPY TESTS AT -30°C AND -40°C

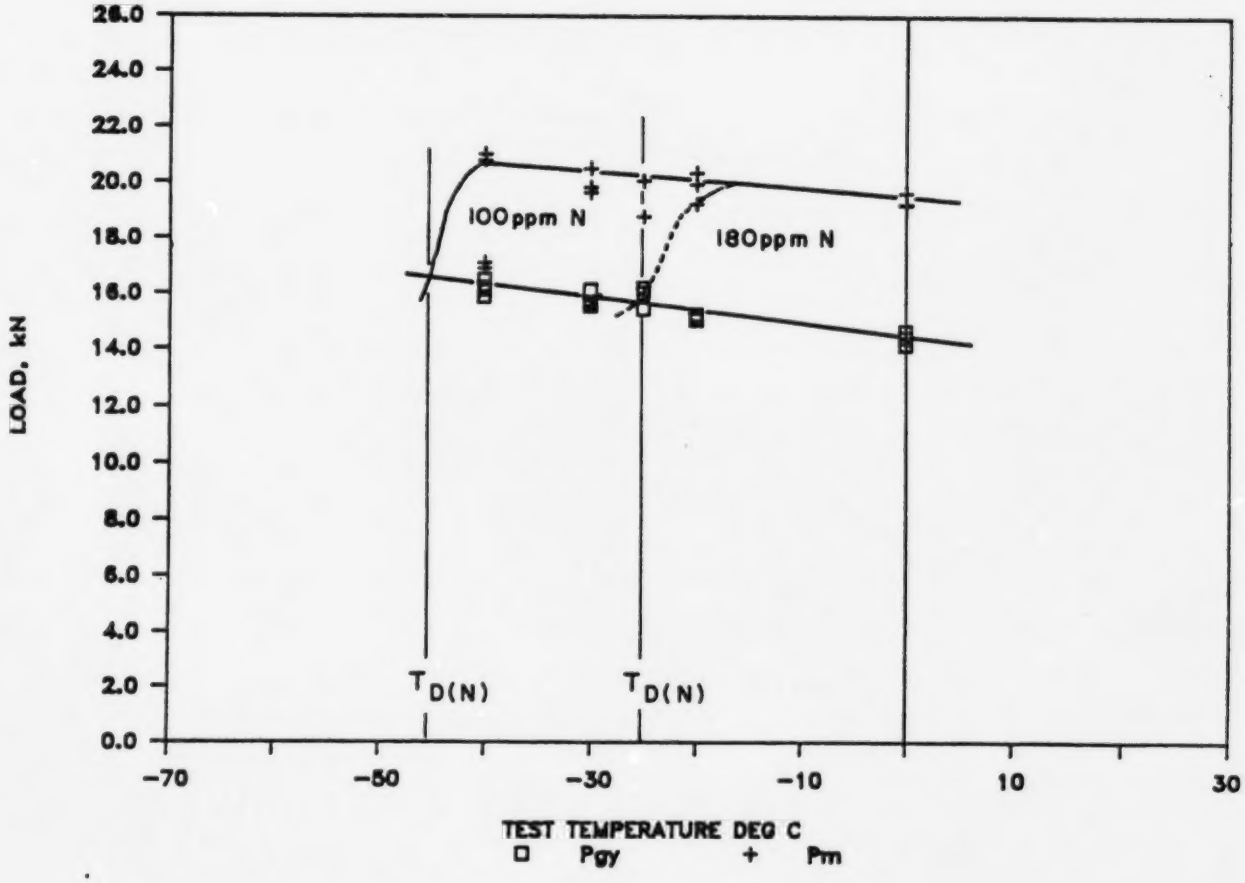

FIGURE 5.22 LOAD-TEMPERATURE DIAGRAM FOR THE TiM WELD WITH 100 AND 180 ppm N

For decreased N levels, the $T_{D(N)}$ temperature decreases from -25°C for 180 ppm to below -40°C for 100 ppm. This results in an increase in the critical cleavage fracture stress from 2240 MPa to 2400 MPa. It should be noted that a reduction in the N content of the weld metal by about 80 ppm has about the same effect on the reduction in the $T_{D(N)}$ temperature as does passing from 8% AF to 84% AF in the weld metal. This underlines the need for the reduction in the N levels to as low a level as possible in order to ensure good impact resistance of the weld metal.

It is generally recognized that interstitial nitrogen embrittles steels and the loss in toughness due to nitrogen is due to dislocation locking[63,80] and solid solution hardening. Due to the ease of diffusion, interstitial N is found preferentially on dislocations. Hence, it would be expected that N will have the most effect on AF due to its high dislocation density. Fractographic evidence shows that this is the case. For welds with lower N levels, the regions of AF failed by ductile tearing (Figure 4.37(a) and 4.42(a)) whereas for high N levels cleavage cracks form in the regions of AF (Figures 4.42(b)&(c)). This embrittling effect of the AF can be explained by the reduced mobility of dislocations which favours the cleavage fracture process. Since it was shown in Section 5.2. that the cleavage fracture stress depends upon the fracture resistance of the AF phase, any reduction in cleavage fracture resistance of the AF phase will have a marked effect on the weld metal as a whole. Hence, in the development of electrodes for low temperature service, not only is it important to control carefully the composition and inclusion density in order to ensure a high proportion of AF, but it is also important to ensure that the N levels in the weld metal be kept as low as possible so that the full benefit of the increased AF content on the toughness of the weld metal can be realized.

Bonnet and Angeli[40] also found a marked effect of N on the toughness of C-Mn welds at -40°C with trends similar to those found in the present study. They found an increasing dependence of N on the absorbed energy for decreasing N levels below 100 ppm. From their data it appears that Ti reduces the detrimental effect of N on toughness whereas V and Nb additions have the opposite effect. Although, high N levels will reduce the impact resistance, it appears that through careful control of the weld metal chemistry that its detrimental effect will be somewhat reduced.

N will also have a detrimental effect on other regions of the weld such as the heat affected zone as was shown by McRobie and Knott[81] for COD tests in simulated reheated weld metal. It was argued that strain-ageing reduces toughness by increasing the localized flow stress.

5.2.7. Possible Avenues for Improved Toughness in As-deposited Weld Metal

The present results suggest several ways in which improved toughness of weld metal can be achieved. An increase in the AF content to nearly 100% should result in slightly lower transition temperatures. This effect will not, however, be large since there will be a corresponding increase in strength which will mitigate the beneficial effect of the increased AF content. Increasing the AF content also reduces the proportion of the FS(A) phase which was shown to have poor cleavage fracture resistance. Every effort should be made to prevent the formation of this phase in the as-deposited weld metal if good impact properties are desired. It was found that the inclusion density of inclusions over 1μm is playing a significant role in the fracture process, the maximum resistance to cleavage fracture occurring for low inclusion densities. As was shown for the Ti-Ca weld, if the size of the maximum inclusion is kept below about 1.3 μm, then the inclusions should have little effect on the cleavage fracture resistance.

By far the most important way in which the impact resistance can be increased, is by decreasing the interstitial N content of the weld. This may be achieved by careful shielding or by alloy additions such as B which has a strong affinity for N.

5.3. COMPARISON BETWEEN EXPERIMENTAL LARGE PASS WELDS AND CONVENTIONAL CSA TEST WELDS

5.3.1. Toughness

The large pass welds were used to obtain Charpy specimens that were mainly low toughness as-deposited weld metal. Instrumented impact tests permitted the correlation of the total absorbed energy and the load-time curves to the microstructure, inclusion size and distribution and fracture morphology. Although the results from the large pass weld permitted a better understanding concerning the factors that influence microstructural development and the toughness, they do not directly indicate the performance of the electrodes when they are used for conventional welds. For this reason, Charpy specimens were taken from conventional CSA test welds which were welded using the same electrodes that were used for the experimental welds. This was done to see if good low temperature toughness can be achieved in the standard welds with these electrodes and to see if correlations can be developed between the experimental and conventional weld metal impact properties.

As was anticipated, all of the electrodes gave better toughness in the standard weld as compared with the experimental weld (see Table 4.7 and 4.12). The increase in toughness is related to the following points. First, the percentage of as-deposited weld metal in the fracture path is reduced for the standard welds as compared with the experimental welds (about 30% as compared to 80% for the experimental welds). Second, the microstructure in the standard welds is finer (i.e. smaller austenite grain size, finer network and smaller grain size of the PF(G), finer AF, etc..). Third, the average level of N in the standard welds is 92 ppm (62 to 141 ppm) which is much less than the average level of 211 for the experimental welds (122 to 279 ppm). The present

results show the detrimental effect of N when it increases from 100 ppm to 182 ppm in the TiM weld (Section 4.3.1.5 and 5.2.7). Since the N levels in the industrial welds are less or equal to 100 ppm (except for the TiCa weld which contains 141 ppm N), improved toughness can be expected in the standard welds as compared to the experimental welds where the N content is higher.

Three of the weld metal compositions have T_t transition temperatures below -60°C, namely TiM(-68°C), SM (-63°C) and possibly Ti-Ca (< -60°C) whereas the other welds have transition temperatures near -45°C (TiH -42°C, TiL -45°C, TiAl -43°C and SH -45°C). If the toughness data from the experimental and standard welds are compared, the electrodes that gave relatively high or low toughness in the experimental welds have similar effects in the experimental welds. The toughness results from the experimental welds can therefore be used to rate the perfomance of an electrode for standard welding proceedures. However, the order of the welds in terms of the T_t transition temperature is not exactly the same for the experimental and conventional welds. For example, for the large pass weld SM, the $T_{t(max)}$ is -30°C which is less than the value for TiM (-23°C) whereas the inverse is true for the conventional welds, $T_{t(max)}$ for TiM is -68°C compared to -63°C for SM. This inversion will be discussed in greater detail in Section 5.3.2.

The differences in the order of the transition temperatures of the weld metal for the experimental and conventional welds shows the difficulty in comparing the toughness of welds that are prepared under different conditions. If the as-deposited weld zone is considered, the chemical composition can change significantly as a function of the welding proceedure used. The conventional weld permits a better transfer of the major alloying elements (Mn, Si and Ti) to the weld metal which results in Mn levels of 1.46 to 1.71%, Si levels of 0.37 to 0.70% and Ti levels of 0.002 to 0.034% in the conventional

welds. These should be compared with 1.31 to 1.47% Mn, 0.23 to 0.47% Si and 0.002 to 0.02% Ti in the experimental welds. This increase in alloying additions can affect the toughness by modifying directly the mechanical properties through solid solution and/or precipitation strengthening or by modifying the microstructure by changing the kinetics of the austenite to ferrite transformation. This last effect combined with the higher cooling rate in the conventional welds can greatly modify the microstructural development in the as-deposited weld metal thereby influencing the toughess.

The inclusion size distribution which can also greatly influence the toughness, depends upon the welding conditions. The higher cooling rate in the conventional welds results in an inclusion size distribution that is finer which reduces the number of inclusions larger than 1.0 μm that have been shown to be detrimental to the cleavage fracture resistance in Section 5.2.2.2. For example, in the TiM and SM welds no inclusions larger than 1.0 μm were observed for the conventional welds.

The toughness will also depend upon the proportion of as-deposited and reheated metal in the fracture path. For the experimental welds , the Charpy specimens are almost completely as-deposited weld metal whereas the Charpy specimens from the conventional welds contain a large proportion of relatively tough reheated metal in addition to the as-deposited weld metal. The conventional welds will, therefore be tougher than the experimental large pass welds due to the increased proportion of reheated metal.

Even if it is not possible to make direct correlations between the experimental large pass welds and conventional welds due to the reasons described above, it appears that electrodes that give relatively good toughness in large pass welds will also give good toughness in conventional welds.

5.3.2. The Conventional Welds TiM-I* and SM-I *

The electrodes for the SM and TiM welds gave the as-deposited and reheated weld metal with the lowest transition temperatures for both the large pass and conventional welds. Contrary to the experimental large pass welds, the TiM-I weld gave lower transition temperatures than SM for the conventional industrial type welds which was in spite of a higher N content (102 ppm as compared to 62 ppm for SM-I). Microstructural observations and inclusion analyses were used to explain the inversion in the order of the transition temperature for these two welds.

5.3.2.1. Effect of Inclusions on the Microstructural Development

Figures 5.23 and 5.24 show typical microstructures of the TiM-I and SM-I welds. Table 5.2 gives the results of a quantitative microstructural analysis, the chemical composition of the welds as well as the results of an analysis of the inclusion size distributions and chemical compositions. Figure 5.25 gives the inclusion size distributions and Figure 5.26 presents the relative intensities of Si, S, Ti and Mn as a function of the inclusion diameter for TiM-I and SM-I.

The TiM-I weld has a higher proportion of AF (57.6%) as compared with SM-I (40.2%). The increase in the proportion of AF in TiM-I is due to an increase in FS (39.6% for SM-I as compared to 18.3% for TiM-I). The proportion of PF(G) is constant at about 12.5% for the two welds. The ferrite veins on the prior-austenite grain boundaries which are composed of PF(G) and FS are larger in the SM-I weld.

* I indicates that this is a conventional CSA test weld.

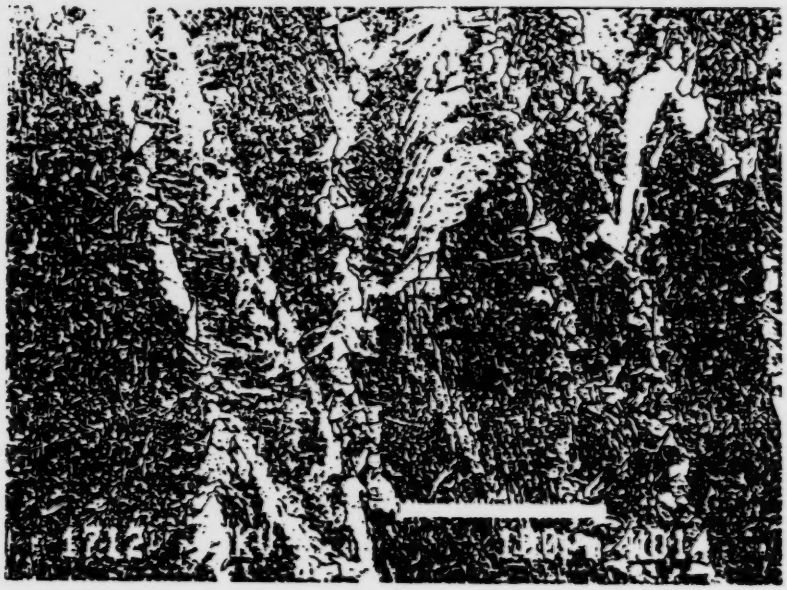

FIGURE 5.23 Micrograph Showing the Caracteristic Microstructure of the Weld TiM-1.

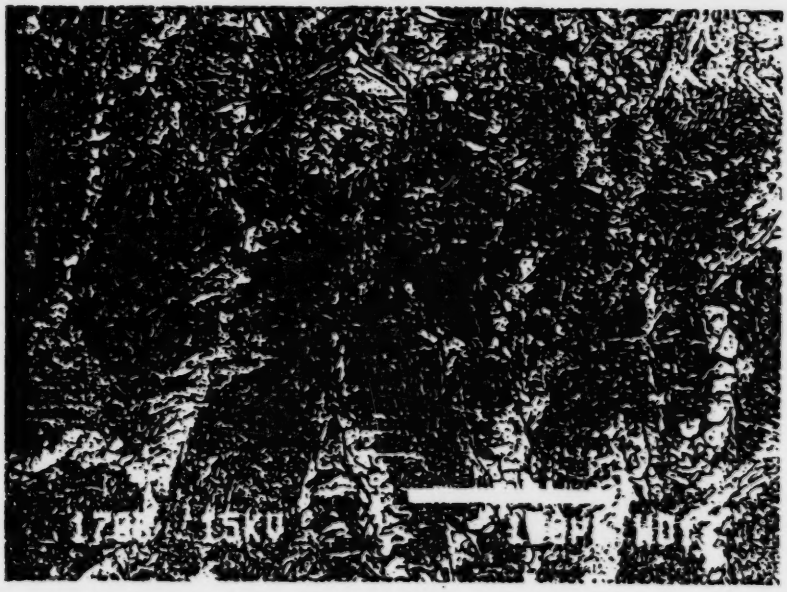

FIGURE 5.24 Micrograph Showing the Caracteristic Microstructure of the Weld SM-1.

TABLE 5.2

SUMMARY OF THE QUANTITATIVE MICROSTRUCTURAL AND INCLUSION ANALYSIS

		TiM-I	SM-I
Chemical composition	Mn (%)	1.68	1.46
	Si (%)	0.52	0.48
	Ti (%)	0.007	0.007
	S (%)	0.010	0.014
	O (ppm)	293	382
	N (ppm)	102	62
Microstructure Analysis	PF (G)	12.5	12.8
	PF (I)	11.5	7.1
	AF	57.6	40.2
	FS (NA)	12.5	28.2
	FS (A)	5.8	11.4
	austenite grain size S/L (mm)	22.3	16.0
Inclusion analysis	Mean diameter (μm)	0.35	0.35
	Mediam diameter (μm)	0.35	0.34
	Volume fraction (%)	0.34	0.43
	N_A ($\times 10^5 cm^{-2}$)	30.52	38.14
	N_A diam$_5$>1μm ($\times 10^5 cm^{-2}$)	0	0
Chemical Composition of Inclusion (average relative intensities	AL	0	0
	Si	25.8	26.2
	S	9.1	8.6
	Ti	6.6	6.5
	Mn	58.5	58.7
	Ca	0	0
AF Nucleation	Fγ (t=0.0175mm)	0.70	0.59
	AF/F	0.82	0.68
	A_{ti} (μm^2)	0.0691	0.0699
	$N_A \times A_{ti}$ ($\times 10^{-4} cm^2/cm^2$)	21.08	26.66

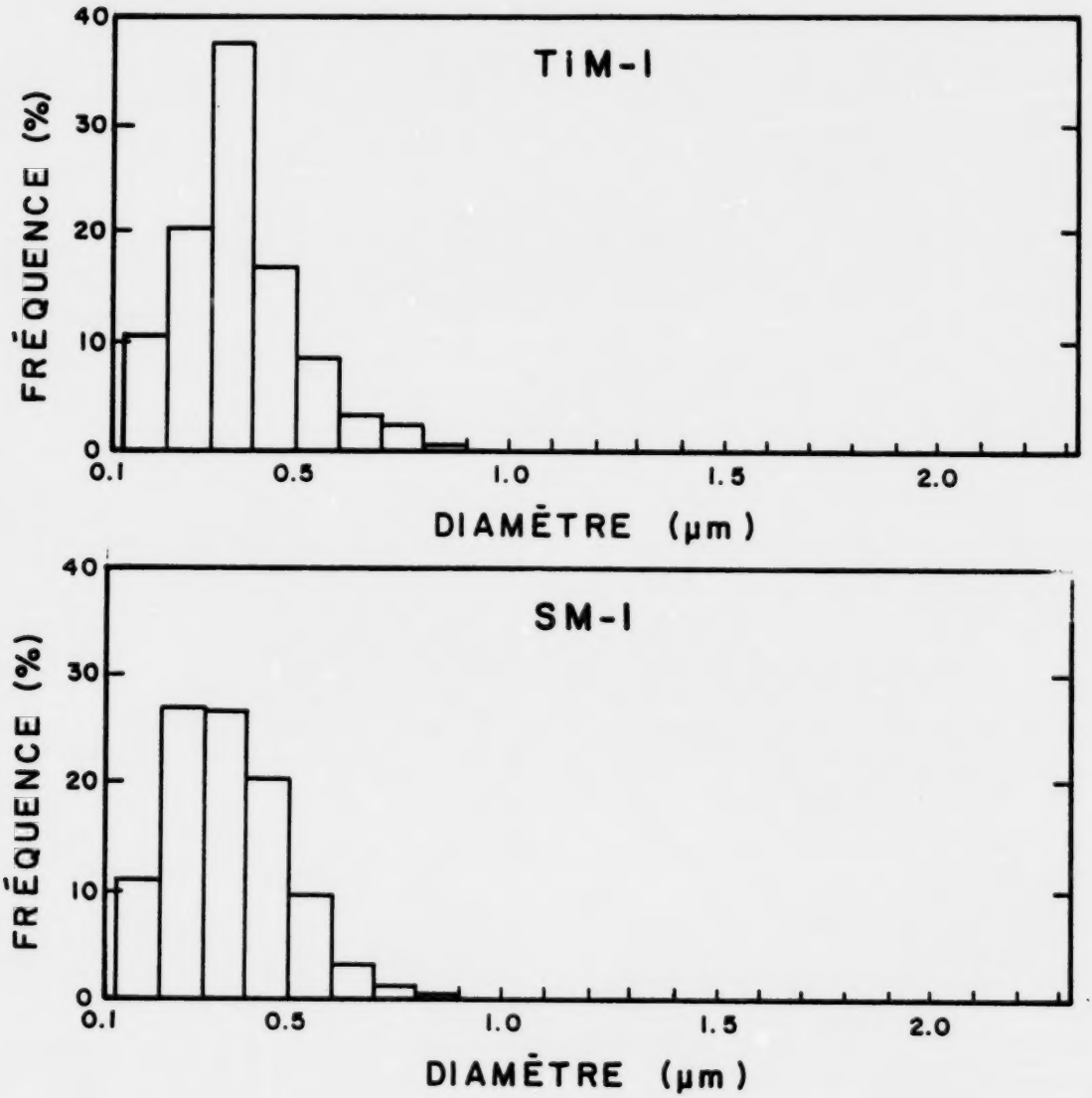

FIGURE 5.25 Inclusion Size Distributions of TiM-1 and SM-1 Welds.

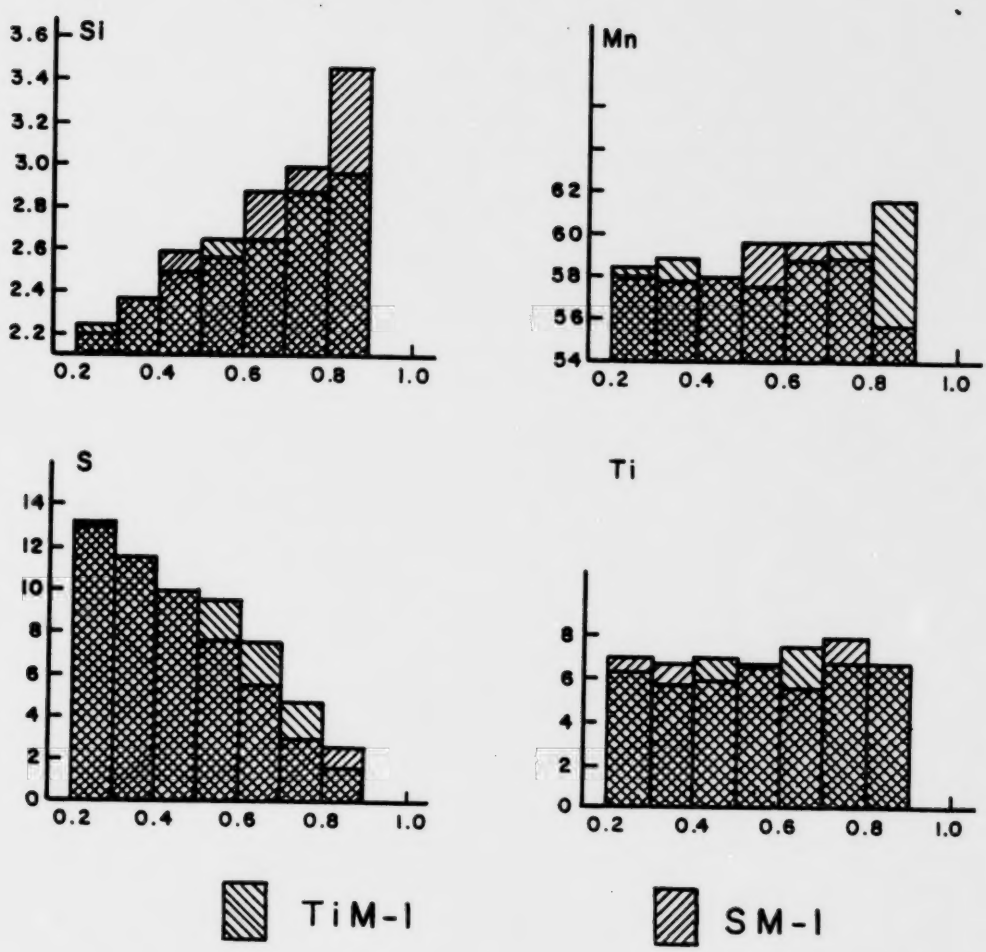

FIGURE 5.26 Relative Intensities of Si, S, Ti and Mn as a Function of the Inclusion diameter for TiM-I and SM-I Welds.

As was mentioned in Section 5.1.3.3., for similar welding conditions, the thickness of the ferrite veins depends upon the level of alloying elements which influence the transformation kinetics as well as the efficency the inclusions for the formation of AF.

The efficency for the nucleation of AF which is described by the AF/F_γ ratio depends upon the total surface area of the Ti rich phases per unit surface area of the as-deposited weld metal. This is a function of the Ti content in the inclusion, the inclusion density as well as the size distribution of the inclusions which determines the total surface area of the inclusions. Since the inclusion size distributions and the Ti content of the inclusions are almost identical for the two welds, it could be concluded that the AF/F_γ ratio should be a function of N_A which is larger in SM-I than TiM-I(chemical composition of the inclusions is similar). The following values were obtained for $N_A.A_{Ti}$:

$$\text{TiM-I} = 20.08 \times 10^{-4}\ cm^2/cm^2$$

$$\text{SM-I} = 26.66 \times 10^{-4}\ cm^2/cm^2$$

These results suggest that SM-I should be more effective in initiating AF than TiM-I but this was not the case if the quantity of alloying elements and thickness t of the ferrite vein are assumed the same for the two welds. If a an average value of t for the two deposits is used, the AF/F_γ ratio is 0.68 for SM-I and 0.82 for TiM-I.

Inclusions do not appear to be the factor that explains the presence of the thicker ferrite veins in SM-I weld which is more likely due to the increased Mn content in the TiM-I weld of 1.68% as compared with 1.46% Mn for SM-I. Mn, being an austenite forming element, lowers the $\gamma \rightarrow \alpha$ transformation temperature and increases the hardenability. Many researchers have shown that

increased Mn levels favours the formation of AF to the detriment of PF(G) and FS [3,13](Section 2.3.4.4.). In the present study, the increased Mn content from 1.46% to 1.68% reduces the likelyhood for the formation of FS and/or PF(G) at the austenite grain boundaries which in turn increases the amount of austenite that can transform to acicular ferrite.

5.3.2.2. Microstructure-Toughness Relationships

Since the amount of as-deposited weld metal is somewhat smaller in the conventional welds, this phase is not the only factor that determines the toughness of the weld metal. However, since this phase is much less tough than the reheated metal, it is the as-deposited weld metal that is the likely region where fracture will initiate in the conventional welds and therefore will affect the transition temperature.

Fractographic observations of the experimental welds (Section 4.2.3) showed that the presence of PF(G) and FS has a negative effect on the toughness of weld metal since these phases are preferential sites for the initiation and propagation of cleavage cracks. The toughness of the weld metal improves when the quantity of these phases are decreased in the weld metal and replaced by AF. This can be achieved by increasing the austenite grain size and/or decreasing the $\gamma \rightarrow \alpha$ transformation temperature which decreases the temperature interval and therefore time for PF(G) and FS growth. This was observed for the TiM-I and SM-I welds. The TiM-I weld has thinner PF(G)+FS veins than does SM-I.

In addition to its role on the microstructural development, Mn influences the toughness directly through solid solution hardening. In the literature in general [3,13], the optimal transition temperatures are achieved for Mn levels around 1.5%. Above this level, there is in general a decrease in

the fracture resistance of weld metal. In the present study, there is an increase in toughness for increases in Mn from 1.46% to 1.68% which indicates that Mn levels above 1.5% can improve the impact properties(some researchers have found optimum Mn levels approaching 1.8%). It can be concluded that for the welding conditions used in this study and similar chemical compositions of the weld metal that higher Mn levels favours the formation of tougher micro-structures by decreasing the width of the PF(G) and FS phases and increasing the amount of AF.

A decrease in the Oxygen level which decreases from 382 ppm in SM-I to 293 ppm in TiM-I has a benificial effect because this results in a decrease in the inclusion density which increases the austenite grain size as well as decreases the detrimental effect of inclusions on the fracture process. These two factors, in addition to the increased Mn levels will increase the toughness of the weld metal.

CONCLUSIONS

The main results of this investigation can be summarized in the following conclusions:

1- The austenite grain size (S/L) for the welds having intermediate levels of Ti (TiM, SM, SH and TiCa) is related to the inclusion density (N_A) which shows that inclusions can retard or block efficiently the austenite grain growth.

2- For TiH and TiAl welds (having high levels of Ti and/or Al and N), the austenite grain size is much finer than would be expected if only inclusion density is considered. This is explained by the precipitation of fine TiN particles which retard grain growth further.

3- Amongst the elements that can be contained in the inclusions (Al, Si, S, Ti, Mn and Ca), the presence of Ti is required for the formation of acicular ferrite. For welds TiM, TiH, SM, SH, TiCa and TiAl, the inclusion contain significant quantities of Ti and the proportion of AF is significant (>48%). TiL does not contain titanium in its inclusions and has a low proportion of AF (8.4%).

4- Microanalysis in the Scanning Electron Microscope (SEM) of inclusions extracted on replicas of the SM weld showed the heterogeneous nature of the inclusions. Ti is concentrated in a phase referred to as the Ti-rich phase.

5- The minimum Ti content of the weld required for the occurrence of the Ti-rich phase in the inclusions is estimated to be about 39 ppm which agrees very well with the results of Devillers et al[19.20].

6- Even though a minimal amount of Ti is required for the formation of AF, the Ti level in the inclusions is not the only factor determining the proportion of AF in the microstructure. The austenite grain size, the inclusion density and the inclusion size distribution are the other factors affecting the amount of acicular ferrite (the amount of alloying elements and the cooling rate will also have an effect but these are assumed to be constant).

7- In general, increasing austenite grain sizes lead to higher proportions of AF. As for the effect of inclusion density and the size distribution, it was studied by defining $F\gamma$ which represents the volume fraction of austenite available for the formation of AF after PF(G) and FS phases have formed. The nucleation efficiency of AF is then defined by the ratio $AF/F\gamma$ and can be related to inclusion density and size distribution.

8- The nucleation efficiency of AF for welds TiM, SM and SH which have similar levels of Ti in the inclusions is directly related to the inclusion density (N_A) times the average surface area of the inclusions (A_{inc}). The effect of the product ($N_A x A_{inc}$) shows the importance of the total surface area occupied by all the Ti containing inclusions in nucleating AF and thus underlines the role of the surface effect on the mechanism of AF.

9- For welds TiL, TiH, TiCa and TiAl containing different levels of titanium in the inclusions, there was no relationship between the factor $N_A x A_{inc}$ and the efficiency of nucleation of the acicular ferrite, $AF/F\gamma$. Except for the TiAl weld, $AF/F\gamma$ is directly related to the value of ($N_A x A_{inc}$) which is

the product of the inclusion density (N_A) times the average external surface area of the inclusions occupied by the Ti-rich phase (A_{Ti}).

10- It follows that the mechanism responsible for the nucleation of AF in the welds studied is related to a surface effect associated with the Ti-rich phase present in the inclusions. Factors such as the number, size and chemistry of the inclusions that will increase the inclusion density of Ti-rich inclusions and the total external surface of the inclusions occupied by the Ti-rich phases lead to a greater amount of AF.

11- The lower value of the efficiency of nucleation of AF, $AF/F\gamma$, observed for the TiAl weld than that expected from the value of $N_A x A_{Ti}$ was argued to be the result of the fact that the Ti-rich phase was predominantly located in the core of the inclusions. In addition, a higher Si level in the weld lead to a higher transformation temperature and larger thickness of PF(G) and FS at the boundaries than for the other welds. The consequence was a overestimated value of $F\gamma$ (calculated from the hypothesis that the thickness of PF(G) and FS is the same for all the welds) thus reducing the ratio $AF/F\gamma$.

12- The dynamic yield strength is directly proportional to the percentage of AF present in the softer FS and PF(G) phases for the welds with varying Ti contents and agrees with the trends found by Tweed and Knott[81] and Widgery[70]. It was concluded that precipitation strengthening is not a major contributor to the increased strength for increasing Ti contents. This relationship did not hold for increasing S content of the weld metal due to a decrease in the hardness of the AF phase with an increase in S content.

13- As is the case for the dynamic yield strength, the critical cleavage fracture stress is directly proportional to the AF content of the weld metal for similar inclusion size distributions and increases to around 2700 MPa for 100% AF.

14- There is a monotonic relationship between the decrease in the cleavage fracture stress from the value predicted by the relationship described in conclusion 13 and the increase in the inclusion density of inclusions larger than 1 μm. Large Al rich inclusions in the Ti-Al weld proved to be very detrimental to the fracture resistance of weld metal. If the maximum inclusion size can be kept below about 1.3μm, the inclusions will have little detrimental effect on the cleavage fracture resistance.

15- The changes in the T_t 50 J/cm^2 transition temperatures as a function of microstructure and alloying additions are due not only to changes in the brittleness transition temperature but also to large changes in the Charpy slope which affects the temperature dependence of the total absorbed energy between the brittleness transition temperature, $T_{D(N)}$ and the T_t. A reduction in the Charpy slope is related to the presence of large volume fractions of large inclusions, M-A microconstituents or grain boundary carbide which can act as sites for cleavage fracture initiation. The high work-hardening rates of AF will also reduce the Charpy slope.

16- The poor impact resistance of the TiL weld is related to the presence of extensive FS(A) which has a large effective grain size which reduces its ability to resist cleavage fracture. The presence of a large number of aligned M-A microconstituents also reduces the fracture resistance of this weld.

17- The improvement in the impact resistance with increasing Ti content is related to the reduction in the amount of FS(A) present and an increase in the quantity of AF which has a much higher cleavage fracture resistance.

18- A model for the fracture of weld metal containing significant proportions of AF was proposed and is based on the stress differential between the softer PF(G) or FS phases and the stronger AF which leads to localized strain at the interface of these phases. This model assumes that near plane-strain deformation occurs in the fracture initiation zone.

19- Nitrogen has a pronounced effect on the weld metal toughness in the transition temperature region. Reductions in the absorbed energy of about 7600 J/cm^2 per weight percent N addition was observed. The increase in the N content from 100 ppm to 180 ppm lead to an increase in the brittleness transition temperature of about 15°C.

20- For the welds with inclusions containing large proportions of the Ti-rich phase, it is likely that a limited improvement in toughness can be obtained by reducing the number and/or size of the inclusions. A more significant improvement, however, is more likely from the reduction in the N content and possibly in the Ti content since the precipitation of TiN appears to be detrimental to the toughness of weld metal.

21- The electrodes used in the production of the experimental TiM and SM welds which have the lowest impact transition temperatures gave T_t (50 J/cm^2) below -60°C when used for conventional welds and therefore achieves one of the objectives of the present study. It should be noted that the conventional welds gave higher toughness values than did the experimental large pass

welds for all of the electrodes studied. This is related to the larger percentage of reheated metal in the Charpy specimen of the conventional welds which has higher toughness due the fineness of its structure.

22- The relative toughness of the conventional weld metal generally follows the trends for the toughness of the large pass welds. The experimental large pass welds can therefore be used to study the effects of changes in the as-deposited weld metal microstructure and composition on the Charpy toughness and at the same time the results can be used to identify electrodes that will give good toughness for conventional welds. Care, however, should be taken when extrapolating the results from the experimental large pass welds to conventional welds. The transfer of alloying elements is more effective in the conventional welds and the increase in alloy content may affect slightly the relative order of the transition temperature for the experimental and conventional welds as was observed for the present study.

REFERENCES

1. BONNET, C., JACQUINOT, G., HUBERT, M. "Note technique de la dispersion des des résultats de resilience en zone fondue multipasses", Technical report no 75-34, A.L., France, 1975.

2. CHUEN, S.L.K., P.H.D. THESIS, Colorado School of Mines, Golden, Colorado, 1984.

3. BONNET, C., Soudage et technique annexes, p. 209, July-August 1980.

4. DOWLING, J.M., CORBETT, J.M. and KERR, H.W., in Proc. of Int. Conf. on Inclusions and Residuals in Steels: Effects and Fabrication and Service Behavior, Ottawa, Canada, 1985.

5. KENNY, B.G., KERR, H.W., LAYOR, L.B. and GRAVILLE B., Metal Construction, 17 (6), p. 374R, 1985.

6. PACEY, A.J., KAYALI, S. and KERR, H.W., Canadian Metallurgical Quaterly, 21, p. 309, 1982.

7. PACEY, A.J., KAYALI, S. and KERR, H.W., Canadian Metallurgical Quaterly, 23, p. 227, 1984.

8. COCHRANE, R.C., Welding in the World, 21 (1/2), p. 16, 1983.

9. ABSON, D.J. and DOLBY, R.E., "A Scheme for the Quantitative Description of Ferritic Weld Microstructure", IIW Doc. IXJ-29 80, 1980.

10. ABSON, D.J. and DOLBY, R.E., Weld Int. Res. Bull., 21 (4) p. 100, 1980.

11. DAVEY, T.G. and WIDGERY, D.J., "A Technique For The Characterisation of Weld Metal Microstructure", IIW Doc. II-389-76, 1976.

12. PARGETER, R.J. and DOLBY, R.E., "Guideline for Classification of Ferritic Steel Weld Metal Microstructure Constituents, Using the Light Microscope" IIW Doc. IX-1377-85, 1985.

13. ABSON, D.J., and PARGETER, R.J., Int. Metals Reviews, 31 (4), p. 141, 1986.

14. RICKS, R.A., HOWELL P.R. and BARRITE G.S., J. Mat. Sci. 17, p. 732, 1982.

15. CHOI, C.L. and HILL, D.C., JOURNALS WELDING, 57 (8), P. 2325, 1978.

16. BRAID, J.E.M. AND McGRATH, J.T., Can.Met.Quart., 25(2), p.131, 1986.

17. TWEED, J.H. and KNOTT, J.F., Met. Sci., 17, p. 45, 1983.

18. McROBIE, D.E. and KNOTT, J.F., Met. Sci. and Tech., 1, p. 357, 1985.

19. DEVILLERS, L., MARANDET, B., KAPLAN, D., RIBES A. and RIBOUD, P.V., Soudage et techniques connexes, p. 229, July-August 1983.

20. DEVILLERS, L., KAPLAN, D., RIBES A. and RIBOUD, P.V., Mémoires et etudes scientifiques, Revues de Métallurgie, p. 43, January 1986.

21. FERRANTE, M. and FARRAR, R.A., J. Mater. Sci. 17, p. 3293, 1982.

22. GRONG, O. and MATLOCK, Int. Metal Reviews, 31 (1), p. 27, 1986.

23. GRAVILLE, B.A., Technology focus (Welding Int. of Canada), V.2, p. 1, 1980.

24. COCHRANE, R.C., WARD, J.L. and KEVILLE, B.R., in Proc. Int. Conf. on the Effects of Residual, Inpurity and Microalloying Elements on Weldability and Weld Properties, paper 8, Abdington, The Welding Institute, 1984.

25. DAVIS, M.L.E., PARGETER, R.J. and BAILEY, N., Metal Construction, 15, p. 338, 1983.

26. EVANS, G.M., Welding Journal, 62 (11), p. 3135, 1983.

27. EVANS, G.M. "Effects of Manganese on the Microstructure and Properties of All Weld Metal Deposits", IIW Doc II A 432-77, 1977.

28. ITO, Y. and NAKANISHI, m., SEARCH SUMITOMO, 15, P. 42, 1976.

29. ABSON, D.S., "A Study of the Influence of C and Si on the Microstructure and Toughness of Submerged arc welds", The welding institute, Report no. 68 - 1978-M, 1978.

30. EVANS, G.M., "The Effect of Silicon on the Microstructure and Properties of C-Nn All-Weld Metal Deposits", IIW Doc II-A-630-84, 1984.

31. BONNET, C. and CHARPENTIER, J.P., in Proc. Intl. Cons. on the Effects of Residual, Impurity and Micro Alloying Elements on Weldability and Weld Properties, paper 8, Abdington, the Welding Institute, 1984.

32. NAKANO, S., SHIGA A. and TSUBOI, J., "Optimising the Titanium Effect on Weld Metal Toughness", IIW Doc. XII-B-182-75, 1975.

33. LAU, T., NORTH, T.H., WEATHERLY, G.C., in Proc. of Conf. on Inclusions and Residuals in Steels Effects on Fabrication and Service Behaviour, p. 487, Ottawa, Canada, 1985.

34. MORI, N., HOMMA, H., OKITA, S. and WAKABAYASHI, M., "Mechanism of Notch Toughness Improvement in Ti-B bearing Welds Metals", IIW Doc. IX-1196-81, 1981.

35. MORI, N., HOMMA, H., OKITA, S. and WAKABAYASHI, M., J. JPM Weld Soc., 50 (2), p. 48, 1981.

36. ABSON, D.J., DOLBY, R.E. and HART, N.H.M., In Proc. Conf. on Trends in Steels and Consumables for Welding, p. 75, London, The Welding Institute, 1978.

37. BARRITE, G.S., RICKS, R.A. and HOWELL, P.R., "Quantitative micro analysis with High Spatial Resolution", p. 112, London, The Metals Society, 1981.

38. TERASHIMA, H. and HART, P.H.M., In Proc Conf. on Effect of Residual, Impurity and Micro alloying Elements on Weldability and Weld Properties, Paper 27, Abdington, The Welding Institute, 1984.

39. EVANS, G.M., "The Effects of Sulphur and Phosphores on the Microstructure and Properties of C-Mn all Weld Metal Deposits", IIW Doc. II-A-640-85, 1985.

40. BONNET, C. and ANGELI, A.G., "Influence of Nitrogen Content on Deposited Weld Metal Notch Toughess" Unpablished Report.

41. PARGETER, R.J., "Investigation of Submerged Arc Weld Metal Inclusions", WIRR 151/1981, 1981.

42. SAGGESSE, M.E., BHATTI, A.R. HAWKINS, D.N. and WHITEMM, J.A., In Proc. Conf. on the Effects of Residual, Impurity and Micro alloying Elements on Weldability and Weld Properties, Paper 15, Abdington, The Welding Institute, 1984.

43. KAYALI, E.S., CORBETT, J.M. and KERR, H.W., J. Mat. Sci. Letts. 2, p. 123, 1983.

44. COURT, S.G. and POLLARD, G., Jour of Mat. Sci. letts 4, p. 427, 1985.

45. LATHABAI, S. and STOUT, R.D., Welding Research Supplements. 11, p. 3035, 1985.

46. FISHER, S.B., HARBOTTLE, G.S. and ALDRIDGE, N., CEGE Report no TPRD 10094/N 82, 1982.

47. RICKS, R.A., BARRITE, G.S. and HOWELL, P.R. In Proc. Conf. on Solid State Phase Transformations, p. 463, Pittsburgh, AIME, 1981.

48. KOUKABI, A., NORTH, T.H., and BELL, H.B., In Proc. Conf. on Trends in Steels and Consumables for Welding, p. 281, London, The Welding Institute, 1978.

49. KANAZAWA, S. NAKASHIMA, A., OKAMOTO, K. and KANAYA, K., Trans. IA4SIJ, 16, p. 486, 1976.

50. BROOKSBANK, O. and ANDREWS, K.W., Jour. of the Iron and Steel Institute, p. 246, April 1972.

51. SERVER, W.L., and IRELAND, D.R., "General Yielding of Notched Three-Point Bend Specimen", Effects Technology Report TR-72-19, 1972.

52. "Rapid Inexpensive tests for Determining Fracture Toughness", Report of the Committee on Rapid Inexpensive Tests for Determining Fracture Toughness, National Academy of Sciences, 1976.

53. KRISHNADEV,M.R., "A Study of strength and Structure Relations in Copper-Bearing Steel, Ph.D. thesis, University of Saskatchewan, 1969.

54. CUTLER, L.R., Ph.D. thesis, Laval University, 1984.

55. L'ECUYER, J.D., M. SC. Thesis, Ecole Polytechnique, Montréal, Québec, 1985.

56. L'ECUYER, J.D., L'ESPERANCE, G., AKBEN, M.G. and BACROIX, B., Acta Metall., 35 (5), p. 1149, 1987.

57. TETELMAN, A.S., WULLAERT, R.A. and IRELAND, D.R., "Prediction of Variation of Fracture Toughness KIC From Small Specimen Tests", Effects Technology Technical Report TR 71-05, 1971.

58. RITCHIE, R.O.,Proc. Annual Meeting of the American Institute of Minning, Metallurgical and Petroleum Engineers, 1978, p.54.

59. MALKIN, J. and TETELAMAN, A.S., "Relation Between KIC and Microscopic Strength for Low Alloy Steels", Engineering Fracture Mechanics, Vol. 3, No. 2, pp. 151-169, 1971.

60. WULLAERT, R., Ph.D. Thesis, Stanford University, 1969.

61. NAKAMURA, H., NAIKI, T., OKABAYASHI, H., KURIBAYASHI, M. and MORIAHIGE, N., Engineering Fracture Mechanics, Vol. 7, 1975, p.541.

62. TOMITA, Y. and OKABAYASHI, K., Met. Trans. A., Vol.17A, 1986, p.1203.

63. PICKERING, F.B., "Physical Metallurgy and the Design of Steels", Applied Science Publishers LTD, London, p.84.

64. COCHRANE, R.C., Effect of Second Phase Particles on the Mechanical Properties of Steels, Iron and Steel Institue, 1971, p.101.

65. TWEED, J.H. and KNOTT, J.F.," Microstructure-Toughness Relationships in a C-Mn Weld Metal", Fracture and the Role of Microstructure, Proceedings of the 4th European Conference on Fracture, Leoben, Austria, 1982, p.127.

66. GIANETTO, J.A., and BRAID, J.E.M., "An Evaluation of Weld Metal Toughness for Low Temperature Offshore Structure Applications.

66. OHWA,T., "Statisical investigation of the effect of alloying elements for the notch toughness of weld metals", IIW Doc.II-221-62,1962.

67. DOLBY, R.E., Welding Inst. Report R/RB/M93/76, 1976.

68. GARLAND, J.G. and KIRKWOOD, P.R., Met. Constr., Vol. 7, No. 275, 1979, p.320.

69. Dieter, G.E., Mechanical Metallurgy, Second Edition, McGraw-Hill,1976, p.217.

70. WIDGERY,D.J., Ph.D thesis, Cambridge, 1974.

71. TREMLETT, H.F., BAKER,R.G., and WHEATLEY,J.M., Br. Welding Journal, 1961, Vol.8,p.437.

72. KLASSEN, R.J., BASSIM, M.N., BAYOUMI, M.R., and WILSFORF, H.G.F., Materials Science and Engineering, Vol. 80, 1986, p.25.

73. HALL, E.O., Proc. Phys. Soc., London, B64, 1951, p.747.

74. PETCH,N.J., J. Iron and Steel Inst., Vol 174, 1953, p.35.

75. MINCHIER, A.L., BOSCH, R.A., and MORGAN, R.P.,"Comercial Production of High-Strength, Titanium-Bearing Hot-Rolled Steel", Proceedings Micro-Alloying 75 Conference, Washington, D.C., October 1975, p. 297.

76. WULLAERT, R., "The Effect of Nickel on the Microstructure and Mechanical Properties of Ferritic Steels", Ph.D. thesis, Stanford University, 1969.

77. KNOTT,J.F., "Micromechanisms of Fibrous Crack Extension in Engineering Alloys", Metal Science, Vol.14, Aug.-Sept. 1980, p.327.

78. IRICIBAR,R., LEROY, G. and EMBURY, J.D., Metal Science, Vol.14,No. 8&9, 1980, p.337.

79. MINTINK, H., in Scandinavian Offshore Symp. Eindhoven, June 1983, Philips.

80. ENRIETTO, J.F., Trans. AIME, Vol. 224,1962,p.43.

81. SMITH,E., Int. J. Fracture Mech., Vol.4.,1968, p.131.

82. DEBIEZ, Soudage et techniques connexes, 11/12, 1982, p.445.

83. DAWSON,G.W.,and JUDSON,P.,in Proc. Conf. on Offshore Welded Structures, paper 3, London, Welding Institute, 1982.

84. CHEVET,B., Soudage et techniques connexes, janvier-fevrier 1976, p.5.

85. JUDSON,P., McKOEWN,D., in Proc. Conf. on Offshore Welded Structures, Paper 4. London, Welding Institute, 1982.

86. EVANS, G.M., Welding Review, Vol 1(2), 1982,p.4.